CONTINENTAL LAND MASS AIR TRAFFIC CONTROL (COLM ATC)

J.A. Pecar and J.E. Henrich
IBM Federal Systems Division
Electronics Systems Center
18100 Frederick Pike
Gaithersburg, Maryland 20760

21 June 1973
Final Report for Period August 1971 – December 1972

GODDARD SPACE FLIGHT CENTER
Greenbelt, Maryland 20771

1. Report No.	2. Government Accession No.	3. Recipient's Catalog No.
4. Title and Subtitle CONTINENTAL LAND MASS AIR TRAFFIC CONTROL (COLM ATC)		5. Report Date 21 June 1973 6. Performing Organization Code
7. Author(s) J.A. Pecar, J.E. Henrich		8. Performing Organization Report No.
9. Performing Organization Name and Address IBM Federal Systems Division Electronics Systems Center 18100 Frederick Pike Gaithersburg, MD 20760		10. Work Unit No. 11. Contract or Grant No. NAS 5-21656
12. Sponsoring Agency Name and Address Goddard Space Flight Center Greenbelt, Maryland 20771		13. Type of Report and Period Covered Final Report August 1971 – December 1972 14. Sponsoring Agency Code
15. Supplementary Notes		

16. Abstract

The Continental Land Mass (COLM) Air Traffic Control (ATC) Study is essentially a vehicle for comparing various satellite systems and techniques relative to providing CONUS-wide ATC services. Three satellite configurations were reviewed:

1. Configuration I: A constellation of satellites transmit synchronizing ranging waveforms to the users. The users measure the relative time-of-arrival of the ranging waveforms. According to some multiple access rules, the users are polled, either from the ground or from satellites, and the measured data relayed to a local or central processor that performs location computations. This concept is DABS compatible.

2. Configuration II: The user autonomously transmits a ranging waveform through at least four satellites to a control center. Time-of-arrival measurements and position calculations are made at the central processor for each user.

3. Configuration III: This configuration differs from Configuration II in that the users are polled and two-way ranging measurements are obtained. The user's position is computed at the central processor.

The study includes consideration for the various ranging waveforms, multiple access alternatives, and the power and bandwidth required as a function of the number of users.

17. Key Words (Selected by Author(s))	18. Distribution Statement
Air Traffic Control (Continental U.S.) Satellite Ranging	

19. Security Classif. (of this report)	20. Security Classif. (of this page)	21. No. of Pages	22. Price*
Unclassified	Unclassified	272	

*For sale by the Clearinghouse for Federal, Scientific and Technical Information, Springfield, VA 22191

TABLE OF CONTENTS

Table of Contents (cont)

Table of Contents (cont)

Table of Contents (cont)

LIST OF ILLUSTRATIONS

List of Illustrations (cont)

List of Illustrations (cont)

List of Illustrations (cont)

LIST OF TABLES

List of Tables (cont)

GLOSSARY

AC	Air Carrier
A/C	Aircraft
ARTCC	Air Route Traffic Control Center
ATC	Air Traffic Control
ATCAC	Air Traffic Control Advisory Committee
BER	Bit Error Rate
BINOR	Binary Optimum Ranging
bps	Bits per Second
CDM	Code-Division Multiplex
CDMA	Code-Division Multiple Access
CEP	Circular Error Probability
COLM	Continental Land Mass
CONUS	Continental United States
dB	Decibel(s)
DLL	Delay-Lock Loop
ERP	Effective Radiated Power
EW	East-West
FAA	Federal Aviation Administration
FDM	Frequency-Division Multiplex
FDMA	Frequency-Division Multiple Access
ft	Foot or Feet
GA	General Aviation
GDOP	Geometrical Dilution of Precision
GHz	Gigahertz (1×10^9 cycles per second)
h	Hour(s)
Hz	Hertz (cycle per second)

IBM	International Business Machines Corporation
IFR	Instrument Flight Rules
IRAD	Independent Research and Development
JPL	Jet Propulsion Laboratory
kbs	Kilobits per Second
kHz	Kilohertz (1×10^3 cycles per second)
LIT	Location Identification Transmitter
LPF	Low-Pass Filter
MAC	Mid-Air Collision
Mb/s	Megabits per Second
MHz	Megahertz (1×10^6 cycles per second)
mi	Mile(s)
mi/h	Mile(s) per Hour
Mil	Military
ms	Millisecond(s)
NAVSAT	Navigation Satellite
NMAC	Near Mid-Air Collision
nmi	Nautical Mile(s)
NS	North-South
NTSB	National Transportation Safety Board
PLACE	Position Location Aircraft Communications Equipment
PLL	Phase-Lock Loop
PN	Pseudo Noise
RF	Radio Frequency
rms	Root Mean Square
s	Second(s)
SID	Steller Inertial Doppler
SDMA	Space Division Multiple Access
SNR	Signal-to-Noise Ratio

TDM	Time-Division Multiplex
TDMA	Time-Division Multiple Access
TWT	Traveling Wave Tube
US	United States
VCO	Voltage-Controlled Oscillator
VFR	Visual Flight Rules
VHF	Very High Frequency
vs	Versus
W	Watt(s)
°	Degree(s)
%	Percent

Section 1

REVIEW OF MAJOR ATC PROBLEMS

Section 1

REVIEW OF MAJOR ATC PROBLEMS

The Continental Land Mass (COLM) Air Traffic Control (ATC) Study is essentially a vehicle for comparing various satellite systems and techniques relative to providing CONUS-wide ATC services. In order to provide a meaningful framework for the study, a review of the ATC operational environment has been made to highlight the significant problem areas. Much of the material presented in Subsections 1.1 and 1.2 has been abstracted from an IBM IRAD Study, Reference 1. Source material includes various Federal Aviation Administration (FAA) and National Transportation Safety Board (NTSB) documents, References 2 through 9.

1.1 MID-AIR AND NEAR MID-AIR COLLISIONS

The mid-air collision (MAC) record of US civil aviation over the past 15 years is shown in Table 1-1. The major item of concern, the mid-air collision between two air carrier (AC) aircraft, occurred only three times during this period. Two of these accidents involved pilot error and the third an anomaly of the control system. The bulk of the accidents involving air carriers are caused by collision with a general aviation (GA) aircraft. The statistics show an increasing trend during 1966 through 1969 in the number of air carrier/general aviation collisions. As expected, the majority of the mid-air collisions, 83%, are between two general aviation aircraft operating in a VFR environment.

How do actual accidents compare with the number of accidents expected on the basis of aircraft populations? To facilitate this comparisions, data on flight hours and operations are summarized in Table 1-2. Since there are too few collisions in any given year from which to draw valid statistical conclusions, the total accidents occurring during the 15-year period are compared against the aircraft population ratios of 1968 and the results shown in Figure 1-1. Collisions in the traffic pattern or during final approach to an uncontrolled airport have been removed because they are a special problem related to airport traffic. All three collision categories involving air carriers are lower than predicted since the air carriers operate almost exclusively under instrument flight rules. General aviation which operates under visual rules approximately 88% of the time is higher than predicted.

Table 1-1

MID-AIR COLLISION RECORD, US CIVIL AVIATION[1]

Number of Accidents by Segment of Aviation Involved						
Year	AC/AC	AC/GA	AC/Mil	GA/Mil	GA/GA	Total
1956	1	1		1	14	17
1957			1	4	10	15
1958			2	2	12	16
1959				3	10	13
1960	1	4		2	19	26
1961					20	20
1962				5	14	19
1963				2	11	13
1964				2	12	14
1965	1			2	24	27
1966		1		1	25	27
1967		2	1	3	20	26
1968		3		1	34	38
1969		3		3	21	27
1970		0		5	32	37
Total	3	14	4	36	278	335

1. Official National Transportation Safety Board Figures
2. Preliminary

Table 1-2

AIR TRAFFIC ACTIVITY, 1968

Flight Hours by Flight Rule (millions)

	IFR	VFR	Total
Air Carrier	7.2	—	7.2
General Aviation	2.9	20.4	23.3
Military	4.9	2.9	7.8
Total	15.0	23.3	38.3

Flight Hours by Aircraft Class (millions)

	Single Engine Piston	Multi-Engine Piston	Prop Jet	Turbo Jet
Air Carrier	0.3	0.1	1.0	5.8
General Aviation	19.0	3.6	0.4	.3
Military	0.9	2.2	0.5	4.2
Total	20.2	5.9	1.9	10.3

Operations (millions)

At airports without FAA towers		57.7
At airports with FAA towers — VFR	14.6	
At airports with FAA towers — IFR	40.5	
Subtotal		55.1
Total		112.8

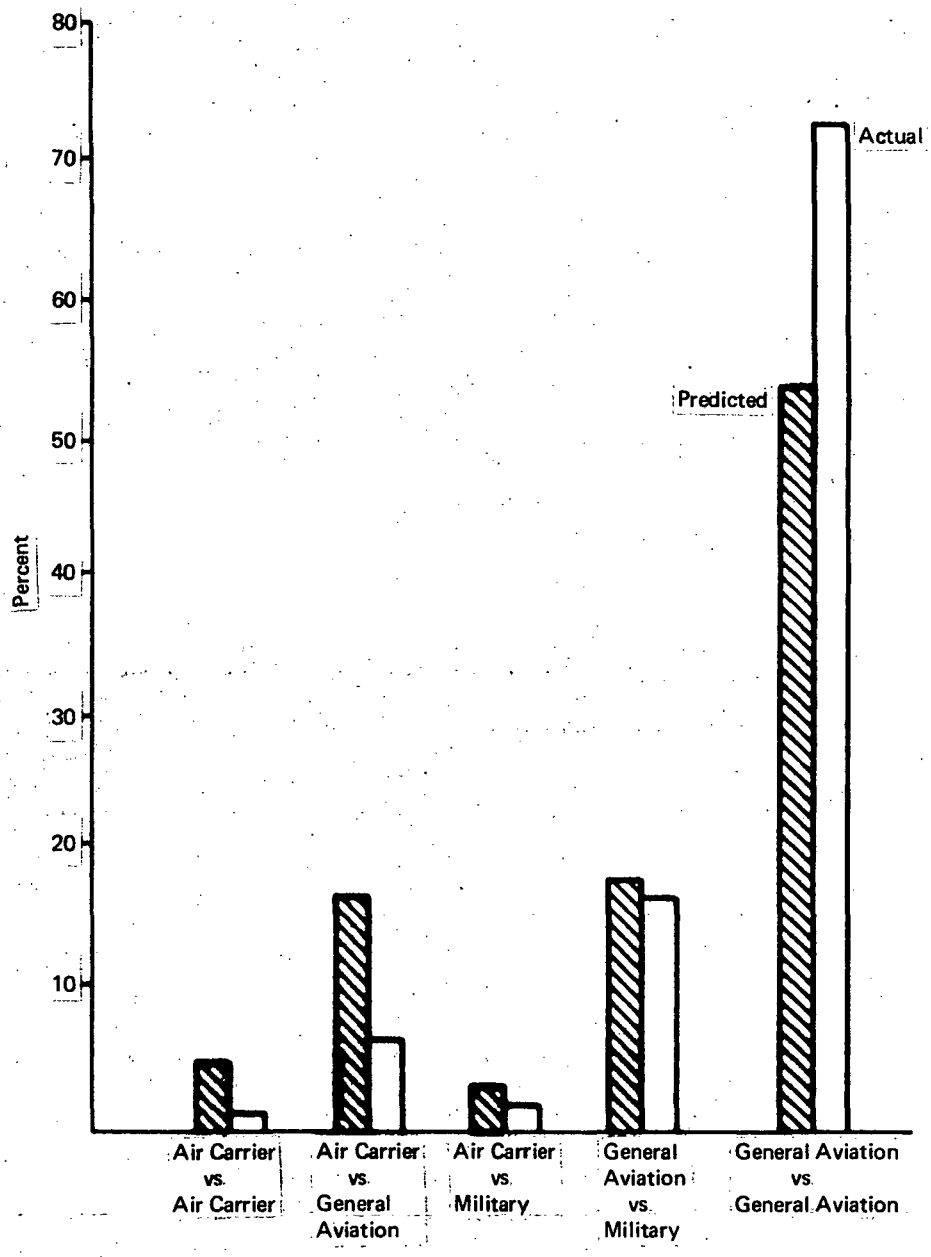

Figure 1-1. Actual vs Predicted Mid-Air Collisions by User

In January 1968, a special FAA group undertook a study of near mid-air collisions. The near miss situation is at best a subjective judgment. Aircraft may pass in close proximity to each other, particularly in a terminal area, without the incident being considered a hazardous condition. A near miss is defined as a situation in which one aircraft passed within close proximity, 500 ft or less, and created an unsafe condition. Near miss incidents were further divided into hazardous and nonhazardous categories. Hazardous near misses are defined as those where

1) Time was not available for an evasive maneuver and avoidance of an accident was strictly by chance

2) Collision might have resulted if evasive action had not been taken by either pilot.

In the past, near misses frequently were not reported by the pilot in order to avoid action under the FAA enforcement program. To obtain as many reports as possible, plus an objective analysis of this situation, immunity to prosecution was granted by the FAA administrator to all pilots or controllers involved in a near mid-air collision. Results of the study are shown in Figure 1-2. Of the 2230 reported incidents, 1102 were judged to be nonhazardous and are not considered in this study. Of the 1128 hazardous incidents, 36% occurred in the en route area and 64% in terminal areas. In Figure 1-3 these incidents are compared to the expected value based on the number of aircraft operations for each flight rule category. Predictions for the en route area are based on total flight hours. Correlation between actual and predicted values for the VFR versus VFR case is extremely good. A higher degree of interference between IFR and VFR aircraft is experienced than would be predicted. The effect of the control system in reducing incidents is clearly shown in the IFR versus IFR case. Returning to Figure 1-2, controller error is responsible for four times as many IFR versus IFR incidents as pilot error.

Sixty-four percent of the hazardous incidents occurred in the terminal area. The majority of the terminal incidents (87%) occurred at the 322 airports equipped with an FAA tower, even though total operations are almost equally divided between tower and nontower airports. There are two major reasons for the low percentage of near mid-air collisions (NMACs) at uncontrolled airports. First, the private pilot is reluctant to report a near miss because of the inconvenience and paperwork involved. Secondly, the private pilot has much higher tolerance for close proximity passing since this is a frequent occurrence in and around the light plane airport during VFR operations.

On the next level of Figure 1-2, terminal incidents are classified by flight rule, and in Figure 1-3 are compared to the expected value. For the terminal area, the number of operations is used as the basis for the expected number of incidents rather than flight hours. IFR versus IFR incidents are only 3%, less than half that which would be predicted. Incidents between IFR and VFR aircraft account for 63% of the total, more than double the number expected. A high degree of interference between

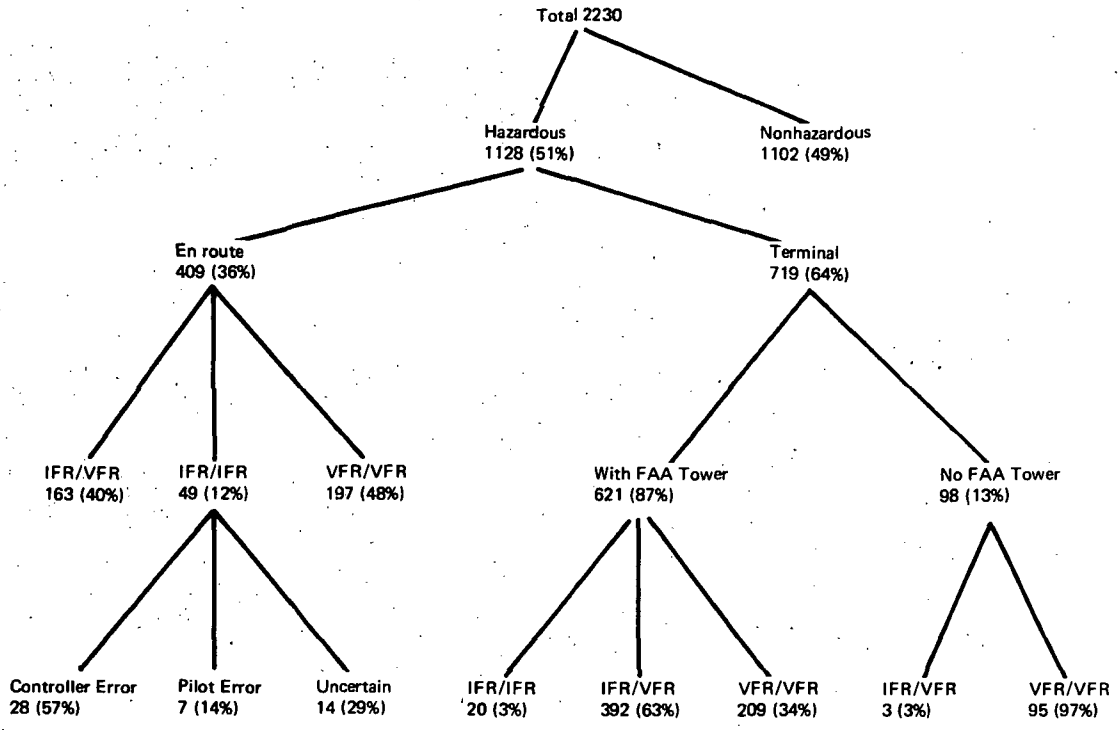

Figure 1-2. Near Mid-Air Collision Study, 1968

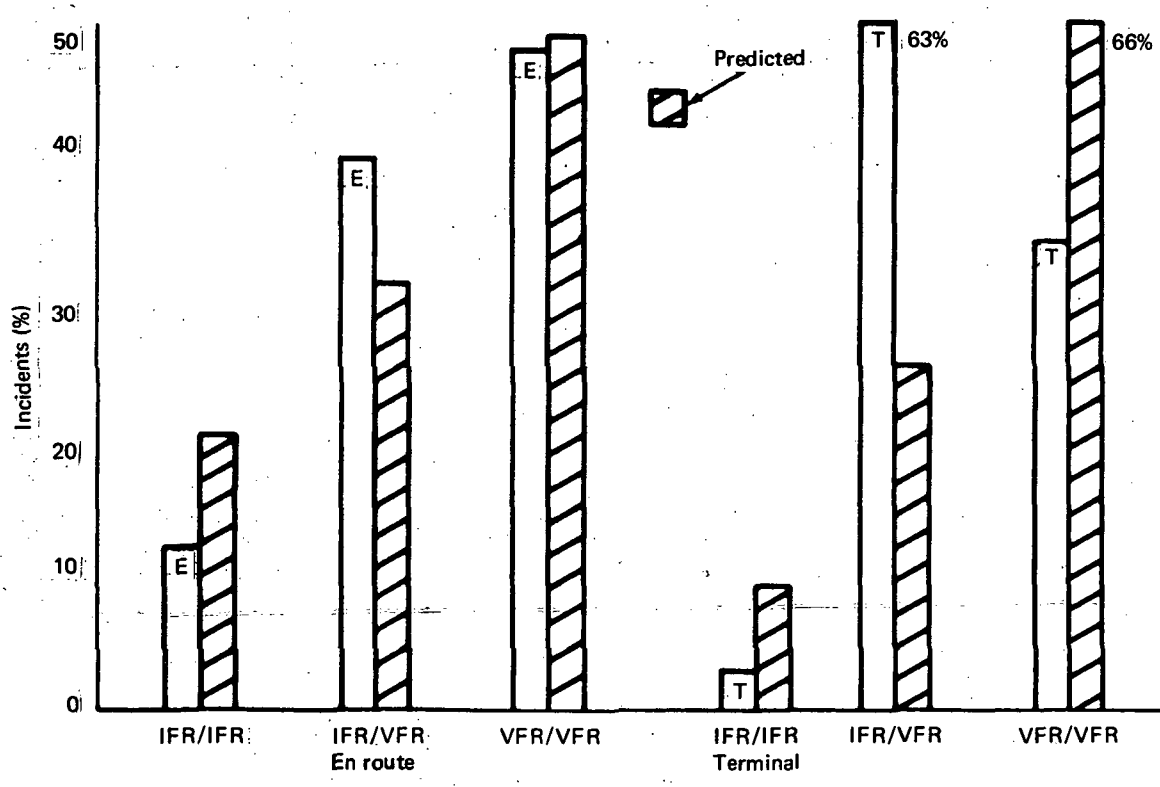

Figure 1-3. Near Mid-Air Collisions — Involvement by Flight Rule En Route and Terminal vs Predicted

aircraft operating at major commercial hubs and nearby general aviation airports is indicated. VFR/VFR incidents accounted for only 34% of the total, approximately half the number expected. The terminal ATC task is generally thought to be more difficult than the en route task since airspace is restricted, aircraft traffic densities higher, and aircraft altitude is frequently changing. Yet, the percentage of total incidents occurring between two IFR aircraft in the terminal area is one-quarter that of the en route airspace.

1.1.1 GEOGRAPHIC DISTRIBUTION

A geographic distribution of mid-air collisions for the years 1966 through 1968 is shown in Figure 1-4. Although they tend to group in California, Florida, Ohio, and New England, collisions are also distributed over low traffic areas. The problem is better defined by a plot of the near mid-air collisions shown in Figure 1-5. Here the incidents are clearly shown clustering around major hubs such as New York, Los Angeles, San Francisco, and Washington. Smaller clusters are shown over the training areas in South Florida, Pensacola, and Phoenix. Incidents occurring away from population centers fall to a great degree on airways and, more specifically, on intersections of airways.

An idea of the concentration of NMACs in the area of major hubs may be obtained from Table 1-3. Total operations at airports within a 50 mile radius of the hub have been estimated*. NMAC incidents occurring in the same area are taken from the 1968 report and the NMAC rate per million operations is determined. The hubs are then listed by incident rate in decreasing order. It is readily apparent that factors other than total number of operations in the area determine the incident rate. Phoenix and Pensacola have relatively low traffic counts but a high proportion of military training flights. The incident rates for New York, Philadelphia and Washington are similar and quite high. San Diego, San Francisco, and Los Angeles possess comparable geographic features and have similar but lower incident rates. No explanation is offered for the very low rates found at Dallas, Miami, Minneapolis, Columbus, and New Orleans.

Distance from terminal at which incidents occurred was also investigated. Number of actual and near mid-air collisions is plotted as a function of distance from the terminal in Figure 1-6. Since many more near mid-air collisions occur than actual mid-air collisions, a relative frequency scale is utilized. Actual mid-air collisions peak roughly 2 miles from the airport while the near mid-air collisions peak slightly more than 3 miles from the terminal. This difference is partially explained in Figure 1-7 which shows the location of 20 mid-air collisions which occurred in 1968 during the landing phase. As the airport is approached, density of traffic increases and the pilot is alert, so the number of incidents reported is high. The majority of accidents, however, occur on or near final approach. Four factors appear to be responsible

1) When on the base leg and final approach, the pilot is preoccupied with landing procedures.

*Operations at tower equipped airports in the area multiplied by the ratio of total operations to operations at tower equipped airports.

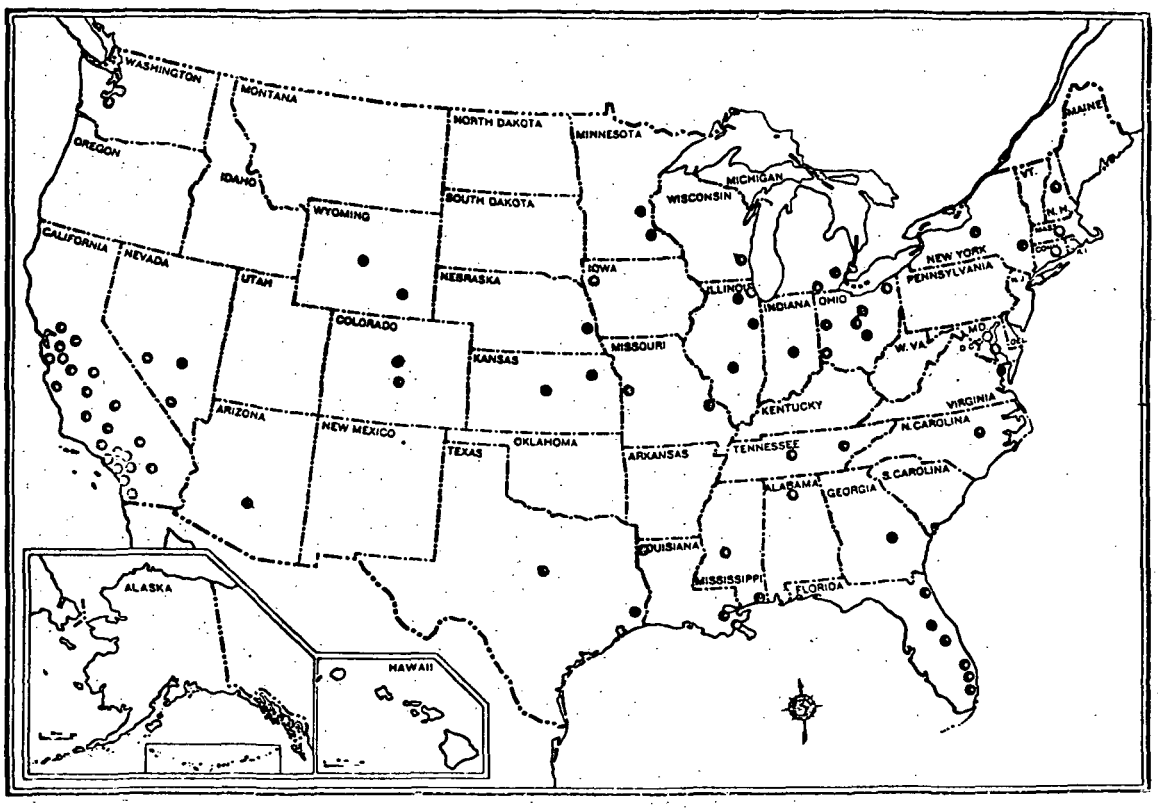

Figure 1-4. Mid-Air Collisions 1966 through 1968

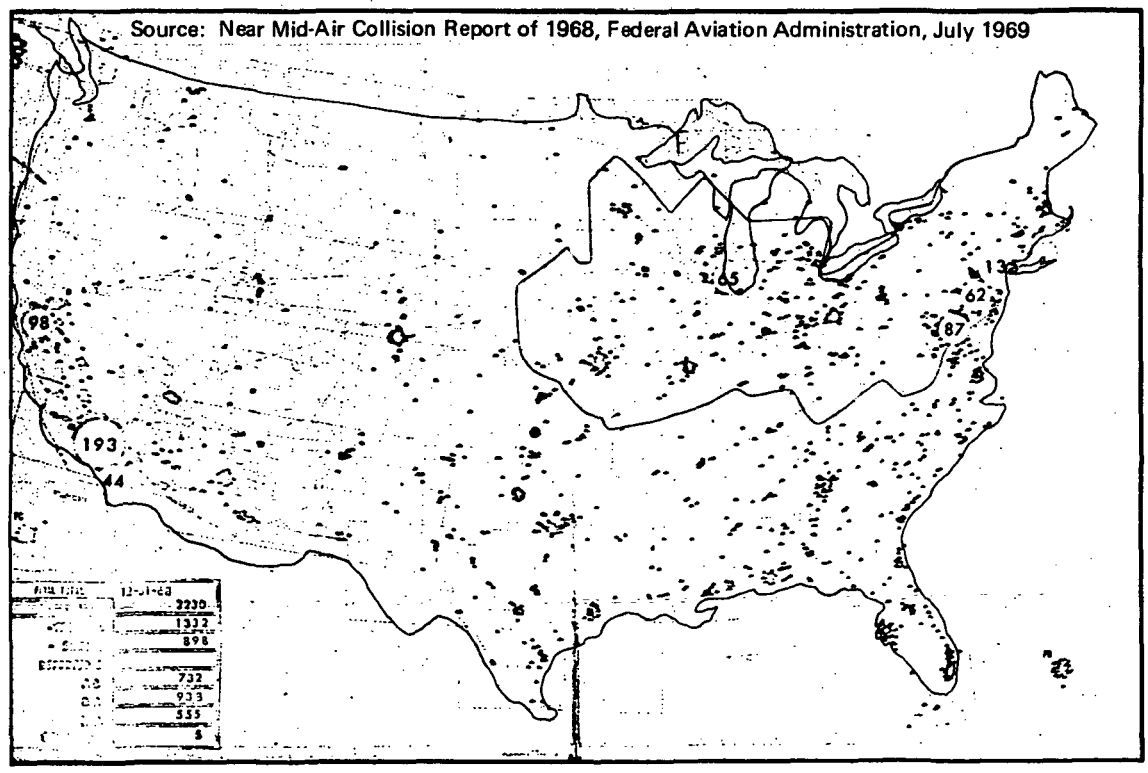

Figure 1-5. Special Near Mid-Air Collision Study, 1968

Table 1-3

NMAC RATE FOR MAJOR HUBS

	Operations [1] (millions)	NMAC	Rate Per Million
Phoenix	0.7	12	17.1
Pensacola	0.3	5	16.6
New York	3.2	53	16.6
Philadelphia	0.9	15	16.6
Washington	1.5	24	16.0
Denver	1.1	17	15.5
San Diego	1.5	19	12.6
San Francisco	3.2	38	11.9
Los Angeles	6.3	74	11.7
Cleveland	0.6	6	11.6
Chicago	1.9	21	11.0
Boston	0.6	6	10.0
Norfolk	0.7	6	8.6
Kansas City	1.3	11	8.5
Seattle	1.4	11	7.8
Dallas	1.7	10	5.9
Miami	1.8	10	5.5
Minneapolis	1.7	9	5.3
Columbus	1.3	6	4.6
New Orleans	0.9	3	3.3

[1]Estimated local and transient operations in 50 mile radius area not including military operations.

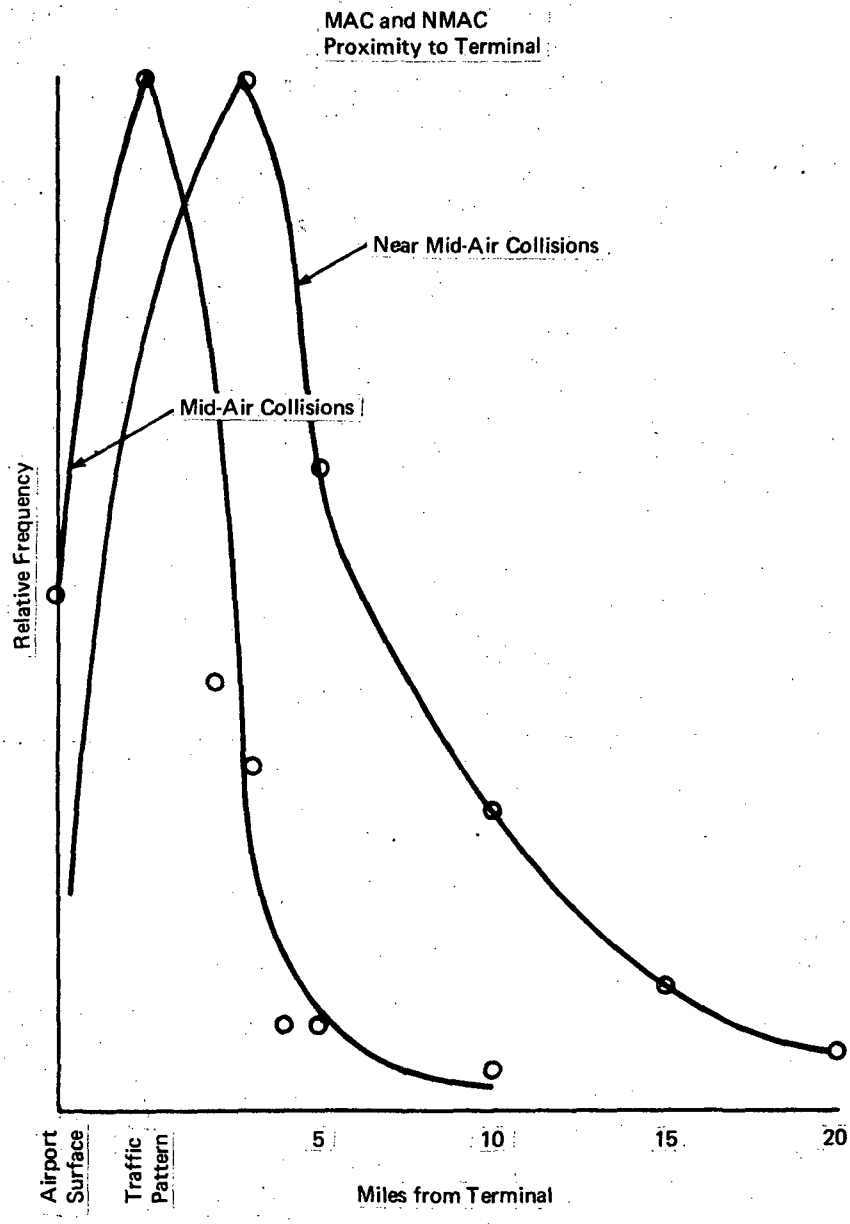

Figure 1-6. MAC and NMAC Proximity to Terminal

2) The airspace through which the flow of aircraft must pass is enormously compressed as the end of the runway is approached.

3) Visibility of the aircraft is poor in the downward direction.

4) Due to the angle of bank, aircraft turning a short base leg have poor visibility of any aircraft already on final.

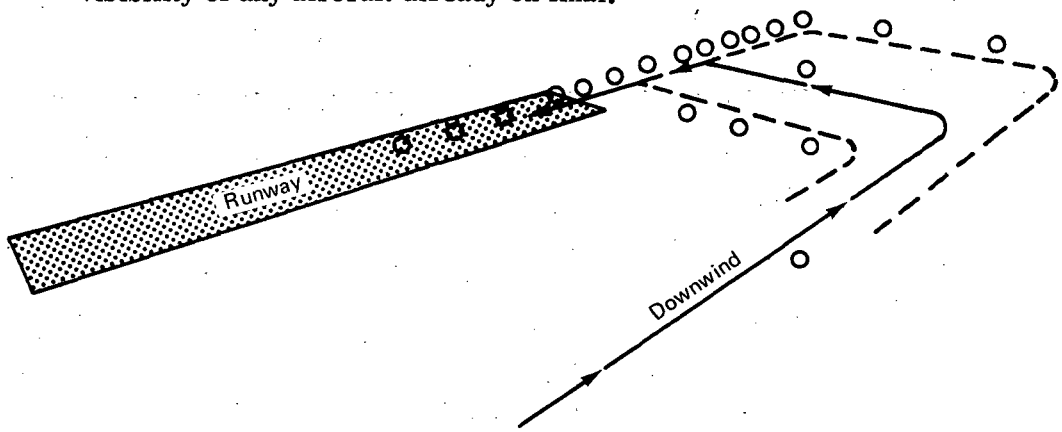

Approximate Position of 20 Mid-Air Collisions that Occurred in the Down-Wind, Base-Leg and Final Approach.

Source: Mid-Air Collisions in US Civil Aviation—1968, NTSB, July 1969

Figure 1-7. Mid-Air Collisions During Landing Phase

1.1.2 OPERATIONAL FACTORS

As expected, the phase of operation significantly affects the number of mid-air collisions. Total collisions for the period 1966 to 1968 are plotted by phase of operation in Figure 1-8, with each aircraft plotted separately. The predominance of accidents in the final approach and traffic pattern have already been discussed. One would intuitively assume that climbing and descending aircraft are a major factor in mid-air collisions. This does not appear to be the case since the bulk of the nontraffic pattern accidents occurred with both aircraft under normal cruise conditions.

Angle of closure is also a significant factor. In Figure 1-9 near miss incidents are compared against actual collisions for both en route and terminal air space. As before, there are many more NMAC incidents than actual collisions so data is plotted on the basis of percentage of total. For the en route area, the majority of the NMAC incidents occur from ahead or from crossing traffic. Actual collisions follow an inverse pattern with the majority of the collisions taking place between overtaking traffic. The same pattern is evident but even more pronounced for the terminal area. Poor cockpit visibility adds to the visibility problems created by weather and sun glare.

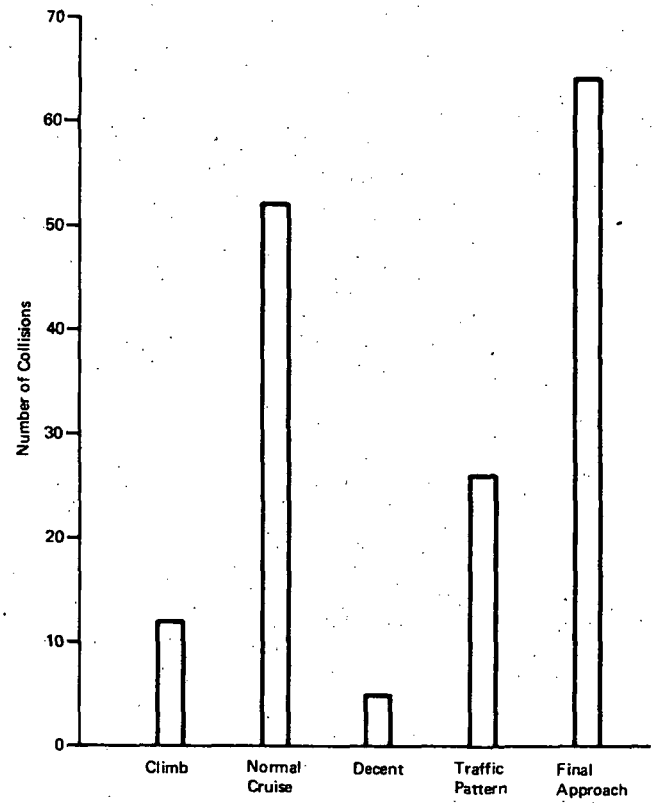

Figure 1-8. Mid-Air Collisions by Phase of Operation, 1966 to 1968

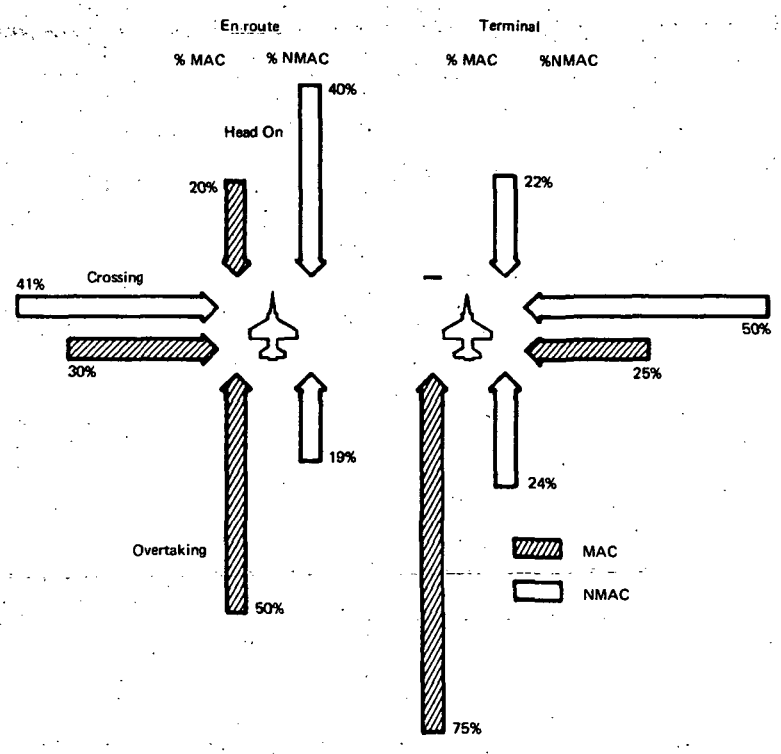

Figure 1-9. Angle of Closure

Closing speed between the two aircraft involved in near miss also seems to be a major factor in mid-air collision situations. Unfortunately, data is available only on NMAC incidents. Closing speeds between the conflicting aircraft are plotted in Figure 1-10. As expected, speeds are lowest in the terminal area and increase through the transition area, and further increase in low altitude en route and are greatest in high altitude en route. Two factors are significant

1) Most low altitude incidents occur in the vicinity of 300 knots, a speed range where see-and-avoid is estimated (Reference 10) to be 95% effective.

2) Above 10,000 feet the majority of incidents occur above 400 knots where the estimate of the effectiveness of see-and-avoid has fallen to 50%.

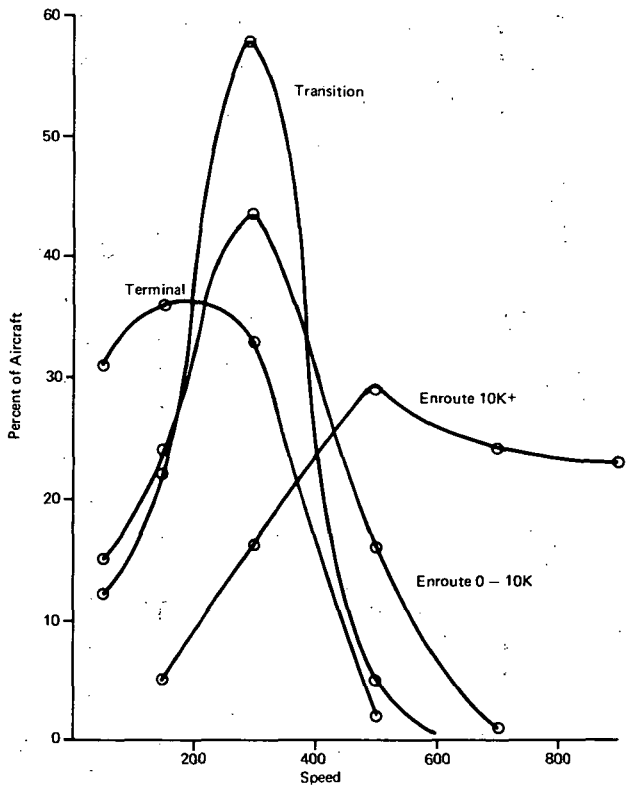

Figure 1-10. Closing Speed at Time of Near Mid-Air Collision

The role of radar advisories in NMAC incidents is shown in Figure 1-11. In the terminal area 85% of the incidents occurred within radar coverage, and in 60% of the incidents one or both aircraft was in contact with an ATC facility. Radar advisories were issued in only 21% of the cases due to controller workload and other reasons. Similar figures are shown for en route airspace. Here radar advisories alerted the

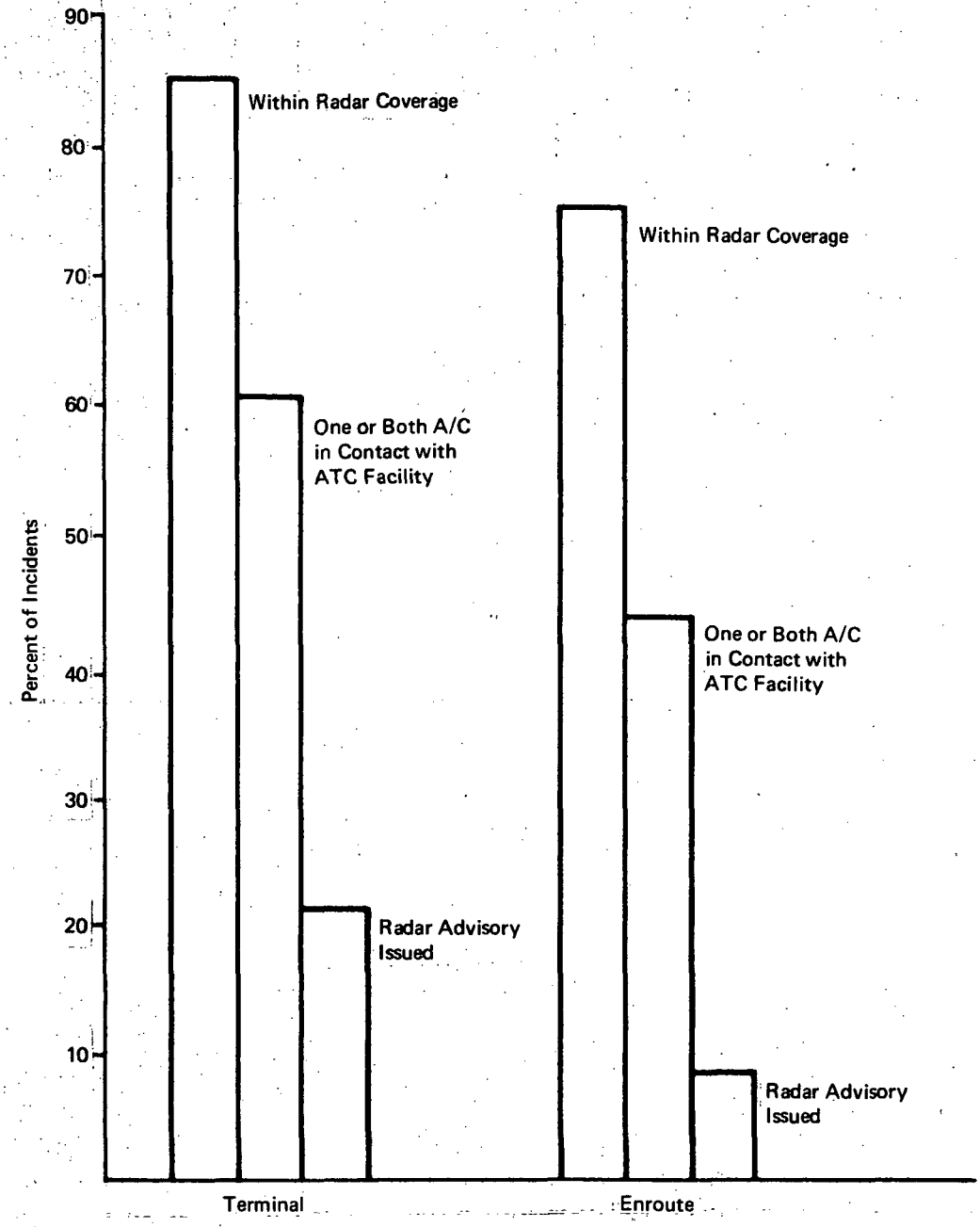

Figure 1-11. Relationship between NMAC and Radar Advisories

pilot to the near miss situation less than 8% of the time. It appears that the usefulness of radar advisory information is limited by the control system's ability to issue advisories and communicate with aircraft rather than lack of radar coverage.

1.1.3 ALTITUDE DISTRIBUTION

The final and perhaps most important aspect of the mid-air collision is the distribution of these incidents by altitude. Figures 1-12 and 1-13 are altitude distribution of near-miss incidents taken from the FAA NMAC report. Incidents in the terminal areas occur at the lower altitudes and IFR/IFR incidents are almost negligible. Incidents between VFR aircraft occur lower than those between mixed traffic. En route incidents between two controlled aircraft are principally a phenomenon of the higher altitudes peaking at 15,000 feet. Although these distributions are as one would expect, the main question is how they compare with aircraft population at each altitude. Official figures on total aircraft population as a function of altitude do not exist so data from a number of sources (References 6 and 7) has been brought together into a composit estimate. The number of flight hours at each altitude has been used for comparison purposes rather than number of flights. Estimated distributions are shown in Figures 1-14 and 1-15. Figure 1-14 is a cumulative plot of the total hours by class of user. General aviation is obviously the dominant factor with the bulk of its hours occuring below 10,000 feet. Figure 1-15 is that of IFR and VFR flight hours. Note that VFR operations extend all the way to 24,000 ft and that both IFR and VFR hours peak below 6000 ft.

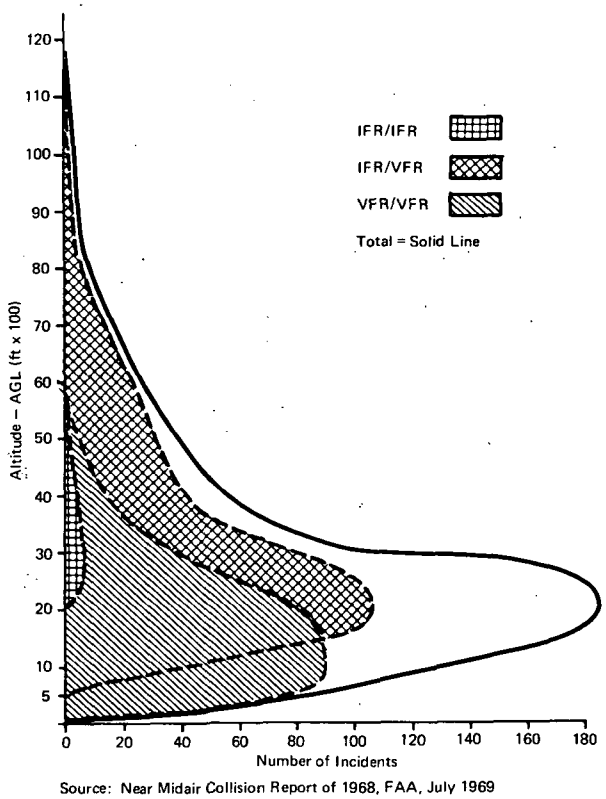

Figure 1-12. Type of Flight by Altitude Distribution (Terminal - 719 Incidents)

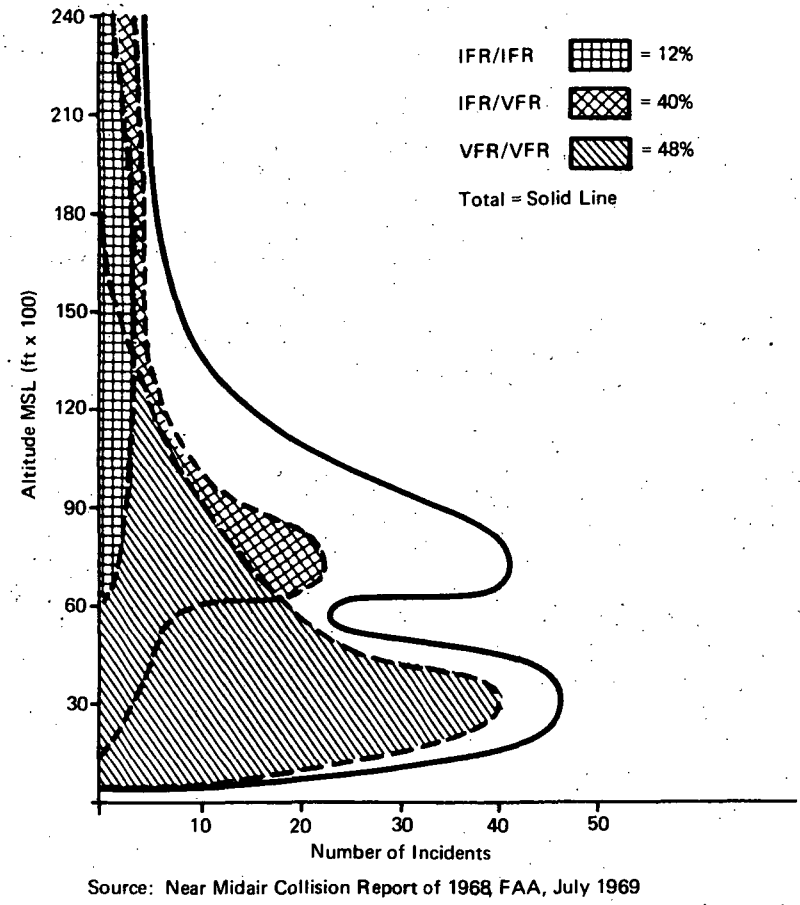

Source: Near Midair Collision Report of 1968, FAA, July 1969

Figure 1-13. Type of Flight by Altitude Distribution (En Route - 409 Incidents)

One would intuitively expect altitude transitioning of jet traffic to be the cause of the high incident rate at intermediate altitudes. Yet, earlier charts, Figures 1-8 and 1-9, show that incidents occur between aircraft in level flight. There appears to be several reasons for this paradox with altitude transition an indirect cause. Altitude maneuvers are complex but relatively safe for controlled aircraft (IFR) since they are closely watched by one or more controllers. Thus, during these maneuvers the controller's attention is somewhat diverted from other aircraft under this control. Attention is also diverted to aircraft at other altitudes. Since the bulk of the air traffic is located below 9000 feet the controller is concentrating on providing separation in these higher density areas. The third factor is speed. At the time of this study, aircraft below 10,000 feet were restricted to 250 knots. Many aircraft routinely descend to the 10,000 feet level at much higher velocities. These higher speeds create problems both in time available for the controller to detect and react to the closing situation, and in time to plan and coordinate handoffs. The majority of the low altitude controller's activity involves lowspeed traffic and he apparently does not react well to the high-speed situation.

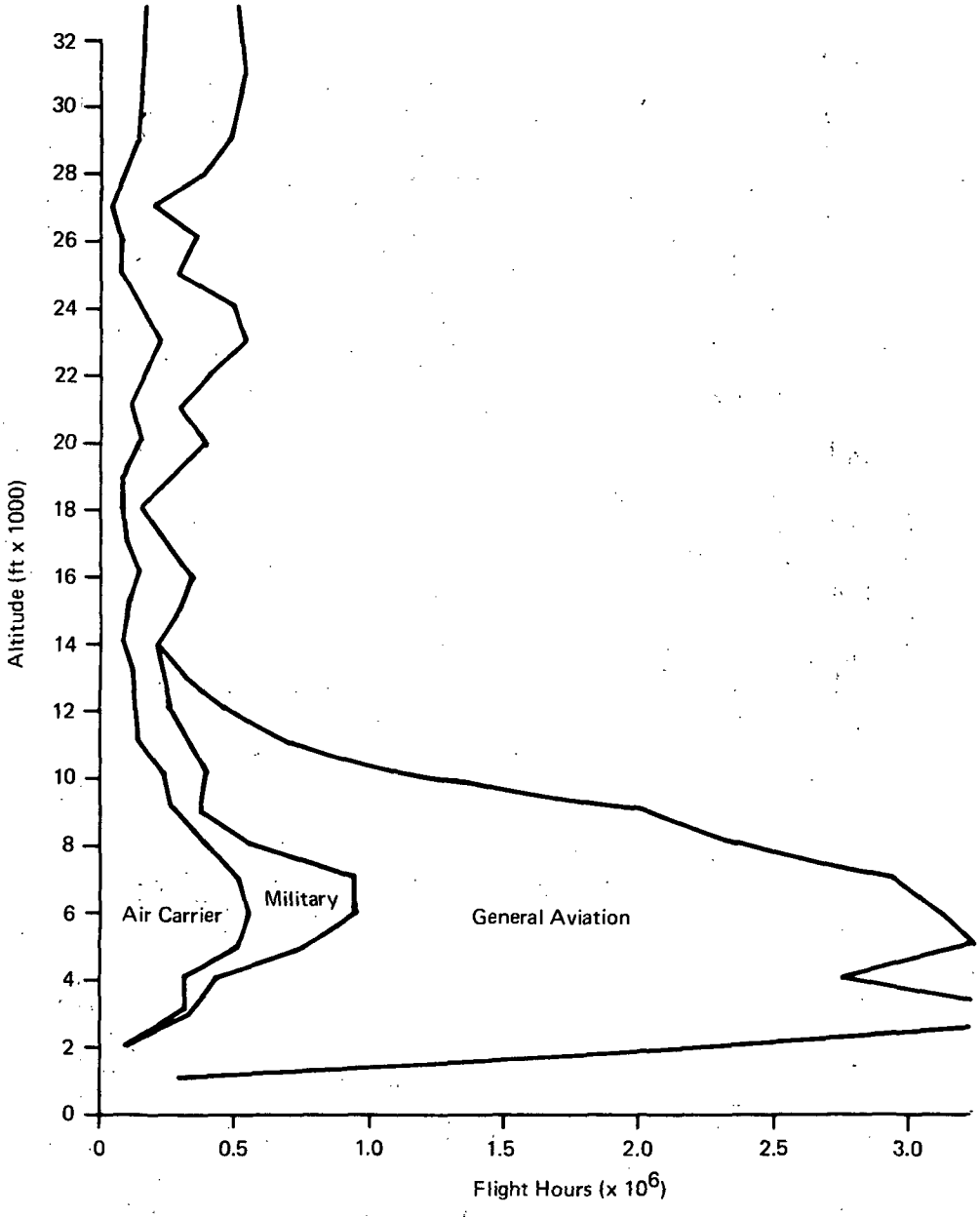

Figure 1-14. Total Hours Cumulative Distribution by Altitude and User

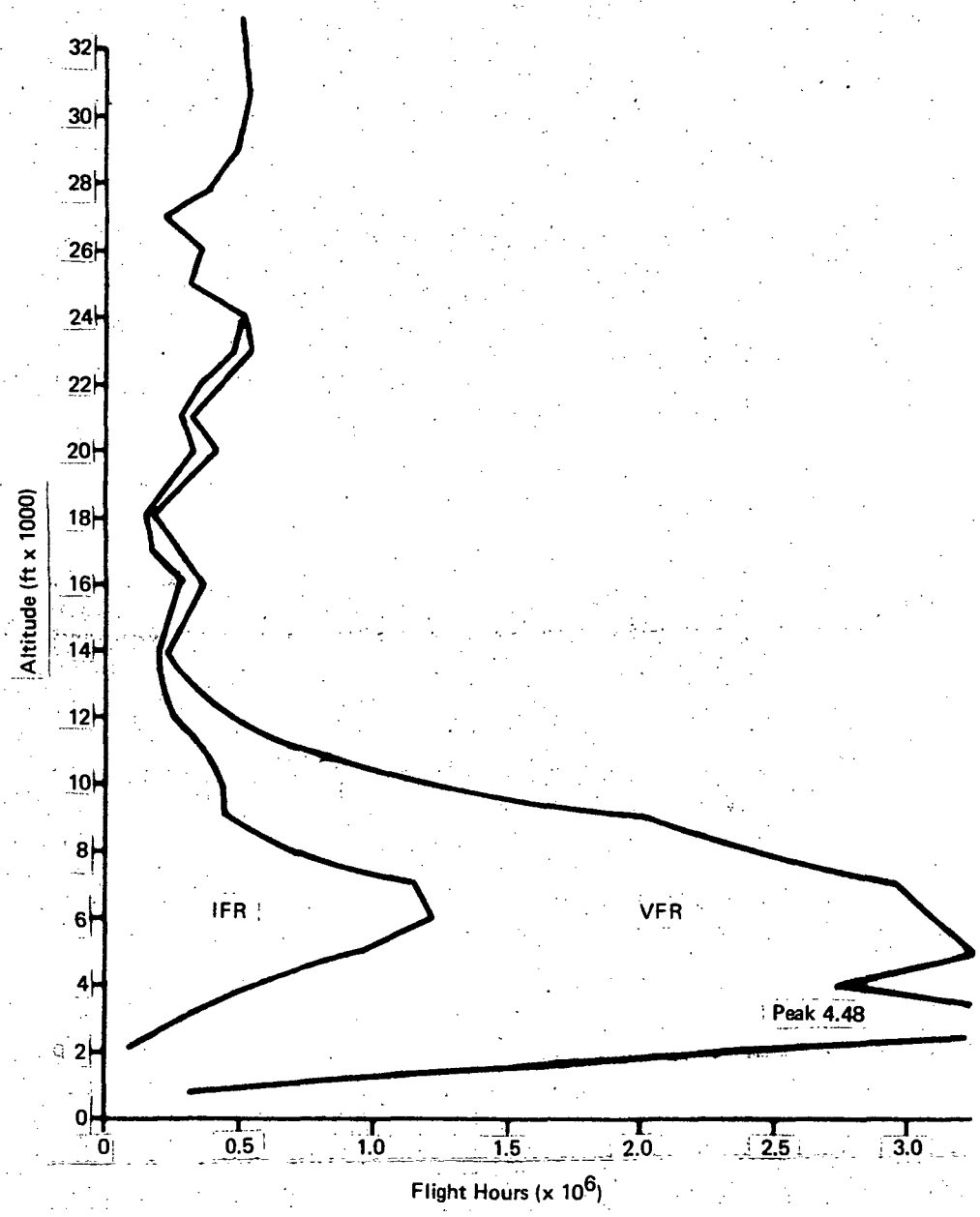

Figure 1-15. Total Hours Cumulative Distribution by Altitude and Flight Rule

1.1.4 CONCLUSIONS

1) This analysis of MAC and NMAC statistics indicates that the CONUS airspace can be divided into five regions, each of which has unique problems and requirements:
   a) High altitude en route
   b) Major air carrier terminals
   c) Low altitude en route
   d) High density general aviation airspace
   e) Nontower general aviation terminal airspace
2) The principal hazard in the terminal area is the mixture of controlled (IFR) and uncontrolled (VFR) or high and low performance aircraft.
3) The present airway navigation system concentrates the traffic into a small percentage of the airspace significantly increasing the collision hazard, especially at the airway intersection points.
4) Visual flight rules are not an effective method of separation of aircraft at speeds in excess of 250 knots and at altitudes in excess of 10,000 ft.
5) A large percentage of the near mid-air collisions take place within radar coverage; but the number of radar advisories issued is small. Lack of communication between the pilot and the control facility reduces the potential effectiveness of radar advisories.
6) Restricted cockpit visibility is the major cause of mid-air collisions at general aviation airports.
7) In a controlled system low activity, and low stress periods are not necessarily the safest since pilot and controller inattention becomes a factor.
8) As a possible corollary to item 7, in the en route phase of flight, controller error is the principle source of near mid-air collisions involving IFR/IFR aircraft.

1.2 REQUIREMENTS FOR ATC COMMUNICATION TO AIRCRAFT

One of the current near critical problems in ATC is in the area of ground to aircraft communications. There is a capacity problem because of the shortage of available VHF channels and high channel utilization under peak loading conditions. There is also a workload problem for both controller and pilot imposed by the need to exchange essential information. The RTCA, the FAA, and others have recognized that an automatic data link system for ATC can provide significant relief in both the capacity and workload areas. The purpose of this subsection is to develop data rate requirements for such a system.

1.2.1 TERMINAL AREA

Terminal ATC is generally concerned with either the first 15 minutes of flight or the last 15 minutes depending on whether a departure or arrival operation is required. In Table 1-4, a set of ATC commands for terminal operations is presented. An estimate of the frequency of command issuance is given (Reference 11) along with an estimate of the message length. The message length includes the overhead items listed in Table 1-5. An 8-bit character was selected to be compatible with the RTCA standard (Document DO-136) and ARINC/AEEC design. More efficient coding could be employed from the standpoint of the rate of information exchange, but at a corresponding loss in error checking capability. A missed approach sequence is described in Table 1-6.

Referring to Table 1-4, there are several assumptions implicit in the frequency with which various commands are given. These assumptions are

1) That a flow control capability will exist which will tend to reduce the frequency of holds
2) That track assignments will consist of coded routing like SIDs and STARs
3) That communications channel switching will be primarily a ground function.

The product of the command message length and the frequency of command occurrence yields the weighted message length shown in Table 1-7. The totals shown in the arrival and departure columns are an estimate of the total number of bits of data which must be transmitted per aircraft.

1.2.2 EN ROUTE AREA

The en route ATC is concerned with the control of aircraft from departure terminal handoff to arrival terminal handoff. An estimate of ATC en route requirements essentially follows the same procedure used for terminal requirements. The en route ATC commands are shown in Table 1-8, with message length and frequency of occurrence (Reference 12). The frequency of command occurrence for route, altitude and speed changes is based on peak day statistics for the Chicago ARTCC, December 1968. The weighted message lengths are shown in Table 1-9.

1.2.3 DATA RATES

The data rates required are a function of traffic loading, in particular the peak loading. The data rate computations are shown in Table 1-10 for both the en route and terminal areas. The en route estimates are based on the ATCAC (Reference 13) load of 2500 IFR aircraft. The traffic distribution is based on the Chicago ARTCC statistics. One way data rate estimates are 1785 bps. Assuming that aircraft acknowledgement is accomplished by parroting the message to the ground, the two way data rate will be 3570 bps.

The terminal data rates are based on the ATCAC (Reference 13) Los Angeles terminal basin peak load for 1990 of 1160 aircraft/hour arriving and departing from several airports. The one way data rate is 1513 bps and the two way rate is 3026 bps.

1.3 REFERENCES

1. "Control Subsystem for the 'Next Generation' Air Traffic Control System", IBM IRAD Study, July 15, 1971.

2. Briefs of Accidents Involving Mid-Air Collisions, U. S. Civil Aviation 1966, National Transportation Safety Board, June 1968.

3. Briefs of Accidents Involving Mid-Air Collisions, U. S. General Aviation, National Transportation Safety Board, 1967.

4. Mid-Air Collision in U. S. Civil Aviation 1968, National Transportation Safety Board, July 1969.

5. Near Mid-Air Collision Report of 1968, Federal Aviation Administration, July 1969.

6. En route IFR Air Traffic Survey Peak Day FY 1969, Federal Aviation Administration.

7. Traffic Patterns for IFR and VFR Aviation, Calendar Year 1969, Federal Aviation Administration.

8. FAA Air Traffic Activity FY 1970, Federal Aviation Administration, August 1970.

9. Air Traffic Control Advisory Committee Vol I, Department of Transportation, December 1969.

10. "Separation of Air Traffic by Visual Means: an Estimate of the Effectiveness of See and Avoid", Proceedings of the IEEE, March 1970.

11. Fred Holland, Mitre, WP 8266, "Computer Sizing of Terminal Area Command and Control for the ATC Advisory Committee," April 11, 1969.

12. Fred Holland, Mitre, WP 8272, "Computer Sizing of En route Command and Control for the ATC Advisory Committee," April 22, 1969.

13. "Report of Department of Transportation Air Traffic Control Advisory Committee," December 1969.

Table 1-4

TERMINAL UP LINK COMMANDS

Commands	Message Length*		Frequency/Flight	
	Characters	Bits	Arrivals	Departures
Enter Hold	35	280	0.25	—
Leave Hold	35	280	0.25	—
Track Assignment	24	192	1.0	1.0
Change Speed	20	160	4.0	2.0
Take Up Heading	20	160	6.0	2.0
Change Frequency**	22	176	1.0	1.0
Intercept Landing System	24	192	1.0	—
Change Altitude	20	160	4.0	2.0
Position for Takeoff	28	224	—	1.0
Cleared for Takeoff	22	176	—	1.0
Missed Approach Sequence***	—	3144	0.01	—
Total	—	—	17.51	10.

* Includes message overhead (see Table 1-5).

** Assumes the implementation of some form of the discrete frequency concept in which the ground system performs most of the frequency switching.

*** Probability of a missed approach is assumed to be 0.01 (see Table 1-6 for details).

Table 1-5

DATA LINK MESSAGE OVERHEAD

Component	Characters	Bits
Synchronization	2	16
Start of Header	1	8
Aircraft Address	7	56
Ground Station Address	4	32
Mode	1	8
Start of Text	1	8
End of Message	1	8
Block Check	1	8
TOTAL	18	144

Table 1-6

UP LINK COMMANDS FOR AIRCRAFT EXECUTING A MISSED APPROACH SEQUENCE

Command	Number	Message Length*		Bits/Sequence
		Char	Bits	
Execute Missed Approach	1	19	152	152
Take Up Heading	8	20	160	1280
Change Speed	4	20	160	640
Change Altitude	2	20	160	320
Enter Hold	1	35	280	280
Leave Hold	1	35	280	280
Intercept Landing System	1	24	192	192
Total	18	—	—	3144

* Includes message overhead (see Table 1-5).

Table 1-7

TERMINAL UP LINK MESSAGES

Commands	Weighted Message Length (bits)	
	Arrivals	Departures
Enter Hold	70	—
Leave Hold	70	—
Track Assignment	192	192
Change Speed	640	320
Take Up Heading	690	320
Change Frequency	176	176
Intercept Landing System	192	—
Change Altitude	640	320
Position for Takeoff	—	224
Cleared for Takeoff	—	176
Missed Approach Sequence	31	—
Total	2971	1728

Table 1-8

EN ROUTE UP LINK COMMANDS

Commands	Message Length*		Frequency/Flight Category			
	Chars	Bits	Arrivals	Departures	Overs	Withins
Enter Hold	35	280	—	—	—	.25
Leave Hold	35	280	—	—	—	.25
Route Assignment	78	624	—	1.0	—	1.0
Change Route **	38	304	.2	.3	.2	.4
Change Speed**	20	160	.8	—	—	.2
Take Up Heading	20	160	3.0	3.0	—	6.0
Change Frequency***	22	176	2.0	2.0	—	2.0
Change Altitude**	20	160	3.9	1.5	.8	3.1
Total			9.9	7.8	1.0	13.20

* Includes message overhead (see Table 1-5)

** Command frequency is based on peak day statistics for Chicago ARTCC, December 1968

*** Assumes the implementation of some type of discrete frequency concept in which the ground system performs most of the frequency switching.

Table 1-9

EN ROUTE UP LINK MESSAGES

Commands	Weighted Message Length (bits)			
	Arrivals	Departures	Overs	Withins
Enter Hold	—	—	—	70
Leave Hold	—	—	—	70
Route Assignment	—	624	—	624
Change Route	61	91	61	122
Change Speed	128	—	—	32
Take Up Heading	480	480	—	960
Change Frequency	352	352	—	352
Change Altitude	625	240	128	496
Total	1646	1787	189	2726

Table 1-10

DATA RATES

	Arrivals	Departures	Overs	Withins
En route (assuming 2500 IFR Aircraft)				
Message Length/Aircraft (bits)	1646	1787	189	2726
Traffic Distribution (%)	34.9	24.8	16.3	24.0
Traffic Count	873	620	407	600
Control Life (minutes)	33.1	40.2	59.3	46.8
Aircraft/Hour	1580	925	412	769
One Way Data Rate (bits/s)	722	459	22	582
Total One Way Rate = 1785 bits/s				

	Arrivals	Departures
Terminal		
Message Length/Aircraft (bits)	2971	1728
Aircraft/Hour	1160	1160
One Way Data Rate (bits/sec)	956	557
Total One Way Rate = 1513 bits/s		

Section 2

COMMUNICATION TECHNIQUES FOR SATELLITE ATC SURVEILLANCE

Section 2

COMMUNICATION TECHNIQUES FOR SATELLITE ATC SURVEILLANCE

2.1 INTRODUCTION

The communications connected with a COLM Air Traffic Control System using satellites are diverse, covering a wide range of operational requirements. A preliminary categorization which can be used to focus the problem and direct attention toward specific topics which are peculiar to satellite systems, and which have not been systematically treated in the past is the following:

1) Voice communications for advisories and control
2) Communications specific to surveillance position location
3) Communications specific to navigation position location
4) Digital data communications other than those required for navigation and surveillance (e.g., company data transmission, weather advisories, etc.)
5) Communications related to satellite control, (e.g., telemetry and housekeeping, ephemeris determination, and satellite electronics timing and synchronization)

The voice communication problem is not peculiar to satellite ATC systems, although the inefficient use of bandwidth, which is characteristic of voice, makes it even more unattractive for satellite relay (with its premium on bandwidth) than for line-of-sight communications. The trend, in present planning, is to replace voice transmissions with formatted binary data links. We have correspondingly assumed that such voice links as remain in the satellite-based system will not be relayed over satellite links, and hence do not constitute a problem appropriate for detailed consideration in this study.

The satellite control communications of item 5 take place over links between the satellites and fixed earth stations. Such links are characterized by high-gain antennas at the ground, and are well understood, having been the subject of attention in many contacts over the past 10 or 15 years. They are, therefore, also not considered in detail.

Items 2, 3, and 4 involve communication paths between the ground control center and the airborne users which use the satellite repeater as a relay point. The

ground-to-satellite segments of these links are not considered critical for the reasons cited above. The satellite-to-user links, on the other hand, are characterized by low-gain nondirectional aircraft antennas, and by a large number of users.

Thus, although the data rate from the control center to each user may be quite low, the satellite-to-user downlink must carry a high data rate, with correspondingly stringent requirements on satellite prime power. For example, 10-bit/second user implies, for 10^5 users, a one megabit per second downlink data rate. In the other direction, the return of data from user to control center, which cannot be avoided for surveillance, imposes a severe multiple-access problem, with all users requiring simultaneous access to the satellite repeater.

From an operational point of view, the most attractive feature of a satellite-based ATC system is its ability to transcend line-of-sight limitations, and to provide surveillance coverage for all users without low-altitude blind spots. Because of the potentially low cost to the user of equipment to provide surveillance, the surveillance aspect is considered to be more critical than the area navigation capability that satellites can provide. Since navigation is inherently a high user cost item, it will probably be limited to large commercial and military users in any practical system.

Consequently, in this section we concentrate primarily upon the surveillance communication problem, and examine in detail the satellite-to-user link. To do this in a systematic way, we first postulate a number of satellite configurations which are sufficiently general to encompass almost all conceivable surveillance and navigation systems.

These configurations are shown in Figure 2-1, and are briefly described as follows:

1) Configuration I - A number of satellites transmit synchronized ranging waveforms to the users. Users with the appropriate equipment can use these signals for area navigation, but, in general, the users will make time-of-arrival difference measurements and store this data temporarily. According to some multiple-access and polling procedure, each user transmits this data through a single relay satellite to the control center, where the measurements are converted to a three-dimensional position fix by hyperbolic computation.

2) Configuration II - Each user autonomously transmits a periodic ranging waveform through at least four satellites to the control center. Time-of-arrival difference measurements are made for each user, and a position fix is computed hyperbolically.

3) Configuration III - This differs from Configuration II only in that the ranging waveforms are elicited by an interrogation waveform which polls each user

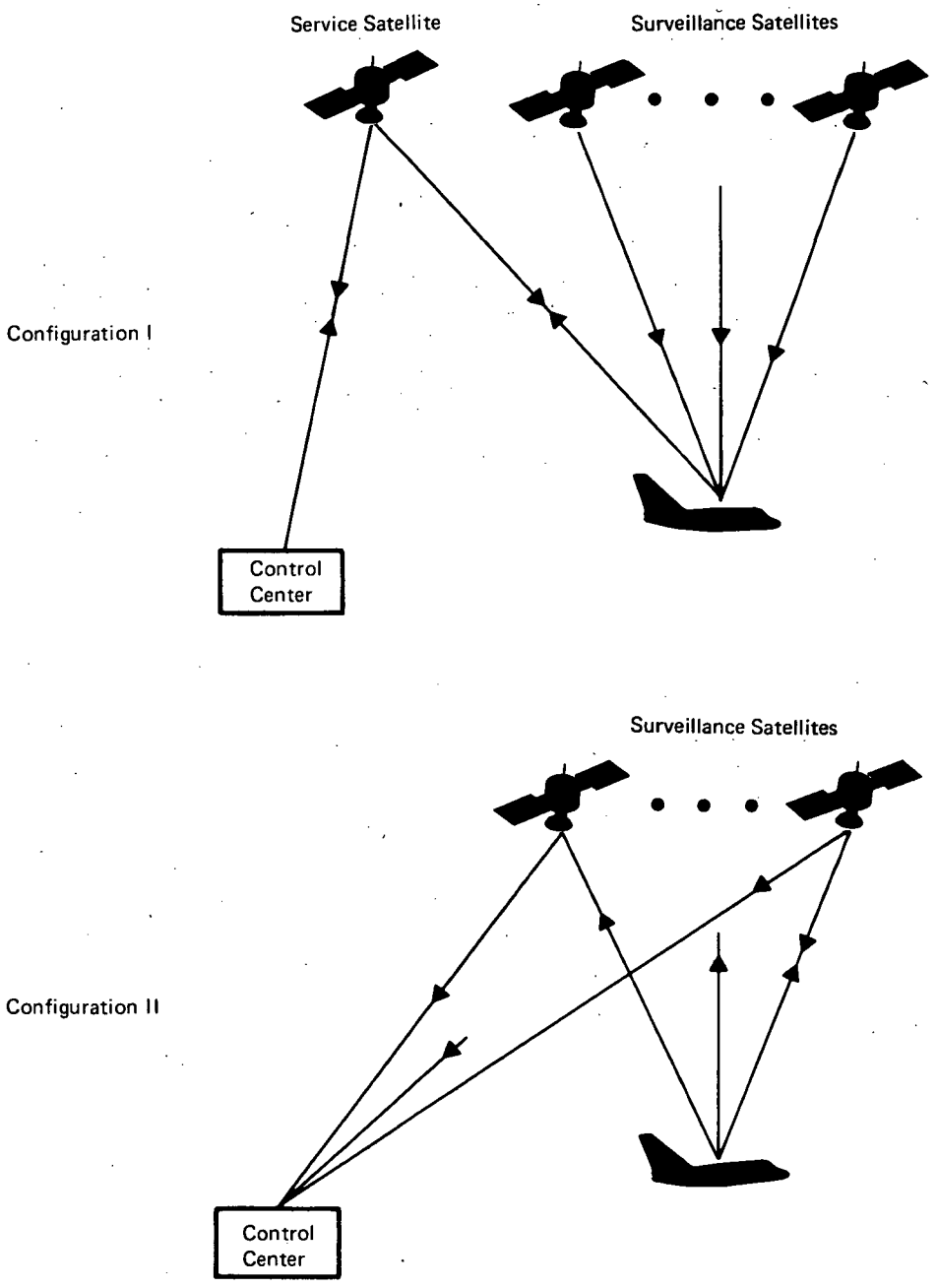

Figure 2-1. Satellite Configurations

Configuration III

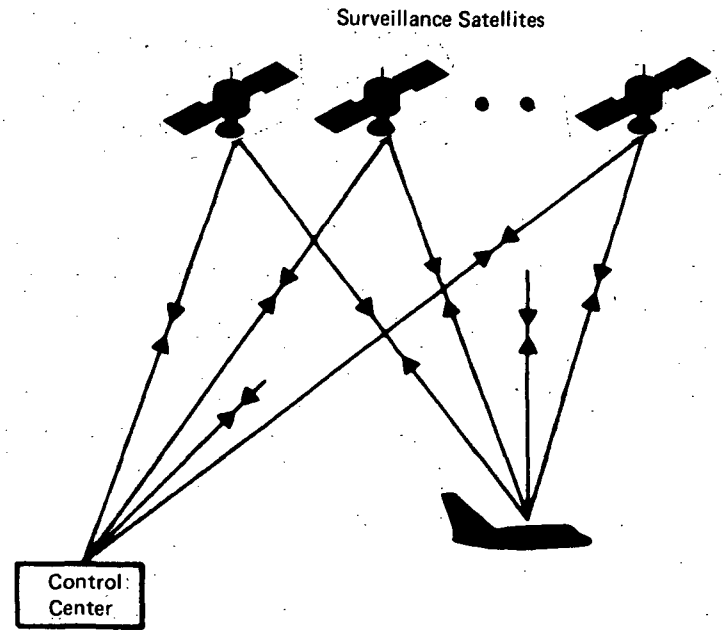

Configuration IV

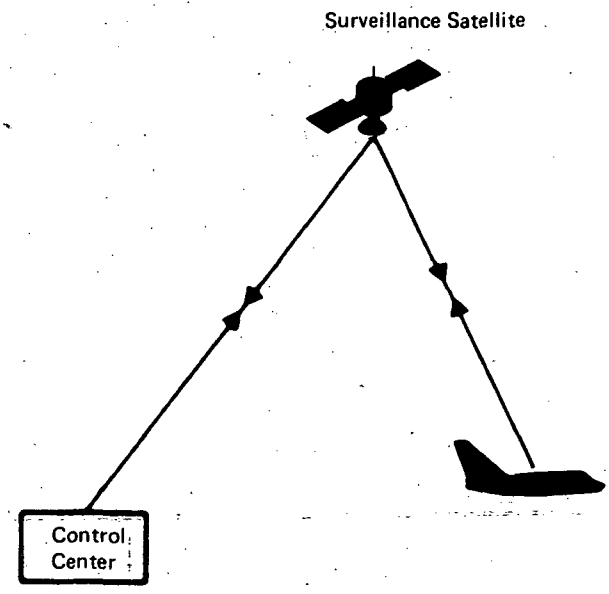

Figure 2-1. Satellite Configurations (cont)

at a specified time. The position fix is then computed by trilateration using the two-way range measurements.

4) Configuration IV - This configuration is characterized by the use of a single satellite equipped with crossed-boom interferometer. Suitable waveforms are transmitted by the users either autonomously or by interrogation, and measurements of phase differences of the signals transponded by the individual interferometer antennas permits a two-dimensional position to be determined. The third dimension is supplied by the user, who includes his pressure or radar altimeter reading as part of his transmission.

In analyzing candidate approaches to the communications aspects of each of these configurations we take a top-down approach which emphasizes the multiple-access and polling problems rather than the details of specific modulation methods. It is the decisions made at these higher levels of system design that have the greatest effect upon the efficiency of the system in terms of bandwidth and power. Specifically, we recognize four levels of design which are described in the following subsection.

2.1.1 ELEMENTS OF SATELLITE COMMUNICATIONS DESIGN

The elements of satellite communications design for ATC surveillance and navigation applications can be viewed as consisting of four separate but related levels of design considerations. These considerations are (1) first level, polling; (2) second level, multiple access; (3) third level, modulation; and (4) fourth level, ranging.

1) First Level - Polling Alternatives

In synthesizing satellite ATC surveillance systems, the most fundamental design decision involves how the operation of polling users is accomplished. Basically there are three alternatives, namely,

a) Autonomous - Asynchronous user generation of position messages are exclusive of external control signals or precise timing standards.

b) Elicited - User position messages are generated in response to central control command or to a central control common timing signal. Group polling may be accomplished, for example, by airspace areas or by user aircraft performance categories, etc.

c) Hybrid: Individual, Group, Common Timing Control - Hybrid techniques utilize advantageous features of both autonomous and elicited polling. That is, such criteria as aircraft performance, flight profile, and airspace density facets may be utilized to determine transitional points between autonomous and elicited techniques to facilitate an optimum position update rate. Under processor control, the polling technique could be altered in real time to emphasize surveillance of high risk airspace areas.

2) Second Level - Multiple Access Alternatives

These alternatives involve the methodology of obtaining signal orthogonality to permit surveillance of many users within the required interval. These alternatives* are

a) TDMA TDMA/CDMA TDMA/FDMA/CDMA

b) FDMA TDMA/FDMA

c) CDMA CDMA/FDMA

d) All the above with SDMA

3) Third Level - Modulation

The third level of investigation, modulation, essentially impacts communication link performance in terms of detection sensitivity, error rate, and information bandwidth. As such, the analysis for a given application is straight forward. However, when combined with conjunctive ranging and reporting configurations, additional modulation requirements exist which impact trade-off selection.

4) Fourth Level - Ranging

In those configurations where user-initiated signals are utilized by the control center to determine position, or, as in Configuration I, where satellite ranging waveforms are used for position location measurements, the impact of ranging signals must be considered with communications requirements. Ranging signal structures considered include

a) Sidetone

b) BINOR**

c) Pseudo-Noise

d) Pulse

e) Pulse Compression

1. Analog

2. Digital

2.1.2 PRINCIPAL SYSTEM PARAMETERS AND ASSUMPTIONS

In the analyses performed in this section, the basic approach is parametric in order to allow the widest possible application of the results. Where specific calculations are made, the numerical assumptions listed on the next page are used.

*TDMA — Time Division Multiple Access
FDMA — Frequency Division Multiple Access
CDMA — Code Division Multiple Access
SDMA — Space Division Multiple Access (multiple antenna beams)
**BINOR — Binary Optimum Ranging

1)	Number of system users (max), N,	10^5
2)	Update interval, T_u,	1 second
3)	Total message length (Configuration I), T_i,	100 bits
4)	Desired data quality, P_e,	10^{-5} bit error rate (BER)
5)	Signal-to-noise (thermal-no CDMA)	13 dB for 10^{-5} BER
6)	Signal-to-noise (thermal with CDMA)	20 dB for 10^{-5} BER
7)	Signal-to-Clutter (CDMA)	13 dB for 10^{-5} BER
8)	Data transmission efficiency	1 bit/Hz

Aircraft-to-satellite link budget is as follows:

1)	User antenna gain	0 dB
2)	Satellite antenna gain	24 dB (CONUS coverage)
3)	Path loss (@ 1.6 GHz)	187 dB
4)	N_0 KT (T=910^{o}K)	-199 dB
	$P_R/N_0 \frac{(dB/Hz)}{W}$	36 dB/Hz for each watt

2.1.3 PRINCIPAL DESIGN PERFORMANCE PARAMETERS

The design performance parameters employed for trade-off comparison relate to either the use of basic resources such as bandwidth and spectrum, or to practical considerations which ultimately limit feasibility. These principal performance parameters are

1) Bandwidth efficiency (users per megahertz)
2) Power/BER (channel quality per watt)
3) Signal process gain required
4) Number of spacecraft required by approach
5) Number of spaceborne antenna per spacecraft
6) Ground center complexity
7) Requirements for return ground to user link (via satellite)
8) Return link requirements, e.g., power, speed, BER.

2.1.4 OUTLINE OF SECTION 2

The next two parts of this section deal with topics which have application to all configurations. Subsection 2.2 presents a trade-off analysis of candidate waveforms for ranging. Subsection 2.3 considers the problem of sequential polling and the design of available polling waveforms for each of the satellite configurations. In subsections 2.4 through 2.7 the multiple access problem is considered in detail for each of the four configurations. Each multiple-access candidate is analyzed using a unified approach as far as possible. The results are presented in a way which is convenient for comparison of candidates. Subsection 2.8 consists of a summary which includes a comparison of the approaches analyzed and a preliminary selection of a number of candidates which appear suitable for further consideration.

2.2 RANGING WAVEFORM ANALYSIS

This subsection presents a comparative analysis of a number of ranging waveform designs. The analysis is applicable to all the configurations, although it is directed primarily toward the requirements of Configuration I, in which navigation signals are processed by the user for later retransmission.

2.2.1 COMPARISON CRITERIA

The comparison is made on the basis of the following four criteria:

1) Ranging power utilization
2) Bandwidth occupancy
3) Attainable fix rate
4) Cost and complexity of user hardware.

The principal operational criteria are ranging accuracy and fix rate, which are linked by the noise bandwidth of the phase-locked loop used for phase measurement. The required loop bandwidth is in turn determined by the received power-to-noise density ratio, the loop center frequency, and the system dynamics. In the following analyses, ranging accuracy is normalized to the ranging signal bandwidth, which is assumed to be determined by the chip rate in binary codes and the upper tone frequency in sidetone signals, and found as a function of P_r/N_o, the signal power-to-noise density ratio at the receiver. The attainable fix rate is taken to be the reciprocal of the ranging phase-locked loop bandwidth.

The cost of the hardware required by the user in each of the candidate techniques is influenced by several factors. Signals must be received from approximately four satellites for each fix, and these signals must access the user's receiver according to some multiple-access discipline. Frequency-division, code-division, and time-

division multiple access methods are considered where applicable, and the implications of each method are determined in terms of number and complexity of the receivers required, bandwidth utilization, and fix rate.

2.2.2 BINARY CODES

2.2.2.1 Continuous PN

The basis of this waveform is a PN sequence which is transmitted continuously by each satellite. In FDM systems each satellite may use the same code, while in code division each satellite will use a different code. For what follows, we initially assume an FDM system.

The fine ranging measurement is made by measuring the phase of the receiver delay-lock loop clock relative to an on-board clock. Practical restrictions limit the accuracy of phase measurements to about 0.01 cycle, which must correspond to the best desired rms error, which is assumed to be about 50 ft. This indicates a minimum code chip rate of 400 kHz. The range ambiguity requirements dictate a code repetition rate not exceeding 100 Hz. The limits for both accuracy and ambiguity resolution are exceeded by the use of an 8191 bit code, for example, a maximal length sequence from a 13 stage shift register. Another well-known code of this length is the JPL code (see Reference 1), which is synthesized from three sequences of 7, 19, and 31 bits, respectively. Typical chip length and sequence repetition rates for an 8192 chip code are 500k chips/second and 61 Hz, respectively.

Continuous transmission of a PN code sequence provides sufficient information for the user to acquire the signal, synchronize with the code, and perform ranging measurements. Using the code parameters of the preceding paragraph, a representation of the code characteristics in time and frequency is shown in Figure 2-2. The spectrum shown is of the binary PN code itself. In practice, the baseband code will be filtered to remove the high frequency components, which will result in de-emphasis of the spectrum lobes above the first null.

The transmission of data in conjunction with the PN waveform can be handled in several ways. The binary data can be modulated directly onto the PN sequence by code phase reversal at the appropriate bit rate. The data, which is narrowband, can also be placed on a separate subcarrier located above the baseband spectrum of the PN signal. The low data rates involved in the satellite transmission make the data transmission a fairly uncritical item in the waveform design. Quantitative support for this statement is obtained from the link characteristics given in subsection 2.1.1, which shows a received signal-to-noise density ratio of 36 dB/Hz for each watt of satellite transmitted power. If 13 dB is assumed to be sufficient E/N_0 for a satisfactory error rate, then -21 dBW/bit/s must be transmitted by the satellite. For the present assumption of no more than 10 bits/s, only -11 dBW of satellite power need be used for data transmission.

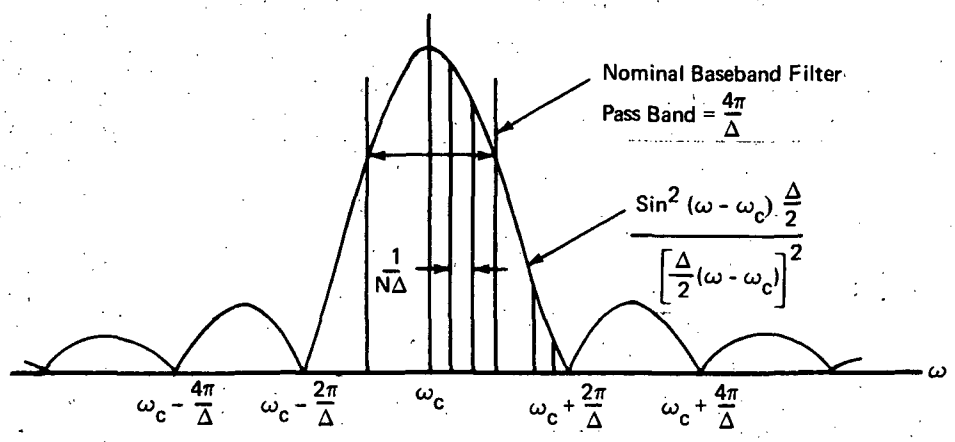

a. PN Code Frequency Spectrum

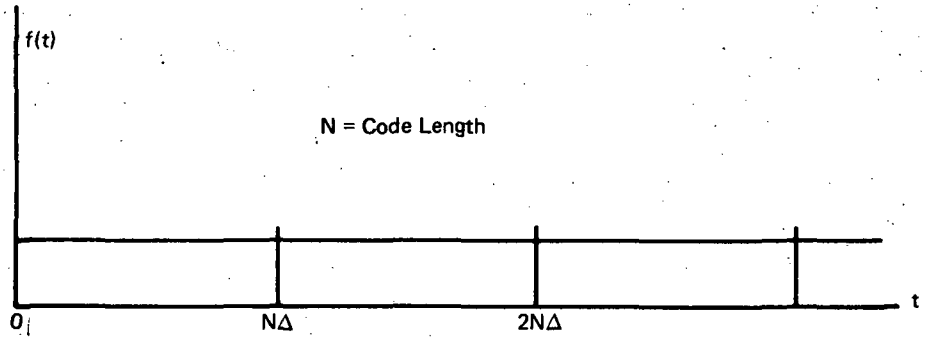

b. PN Code Time Profile

Figure 2-2. Code Characteristics in Time and Frequency

Although acquisition of the code signal is only done by each user upon take-off (or if synchronization is lost due to noise) it is noted that the use of a composite code such as the JPL code permits rapid acquisition, with each code component being acquired in turn. For example, an analysis given in Reference 1 gives an acquisition time of 1.0 second with a P_r/N_0 of 42 dB/Hz. This figure assumes a 99.9% required probability of acquisition.

2.2.2.1.1 Range Measurement

The range measurement is performed by measuring the phase of the clock generated in the receiver delay-lock loop, while coarse range is determined by the offset between the received code and the reference code generated by the loop. For FDMA (i.e., a separate frequency channel per satellite), we assume coherent demodulation of the PN sequence by a delay-lock loop such as that shown in Figure 2-3. The presence of several signals in the same channel precludes the use of coherent demodulation; thus, for CDMA, a noncoherent receiver is required such as shown in Figure 2-4.

CDMA performance is discussed in the next subsection. The ranging accuracy is determined by the mean-square phase jitter at the VCO output. In a coherent receiver, two factors contribute to this jitter: (1) the thermal noise at the input, assumed to be Gaussian and white across the IF bandwidth, and (2) the self-noise generated by the correlation process, which results from the fact that under locked conditions the input is time-displaced from both reference code generator outputs by one-half a chip length.

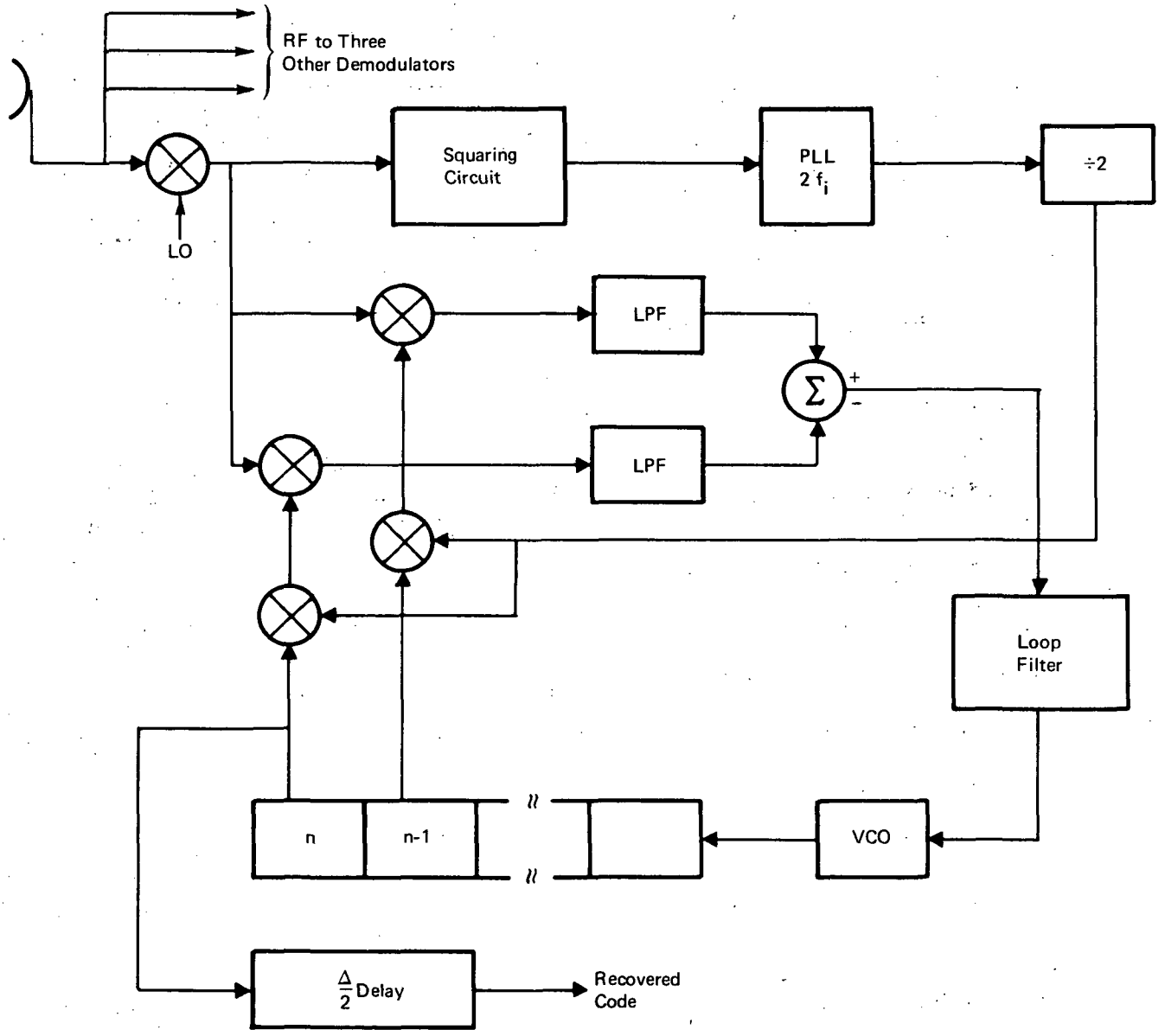

Figure 2-3. Coherent Delay-Lock Loop for FDMA Satellite Signals

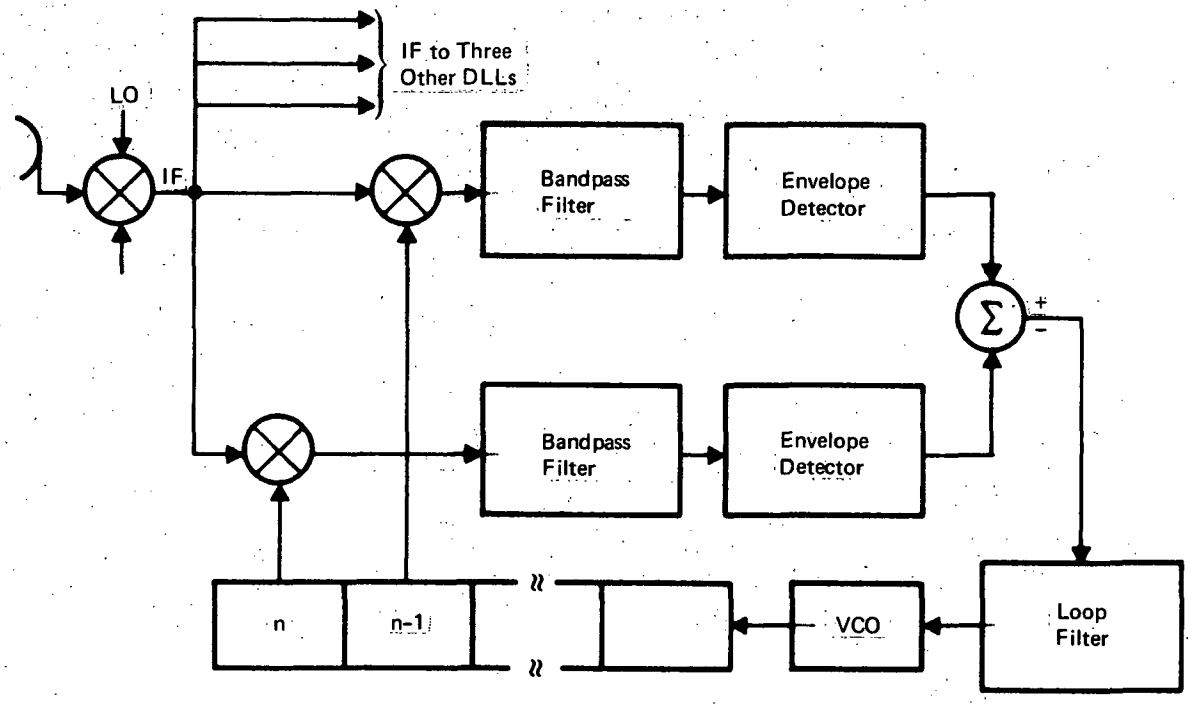

Figure 2-4. Envelope-Correlator Delay-Lock Loop for CDMA Satellite Signals

Gill (Reference 2) analyzed a delay-lock loop of the type shown in Figure 2-3, and derived an expression for the mean-square error resulting from the thermal noise. The error normalized to the chip length Δ (and hence to the RF bandwidth) is given by

$$\frac{\sigma_t}{\Delta} = \left[\frac{B_n N_o}{2P_r}\right]^{1/2} \tag{2-1}$$

where B_n = loop noise equivalent bandwidth

P_r/N_o = received signal-to-noise density ratio.

The normalized self-noise of the correlation process is given by (see Reference 3):

$$\frac{\sigma_n}{\Delta} = \left\{\frac{\Delta B_n}{4}\left[1 + 24\left(\frac{\epsilon}{\Delta}\right)^2\right]\right\}^{1/2} \tag{2-2}$$

where, ϵ is the delay-measurement error. Under in-lock conditions, $\epsilon \approx 0$, and the following term can be written:

$$\frac{\sigma_n}{\Delta} \approx \left(\frac{\Delta B_n}{4}\right)^{1/2} \tag{2-3}$$

Under in-lock conditions, it is reasonable to assume statistical independence between the self-noise and the other error contributions. Therefore, the total normalized error becomes

$$\frac{\sigma}{\Delta} = \left(\frac{\sigma_t^2}{\Delta^2} + \frac{\sigma_n^2}{\Delta^2} \right)^{1/2}$$

$$= \left[\frac{B_n N_o}{2P_r} + \frac{\Delta B_n}{4} \right]^{1/2} \qquad (2\text{-}4)$$

An effect which must be considered in evaluating error performance by means of Equation 2-4 is the delay-lock loop threshold. This arises from the shape of the loop discriminant curve shown in Figure 2-5, which shows the correlator output as a function of delay error. For errors lying in the interval $(-\Delta/2, \Delta/2)$ the discriminant is linear. Errors exceeding this range, however, cause the loop to lose lock. The chip length should be chosen such that the mean square error is less than about 0.3Δ (Gill, Reference 1). For a minimum range error of 50 ft, this condition is satisfied for $\Delta > 170 \times 10^{-9}$ seconds.

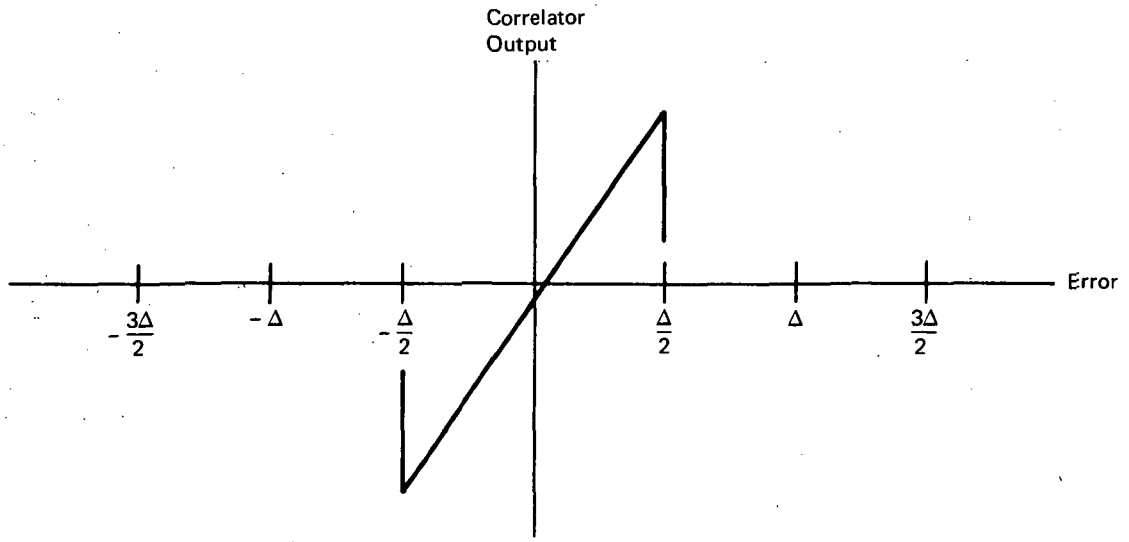

Figure 2-5. Delay-Lock Loop Discriminant

Equation 2-4 is plotted in Figure 2-6 for $\Delta = 10^{-6}$ seconds, and two values of loop noise bandwidth. The performance degradation at high signal-to-noise density ratios arises from the correlator self-noise. The threshold of the delay-locked loop is also shown at $\sigma = 0.3\Delta$.

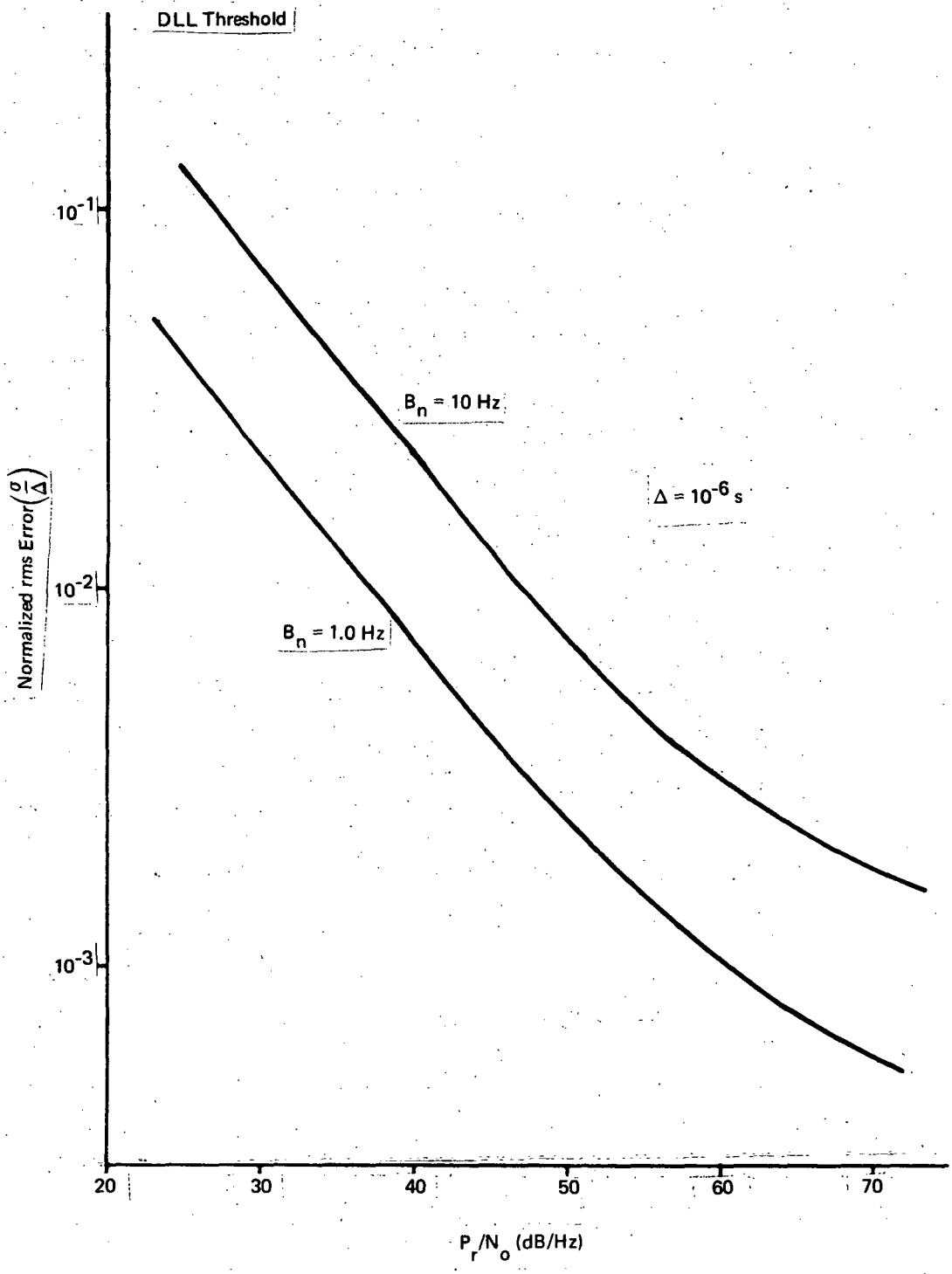

Figure 2-6. Ranging Accuracy PN-FDMA

2.2.2.1.2 Fix Rate

The fix rate which can be achieved is determined directly by the rate at which independent samples can be taken of the loop delay estimate. This depends upon the loop bandwidth, and is assumed to be its reciprocal. The curves of Figure 2-6, therefore, correspond to fix rates of 1 and 10 per second. In any practical application, a tradeoff must be performed between desired fix rate and error performance.

2.2.2.1.3 Multiple-access Techniques

As indicated above, the multiple satellite signals can access the user receiver either by frequency division or code division. The use of code division will affect performance by increasing the interference level. An essential tradeoff to be considered is between RF bandwidth and range error. A secondary tradeoff arises from consideration of user costs. Each frequency occupied by a separate signal implies additional receiver front-end complexity with its attendant cost in space, weight, and power. It should be noted that a separate delay-lock loop is required for each satellite signal regardless of the multiple-access technique used.

2.2.2.1.4 CDMA Performance Analysis

In the foregoing analysis of PN-FDMA ranging, a coherent receiver is assumed. In CDMA signaling, the presence of multiple carriers in the same frequency band makes coherent reception infeasible. The ranging PN signal must be recovered by means of square-law envelope-detector delay-lock loop such as shown in Figure 2-4. The normalized error performance of such a system for a single input signal is given by (Gill, Reference 2):

$$\frac{\sigma}{\Delta} = \left[\frac{B_n N_o}{2P_r} + \frac{B_1 B_n N_o^2}{P_r^2} + \frac{\Delta B_n}{4} \right]^{1/2}, \qquad (2\text{-}5)$$

where B_1 is the bandpass filter bandwidth, assumed to be 10 kHz to account for doppler uncertainty. This expression differs from that of Equation 2-4 in the addition of the middle term. This term arises from the action of the envelope detector, which has a signal suppression effect at low signal-to-noise ratios.

In analyzing the effect of code-division multiple-access upon error performance, one can proceed by assuming that the interfering signals are constant-amplitude sinusoids of random, uniformly distributed phase angles. The resultant interference will be assumed Gaussian and white across the RF bandwidth. Then, if the power in

each signal is equal to P_r at the receiver, and assuming three interfering signals, the effective noise power density becomes

$$N_{EFF} = N_o + \frac{3P_r}{B_{RF}} \tag{2-6}$$

The error performance for the code division system is then found by replacing N_o by N_{EFF} in Equation 2-5. If we let $B_{RF} = 1/\Delta$, the result is

$$\frac{\sigma}{\Delta} = \left[\frac{B_n}{2P_r}(N_o + 3P_r\Delta) + \frac{B_1 B_n}{P_r^2}(N_o + 3P_r\Delta)^2 + \frac{\Delta B_n}{4}\right]^{1/2} \tag{2-7}$$

Note, that for fewer than three interfering signals, the Gaussian assumption can no longer be made realistically, and the analysis involves a detailed investigation of the cross correlation properties of the codes. In general, no closed form analytical procedures are available, however, Gold (Reference 4) and others have completed significant work which allows reasonable performance estimates to be made on the basis of computer analysis. Equation 2-7 is plotted in Figure 2-7. The deterioration of performance from the FDMA case at high received signal power is shown by comparison with the dashed curves, which are identical to those in Figure 2-6. At low signal-to-noise ratios, a performance degradation is noted arising from the effect of the envelope detector.

2.2.2.1.5 Summary

The principal feature of PN ranging is the ability of several signals to share the same frequency band. In view of the scarcity of the spectrum resource and the inherently wideband nature of ranging signals, this is a significant asset.

Ranging performance in noisy environments is dependent upon the presence in the signal of high-frequency "fine structure" while the resolution of ambiguities requires the inclusion of low-frequency components. These two requirements place a lower bound on the code chip rate and a lower bound on the code sequence length. Short codes which have lengths close to the lower bound are generally easier to generate and to acquire. Longer codes may be desirable in some applications where privacy is a factor and the longer acquisition time can be tolerated. Composite or separate codes could be used in a system which accommodates both military and civilian users with the same satellites.

For a given satellite transmitted power, the ranging accuracy and fix-rate achieved are determined essentially by the delay-lock receiver bandwidth. This, in turn, is determined primarily by the Doppler rate that is expected to be encountered. Reasonable aircraft performance assumptions lead to practical loop bandwidths of 1 to 10 Hz.

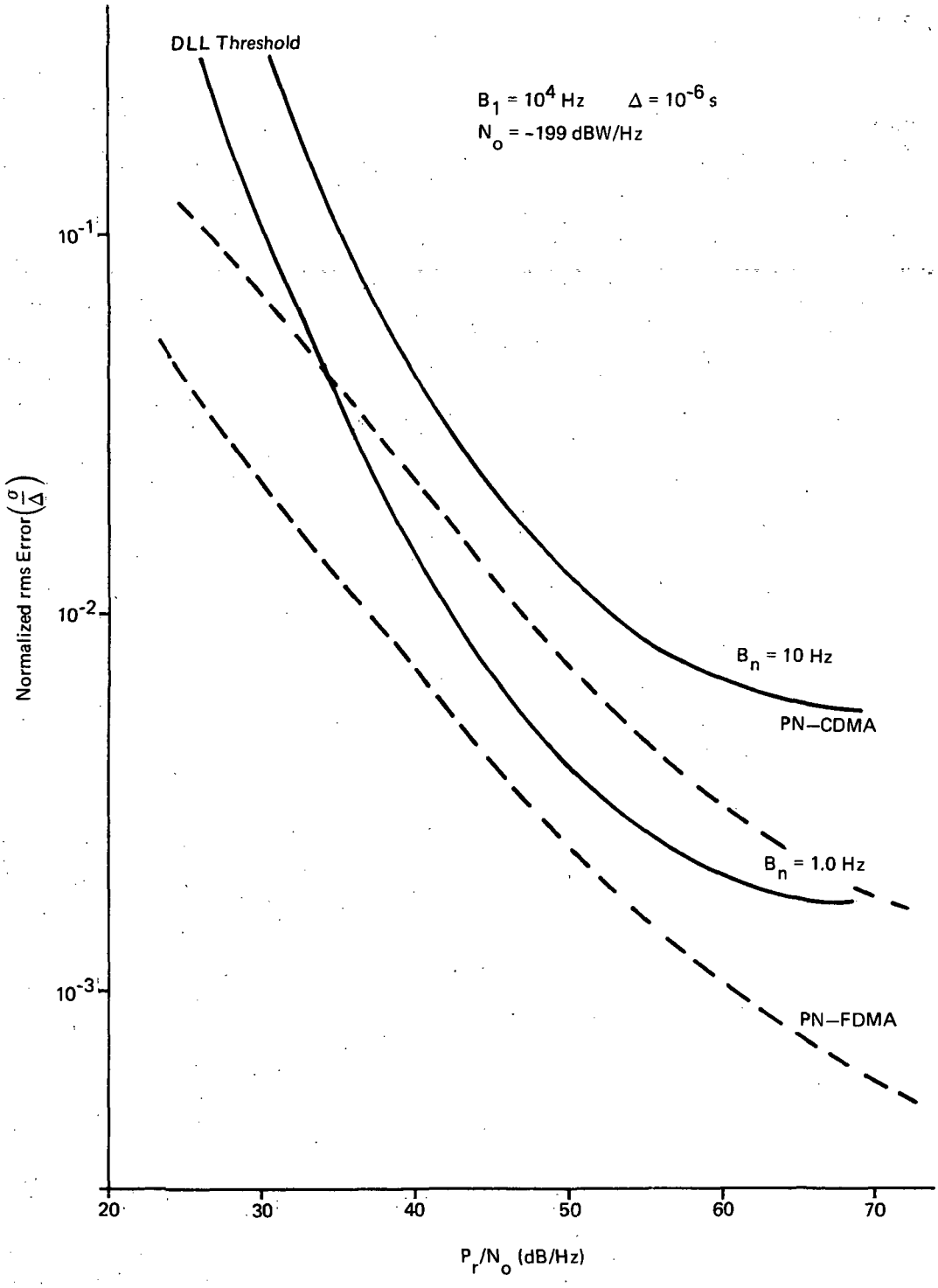

Figure 2-7. Ranging Accuracy PN-CDMA and PN-FDMA

2.2.2.2 BINOR Code

In order to reduce the acquisition time required for long binary PN codes, Stiffler (Reference 5) has developed a code referred to as the binary optimum ranging (BINOR) code, which is distinguished by the characteristic that the acquisition time required in the receiver requires on the order of $\log_2 N$ trials for a code of length N, whereas a PN receiver normally can require up to N trials. The code is synthesized by majority logic from a set of $\log_2 N$ square waves of harmonically related frequencies. Acquisition is accomplished by noting the polarity of each of $\log_2 N$ successive partial correlations with the component square waves. The spectrum and time profiles of the BINOR code are essentially equivalent to those of PN-FDMA as fiven in Figure 2-2. A typical receiver structure is shown in Figure 2-8.

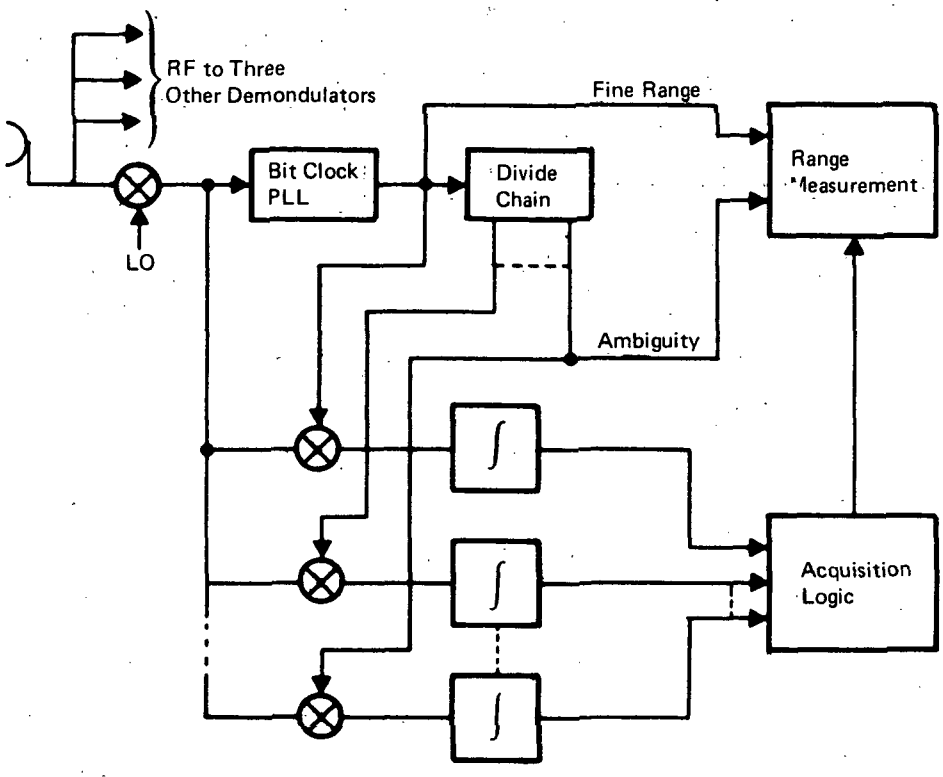

Figure 2-8. Binary Code Receiver

The transmission of binary data using the BINOR waveform cannot be done by code phase reversal because of the acquisition procedure, which is sensitive to code polarity. Data transmission must be by separate carrier adjacent to same frequency band. The same calculations of power required for data transmission as were made for PN also hold in this case.

2.2.2.2.1 Phase Measurement

Once the code has been acquired by the user, the phase measurement is made on the lowest frequency square wave, which is derived from the recovered bit clock by a divider chain. The phase jitter on the low-frequency square wave is thus equal to the bit clock recovery phaselocked loop. The normalized mean square delay error resulting from this jitter is given by the expression

$$\frac{\sigma_t}{\Delta} = \frac{1}{\pi}\left[\frac{B_n N_o}{2P_r \rho^2}\right]^{1/2} \tag{2-8}$$

where B_n is the equivalent noise bandwidth of the bit-clock phase-locked loop, and ρ is the correlation coefficient between the clock and the received signal, which is given by

$$\rho = \sqrt{\frac{2}{(\log_2 N)\,\pi}} \tag{2-9}$$

Since, from Equation 2-9, the correlation coefficient is dependent upon $\log_2 N$, the ranging accuracy is a function of the code length N. Hence, a lower bound on accuracy is imposed by the ambiguity resolution. Assuming, for equivalence with the PN code, a chip length of 1 μs and a code length of 8192 chips; then 13 square waves are required for code synthesis. Equation 2-8 is plotted in Figure 2-9 for $\log_2 N = 13$ and typical values of loop noise bandwidth.

2.2.2.2.2 Fix Rate

As in the case of PN ranging, the attainable fix rate is dependent upon the recovery loop bandwidth.

2.2.2.2.3 Multiple-access Methods

Due to the uniqueness of the BINOR code, code-division multiple-access cannot be used. Frequency separation of the signals is the only viable method. Separate code receivers are required for each satellite, and sufficient bandwidth for four simultaneous transmissions must be available.

2.2.2.2.4 Summary

The BINOR code differs from PN codes primarily in its regular structure which permits rapid acquisition. The regular structure, however, also implies a loss of

the desirable autocorrelation characteristics which permit the use of a delay-locked loop receiver for PN codes. Although a DLL could be used to receive the BINOR code, its performance is not easy to predict. The foregoing analysis assumes that a phase-locked loop, locked to the bit clock, is the principal instrument of phase measurement. This implementation causes the performance to be dependent upon code length, and results in a loss of about 2 dB in power requirement over a PN-FDMA code with equivalent parameters.

Besides rapid acquisition (about 0.2 s for the code described above), the BINOR code has the advantage in that the synchronizing and recovery circuitry, being primarily digital, is relatively inexpensive. This claim (Reference 1) has not been investigated in detail.

It is concluded that for the accuracy and ambiguity requirements of the present problem the BINOR code achieves ranging accuracy only slightly inferior to that of PN-FDMA. The acquisition performance of BINOR is superior to PN, being about 0.2s at $P_r/N_o = 42$ dB/Hz.

2.2.3 SIDETONES

In a sidetone ranging scheme, a set of sinusoidal tones is transmitted. The frequency of the highest frequency tone is determined by the range accuracy required, assuming the same limitation on phase measurement resolution as in the case of binary codes. The lowest frequency is set by the ambiguity resolution required. The intermediate tones are used to resolve the ambiguity in each successively higher tone. The problem of optimum tone frequency selection has been discussed by several investigators, e.g., Reference 1 and Reference 6. A typical sidetone spectrum is shown in Figure 2-10.

2.2.3.1 Phase Measurement

The mean-square error in the time delay measurement made with a tone ranging system is determined by the upper tone frequency, f_m, the number of tones, and the received signal-to-noise ratio, and is given by

$$\sigma_t = \frac{1}{2\pi f_m \sqrt{\frac{2P_r}{nB_n N_o}}} \tag{2-10}$$

where n is the number of tones. The assumption that each tone contains 1/n of the total power is implicit. Normalized to the half-period of the upper tone, T_m, this is

$$\frac{\sigma_t}{T_m} = \frac{1}{\pi \sqrt{\frac{2P_r}{nB_n N_o}}} \tag{2-11}$$

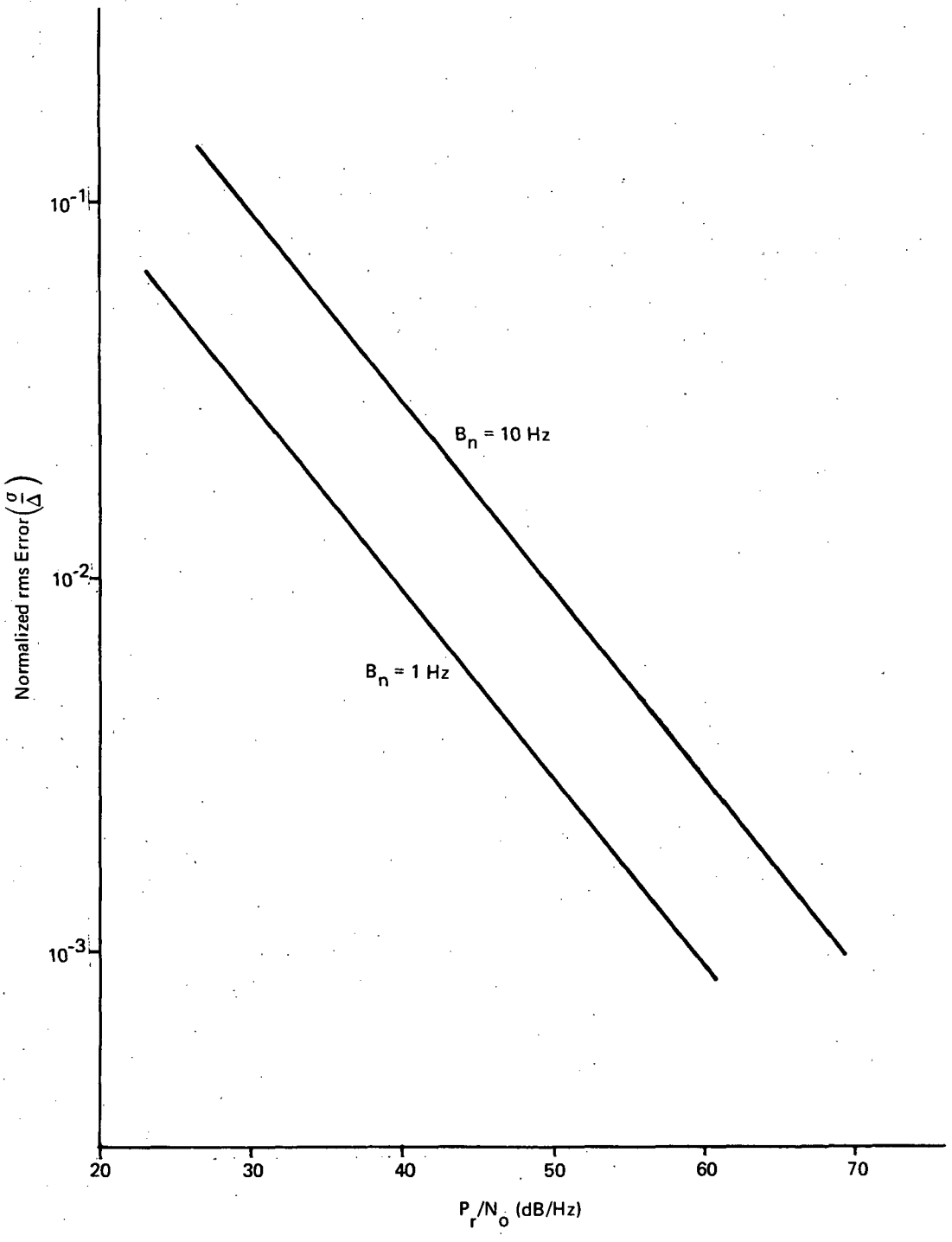

Figure 2-9. Ranging Accuracy, BINOR Code

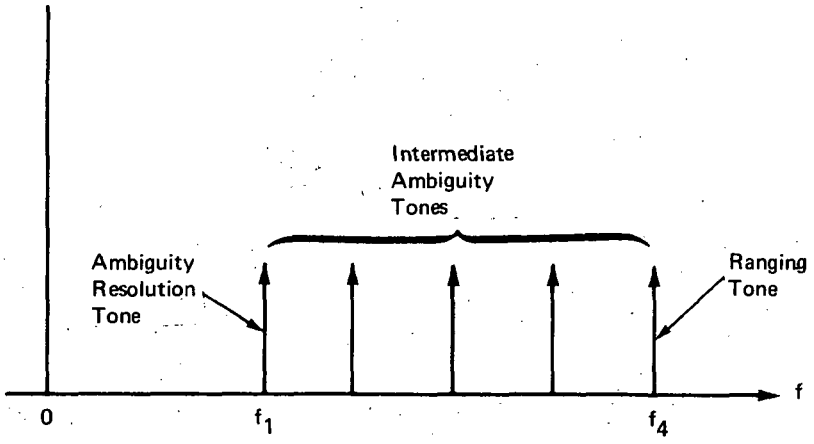

Figure 2-10. Typical Sidetone Spectrum

This normalization permits a comparison with the corresponding normalized error for the binary code given by Equations 2-4 and 2-7. Equation 2-11 is plotted in Figure 2-11 for n=5. If we assume a parallel between binary code clock rate and fine ranging tone frequency, then we can conclude (in a general sense) that performance is equivalent per unit bandwidth to a digital code for a tone system using 10 tones. For fewer tones, the performance is relatively better.

2.2.3.2 Data Transmission and Spectrum Compaction

Unlike the spectra of the binary codes, which contain discrete components every 1/N Hz where N is the ambiguity resolution period, the spectrum of a sidetone waveform consists of a small number of components and a large amount of unused spectral capacity. The availability of the unused capacity can be increased by frequency-translating the component tones to more closely-spaced spectrum positions. A systematic way of doing this is, for a sequence of tones f_1, f_2, ..., f_n transmitting the tones $f_n - f_{n-1}$, $f_n - f_{n-2}$, ..., $f_n - f_i$, f_n.

For example, if a sequence 0.4 kHz, 2 kHz, and 10 kHz is required, the transmitted set would be 10 kHz, 9.6 kHz, and 8 kHz. Provided that $f_n - f_{n-1} < f_1$, this procedure results in a compaction of the overall spectrum. The required tones are synthesized in the receiver from the received set.

The reduction in accuracy that results from spectrum compaction is found as follows. In the receiver, the tone f_i is found as the difference of the two received tones $f_n - f_i$ and f_n. If the phase error variance in the recovery of each of these tones is equal to σ_ϕ^2, and the two errors are assumed independent, then the rms phase error is equal to $\sqrt{2}\ \sigma_\phi^2$. The rms ranging power utilization is therefore reduced by 3 dB.

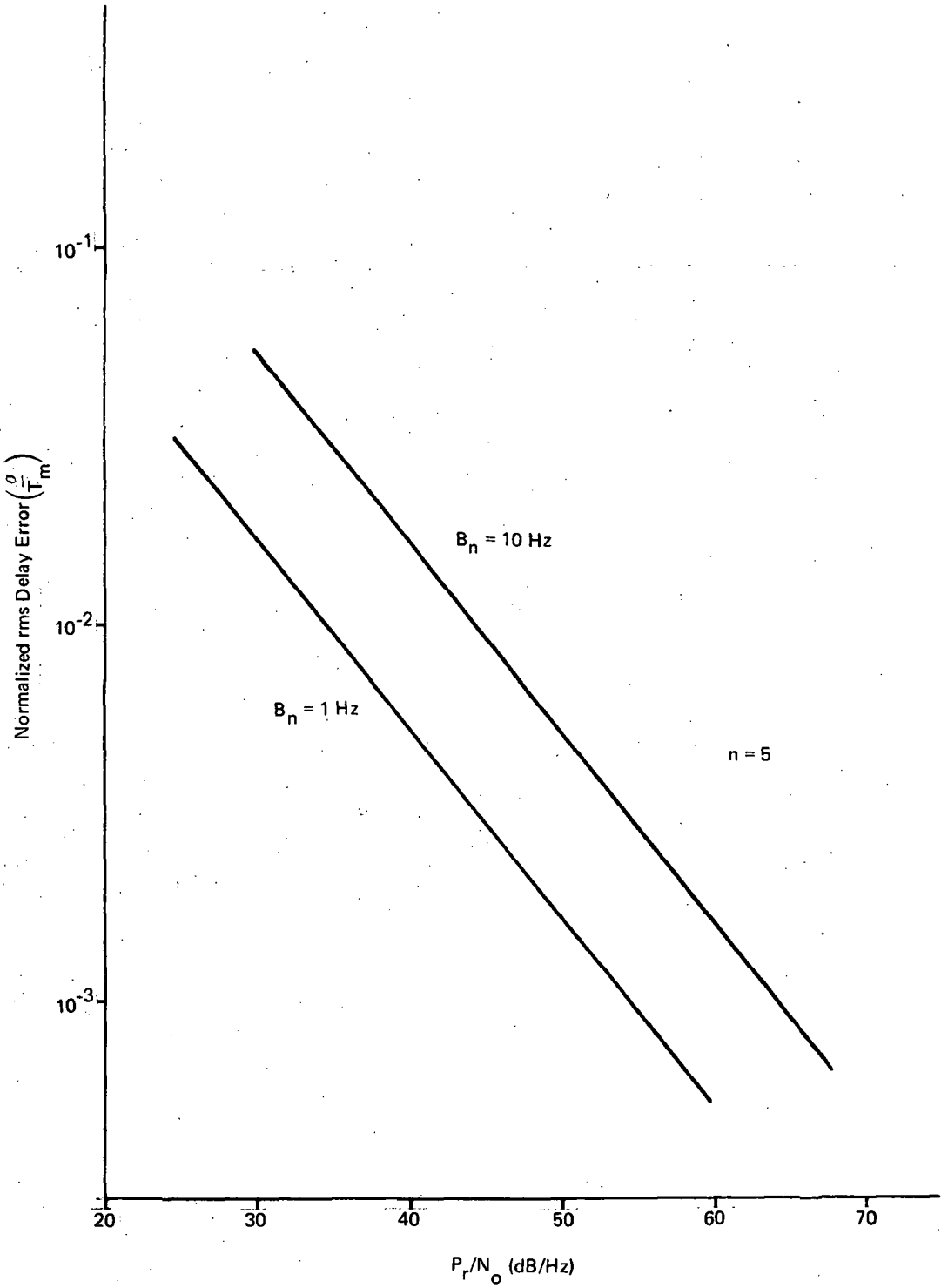

Figure 2-11. Ranging Accuracy Sidetones

Data transmission in conjunction with the sidetone waveform must be placed on a separate carrier and positioned in the spectrum between the tones and the main carrier. The reduction of power available for ranging due to the transmission of data is -24 dBW/bit/s, as computed in the preceding subsection. The 10 bits/s assumed for this system requires negligible power.

2.2.3.3 Fix Rate and Multiple-Access

Sidetone ranging fix rate is determined solely by the receiver PLL bandwidth for the high frequency tone. Frequency-division multiple-access is required.

2.2.3.4 Summary

The ranging accuracy of a sidetone ranging waveform is primarily determined by the amount of power in the highest frequency tone. Thus, proliferation of tones reduces performance. In this respect, sidetone ranging is similar to BINOR code ranging which loses accuracy with an increase in the number of synthesizing square waves. A sidetone waveform, however, does not require a component tone at every harmonic of the ambiguity resolution frequency as does the BINOR code; thus, it is inherently more flexible and efficient. Its performance is also an improvement on PN ranging.

Reception and demodulation of a sidetone waveform involves a set of PLLs, one locked to each tone frequency. This set follows a coherent demodulator and carrier PLL.

Sidetone ranging achieves a somewhat better utilization of ranging power than digital codes for the problem parameters under consideration.

2.2.4 PULSE RANGING TECHNIQUES

Pulse ranging systems differ from the CW methods discussed in the preceding subsections in several important respects. Ranging accuracy is determined by the resolution of the time-of-arrival of a narrow pulse. Pulse receivers inherently operate in an incoherent mode, using matched filter detection rather than serial correlators or phase-locked loops. Thus, signal acquisition is not a factor in pulse ranging, the low duty cycle of the pulse signals makes time-division multiple-access a natual operating mode, and peak power devices are appropriate.

The principal constraining factor in the generation of pulse ranging signals onboard a satellite is the limitation on the peak power that can be generated by satellite transmitting equipment. The present state-of-the-art in high-power devices for spaceborne applications is about 500 W (with some laboratory bulk effect devices producing an order of magnitude more peak power) at L-band using a Gunn effect negative-resistance oscillator. The device efficiency under these conditions is about 30%.

In order to mitigate the peak power problems, proposals for satellite-generated pulse waveforms generally assume the use of pulse compression techniques to obtain short, high-energy detected pulses by filtering the longer duration, lower power pulses which are actually transmitted by the satellite. Well-known methods for implementing pulse compression signaling are by the use of short PN codes and by the use of linear frequency modulation. The following analysis is general, and applies to both techniques. For comparison, an uncompressed pulse ranging approach is also analyzed. Figure 2-12 shows a PN pulse spectrum and profile.

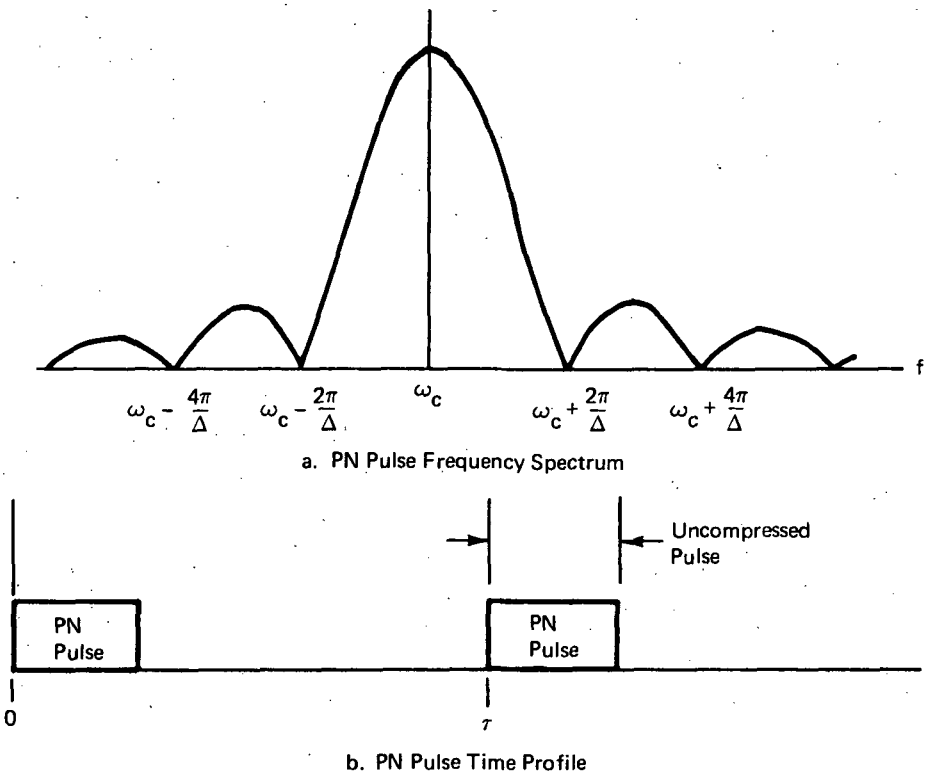

a. PN Pulse Frequency Spectrum

b. PN Pulse Time Profile

Figure 2-12. PN Pulse Spectrum and Profile

The functions to be performed by the pulse ranging waveform are identical to those performed by the CW waveforms — range measurements, ambiguity resolution, and data transmission. The range accuracy achieved is directly related to the compressed pulse bandwidth and received pulse energy to noise ratio as discussed below. Ambiguity resolution is determined by pulse repetition rate, which must therefore be less than 100 Hz (for 10^7 ft maximum range difference). Data transmission can be accomplished in a number of ways. Optimum error rates can be achieved by using antipodal binary codes with dual matched-filter reception.

2.2.4.1 Range Measurement

Assume the rise time of the compressed pulse at the output of the matched filter is τ_b. If the time-of-arrival is measured at the leading and trailing pulse edges and the two readings are used to obtain an average measurement, then (Reference 6) the delay error is given by

$$\sigma_t = \left(\frac{2\tau_b}{4B\ E/N_o} \right)^{1/2} \tag{2-12}$$

where E is the pulse energy, and B is the IF bandwidth. If $B = 1/\tau_b$, then

$$\sigma_t = \frac{1}{2B\sqrt{\frac{E}{N_o}}} \tag{2-13}$$

This can be related to peak P_r/N_o by noting that

$$\frac{E}{N_o} = \frac{P_r T}{N_o} \tag{2-14}$$

where T is the duration of the uncompressed pulse. In pulse ranging, different fix rates are obtained by averaging the range measurement over different numbers of received pulses. For averaging over n pulses, assuming independence, the error variance is reduced by 1/n. Then Equation 2-13 is

$$\sigma_t = \frac{\tau_b}{2\sqrt{\frac{nP_r T}{N_o}}} \tag{2-15}$$

Equation 2-15 is plotted in Figure 2-13 for $T = \tau_b = 1.0\ \mu s$, that is, no pulse compression effect. It is observed, for example, that for $\sigma = 10^{-1}\mu s$ (100 ft ranging error), and n = 1, the required peak P_r/N_o is 74 dB/Hz. The assumed link provides 34 dB/Hz/W of satellite power; hence, 40 dBW, or 10 kW of peak power must be transmitted by the satellite.

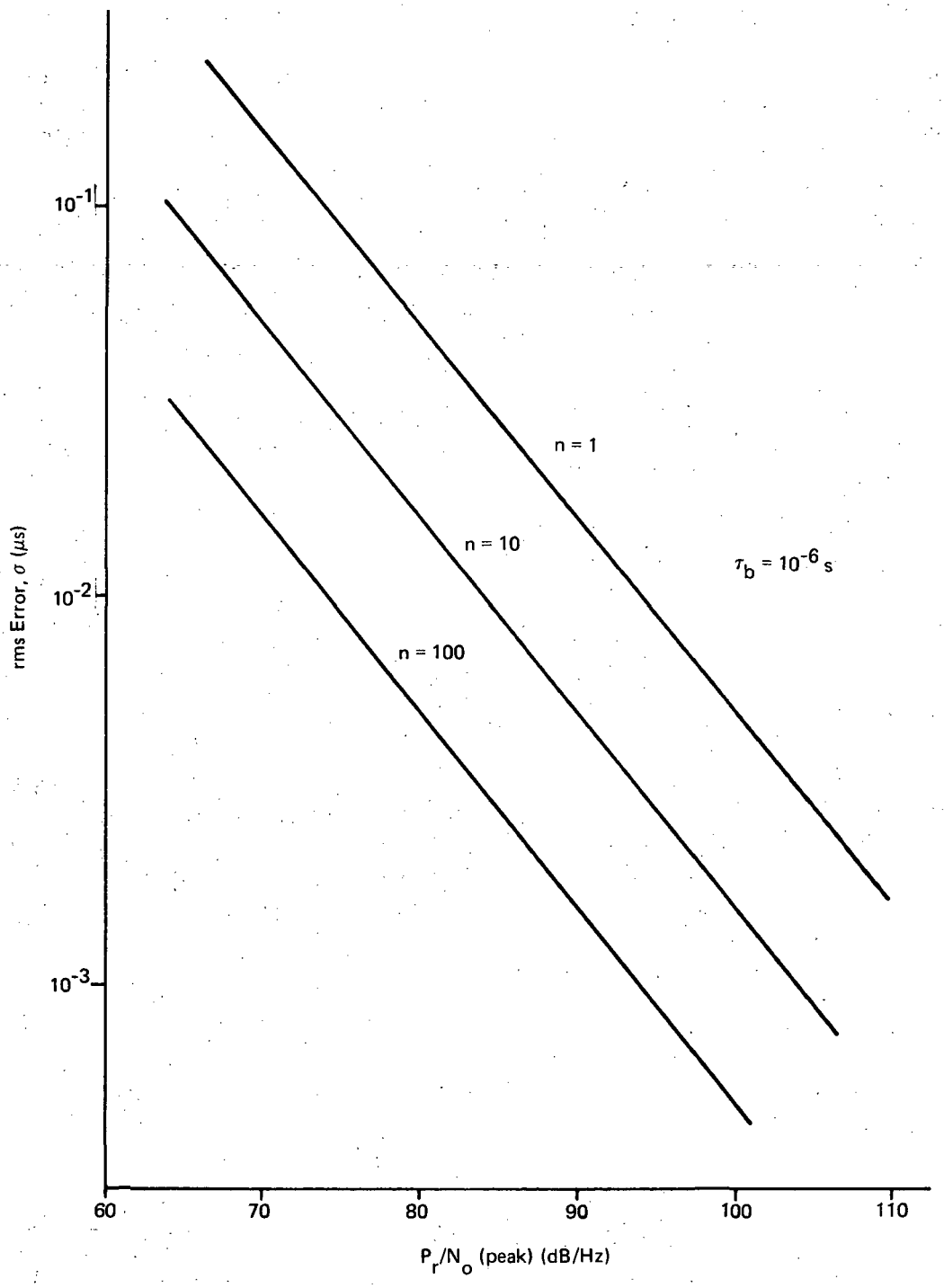

Figure 2-13. Ranging Accuracy Pulse

In Figure 2-14 an uncompressed pulse length of 10^{-4} seconds and 100 pulses per second are assumed. The normalized range error, σ/τ_b, is shown as a function of both peak and average transmitter power. The compression provides 20 dB reduction in required peak power; thus, the same performance as in the above example can be achieved with 100 W peak assuming as before a 1.0 μs compressed pulse length.

The use of pulse compression provides the ability to differentiate (by signal or code design) between signals from different satellites, perhaps eliminating the need for staggering transmission between satellites.

2.2.4.2 Data Transmission

The transmission of satellite data is conceptually straightforward for pulse signals. Two signal codes are used with dual matched-filter reception. In the case of chirp signals, the binary signaling states can be represented by an increasing or decreasing chirp frequency, while binary codes can be modulated by binary phase reversal. The ranging signals and data transmission signals are the same.

In the matched-filter reception of pulse signals, attention must be paid to both the probability of a missed pulse and to the probability of a false alarm. False alarm rates can be kept very low by using predictive pulse gating based upon a priori knowledge of the pulse repetition frequency.

2.2.4.3 Multiple-access Techniques

The low duty cycle of the pulse signal from each satellite makes time division the most attractive and bandwidth-efficient multiple-access scheme. The user equipment consists of a single pulse receiver with the necessary timing and data decoding circuitry.

2.2.4.4 Summary

Other than PN-CDMA, pulse ranging is the only system that permits operation in a single frequency channel. On an average power basis, it achieves ranging accuracy comparable to that of a sidetone waveform (see Figure 2-10). The inherently TDMA nature of pulse transmission leads to somewhat simpler user equipment since receiver duplication for multiple signals is not required.

The principal drawback to pulse ranging is the requirement for the generation of relatively high peak powers on board the satellite. Present approaches to the design of spacecraft transmitters emphasize the use of constant power output devices, such as TWTs. As mentioned previously, devices presently under development will meet the power requirements for pulse systems using compression ratios of at least 100:1, but the peak power requirements for uncompressed pulses currently are beyond the state-of-the-art.

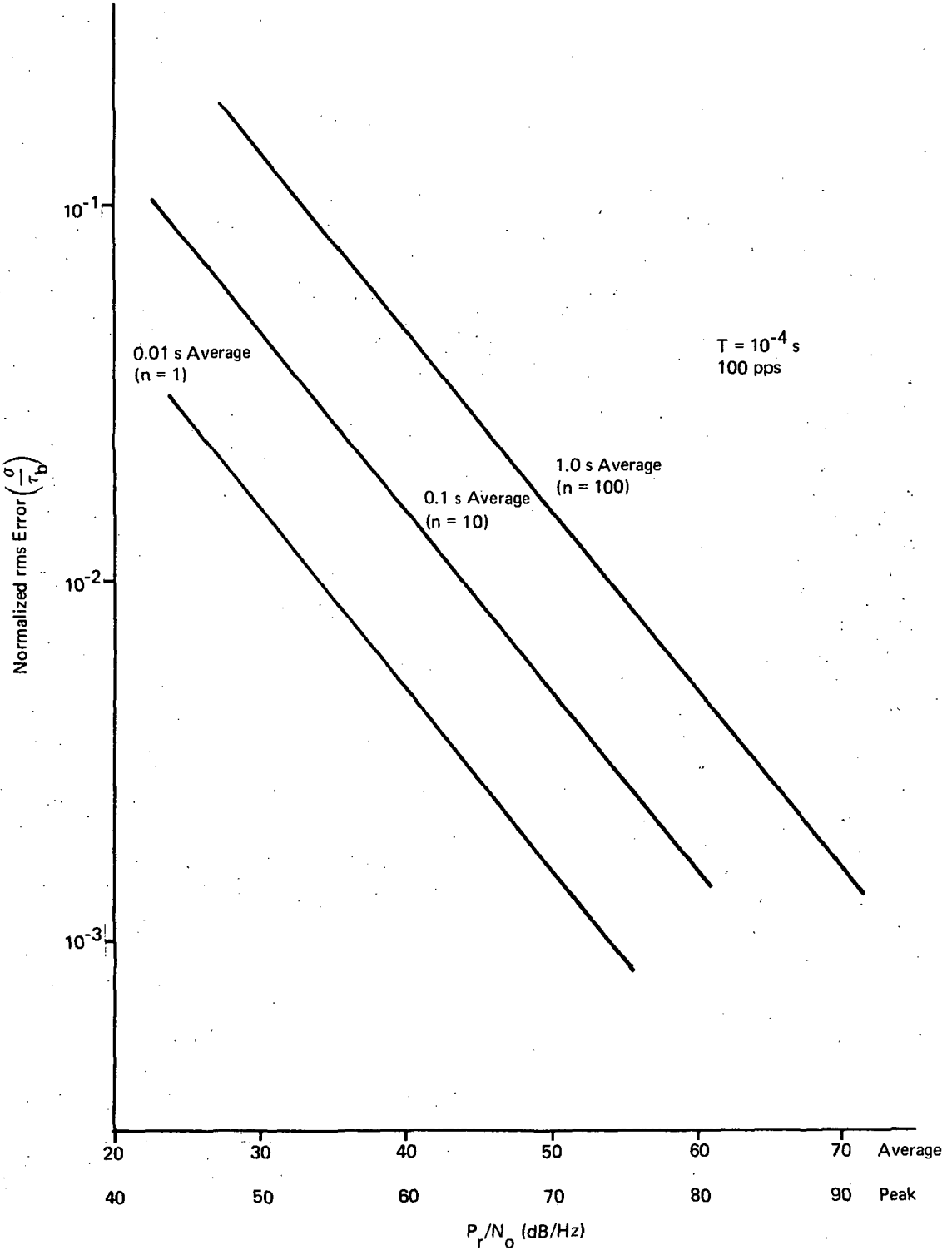

Figure 2-14. Ranging Accuracy Pulse Compression

2.2.5 MULTIPATH PERFORMANCE

This subsection briefly discusses the problem of multipath reception and its effects upon the ranging waveforms.

The reception by an aircraft of a satellite signal is susceptible to interference from the signal reflected upward from the ground plane. The severity of the interference is determined primarily by the strength of the spurious signal, its dispersion in time and in frequency, and the difference in propagation time over the two paths.

The strength of the reflected signal, its time and frequency dispersion are in turn dependent upon the nature of the reflecting surface as described by its reflectivity coefficient and its average roughness, and upon the wave incident angle. The reflectivity coefficient, which is a function of incident angle, determines spurious signal strength, while the surface roughness determines the dispersion of the reflected signal in time and frequency. To a first-order-of-approximation the reflectivity coefficient is dependent only upon the incident angle and the dielectric constant of the surface. The total reflected power is independent of roughness. Experimental measurements of reflectivity coefficients (Reference 8) for asphalt and short grass at L-band give results which for low elevation angles (10^{o} to 40^{o}) are generally less than -10 dB. At higher angles the aircraft antenna, being hemispherical in coverage pattern, can be expected to provide additional discrimination against reflected signals. The prediction of quantitative performance of any given configuration of aircraft antenna, wave polarization, satellite elevation angle, and surface material can generally be done only by computer simulation or experimental measurements.

The effects of surface roughness appear as a dispersion in the frequency of the reflected wave which, at L-band, is generally negligible, and a random dispersion in the path length traveled by the reflected wave which appears as a random time dispersion in the interfering signal. At L-band, and assuming a surface roughness which is just sufficient to differentiate it from a smooth surface ("critical roughness") this time dispersion is on the order of 5 μs, which cannot be considered negligible with respect to the baseband signals under consideration. In evaluating the ranging waveforms for a particular system application the effects of the time dispersion of the multipath signal must be investigated by simulation and experiment. Note that time dispersion due to roughness is of the same order of magnitude as the time delay due to path length difference.

Since the analytical prediction of multipath performance as a function of waveform design, on a quantitative basis, is relatively intractable, all that can be done is to evaluate the waveform candidates against certain qualitative design principles which lead to good multipath rejection.

Ranging measurements are based upon the cross-correlation of the received waveform with a stored replica, and it is intuitively evident that waveforms having autocorrelation functions (approximately an impulse function) are the most desirable. Blasbalg

(Reference 8) has demonstrated this result rigorously by showing that optimum multipath rejection is achieved by signals having the flat spectrum of white noise. According to this principle, multipath performance is improved by narrowing the central peak of the autocorrelation function and reducing the sidelobes. Reducing the width of the peak is achieved by raising the clock rate for binary signals, reducing the compressed pulse width for pulse coding, and raising the upper tone frequency for tone ranging signals. As a rough rule, the width of the correlation peak should be small compared to the path length differential delay. The reduction of sidelobes in the correlation function implies the removal of periodic components in the baseband spectrum (i. e. flattening the spectrum). Both of these criteria argue in favor of the use of noiselike (PN) signals and against the use of signals with strong specular components such as sidetones and the BINOR code.

Multipath performance in a satellite system is strongly dependent upon the elevation angle of the satellite. At low elevations the differential delay becomes small while the reflectivity coefficient increases. Thus the spurious signal strength increases under conditions in which the increase of signal bandwidth is least effective. This double deterioration may argue in favor of a multisatellite constellation in which at least four satellites will always be at sufficiently high elevations that the multipath is acceptable.

2.2.6 VELOCITY MEASUREMENT

Signaling waveforms which permit coherent carrier recovery can be used for direct measurements of the radial velocity of the user relative to the satellite. Radial velocity measurements from three satellites permit the calculation of user velocity in x, y, and z. The measurement is implemented by determining the frequency of the carrier received from the satellite and calculating radial velocity from the equation

$$v_r = f_d \lambda \tag{2-16}$$

where f_d is the Doppler frequency. Knowledge of the frequency transmitted is assumed, and λ is the wavelength of the transmitted frequency. The mean-square velocity error resulting from thermal noise at the receiver input is given by

$$\sigma_{v_r}^2 = \frac{\lambda^2 \sigma_p^2 B_1^2}{(2\pi)^2} \tag{2-17}$$

where σ_p^2 is the phase-error variance at the output of the carrier recovery phase-locked loop and B_L is the loop bandwidth. The phase-error variance is given by

$$\sigma_p^2 = \frac{N_o B_1}{2P_r} \tag{2-18}$$

where P_r is the carrier power. Substituting (2-18) in (2-17) gives the result

$$\sigma_{v_r}^2 = \frac{\lambda^2 B_1 N_o}{8\pi^2 P_r} \tag{2-19}$$

Under the assumptions that $\lambda = 0.65$ ft , $P_r/N_o = 40$ dB/Hz, and the desired rms velocity error is 1 ft/s, the required loop bandwidth is

$$B_1 = \frac{8\pi^2 P_r \sigma_{v_r}^2}{\lambda^2 N_o}^{1/3}$$

$$= \frac{8\pi^2}{0.422} \times 10^4 ^{1/3}$$

$$= 123 \text{ Hz}$$

It is noted that only those waveforms with a continuous carrier; i. e. PN-FDMA, PN-CDMA, BINOR, and sidetones; can be used for velocity measurement.

2.2.7 SEPARATION OF FUNCTIONS

In the foregoing analyses of candidate ranging waveforms, we implicitly assumed that the satellite transmission consists of the repetitive transmission of a single ranging waveform containing no periodicity of a longer period than that required for ambiguity resolution. Carrier synchronization, code (or frequency) acquisition, and range measurements are all carried out on the same waveform. Improved performance can, however, be obtained if the functions of ranging and ambiguity resolution are carried out on different waveforms at different times.

The fundamental expression for delay resolution, from which the expressions for ranging accuracy in the preceding subsections are directly or indirectly derived, is

$$\sigma_t = \frac{1}{(2\pi\beta)\sqrt{\frac{2S}{N}}} \tag{2-20}$$

where β is the effective signal bandwidth defined by

$$\beta = \frac{\int_{-\infty}^{\infty} \omega^2 \left| F(\omega) \right|^2 d\omega}{\int_{-\infty}^{\infty} \left| F(\omega) \right|^2 d\omega} \qquad (2\text{-}21)$$

where $F(\omega)$ is the Fourier transform of the signal. A single sinusoid at frequency ω has, from Equation (2-21), an effective bandwidth ω. In ranging measurements, therefore, the optimum use of a baseband channel of width ω_c is obtained by transmitting a single sinusoid of frequency ω_c at full power. This is equivalent to a sidetone ranging waveform containing only a single tone. The lower frequency components, which are included in all the waveforms considered here, are required only for ambiguity resolution; their effect on ranging accuracy is to reduce it by reducing the effective bandwidth of the signal.

This point was recognized in the design of the TRW NAVSAT navigation waveform (Reference 1). This waveform is based upon the use of the BINOR code for acquisition and ambiguity resolution while range measurements are performed during periodic transmission of a bit-clock signal at full power. The ranging accuracy performance, thus obtained, is that of a sidetone system consisting of a single tone (n = 1 in Figure 2-11). It is clear, however, that both PN-FDMA codes and sidetone ranging waveforms are susceptible to the same approach. When viewed in this way, it is seen that the essential differences in the waveforms consist of differences in the method used for ambiguity resolution.

With functions thus separated, each waveform consists of a sequence of code (or multitone signal) of sufficient length to permit both initial acquisition and resynchronization of the ambiguity-resolving loops (DLL for PN codes, and PLL for sidetones). This segment is followed by a segment of pure bit clock (or high-frequency tone) during which the precision range measurements are made. With this waveform structure, the approaches yield equal performance in both ranging and ambiguity resolution. Comparative decisions between them must be made on the basis of considerations other than these — primarily the cost and complexity of user equipment. We note that neither PN-CDMA nor pulse waveforms are viable candidates for separation of functions; hence, since all other candidates occupy the same bandwidth, bandwidth is not a factor in the comparison.

In discussing the separation in functions in time we note that the data transmission function can also be separated in time from ranging and ambiguity determination, and transmitted during a short time segment when full carrier power can be devoted to it. In this way a much higher data rate can be supported than in the case with continuous transmission at low power, and data can be sent with a low duty cycle. This approach may simplify the receiver compared to the user of a separate carrier.

2.2.8 DISCUSSION AND CONCLUSIONS

In this subsection, the normalized delay error curves are used as the basis for comparison of performance from an operational point of view. For convenience, these curves are reproduced in Figure 2-15. In addition to the performance curves for the five waveforms considered in detail, two additional curves are shown. One of these shows the ranging accuracy that is achieved by separating the waveform functions as discussed in the preceding subsection. It is equivalent to the performance that would be obtained by a single sinusoid at the highest baseband frequency. The second additional curve gives the performance of a pulse ranging system operating with no compression and with no averaging over groups of pulses. Although this curve is plotted with the same normalized ordinate as the other curves, it holds only for a pulse length of 10^{-6} second. Separate labeling of the abscissa shows the peak power that must be transmitted from the satellite for each of the pulse waveforms. The average power abscissa holds for all the curves.

It is seen that sidetones, PN-FDMA, and BINOR waveforms achieve roughly equivalent performance, with the differences between them arising from differences in effective bandwidth. Of the three, sidetones are the most efficient in the utilization of ranging power. This is an intuitively satisfying conclusion, since in a sidetone system power is allotted only at those specific points in the spectrum where it is required, whereas in the binary code waveforms power is diffused over the entire baseband. Although this feature contributes to the ranging efficiency of sidetone waveforms, it is, as discussed below, an disadvantage in other respects.

The performance of the 100:1 pulse compression waveform is essentially equal to that of the five-tone sidetone waveform for equal average power. A 3-dB factor in its performance arises from the assumption that two delay measurements are made on each pulse. If only one measurement is made then the pulse performance curve becomes equal to that of PN-FDMA.

PN-CDMA suffers in performance both at high and low values of transmitted power relative to the FDMA and TDMA waveforms. The deterioration in performance of this approach must be traded against the reduction in required RF bandwidth.

The curves of Figure 2-15 can be viewed from several different perspectives. For example, if the rms error is fixed at the same value for each waveform the curves become those of required RF bandwidth (per satellite for FDMA and TDMA, and total for CDMA) as a function of transmitted power. Similarly, for a fixed bandwidth, the curves show rms error performance as a function of transmitted power.

To determine the overall bandwidth efficiency of each waveform the total bandwidth required by the particular multiple-access scheme must be taken into account. Of the waveforms analyzed, only in PN-CDMA and pulse signaling can the signals from all satellites be accommodated in a single RF channel. The remaining waveforms require FDMA and use one channel per satellite. This factor must be taken into account in using the curves of Figure 2-15 to determine relative bandwidth efficiency of the different waveforms.

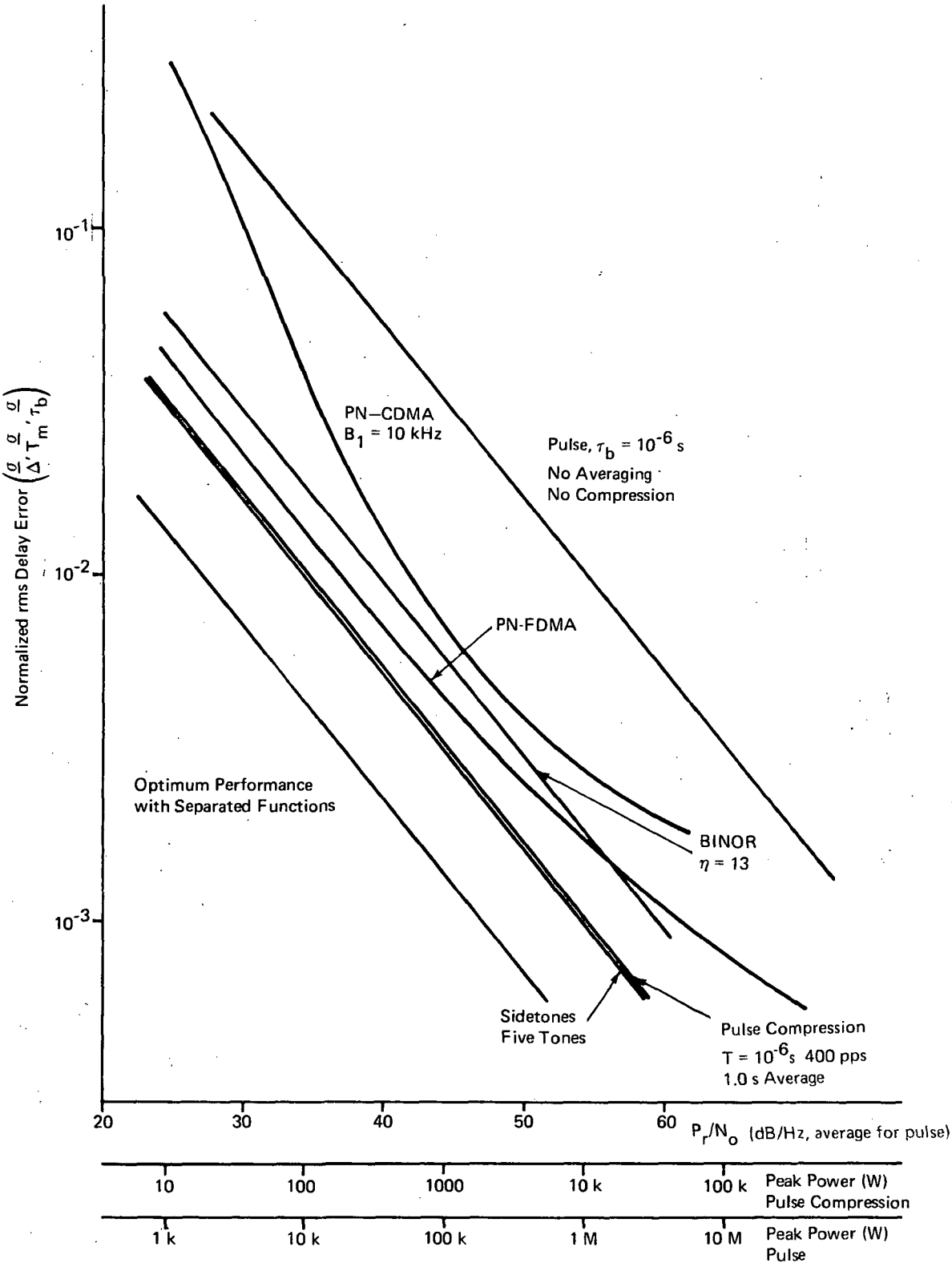

Figure 2-15. Comparative Ranging Performance

It is reasonable to conclude on the basis of Figure 2-15 that the ranging performance and bandwidth occupancy of sidetones PN-FDMA and BINOR are sufficiently close that a decision between them should be made on the basis of other considerations, such as user set complexity and susceptibility to multipath interference.

The fix rates attainable by the candidate waveforms are determined by the receiver loop noise equivalent bandwidth (or averaging time for pulse waveforms). Since this parameter can be independently chosen it is concluded that attainable fix rate is not a significant trade-off factor in selecting between the approaches considered.

In contrast to the conclusions relating to the efficiency of utilization of power for ranging purposes, the discussion of subsection 2.2.5 points to the conclusion that waveforms with relatively flat spectra, such as binary, are less susceptible to multipath interference than are waveforms with strong specular components. The difficulty of obtaining quantitative estimates of this effect prevents a trade-off being made at the level of this study, except to note the importance of investigating this area, particularly since the ranking of waveforms relative to multipath susceptibility appear to be opposite to the ranking for ranging performance.

In considering the user set complexity required to implement receiving and processing circuitry for the waveforms considered, several observations can be made. The waveforms that require separate RF channels (PN-FDMA, sidetones, and BINOR code) require a wideband RF receiver and a separate demodulator and baseband processor for each satellite signal. The use of PN-CDMA places all the signals in a single RF channel, but separate processors are still required for demodulation and processing for each satellite. Comparison of these approaches requires further design of the user set to permit a cost comparison to be made at a lower level of design detail. The only approach which seems to offer a clear advantage in user costs is the pulse system, in which all the satellite signals time-share a single channel and a single receiver.

As a result of the investigation reported herein, it is concluded that none of the waveforms considered offers a clear and uniform advantage over the others relative to the comparison criteria taken into account. Selection of a waveform for a particular system application must be done on the basis of evaluation against what may be called secondary criteria, many of which will be system-specific. The selection may be made on the basis of these secondary criteria with reasonable confidence that the system performance in ranging and position location will not be severely degraded regardless of the selection.

2.3 SEQUENTIAL POLLING

This Subsection discusses the mechanism of polling and response which lies at the heart of elicited-response surveillance systems. The discussion is concerned with specific polling procedures and the design of the interrogation waveform.

Elicited-response systems depend upon the use of interrogation waveforms that key user responses, at appropriate times. The interrogation waveforms are transmitted on the satellite downlinks to groups of users who respond to the recognition of a specific point in the waveform. The basic problem in a sequential polling waveform design is to assure that the responses in a given frequency channel do not overlap at the repeaters of the relay satellites unless protection is provided by the use of code division multiple access. Stated another way, the problem is to sequence responses from groups of users using the same response waveform in the most efficient way. The questions to be answered are

1) In what order and with what time spacing must the users be interrogated?

2) What is the best signal design for the interrogation waveform?

The answer to the first question depends upon whether a system with a single response path (Configuration I) or a system with multiple paths (Configuration III) is being considered. In Configuration I, two approaches to range-ordered polling can be considered. For Configuration III, the requirement to avoid signal overlaps simultaneously at several satellites imposes additional constraints which dictate a different approach to the problem.

2.3.1 RANGE-ORDERED POLLING

Consider the situation shown in Figure 2-16. A group of users is to be polled by an interrogation waveform such that their response messages, each of length τ_m, are sequenced through the repeater of the relay satellite. The number of users that can be polled in a time T_u is clearly maximized by minimizing the guard time between messages. If the control center has knowledge of the positions of all users, this can be done by placing the interrogation point for user j in the interrogation waveform at a time τ_j, where τ_j is given by

$$\tau_i = (j - 1)\,\tau_m - \frac{\Delta r_j}{c} \qquad (2\text{-}22)$$

in which τ_m is the message length, Δr_j is the range difference between user j and user j + 1, and c is the signal propagation speed. The situation is shown in Figure 2-17 in which the horizontal axis represents time and the vertical axis represents distance between the satellite repeater and the users. A single frame of polling and response is shown, although in practice the process is continuous. Equation 2-22 can be understood by observing that if all the users are at the same range the second term is zero

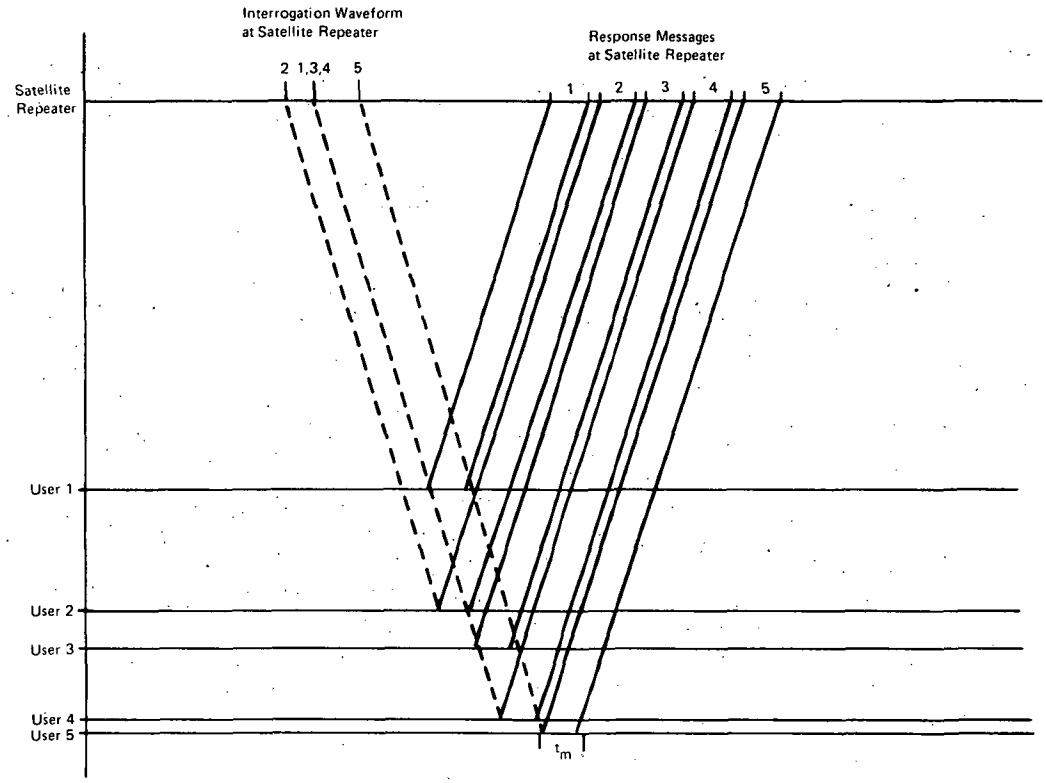

Figure 2-16. Range Polling – Operational Configuration

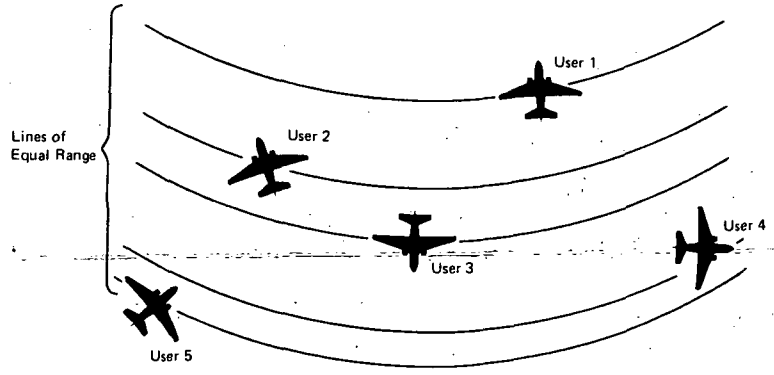

Figure 2-17. Range-Ordered Polling with Minimum Guard Time

and the interrogation points are spaced by the message length. The second term corrects for the propagation delay resulting from unequal ranges. It is noted that the order of the interrogation points is not the same as the order of the responses, and also that more than one user may have to respond at the same (or almost the same) point. This rolling method is referred to as "minimum guard time" range-ordered polling.

The implementation of this minimum guard time approach introduces several difficulties. First, the processor at the control center must compute the propagation delays for each user at each interrogation scan, and order the interrogation waveform to assure the correct sequential response. Second, the ordering of the interrogation waveform must be changed every scan to reflect changes in user positions regardless of whether the ordering by range has changed.

This approach maximizes the number of users that can be polled sequentially. The number of users, N, that can be polled in a given time T_u is limited only by the message length, and is given by

$$N = \frac{T_u}{T_m} \tag{2-23}$$

The implementation difficulties encountered in minimum guard time polling can be eased considerably at a slight sacrifice in capacity. Assume that the interrogations are ordered by user range, and are spaced at the transmitter at intervals equal to T_m. Then for users at the same range the responses will be sequenced through the repeater with essentially zero guard time, as in the previous approach. The responses from users whose ranges differ by an amount Δr_i will be spaced at the satellite by a time interval equal to $2\Delta r/c$. If r_i is the range difference between the i'th user and the (i + 1)'th user, then the total time, T_u, required for the responses from N users is

$$T_u = \frac{2}{c} \sum_{i=1}^{N} \Delta v_i + N\tau_m \tag{2-24}$$

If R is the range difference between the closest and furthest users, then,

$$\sum_{i=1}^{N} \Delta r_i = \Delta R \tag{2-25}$$

and

$$T = \frac{2\ \Delta R}{c} + N\tau_m \tag{2-26}$$

For specified T, Equation 2-26 limits the number of users that can be polled using this technique. N is given by

$$N = \frac{T - \frac{2\,\Delta R}{c}}{\tau_m} \tag{2-27}$$

This simplified range-ordered polling scheme represents a decrease of $2\,\Delta R/c\,\tau_m$ in the number of users from the minimum guard time approach. An estimate of the magnitude of this reduction can be made using the typical figures of $T_u = 1$ second, $\tau_m = 10^{-5}$ second, and $\Delta R = 3000$ miles (CONUS). Then,

$$\frac{2\,\Delta R}{c\,\tau_m} = \frac{2 \times 3000}{1.86 \times 10^{5} \times 10^{-5}}$$

$$= 3220$$

which represents a loss of some 3% of the 10^5 users which could otherwise be polled.

2.3.2 SEQUENTIAL POLLING FOR MULTIPLE SATELLITES

The conceptual simplicity of the range-ordered polling method depends upon the assumption that the user signals return to the control center by way of a single satellite, and hence, this method of polling is confined to use only with a Configuration I system. Assuming only time orthogonality, in the multisatellite elicited polling associated with Configuration III, the problem is complicated by the fact that the response messages must be sequenced in such a way that no overlap occurs at any of the relay satellites. Clearly, if a set of users are range-ordered with respect to one satellite, the same range-ordering cannot hold for any other satellite. Another approach to the problem must be taken.

Assume that a group of N users is distributed randomly over the total coverage area of interest, with the maximum possible distance between any pair being ΔR, and consider a low-elevation satellite as shown in Figure 2-18. Assume also that the interrogation signal is being transmitted by the same satellite. If User 1 and User 2 are interrogated successively, then the response messages will not overlap if the interrogations are spaced by an interval τ given by

$$\tau = \frac{2\,\Delta R}{c} + \tau_m \tag{2-28}$$

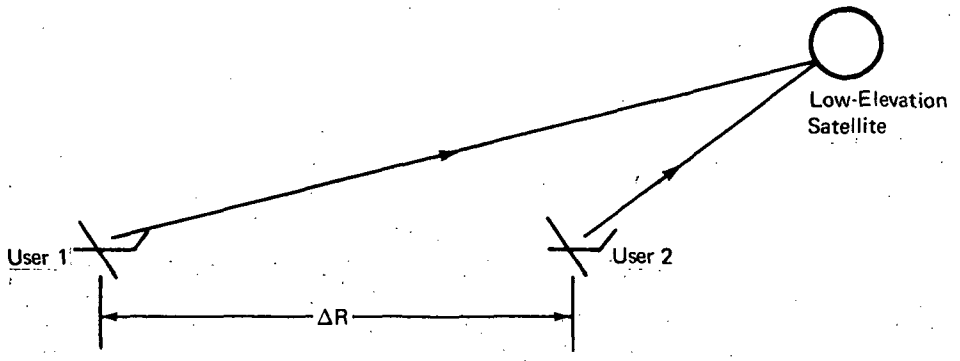

Figure 2-18. Low-Elevation Satellite

If no overlap is assured for the lowest elevation satellite, it is also assured for satellites at higher elevations. For a specified polling interval of T_u seconds, the number of users that can be polled is

$$N = \frac{T_u}{\tau}$$

$$= \frac{T_u}{\frac{2\,\Delta R}{c} + \tau_m} \qquad (2\text{-}29)$$

A generalization of this idea is obtained by dividing the total coverage area, A_T, into n equal-area square cells of dimension $A^{1/2}$, where A is the cell area. Within each cell, users may be interrogated in random order, with no overlap of messages provided that the successive interrogations are spaced by an interval given by Equation 2-28. In this case, we have

$$\Delta R = (2A)^{1/2} \qquad (2\text{-}30)$$

since the maximum possible separation of users within a cell is the length of the cell diagonal. In polling all users, the procedure is to interrogate all the users in a given cell, with spacing given by Equation 2-28 before passing to the next adjacent cell, according to a prespecified and fixed cell order. In determining the number of users that can be interrogated using this procedure, Equation 2-29 must be modified to reflect the fact that when the interrogation sequence moves from one cell to another, the maximum distance between the last user polled in one cell to the first user polled in the next cell in greater than ΔR. For simplicity, we ignore the fact that the true distance is the diagonal across two cells, and use $2 \times (2A)^{1/2}$ as an approximation. The interrogation interval in this case is

$$\tau' = \frac{4(2A)^{1/2}}{c} + \tau_m \qquad (2\text{-}31)$$

which exceeds the value given by Equation 2-28 by $2(2A)^{1/2}/c$. This additional amount must be allowed for each of the n cells. In a total polling interval of time T_u, there will be N polling intervals of length τ, and n cell-transition intervals of length $2(2A)^{1/2}/c$. Summing these intervals and equating to T_u gives

$$T_u = N\left[\frac{2(2A)^{1/2}}{c} + \tau_m\right] + n\left[\frac{2(2A)^{1/2}}{c}\right] \qquad (2\text{-}32)$$

Solving for N,

$$N = \frac{T_u - n\left[\frac{2(2A)^{1/2}}{c}\right]}{\left[\frac{2(2A)^{1/2}}{c} + \tau_m\right]} \qquad (2\text{-}33)$$

The question to be investigated is how the cell area, A, should be chosen to maximize N for a given T_u, τ_m, and A_T. Noting that

$$n = \frac{A_T}{A},$$

Equation 2-33 can be rewritten

$$N = \frac{cT_u - 2A_T\sqrt{2}\,A^{-1/2}}{2\sqrt{2}\,A^{1/2} + c\tau_m} \qquad (2\text{-}34)$$

Differentiating Equation 2-34 with respect to $A^{1/2}$ and equating the result to zero leads to

$$A - \left[\frac{4A_T\sqrt{2}}{cT}\right]A^{1/2} - \frac{A_T\tau_m}{T_u} = 0 \qquad (2\text{-}35)$$

The solution for the positive real root of Equation 2-35 is

$$A^{1/2} = \frac{2A_T\sqrt{2}}{cT} + \frac{1}{2}\left[\frac{32A_T^2}{(cT)^2} + \frac{4A_T\tau_m}{T_u}\right]^{1/2} \qquad (2\text{-}36)$$

It is easy to verify that $A^{1/2}$ given by this expression corresponds to a maximum of N, which we denote by N_m. Table 2-1 gives a tabulation of values of N_m and $A^{1/2}$ for various values of A_T, T_u, and τ_m. The number of cells, n, is also given.

Table 2-1

N_m, n, AND $A^{1/2}$ FOR VARIOUS VALUES OF A_T, T_u, AND τ_m

A_T (mil^2)	T_u (s)	τ_m (μs)	N_m	n	$A^{1/2}$ (mi)
4×10^6	10	1	26,742	26,963	12.2
		10	24,670	25,682	12.5
		100	12,670	18,310	14.8
	3	1	2,431	2,439	40.0
		10	2,396	2,427	40.0
		100	2,324	2,391	41.0
	1	1	270	271	12.2
		10	269	270	12.2
		100	257	257	12.5
4×10^5	1	1	2,674	2,696	12.2
		10	2,440	2,568	12.5
		100	1,267	1,831	14.8

The value of A_T of 4×10^6 square miles corresponds to a CONUS coverage system. A_T of 4×10^5 square miles corresponds to a system in which the CONUS area is divided into ten sectors, within each of which the interrogation procedure is independent of the others. The table entries for N_m and n for $A_T = 10^5$ square miles are per sector.

The number of users that can be interrogated using this procedure is quite low, particularly for small values of T. This is not surprising when it is noted that the channel duty cycle is low. That is, the message length is generally short compared to the interval between successive response messages. In designing a practical system, the capacity that is unused under a strict TMDA procedure is filled by users separated by code division. Various ways of doing this are analyzed later in Subsection 2.5.

As long as a user remains in the same cell, he can respond at the same point in the interrogation waveform. When he moves from cell to cell, his response point in the interrogation sequence must be changed. The frequency with which this occurs is important, as it affects the processing load imposed on the control center and also the data rate on the link from control center to user. The smallest cell dimension in Table 2-1 corresponds to an update rate per user of about 3 minutes at an average speed of 250 mi/h. The required downlink data rate is investigated in the next subsection.

It should be noted that the determination of N_m makes no assumptions about the distribution of users, and the analysis is valid for any distribution, except the unlikely case in which all the users occupy the same cell. In this case, N_m is larger, but it is obviously not of practical interest.

2.3.3 DESIGN OF THE POLLING WAVEFORM

The polling waveform must perform several functions. It must

1) In two-way ranging measurements (Configuration III), be designed with sufficient fine structure to permit the user to recognize and respond to its assigned interrogation point with a time accuracy determined by the required position error
2) Transmit data for changing interrogation points when necessary
3) Transmit data to selected users for collision avoidance
4) Operate within the downlink power restrictions imposed by the low user antenna gain and satellite prime power limitations.

The requirement of Item 1 is relaxed somewhat in Configuration I, in which the interrogation signal is not itself part of a ranging measurement.

First consider the requirements of interrogation: there are two basic approaches that can be taken. First, the users can be polled by transmission of user addresses. When a user recognizes his address, he responds with the appropriate message. This approach has the advantage that changes in the polling sequence and can be accomplished simply by rearrangement of the addresses by the control center. No specific data transmission to the user is necessary to change response points. A second possibility is to transmit a common timing waveform which is received and monitored by each user. The waveform repeats every polling scan. Each user is assigned a point in the timing waveform to respond. An obvious candidate for the timing waveform is a long PN sequence. Using this approach, the polling sequence must be changed by signaling each affected user to change his response point. The basic criterion which is used to evaluate the merits of these two possibilities is the data rate required on the satellite to user downlink. A secondary criterion is the processing load imposed on the control center to generate and update the polling sequence.

2.3.3.1 Configuration I

In Configuration I, it is easy to show that minimum guard time range-ordered polling imposes an excessive bit rate requirement on the downlink. The sequencing requirement necessitates a waveform with a fine "granularity" of response points which can only be satisfied by a common timing waveform. But a common timing waveform requires explicit update messages when the user response points change, which must be done every scan. Assume N users, and B bits per update message, and a scan time of T seconds. The downlink data rate R is

$$R = \frac{NB}{T} \tag{2-37}$$

For $N = 10^5$, $B = 10^2$ bits, and $T = 1$ second, $R = 10^7$ bits/s. The postulated satellite link, with a characteristic of 36 dB/Hz/W, would require about 50 kW of transmitted satellite power to achieve a bit rate with a 13 dB E/N_o. The minimum guard time approach can be dismissed on this basis alone.

The use of a common timing waveform with the simplified range-ordered polling method can also be dismissed by the same argument, since the range-ordering will change from scan to scan. Consider the implementation of this method with discrete-address polling. The polling addresses must be transmitted with a spacing essentially equal to the response message length. Assuming M bits for each address and a response message length of τ_m seconds, the downlink data rate is

$$R = \frac{M}{\tau_m} \tag{2-38}$$

which is independent both of the total number of users and the scan time. Equation 2-38 is plotted in Figure 2-19 with M assumed to be 20 bits. It is noted that the rates are sufficiently high that the downlink power may be the controlling factor in establishing the polling rate using this method.

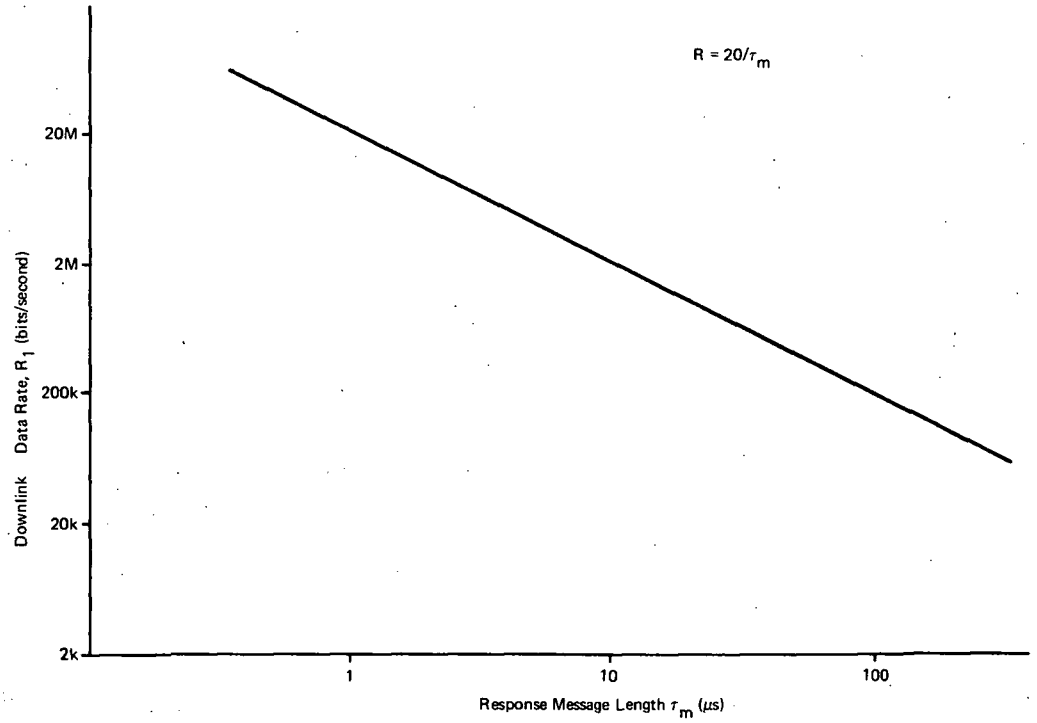

Figure 2-19. Downlink Data Rate Discrete-Address Polling

2.3.3.2 Configuration III

In the multisatellite elicited-response system, the rate at which users can be interrogated is limited by the geometric considerations discussed previously. The discrete-address data rate can be found directly from the scan time T_u, and the number of users, M:

$$R = \frac{NM}{T_u} \tag{2-39}$$

For example, for $N = 10^5$, M = 20 bits, and T_u = 1 second, R = 2 Mb/s. This rate requires 10 kW satellite power, and appears to be unworkable for this reason.

To find the bit rate for the common timing waveform, the rate at which update messages must be sent must be found. This is equal to the rate at which users move between cells. Assuming an aircraft speed v and a cell dimension $A^{1/2}$, the average number of cell transitions per second, M, with uniform user density is given by

$$M = \frac{Nv}{A^{1/2}} \tag{2-40}$$

The data rate for M-bit update messages is then

$$R = \frac{MNv}{A^{1/2} \times 3600} \text{ bits/second} \tag{2-41}$$

For M = 150, $N = 10^5$, v = 250 mi/h, and $A^{1/2}$ = 25 miles, R = 41.5 kb/s. The required satellite power for this data rate is about 200 W.

2.2.3.3 Waveform Structure

When a user moves from cell to cell, his interrogation point in the polling waveform is moved to a point associated with the cell he is entering. This implies that such a point is available (that is, unoccupied), otherwise the change of the one interrogation would require the change of many others. An approach that accomplishes this is to preassign segments of the waveform to each cell, with the duration of the segment determined by the maximum number of users expected in that cell. This is shown in Figure 2-20. The success of this approach depends upon providing sufficient capacity that the probability of a cell becoming saturated is suitably low.

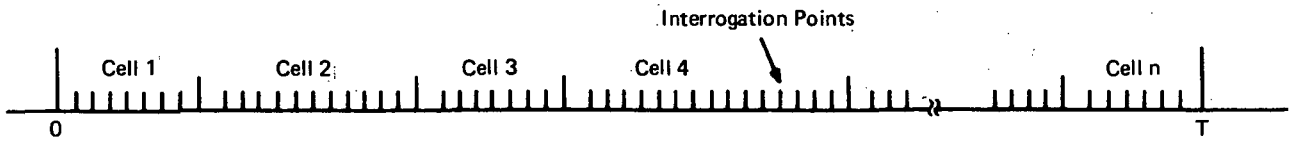

Figure 2-20. Interrogation Waveform Structure

2.3.4 SUMMARY

In this subsection we have discussed some of the aspects of the polling problem for elicited-response systems. Sequential polling methods for both single-satellite and multiple-satellite response systems were considered, and some of the implications of the polling procedure on the downlink interrogation signal design were investigated.

In the single-satellite (Configuration I) system, two approaches to range-ordered polling were considered. The first, which involves sequencing the user responses through the satellite repeater with essentially zero guard time, was found to require excessive downlink power in the interrogation signal, in addition to being undesirable because of the load it imposes on the ground processor. The second simplified approach is feasible with discrete-address interrogation, and involves only a small loss in capacity.

For multiple-satellite (Configuration III) signaling range-ordered polling cannot be used, and a range-cell approach to polling was developed. It was shown that the cell arrangement can be chosen to maximize the number of users interrogated. In this case the common timing waveform is the preferred interrogation signal design. It is noted that the ground processing load imposed in Configuration I range-ordering can be reduced by adopting a range-cell approach at some sacrifice in capacity.

2.4 CONFIGURATION I ANALYSIS

The objective of the following paragraphs is to describe the aircraft-to-satellite performance of pairs-of-polling and multiple-access schemes in terms of the performance parameters of Subsection 2.1.3. The determination of polling/multiple access pairs is the most significant design decision to be made in selecting preferred ATC surveillance communications techniques. A uniform analytical procedure will be developed so that alternatives can be viewed and interpreted on an equal basis. Subsequent subsections will apply the result to Configurations II, III, and IV. The ground-to-satellite links are not considered to involve practical technical limitations since large aperture ground antennas can be used.

In Configuration I, the user derives his position information from a navigational system such as

1) IMU
2) Omega/Loran
3) Navigational Satellites.

These navigational systems can be assumed to be independent of the ATC system. It is assumed that regardless of the navigational data source, the user makes suitable measurements on the received navigation signals, and the resultant data is formatted for transmission to the ground center. Investigation of Configuration I, then, revolves about purely communications link considerations, since ranging and position determination is independent. For this analysis a performance matrix for each polling technique and multiple access technique was prepared. The analysis leading to the contents of these matrixes is presented in Appendix A for each multiple access technique.

2.4.1 ANALYSIS PROCEDURE

To illustrate this unified analysis procedure the data sheet for elicited TDMA/CDMA is presented in Table 2-2. Essentially the top of the data sheet describes the multiple access technique and applies realistic signal-to-noise factors. Subsequently the expressions for the prime performance parameters are presented and calculated as a function of number of system users and transitional points between access techniques. From the results of these analyses a normalized bandwidth factor was derived, calculated, and plotted for each polling-multiple access technique. These graphs illustrate the interrelated trends of key resource parameters of bandwidth, user transmitter power, and code process gain as a function of the number of system users. The resultant plot is shown in Figure 2-21 for elicited TDMA/CDMA. Similar graphical presentations for each technique are contained in Appendix A.

Table 2-2 and Figure 2-21 will be described in some detail illustrating the content and use of the additional figures supplied in Appendix A.

The description, elicited TDM/CDM implies that user aircraft transmit only upon interrogation, and that responses are caused to fall into particular time slots relative to the satellite as illustrated in Figure 2-22. Furthermore, more than one user can occupy a particular time slot, via CDMA, and the number of users per slot, N_S, is controlled (by assignment) and is given by the total number of system users divided by the number of time slots, N/R_T. The first entry in Table 2-2 is the signal or code division process gain which is required to accommodate N total system users with R_T time slots (R_T varies from 10 to 1000). The process gain (PG) requirement was taken to be that PG which would result in signal-to-clutter (desired signal-to-other signals) ratio corresponding to a BER* of 10^{-5}. The second entry, T_i, is transmit time per interrogation, during which M bits must be transmitted. This results in a real time data rate of M/T_i and a message bandwidth of $B_i = D/Hz$ (assuming a 1-bit/Hz modulation efficiency), for the third and fourth table entries. Since this example is elicited, or ordered, the probability of a clear channel does not apply and is entered as unity. The sixth entry, total bandwidth B_T, reflects the process gain requirements and the message bandwidth and is given as the product of the desired signal-to-clutter ratio, the maximum number of simultaneous users per time slot, and the detection bandwidth.

*Bit error rate.

Table 2-2

PARAMETRIC ANALYSIS OF ELICITED TDMA/CDMA

Parameter	*Expression*	*Comment*
N_S	$N_S = \frac{N}{R_T}$	Number of Coded Users per Time Slot
R_F	$R_F = 1$	Number of FDM Channels
R_T	R_T = Variable	Number of Time Slots
SNR_c	$SNR_c = 20$ (13 dB)	Signal-to-Clutter Ratio Necessary for $P_e = 10^{-5}$

Calculated Parameter	Expression	$R_T = 10$					$R_T = 100$					$R_T = 1000$				
Number of Users	$N = R_T N_S$	10	10^2	10^3	10^4	10^5	10	10^2	10^3	10^4	10^5	10	10^2	10^3	10^4	10^5
Processing Gain (dB)	$PG = SNR_c N_S$	0	23	33	43	53		0	23	33	43		0	0	23	33
Transmit Time (s)	$T_i = \frac{T_u}{R_T}$	10^{-1}	10^{-1}	10^{-1}	10^{-1}	10^{-1}		10^{-2}	10^{-2}	10^{-2}	10^{-2}		10^{-3}	10^{-3}	10^{-3}	10^{-3}
Real Time Data Rate (bps)	$D = \frac{M}{T_i}$	10^3	10^3	10^3	10^3	10^3		10^4	10^4	10^4	10^4		10^5	10^5	10^5	10^5
Message Bandwidth (hertz)	$B_i = D$	10^3	10^3	10^3	10^3	10^3		10^4	10^4	10^4	10^4		10^5	10^5	10^5	10^5
Probability of Clear Channel	$P_c = 1$ for $P_E = 10^{-5}$; $SNR_c = 20$	1	1	1	1	1		1	1	1	1		1	1	1	1
Total Bandwidth	$B_T = SNR_c N_S \frac{M}{T_i}$ $N \geq 2$	10^3	2×10^5	2×10^6	2×10^7	2×10^8		10^4	2×10^6	2×10^7	2×10^8		10^5	10^5	2×10^7	2×10^8
User Transmit Power (W)	$T_{xp} \cong$ $\text{antilog}\left[\frac{-23 + 10 \log \frac{M}{T_i} + \log 5}{10}\right]$	5	10	10	10	10		50	250	250	250		500	500	500	500
Number of Users/MHz	$\frac{N}{B_T} \times 10^6$	10^4	500	500	500	500		10^4	500	500	500		10^3	10^4	500	500
Timing Accuracy	$A \cong \frac{1}{D}$	10^{-3}	10^{-3}	10^{-3}	10^{-3}	10^{-3}		10^{-4}	10^{-4}	10^{-4}	10^{-4}		10^{-5}	10^{-5}	10^{-5}	10^{-5}
Parallel Receiver Signal Processor	R_F	1	10	10^2	10^3	10^4		1	10	10^2	10^3		1	1	10	10^2

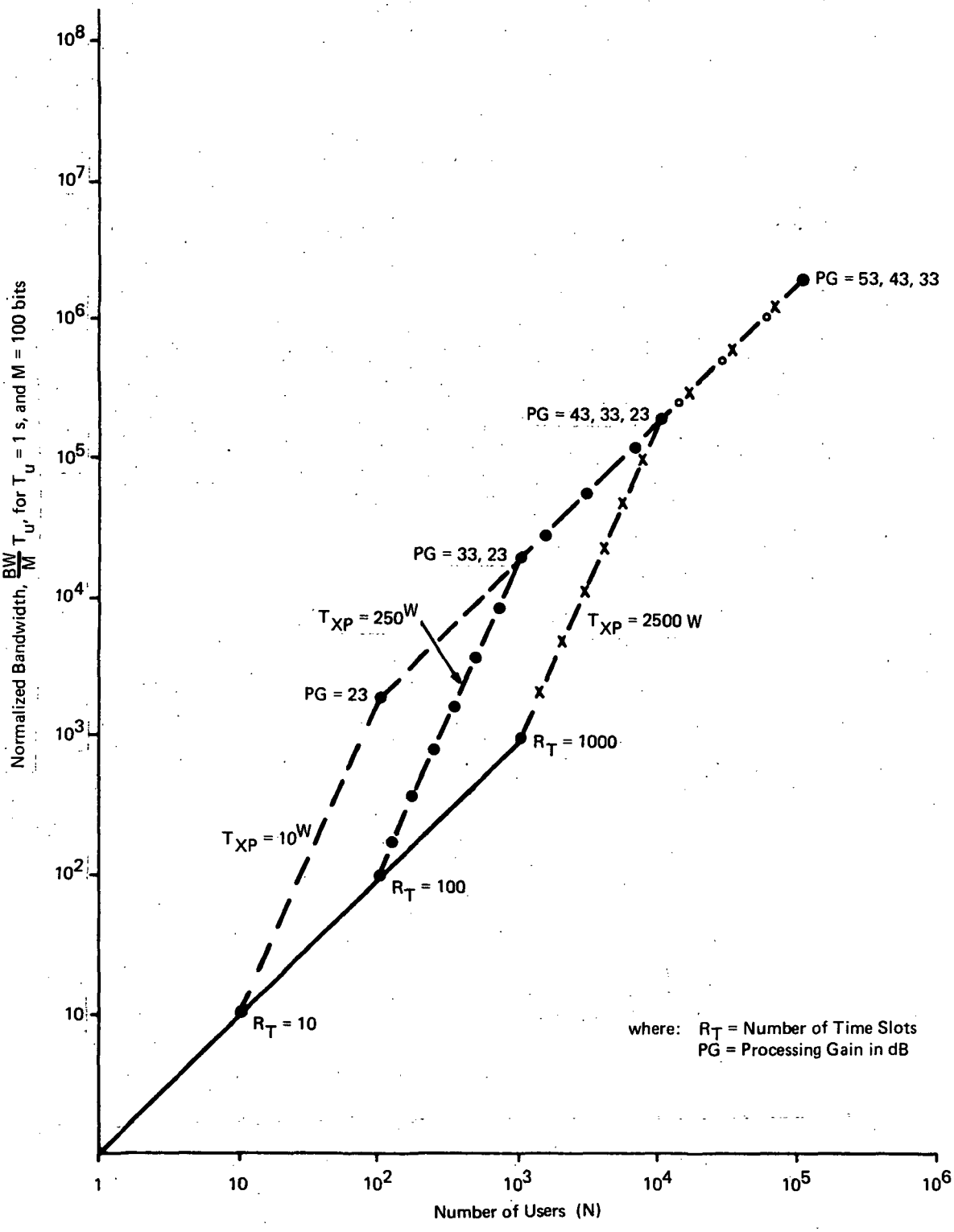

Figure 2-21. Normalized Bandwidth vs Number of Users for Elicited TDMA/CDMA

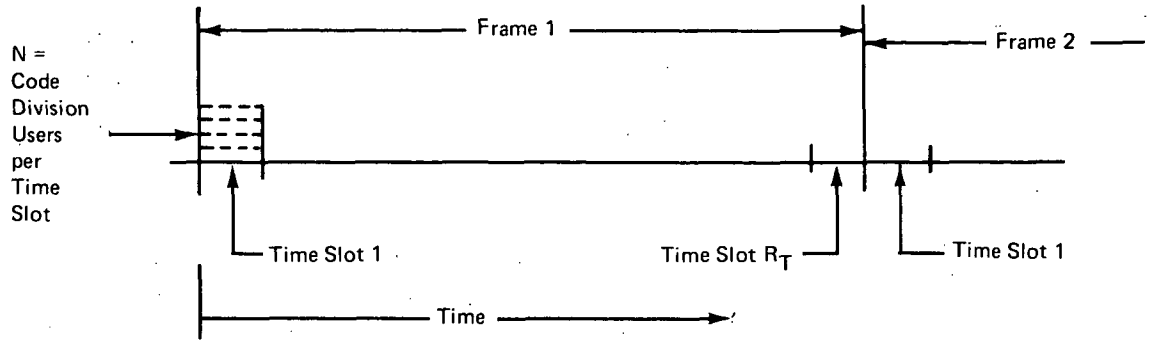

Figure 2-22. Time Profile for Elicited Polling, TDMA/CDMA Multiple Access Pair

The seventh entry, required transmit power, is calculated on the basis that a 20-dB signal-to-thermal noise is necessary, where CDMA is used, so that the BER is principally a function of the signal-to-clutter ratio. The eighth entry is the total number of system users per megahertz, an indication of the relative spectrum utilization of each candidate.

The next entry is the timing accuracy required by both the interrogation signal and the user response if less than one data bit overlap is to occur in the time division format. It is interesting to note that approaches which use elicited TDMA can impose position location accuracy requirements on the navigation system. For example, in Table 2-2 with 1000 time slots, the position of the aircraft must be known at the time of transmission to within 10^4 ft in order to ensure proper arrival time at the satellite. If the ground control station is controlling the transmit time of the user response, the impact of the delay between transmission and the aircraft velocity on this requirement is evident.

Finally, Table 2-2 illustrates the minimum number of parallel ground signal processors needed to accommodate the requirements of N users. Here it is evident that the use of TDMA reduces the number of processors from N to N divided by the number of time slots.

Figure 2-21 summarizes the parametric variation of total (normalized) bandwidth occupancy, transmitter power, and processing gain as a function of the total number of system users. The figure shows the tradeoff between transmitter power and signal processing gain. For example with $N=10^5$ and 10 time slots, 10 W of transmitter power and 53 dB of signal processing gain is required. From a conservative point of view, this signal processing gain probably represents a borderline state-of-art specification. With $N=10^5$ and 100 time slots the transmitter power is 750 W and the process gain is 43 dB, perhaps the best compromise for elicited TDMA/CDMA combinations since the timing requirements to support this degree of TDMA are minimal. In any case, for large N, the bandwidth occupancy can be seen to be independent of the mix of TDMA and CDMA. The real value of these curves can best be derived by overlapping or comparison with other alternatives such as autonomous TDMA/CDMA, etc. Operating points for the popular proposed ATC systems can be located and tradeoff for parameter variation can be interpreted.

Similar analytical procedures and graphical presentations were made for a polling-multiple access pairs and are presented in the appendices.

2.4.2 SYSTEM FIGURE OF MERIT

The analysis in the foregoing subsection can be further generalized by eliminating the link assumptions and the assumption relative to modulation efficiency, and guard frequency and guard time allocations. As indicated above the principal resources are transmitter power, total occupied bandwidth, and signal processing gain. A preferred system approach would minimize the product of these three items, i.e., $T_{xp} \cdot B_T PG$. For convenience, a figure-of-merit describing this performance was defined as

$$Q = T_{xp}\left[\frac{L_{fs}\, G_{ac}\, G_{sc}}{KT}\right] \cdot B_T \cdot PG$$

where

$$\frac{L_{fs}\, G_{ac}\, G_{sc}}{KT}$$

is the product of free space loss, aircraft antenna gain, and spacecraft antenna gain divided by KT, which is the Johnson noise in a 1-Hz bandwidth. Table 2-3 illustrates the form which this product takes for polling/multiple access pairs. The entries are general enough to facilitate the comparison of any candidate approaches. As an example, let us compare the figure-of-merit for autonomous FDMA and TDMA:

$$Q_{A\text{-}FDMA} = \frac{P_r\, T_D}{N_o}\left(\frac{M}{T_u}\, C_1\right)^2 NC_F$$

$$Q_{A\text{-}TDMA} = \frac{P_r\, T_D}{N_o}\left(\frac{MNC_1\, 10^5}{T_u}\right)^2$$

where

T_D = time interval per bit
C_1 = constant for modulation efficiency
C_F = constant for FDM guard channel space.

Here,

$$\frac{P_r\, T_D}{N_o}$$

is the detected signal-to-noise ratio per data bit, a design factor to be specified and one which affects both candidates equally. We observe that the

$$\frac{MC_1}{T_u}$$

Table 2-3

UP LINK TRANSMITTER POWER, TOTAL BANDWIDTH, SIGNAL PROCESS GAIN AND FIGURE OF MERIT FOR ALTERNATIVE CONFIGURATION I APPROACHES

		FDMA	TDMA	CDMA	TDMA/FDMA	FDMA/CDMA	TDMA/CDMA
$T_{xp}\left[\frac{L_{fs}G_{ac}G_{sc}}{KT}\right]$ =	Elicited	$\frac{P_R T_D}{N_o}\cdot\frac{M}{T_u}\cdot C_1$	$\frac{P_R T_D}{N_o}\frac{MN}{T_u}\cdot C_1 C_T$	$\frac{P_R T_D}{N_o}\frac{M}{T_u}C_1$	$\left.\frac{P_R T_D}{N_o}\frac{MNC_1C_T}{T_u R_F}\right\vert_{N>R_F}$ $\left.\frac{P_R T_D}{N_o}\frac{MC_1}{T_u}\right\vert_{N<R_F}$	$\frac{P_R T_D}{N_o}\frac{M}{T_u}C_1$	$\frac{P_R T_D}{N_o}\cdot\frac{MR_T C_1 C_T}{T_u}$
	Autonomous	$\frac{P_R T_D}{N_o}\cdot\frac{M}{T_u}\cdot C_1$	$\frac{P_R T_D}{N_o}\frac{MNC_1 10^5}{T_u}$	$\frac{P_R T_D}{N_o}\frac{M}{T_u}C_1$	$\left.\frac{P_R T_D}{N_o}\frac{MNC_1C_T10^5}{N T_u R_F}\right\vert_{N>R_F}$ $\left.\frac{P_R T_D}{N_o}\frac{MC_1}{T_u}\right\vert_{N<R_F}$		$\frac{P_R T_D}{N_o}\frac{MR_T C_1}{T_u}$
B_T =	Elicited	$N\frac{M}{T_u}\cdot C_1 C_F$	$\frac{MN}{T_u}\cdot C_1 C_T$	$\frac{P_R T_D}{N_c}\frac{MN}{T_u}C_1$	$\left.\frac{MNC_1C_TC_F}{T_u}\right\vert_{N>R_F}$ $\left.\frac{MNC_1C_F}{T_u}\right\vert_{N<R_F}$	$\frac{P_R T_D}{N_c}\left(\frac{MNC_1}{T_u}\right)C_P\Big\vert_{N>R_F}$	$\frac{P_R T_D}{N_c}\cdot\frac{MNC_1C_T}{T_u}$
	Autonomous	$N\frac{M}{T_u}\cdot C_1 C_F$	$\frac{MNC_1 10^5}{T_u}$	$\frac{P_R T_D}{N_c}\frac{MN}{T_u}C_1$	$\left.\frac{MNC_1C_T10^5}{T_u}C_F\right\vert_{N>R_F}$ $\left.\frac{MNC_1C_F}{T_u}\right\vert_{N<R_F}$	$\left.\frac{MNC_1C_F}{T_u}\right\vert_{N<R_F}$	$\frac{P_R T_D}{N_c}\cdot\frac{3MNC_1}{T_u}$
PG =	Elicited	1	1	$\frac{P_R T_D}{N_c}N$	1	$\left.\frac{P_R T_D}{N_o}\frac{N}{R_F}\right\vert_{N>R_F}$	$\frac{P_R T_D}{N_c}\cdot\frac{N}{R_T}$
	Autonomous	1	1	$\frac{P_R T_D}{N_c}$	1	$1\Big\vert_{N<R_F}$	$\frac{P_R T_D}{N_c}\frac{3N}{R_T}$
$Q = T_{xp}\cdot[L]\cdot B_T\cdot PG =$ where $[L]=\left[\frac{L_{fs}G_{ac}G_{sc}}{KT}\right]$	Elicited	$\frac{P_R T_D}{N_o}\left(\frac{M}{T_u}C_1\right)^2 NC_F$	$\frac{P_R T_D}{N_o}\left(\frac{MNC_1C_T}{T_u}\right)^2$	$\frac{P_R T_D}{N_o}\left(\frac{MNC_1}{T_u}\right)^2\left(\frac{P_R T_D}{N_c}\right)^2$	$\left.\frac{P_R T_D}{N_o}\left(\frac{MNC_1C_T}{T_u}\right)^2\frac{C_F}{R_F}\right\vert_{N>R_F}$ $\left.\frac{P_R T_D}{N_o}\left(\frac{MC_1}{T_u}\right)NC_F\right\vert_{N<R_F}$	$\frac{P_R T_D}{N_o}\left(\frac{MNC_1}{T_u}\right)^2\left(\frac{P_R T_D}{N_c}\right)^2\frac{C_F}{R_F}$ $N>R_F$	$\frac{P_R T_D}{N_o}\left(\frac{MNC_1C_T}{T_u}\right)^2\left(\frac{P_R T_D}{N_c}\right)^2$
	Autonomous	$\frac{P_R T_D}{N_o}\left(\frac{M}{T_u}C_1\right)^2 NC_F$	$\frac{P_R T_D}{N_o}\left(\frac{MNC_1 10^5}{T_u}\right)^2$	$\frac{P_R T_D}{N_o}\left(\frac{MNC_1}{T_u}\right)^2\left(\frac{P_R T_D}{N_o}\right)^2$	$\frac{P_R T_D}{N_o}\left(\frac{MNC_1C_T10^5}{T_u}\right)^2\frac{C_F}{R_F}$ $\frac{P_R T_D}{N_o}\left(\frac{MC_1}{T_u}\right)^2 NC_F$	$\frac{P_R T_D}{N_o}\left(\frac{MC_1}{T_u}\right)^2 NC_F$	$\frac{P_R T_D}{N_o}\left(\frac{3MNC_1}{T_u}\right)^2\left(\frac{P_R T_D}{N_c}\right)^2$

factor; i.e., the number of bits per message, M, times the modulation efficiency (bandwidth in Hz divided by the number of bits per second) C, divided by the interval between messages, Tu; appears squared for both candidates. Consequently, the Q factor is more sensitive to changes in these design factors than to SNR. Finally it is most interesting to note that Q for autonomous TDMA is a function of 10^5 and N squared. The 10^5 factor results from a requirement for the probability of a clear transmission of $1-10^{-5}$. For 10^5 users this means that on the average two users are overlapped all the time and the ground processor must continually input data from two users.* In any event the A-TDMA scheme increases Q as the square of the number of users whereas the Q for A-FDMA varies only linearly with N and C_F, the frequency guard band.

The following additional observations can be made from Table 2-3:

1) Q varies as N^2 for all candidates excepting those which employ FDMA, the FDMA hybrids vary as N^2/R_F where R_F is the number of FDMA slots. For pure FDMA, Q varies linearly with N.

2) All candidates with CDMA include a factor $(P_r T_D/N_c)$ which is the desired signal-to-clutter ratio (clutter is effective noise power due to all other code division signals)

3) Autonomous TDMA without FDMA involves a factor approximately equal to the reciprocal of the probability of two transmissions overlapping. For large N, and the condition that only two signals overlap, this factor is equivalent to one additional N^2 multiplier.

4) For the autonomous TDMA/CDMA hybrid if enough process gain is provided to allow for three times the expected number of signal overlaps than the additional N^2 factor associated with autonomous TDMA is reduced to nine times the ordinary CDMA $(P_r T_D/N_c)$ factor.

The net conclusion from the above analytical procedures is that if the performance of satellite ATC surveillance systems are to be compared only on user ATC transponder power, total system bandwidth, and processing gain then candidates involving FDMA are desirable. We observe that for a "tactically" oriented system; i.e., those with many divergent low-power, low-antenna-gain users; that this conclusion is consistent with minimum user costs and the traditional command and control approaches. It is also observed that in trunkline, point to point systems, wherein the system measure of performance is strictly capacity per megahertz, that an entirely different basis for comparison and selection of techniques is appropriate. Considering that transmitter power, total system bandwidth, and signal processing gain are limited resources constrained either by availability or state-of-art, the above analysis offers a useful evaluation tool for comparing the many possible ATC surveillance schemes. The foregoing evaluation procedure can be used for all possible ATC satellite configurations and therefore provides a uniform basis for comparing system approaches which can be radically different.

---

*Systems with smaller numbers of users (N) could conceivably tolerate overlap rates greater than 10^{-5} in which case the multiplicative penalty for A-TDMA would be reduced.

Figure 2-23 graphically represents the results for the standard link assumption, fix intervals, $C_I = C_T = C_F = 1$, etc., that have been assumed for this study. A detailed analysis of all of the candidates has been completed and documented in Appendix B. Based on these results, a preliminary elimination of Configuration I candidates can be made on the basis that an eventual growth to 10^5 simultaneous users is necessary. The results of this elimination procedure and the rationale is illustrated in Table 2-4. The effects of space division multiplex, i.e., the use of multiple antenna beams will be treated subsequently.

2.4.3 SPACE DIVISION IMPLEMENTATION IMPACT ON TECHNIQUE ANALYSIS

The foregoing multiple-access/polling techniques can be implemented in conjunction with space division satellite techniques. A space division implementation is feasible by configuring 10 to 20 antennas on a spacecraft. If each antenna pattern is designed to cover a subdivision of the COLM area such that a near uniform traffic density exists for each antenna beam, critical code, power, or bandwidth requirements of the foregoing techniques can be reduced. In accomplishing this implementation several operational problems exist. One problem is range ordering in an elicited TDMA technique. Another problem is frequency, code, or time slot management between adjacent and overlapping beam patterns. The ground processor may have to have flight plans stored for each active aircraft, and direct aircraft to change frequency or code as they move from one beam zone to another. These facets of space division are not considered in depth. Rather, the analysis is constrained to deriving the impact of a 10 beam space division system on each of the foregoing techniques. For this analysis, it is assumed that 10^5 users are uniformly distributed between the 10 beams.

Table 2-5 summarizes the effect of using space division on most of the previously described candidates. The transmitter power reduction reflects not only reduced N factors but also an increase in spacecraft antenna gain of 10 dB. Both E-TDMA and A&E-FDMA/CDMA are subsequently added to the list of potential candidates.

2.4.4 SUMMARY AND CONCLUSIONS

As derived from figure-of-merit calculations, the two candidates retained for further trade-off analysis against other configurations are elicited TDMA/FDMA and autonomous or elicited FDMA. Both of these candidates provide the least user complexity in terms of power and implementation while utilizing bandwidth effectively. Although the TDMA/FDMA approach requires the ground control to user link for all surveillance replies, a reduction in system timing and channelization accuracy requirements relative to pure TDMA occurs.

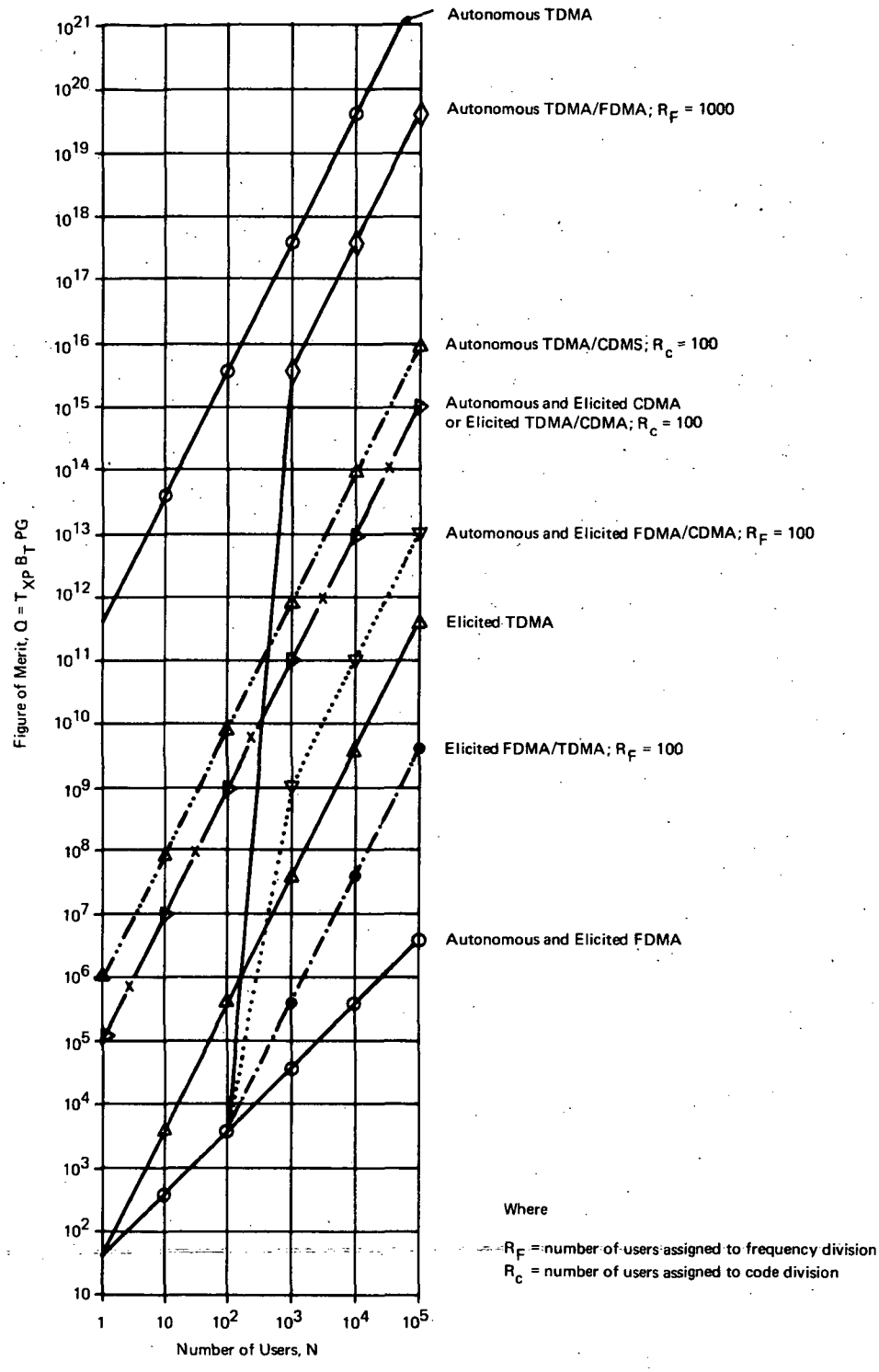

Figure 2-23. Comparison of Polling Multiple Access Technique

Table 2-4

SUMMARY OF CANDIDATE ELIMINATION

Technique	Rationale for Elimination
Autonomous TDMA	Excessive Bandwidth (10^{12} Hz) Excessive User Transmitter Power (5×10^9 W)
Autonomous TDMA/ FDMA	Excessive Bandwidth (10^{12} Hz)
Elicited TDMA	Requires 10 foot Position Location to Implement Requires Uneconomical User Transmit Power (5×10^4 W)
Autonomous and Elicited CDMA	Excessive Processing Gain (63 dB) Requires 10^5 Codes
Elicited FDMA	No Advantage over Autonomous FDMA Unless Ground-User Link Used for Advisory Messages
Autonomous and Elicited FDMA/ CDMA	Excessive Bandwidth
Elicited TDMA/ CDMA	Requires Ground Control to User Link, and Offers no Bandwidth Advantage
Autonomous TDMA/ CDMA/FDMA	Excessive Bandwidth
Autonomous TDMA/ CDMA	Excessive Bandwidth (6×10^8 Hz)
Technique	**Rationale for Candidate Retention**
Elicited TDMA/ FDMA	Bandwidth = 10^7 Hz T_{xp} = 50 W Reasonable Implementation for R_T = 100 Effective Bandwidth Utilization, but Requires Ground-User Link
Autonomous FDMA	Bandwidth = 10^7 Hz T_{xp} = 50 W Best Figure-of-Merit, no Ground-User Link Continuous Surveillance, but Requires 10^{-8} Frequency Stability and in Addition Requires a Methodology of Eliminating Doppler Shift Ground Station Must Process 10^5 Separate Signals

Table 2-5

SUMMARY OF APPROACHES INCORPORATING SDMA

Approach for $N = 10^5$	PG	T_{xp} (W)	B_T	Comments
Eliminated Candidates				
A-TDMA/SDMA	1	5×10^5	10^{11}	Power and bandwidth excessive
E-TDMA/SDMA	1	5×10^2	10^6	Power marginally high
A&E CDMA/SDMA	53 dB	0.25	2×10^7	Process gain marginally high, bandwidth relatively high
A-TDMA/CDMA/ SDMA $R_T = 100$	38 dB	25 W	6×10^7	Excessive bandwidth
A-TDMA/CDMA/ SDMA $R_F = 1000$	1	5×10^3	10^{11}	Excessive bandwidth and power
Retained Candidates				
A&E FDMA/SDMA	1	0.05	10^6	Most efficient but requires ground control of frequency management
E-TDMA/CDMA/ SDMA $R_T = 100$	33 dB	25	2×10^7	Relatively high bandwidth — requires CPU time slot management
E-TDMA/FDMA/ SDMA	1	5.0	10^6	An efficient approach — requires CPU time/frequency slot management
A&E-FDMA/CDMA/ SDMA	43	0.25	2×10^7	Flexible approach requiring less ground CPU management, but more bandwidth

The pure FDMA approach while being the least complex for the user and efficiently utilizing bandwidth has a requirement for accurate carrier stability on the order of 10^{-8}. Furthermore, a method eliminating Doppler shift would be necessary which would increase the on-board complexity somewhat. Each system would require a separate receiver-preprocessor at the ground processor. However, these could be implemented on a growth basis as the system requirements grow to the 10^5 capacity. In fact, the system would not be limited to 10^5 users as long as bandwidth was made available for expansion.

In conclusion, these two approaches are feasible and worthy of further tradeoff against approaches with other configurations because of their bandwidth efficiency/ power efficiency, and implementation complexity.

2.5 CONFIGURATION II ANALYSIS

Configuration II, shown schematically in Figure 2-24, is characterized by the lack of a polling signaling path between the control center and the users. User signals are generated autonomously and sent through at least four satellites to the control center. Position location is done at the control center hyperbolically, using time-of-arrival difference measurements. Although this configuration can inherently be used for navigation by providing suitably timed signals from satellites to user and appropriate processing equipment on-board, only the surveillance communication problem is considered here.

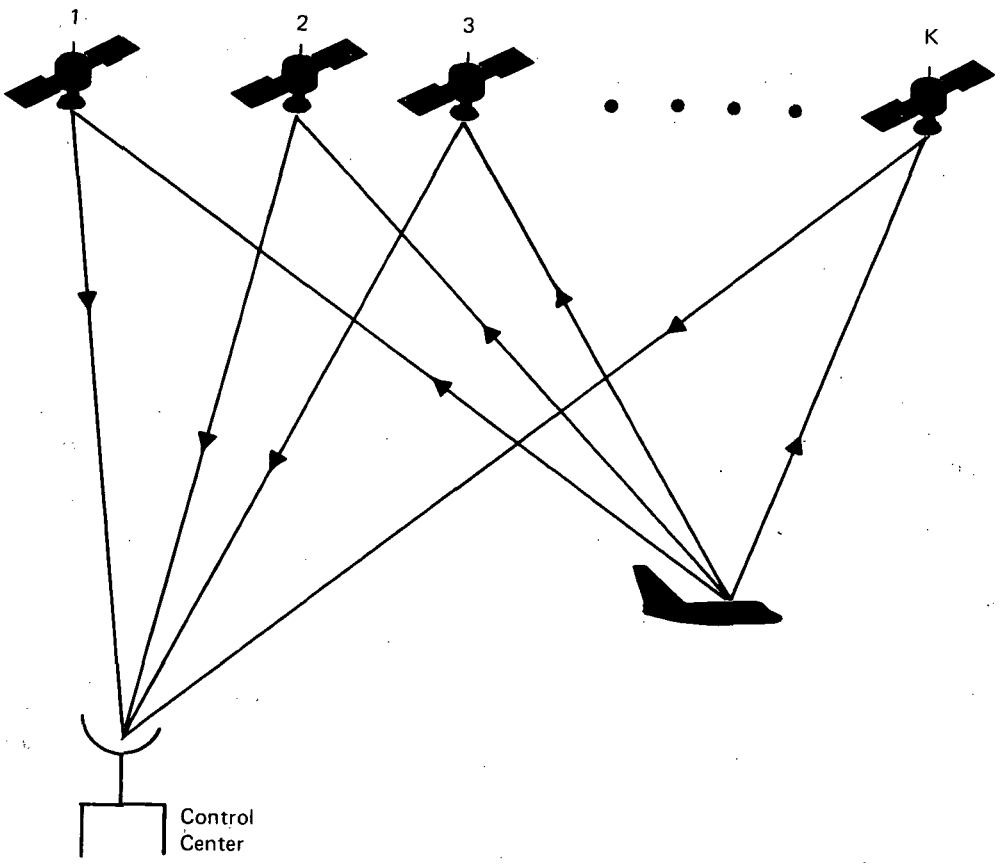

Figure 2-24. Configuration II

Many of the results obtained in the analysis of autonomous polling in Configuration I are directly applicable to Configuration II. There are, however, some significant differences arising from the different functions performed by the transmitted signals. In Configuration I the user transmits a long (about 100 bits) data sequence which contains the data necessary for the control center to compute his position. No time-of-arrival measurements are made directly on the signal. Because of this, a wider range of signaling possibilities exists with Configuration I than Configuration II.

In Configuration II, the user signals must satisfy two criteria: (1) they must permit the control center to make time-of-arrival measurements with sufficient accuracy to satisfy the system error requirements, and (2) they must, either implicitly by time, frequency, or code, or explicitly by data content, identify the transmitting user. The first criteria imposes the requirement that the signal be of sufficient effective bandwidth to permit range measurements. This is the essential difference between Configuration I and Configuration II signaling. In the next subsection the analysis of Subsection 2.4 is adapted as required to indicate the performance of Configuration II.

The following basic parameter assumptions will be made where numerical results are computed:

1) B_S = minimum bandwidth required to transmit a ranging signal
   = 10^7 Hz
2) T_u = 1 second
3) M = 20 bits when user ID is transmitted
   = 1 bit where ID is not needed.

The analyses of the various multiple access-methods have been performed within the same framework as that used for Configuration I; the data sheets which summarize the results are in Appendix E, Tables E-1 through E-6.

The following paragraphs discuss the significant features of each method.

2.5.1 TDMA

As in Configuration I, autonomous TDMA is taken to mean that the users transmit autonomously with no provisions for signal separation other than the low probability of overlap which is assured by the short pulse duty cycle. The signals must contain explicit identification, hence a provision for 20 bits of data is made.

In autonomous TDMA, the addition of users can only be done by shortening the pulse length for all users in order to maintain the desired probability of error. An increase in N, therefore, can only be achieved by a directly proportioned increase in required bandwidth and user power.

2.5.2 FDMA

Autonomous FDMA implies that a separate frequency channel is assigned to each user. The results in this case are significantly different from Configuration I. Since identification of the user is implicit in the frequency channel assignment, the user sends only one bit of data per transmission. Although this is reflected in the low user power requirement, the bandwidth is not similarly reduced since 10^7 Hz is required per user for transmission of the ranging signal. Increase in the number of users is reflected in a proportional bandwidth increase with no change in user power.

2.5.3 CDMA

In autonomous CDMA all users transmit in a common frequency channel of width B_S, with signal separation accomplished by PN code recognition. The transmissions are continuous rather than pulsed; and since user identification is implicit in the code, only one bit of data is sent per transmission. User power in this approach is independent of the number of users. Since each user transmits one bit per second with a 10^7 Hz signal bandwidth, 70 dB signal processing gain is available, which is sufficient to provide adequate clutter margin for up to 10^5 users. (Note that the achievement of 70 dB processing gain in practice is not feasible.)

2.5.4 TDMA/FDMA

The TDMA/FDMA system arbitrarily assumes a number of separate frequency channels. Appendix E shows data for 10, 100, and 1000 channels. The users are evenly divided among the frequency channels, and within each channel the users transmit pulse ranging waveforms autonomously, with the pulse length determined by the desired probability of overlap of 10^{-5}. A 20-bit identification is required in each signal. As in autonomous TDMA, increasing the number of users is accomplished by increasing bandwidth, data rate per transmission, and user power. The total bandwidth requirement is determined only by the number of users, and not by the channelization.

2.5.5 FDMA/CDMA

An FDMA/CDMA system is constructed by channelization of the bandwidth and assignment of equal numbers of users to each channel. Within each channel, signal separation is by code division. The data rate is one bit per transmission, and the transmission for each user is continuous. As in the case of pure CDMA, the available processing gain resulting from the signal bandwidth to data bandwidth ratio far exceeds that required.

2.5.6 TDMA/CDMA

In TDMA/CDMA all users transmit in the same frequency channel, and each is assigned a different pulse code. In this case, signal overlaps are acceptable, and the pulse lengths are determined such that the expected number of overlapping signals (assuming randomly timed transmissions) is one-third of the number that can occur without exceeding the 13 dB signal-to-clutter ratio. The signal processing gain available is determined by the pulse length, since the signal bandwidth is fixed, and in all cases it exceeds the required gain for up to 10^5 users. User power is independent of the number of users.

2.5.7 COMPARISON AND ELIMINATION

The critical comparison criteria are required system bandwidth, user power, and required signal processing gain. Placing realistic attainable limits on these parameters leads to a first-level comparison which results in the elimination of all but one of the six candidates discussed in this section. The limits imposed are

1) Bandwidth — 10^8 Hz for 10^5 users
2) Use power — 5 kW peak
3) Processing gain — 40 dB.

Autonomous TDMA exceeds the bandwidth and power limits. FDMA exceeds the bandwidth limit (note that this differs from the Configuration I results). CDMA, while meeting bandwidth and power requirements requires excessive signal processing gain.

In the hybrid methods, TDMA/FDMA and FDMA/CDMA both require excessive bandwidth. The only method with reasonable values in all three of the primary criteria is TDMA/CDMA, for at least 10^3 time slots. In practical terms, however, a difficulty in implementing this approach arises from the fact that it appears that each user requires a separate code. An alternative to the assignment of separate codes to each user is to allow groups of users all having the same code to transmit at slightly different pulse repetition rates. (See Subsection 2.8.1.2 for a description of the LIT system.)

A preliminary conclusion from the foregoing analyses is that there is no pure or hybrid multiple-access approach using only time, frequency, and code orthogonality that meets the practical limitations set forth above for the Configuration II communication configuration. This conclusion is supported by the fact that the LIT (Reference 9) surveillance system, which is a Configuration II system, uses a form of quasi-orthogonality based upon pulse repetition rate to obtain the additional signal separability required in a TDMA/CDMA hybrid without using a large number of codes. The above analyses indicate that there is no alternative but to introduce such quasi-orthogonality in order to obtain a practical system. With modifications of the LIT type to solve the code design problem, the TDMA/CDMA hybrid is the strong Configuration II candidate.

2.6 CONFIGURATION III ANALYSIS

Figure 2-24 can be used for visualization of Configuration III by the addition of an interrogation signaling path passing either from the control center through one satellite to all users, or through more than one satellite to a specific group of users. Which alternative is followed is primarily a question of downlink data rate and satellite power limitation, and does not materially affect the results of the multiple access analysis presented in this subsection.

It was seen in Subsection 2.5 that the multiple-access analysis for multisatellite autonomous signaling could, with certain modifications, be adapted directly from the single-satellite analyses of Configuration I. There is, however, an essential difference in elicited-response multiple-access between single and multiple satellite configurations. This difference is the fundamental limitation on TDMA interrogation that exists in Configuration III, which was discussed in some detail in Subsection 2.3. This limitation makes the analysis framework of Configurations I and II inappropriate for Configuration III.

The multiple-access methods considered for use in Configuration III are the same six as have been analyzed for Configuration II — TDMA, CDMA, FDMA, TDMA/FDMA, CDMA/FDMA, and TDMA/CDMA. Each of them has a somewhat different operational meaning in Configuration III. The six candidates are described and analyzed in the next subsection.

2.6.1 TDMA

Elicited-response TDMA signaling in Configuration III refers specifically to the time-sequential polling process described in Subsection 2.3. The limit upon the rate at which sequential users can be interrogated was seen to be determined primarily by the system geometry, and secondarily by the response message length. It was also found that a range-cell polling procedure can be designed to maximize the allowable number of users for a given poll repetition rate, T_u, and total area of coverage.

In the analyses of Configurations I and II, the number of users was taken to be the primary independent variable, with system bandwidth, processing gain, and user power determined as functions of the number of users. It is more convenient in Configuration III to take T_u and the message length, T_i as independent variables and determine the number of users that can be accommodated assuming optimization of the range-cell polling. The details of the analysis are in Subsection 2.3.2 and the results for a number of cases are given in Table 2-1. For a more complete definition of performance, these results will be extended to include required user power.

In an elicited-response TDMA system, the user response pulses are uniquely identified by the receive time slot in which they occur. No explicit identification is required in the pulse. It is assumed that each response pulse consists of a short pulse-compression PN code which permits full utilization of the channel bandwidth for SNR improvement. All users can use the same code, hence the receiver consists of a single matched filter. The data rate sent by the user is one bit per pulse. The user pulse power required for the postulated user-satellite link (36 dB/Hz/W), assuming a desired E/N_0 of 13 dB is given by

$$T_{xp} = \log^{-1}\left[-23 + 10 \log \frac{M}{T_i}\right] \qquad (2\text{-}42)$$

where M is the number of bits per pulse. Equation 2-42 is plotted in Figure 2-25 for M = 1 and also for M = 20, which shows the power requirement for the case in which an explicit identification is required in each response.

It is noted that since all users transmit in the same frequency channel, the system bandwidth is independent of the number of users up to the limit imposed by the polling restrictions.

2.6.2 FDMA

FDMA in the context of this analysis implies that each user responds in a separate frequency channel to its interrogation. Since there is no problem of signal overlap, the geometric polling restrictions do not apply, and the users can operate independently of each other. This further implies that the analysis and results of Configuration II are directly applicable. The only operational differences in Configuration III FDMA are that the use of an interrogation signal permits the use of trilateration for position location and also establishes a control center-to-user data path which can be used for collision-avoidance advisories.

2.6.3 CDMA

The same argument holds for CDMA as made above for FDMA. From a signaling point of view there is no distinction between Configurations II and III, and the analysis of Subsection 2.3 applies directly.

2.6.4 CDMA/FDMA

As in the preceding two cases, the analysis of Configuration II applies directly.

2.6.5 FDMA/TDMA

This method is implemented by channelizing the spectrum into a number, R_F, of frequency channels. Within each channel, interrogation and response proceed according to the geometrical restrictions discussed previously. This hybrid is a straightforward extension of pure TDMA in which additional users are accommodated by increasing the bandwidth in increments of the basic 10^7 Hz minimum imposed by the ranging accuracy requirements. The total system bandwidth for a given T_u and T_i is given by

$$B_T = \left[\frac{N}{N_M} \right] \tag{2-43}$$

where [ ] denotes next highest integer. N is the number of users with which the system is to operate, and N_M is found from Table 2-1.

The user power requirements given in Figure 2-25 apply to this case directly.

2.6.6 TDMA/CDMA

The basic framework of elicited-response TDMA for Configuration III can be generalized to include CDMA in several ways. Three possibilities are considered. In all cases the users respond in a common frequency channel of width B_T. It was noted in Subsection 2.3.2 that TDMA used alone in multisatellite signaling resulted in an inefficient use of bandwidth because of the low duty cycle of channel utilization. The use of CDMA allows multiple responses to occupy the same time slot, and hence raises the bandwidth efficiency to the same order of magnitude as that achieved in Configurations I and II. As in the preceding analyses, we are concerned primarily with the system utilization of bandwidth, user power, and process gain. The following subsections give the pertinent analyses for each approach. These three are considered as separate candidates in the comparative analysis of Configuration III approaches given in the next subsection.

The three approaches are distinguished by the way in which the range cells are established and the different codes are assigned to groups of users. The first approach is characterized by a CONUS range-cell arrangement, and a corresponding TDMA interrogation method. Each interrogation triggers responses from a group of users in the same cell, with each user in the group being assigned a different code. In the second approach, the CONUS area is divided into a number of sectors. A range-cell polling scheme is organized independently in each sector, and the interrogation in all sectors proceed simultaneously. All the users in each sector respond with the same code, and are separated by TDMA. Different sectors are assigned different codes. In the third approach, no range cells are used. TDMA interrogations take place at a rate determined by the CONUS propagation delay, with a large group of users responding to each interrogation.

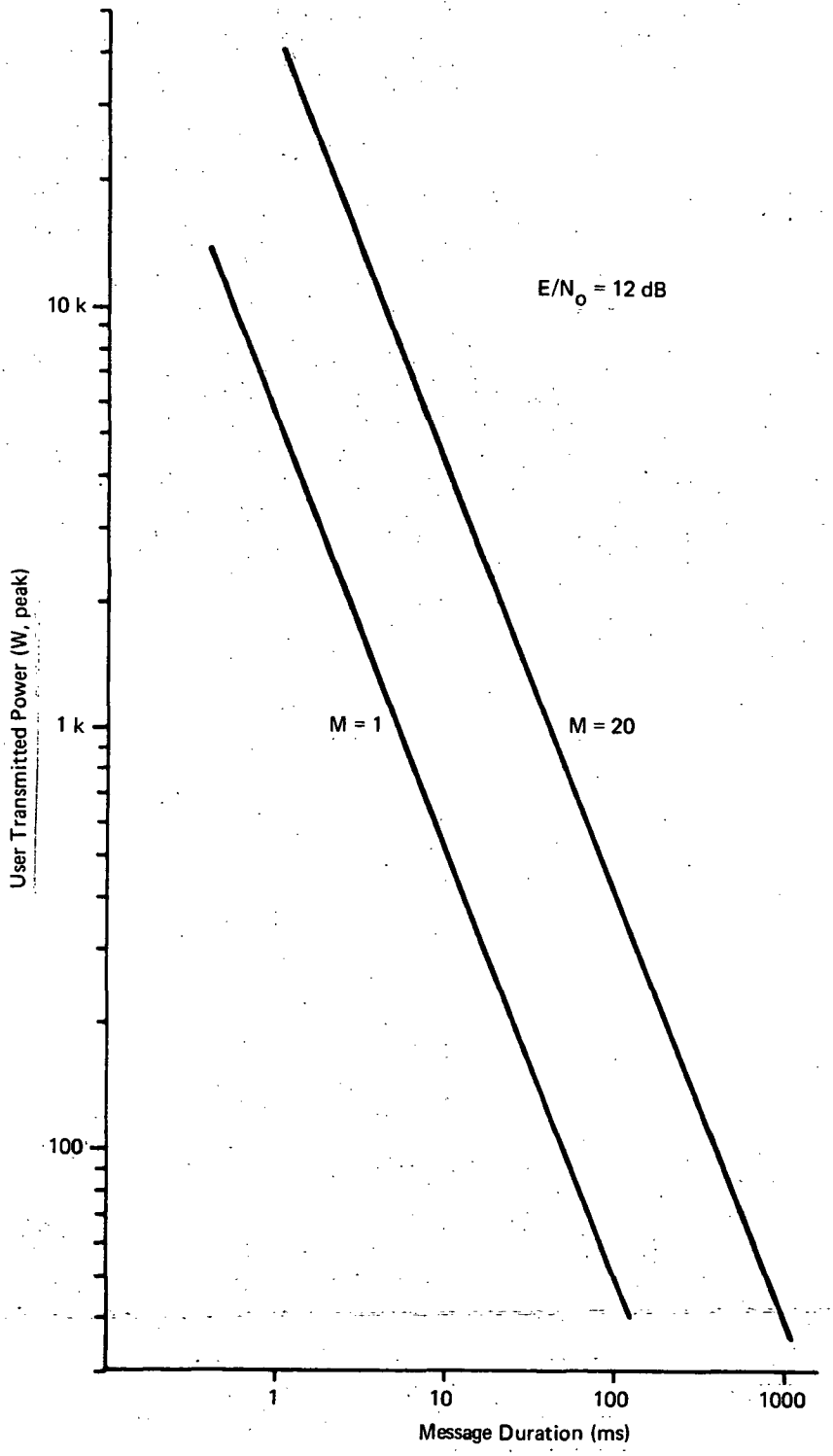

Figure 2-25. User Power Requirements Configuration III TDMA

2.6.6.1 CONUS Beam

Assume a sequential polling signal being transmitted on a CONUS coverage beam to all the users in the system. The interrogation points are spaced by a time interval determined by the area of coverage, A_T, the interrogation scan time, T_u, and the message length T_i. To generalize the results we let

$$T_i = MT_D \tag{2-44}$$

where M is the number of bits per message and T_D is the bit duration.

The users in each range-cell are divided into K groups, each containing R users. Within each group, each user is assigned a different response code. Each polling interrogation point keys responses from all the users in one group. If N_M is the number of users that can be interrogated using TDMA with an optimum range-cell procedure, it allows the system to interrogate $N_M \times R_c$ users per scan. The clutter which results from multiple responses is overcome by the signal processing gain obtained from pulse-compression. It is noted that since no assumption of a uniform distribution of users among range cells is made, the number of groups, K, will vary from cell to cell depending upon the level of cell occupancy. Some cells may have less than R_c users. In general, a cell will have K - 1 groups of R_c users, and one incomplete group. For simplicity we assume an integral number of groups. It is noted that this method requires that as a user moves from cell to cell both his response code and his interrogation point are changed by control center signaling.

We are interested in determining the bandwidth efficiency and user power requirement for this approach. Assume that the total channel bandwidth is B_T. Then the signal processing gain (PG) achieved by pulse compression is

$$PG = B_T T_D \tag{2-45}$$

The processing gain required is determined by the clutter level. If the R_c users who respond to a given interrogation are randomly distributed over the cell (because of the relatively small cell size this is a reasonable assumption), then the response pulses at the receiver occur at random times in an interval $\tau + T_i$, where $\tau + T_i$ is the spacing between interrogations. The expected number of overlapping pulses is (with some simplifying assumptions)

$$E\left[\text{overlapped pulses}\right] = \frac{R_c T_i}{\tau + T_i} \tag{2-46}$$

For a margin of safety, we allow three times this number of simultaneous pulses to occur. Allowing a 13-dB signal to clutter margin, we can then write the required signal processing gain as

$$(PG)_{req} = \frac{3 \times 20 \times R_c T_i}{\tau + T_i} \tag{2-47}$$

Equating the required processing gain to the available gain, we have

$$B_T T_D = \frac{60 R_c T_i}{\tau + T_i} \pi \tag{2-48}$$

Using Equation 2-44 and noting that the total number of users $N = N_M R_c$, this becomes

$$B_T = \frac{60 NM}{N_M (\tau + T_i)} \tag{2-49}$$

The system bandwidth efficiency, expressed in users per MHz, is then

$$\frac{N}{B_T} \times 10^6 = \frac{NM (\tau + T_i)}{60 M} \tag{2-50}$$

The user pulse power requirement for this method is found as follows. Assuming a 20-dB desired E/N_o, we have

$$\frac{E}{N_o} = \frac{P_r T_D}{N_o} = 100 \tag{2-51}$$

where P_r is the received power. Since, with the given link assumptions, we have

$$\frac{P_r}{N_o} = 4000 T_{xp} \tag{2-52}$$

then

$$T_{xp} = (40 T_b)^{-1} \tag{2-53}$$

Figure-of-merit Equations 2-47, 2-49, and 2-53 can be used to calculate a figure-of-merit corresponding to that used in the analysis of Configuration I:

$$Q = T_{xp}\, B_T \times PG$$

$$= 3 \left[\frac{M\, R_c}{\tau + T_i} \right]^2 \qquad (2\text{-}54)$$

2.6.6.2 CONUS Beam, Multiple Sectors

There are operational advantages which can be put forward in favor of dividing CONUS into a number of sectors, each under the control of a semiautonomous control center. Two advantages which are immediately clear are (1) the number of aircraft under the control of each sector control center is smaller than the CONUS control center, hence the polling signal design is simpler and the ground processing load is reduced over that required for a CONUS system, and (2) there is a close match with the existing ATC system which divides the country into semiautonomous sectors. Previous discussions of satellite approaches to multisector surveillance have generally assumed a multi-beam satellite antenna, with spot beams illuminating each sector. In this subsection we describe and analyze an approach which achieves the operational advantages of multiple sector surveillance, while using a CONUS antenna beam for both uplink and downlink signaling.

Assume that the CONUS area is divided into L equal area sectors. Within each sector a control center transmits an interrogation waveform to the users in that sector. The interrogation signal can be a different long PN code for each sector occupying the same frequency band. Users in each sector acquire the appropriate interrogation signal.

Within each sector, an optimum range-cell polling procedure is followed, with the range cells designed on the basis of an area of coverage equal to A_T/L, where A_T is the total CONUS area. (See Table 2-1 for typical parameters for L = 10.) The users in each sector are thus separated by TDMA and can respond with the same code. There are L codes, one for the users in each sector, and all users respond through the same satellite repeater. The required signal processing gain to overcome clutter with the same assumptions as the preceding section is

$$(PG)_{req} = \frac{60\, L\, T_i}{\tau + T_i} \qquad (2\text{-}55)$$

and the available processing gain is given by Equation 2-45. Therefore, we have in this case,

$$B_T\, T_D = \frac{60\, L\, T_i}{\tau + T_i} \qquad (2\text{-}56)$$

and since $N = N_M L$ (where N_M is now maximized over the reduced area), and $T_i = MT_D$,

$$B_T = \frac{60\ NM}{N_M (\tau + T_i)} \tag{2-57}$$

This is identical in form to Equation 2-49 except that the same assumptions of T_u and T_i will result in different performance because of the difference in sector area. Equation 2-50 for bandwidth efficiency is also valid for this case, as is Equation 2-53. The expression for the system figure-of-merit is

$$Q = 3\left(\frac{ML}{\tau + T_i}\right)^2 \tag{2-58}$$

2.6.6.3 CONUS Beam, No Range Cells

The third TDMA/CDMA hybrid to be considered is constructed by dividing all the users over the system coverage area (CONUS) into P groups, each containing R_c users. Within each group R_c response codes are assigned. The code assignments and group breakdown are permanent, and are independent of user position. A single interrogation waveform contains interrogation points spaced by the two-way propagation delay across the entire coverage area. For CONUS, this is about 30 ms. Each interrogation keys responses from all the users in one group, hence P interrogations are required for a complete scan.

The analysis depends upon the assumption that all the users in each group are randomly distributed over the system coverage area. Then, the R_c response pulses from each group will occur at the receiver at random times over a 30-ms interval. By a derivation similar to that used in the preceding sections, it can be shown that

$$B_T T_D = \frac{60\ R_c\ T_i}{\tau + T_i} \tag{2-59}$$

whence

$$B_T = \frac{60\ MR_c}{\tau + T_i}$$

$$= \frac{60\ MN}{P\ (\tau + T_i)} \tag{2-60}$$

since $N = PR_c$. In this case there is a simple relationship between P and the scan time T_u given by

$$\frac{T_u}{P} = 30 \times 10^{-3} \text{ second}$$

and therefore,

$$B_T = \frac{1.8\ MN}{T_u\ (\tau + T_i)} \tag{2-61}$$

The bandwidth efficiency is then

$$\frac{N}{B_T} \times 10^6 = \frac{T_u\ (\tau + T_i)}{1.8\ M} \times 10^6 \tag{2-62}$$

2.6.7 COMPARISON AND DISCUSSION

The multiple-access methods discussed in this subsection are compared on the basis of bandwidth efficiency, required signal processing gain, and user transmitted power. A discussion is given of implementation feasibility and operational factors.

In Table 2-6 the comparison parameters are elevated for each method under the following assumptions:

1) $T_u = 1$ second
2) $T_i = 10^{-5}$ second (where applicable)
3) $M = 1$ bit per transmission
4) $N_M = 270$ (from Table 2.1).

In constructing the table, the methods that incorporate TDMA were analyzed under the assumption of an optimum range cell polling procedure (except, of course, TDMA/CDMA Method 3). The assumed restriction that the ranging signal bandwidth cannot be less than 10^7 Hz was also observed where applicable.

2.6.7.1 Bandwidth Efficiency

As has already been noted, the bandwidth efficiency of methods that use TDMA without any element of code division is low, and is fixed by the polling procedure. In the cases of CDMA and CDMA/FDMA, the dependence of the bandwidth efficiency upon N arises from the assumption of fixed bandwidth, with additional users being accommodated by code division up to the limit of the available signal processing gain. The factor of two which separates TDMA/CDMA Method 3 from Methods 1 and 2 is a result of the fact that Method 3 does not use range-cell polling. The loss in efficiency in the use of range-cell polling results from the extra delays incurred in moving from cell to cell and the fact that the number of cells is approximately equal to the number of users (see Subsection 2.1.3).

Table 2-6

EVALUATION OF COMPARISON PARAMETERS

Method	Bandwidth Efficiency (users/MHz)	Processing Gain Required	User Peak Power (W)
TDMA^{+}	27	1	500
FDMA*	0.5	1	0.005
CDMA*	0.1 N	20 N	0.025
FDMA/CDMA*	0.1 N/R_F	20 N/R_F	0.025
FDMA/TDMA^{+}	27	1	500
TDMA/CDMA^{+} 1.	8350	1.2 N $\times 10^{-3}$$^{++}$	2500
TDMA/CDMA^{+} 2.	8150	1.22 $\times 10^{-3}$$^{++}$	2500
TDMA/CDMA^{+} 3.	16,650	0.60 N $\times 10^{-3}$$^{++}$	2500

*Continuous transmission and bandwidth fixed by ranging requirements

$^{+}$Pulse transmission, $T_i = 10^{-5}$ seconds

$^{++}$cf. Equations 2-47 through 2-49

2.6.7.2 Processing Gain

To clarify the implications of the processing gain requirements, Table 2-7 shows the values for $N = 10^5$ for those methods that use code division. This table also shows the number of codes required to accommodate these many users, which is a significant parameter in CDMA methods.

Table 2-7

PROCESSING GAIN

Method	Processing Gain Required $N = 10^5$ (dB)	Number of Codes Required
CDMA	56	10^5
FDMA/CDMA	56 - 10 log R_F	$10^5/R_F$
TDMA/CDMA 1.	21	370
TDMA/CDMA 2.	21	L (= No. of sectors)
TDMA/CDMA 3.	18	3000

2.6.7.3 User Power

Under the above set of parameter assumptions, the required user peak power is the same for all methods which incorporate TDMA without CDMA. In CDMA/TDMA hybrids there is a 7 dB increase in the required power to reflect the fact that the signal to thermal noise ratio is increased to 20 dB in order that the signal-to-clutter ratio be the determining factor in error performance. FDMA, CDMA, and their hybrid have continuous low power requirements. The average power is comparable in all cases.

Based on the data summarized in Tables 2-6 and 2-7 some preliminary conclusions can be drawn concerning the relative merits of the methods considered.

TDMA, FDMA, and their hybrid (TDMA/FDMA) are low in bandwidth utilization relative to the other methods. Pure CDMA requires unrealizable signal processing gain for a reasonable numbers of users. This problem is alleviated in the FDMA/CDMA hybrid, but at the cost of excessive bandwidth. The best bandwidth utilization is achieved by the TDMA/CDMA hybrid, particularly Method 3. The processing gains required in all three methods are realizable. The number of codes is, however, very high for Method 3, and quite high for Method 1. Method 2 requires only as many response codes as there are sectors, typically ten.

Based on these observations, it is concluded that the TDMA/CDMA hybrid as described in this subsection is the most attractive candidate, particularly in the Method 2 realization. Methods 1 and 3 cannot be dismissed, however, without further investigation of the code design and selection problem.

2.7 CONFIGURATION IV ANALYSIS

The distinguishing feature of Configuration IV is that it implements a surveillance system using only a single satellite. Position location using only one satellite can only be done by the use of multiple, spaced antennas and interferometry techniques. With a two-dimensional antenna array an interferometer can locate a user in two dimensions with an accuracy of about 1 km. Altitude data must be measured by an on-board altimeter and the reading transmitted to the ground on the same signal that is used for interferometer measurements.

The principles of interferometer position location have been described in some detail elsewhere (Reference 10). The significant features for the purposes of the present multiple access study are as follows:

1) Position location accuracy is essentially independent of the signal frequency, and is dependent upon antenna separation. Using a maximum separation of 250 ft, an accuracy of 1 km requires a receiver E/N_o of about 36 dB.

2) Altimeter data and user identification (when required) must be transmitted on the ranging signal.

3) The use of pseudo-random signaling for interferometer has not been investigated in detail. In this report we consider only FDMA, TDMA, and their hybrid, both with elicited and autonomous signaling.

Since only a single satellite is used, the polling considerations discussed for Configuration I apply to this case directly. Range-ordered polling for the elicited-response case is assumed, thus negligible guard time is allowed between successive responses in TDMA.

The principal operational differences between interferometer position location and the other methods considered are the relatively low accuracy, the two-dimensional limitation, and the high E/N required to achieve the 1 km accuracy.

In the calculation of parameters for various multiple-access methods we assume a scan time, T_u, of 1 second, a 40-bit transmission for altitude and ID, with a probability of error of 10^{-5}. This is exceeded if a 36 dB E/N_o is achieved, where E is the total energy in the 40-bit transmission. We also assume a 6 kHz minimum bandwidth per user to allow for Doppler effect and oscillator instabilities, regardless of the actual data rate.

The results of the multiple-access analysis are given in Appendix F, Tables F-1 through F-5.

As in the other configurations, it is clear that multiple-access using autonomous TDMA requires an excessive amount of bandwidth to achieve the desired low probability of overlap (10^{-5}), and also requires unworkably large amounts of user power to obtain satisfactory measurements with the required short transmission times. Pure FDMA without Doppler drift correction has a low bandwidth efficiency and requires on the order of 600 MHz to accommodate 10^5 users. Pure elicited-response TDMA has a high bandwidth efficiency, but the power requirements are very high (100 kW for 10^5 users.

The most promising approach lies in the elicited TDMA/FDMA hybrid which represents a compromise solution between excessive bandwidth and excessive power. For example, with channelization into 100 channels 10^5 users can be accommodated in 46 MHz of bandwidth at a transmitted power level of 1000 W.

2.8 SUMMARY AND CONCLUSIONS

The use of satellite technology in future ATC systems appears certain. The variety of possible satellite ATC systems, although not specifically enumerated herein, were referred to by inference and obviously are limited only by the imagination of system engineers. Since each alternative provides different levels and categories of service and involves different assumptions, the question naturally arises as to whether there exists any general method of classifying and evaluating, in a total resource cost fashion, the performance of ATC candidates. The results of this study effort provides at least a partial answer to this question. Both communications and position location techniques have been classified so as to emphasize fundamental technique trade-offs. In this section the major communications design decisions have been identified. To assure that no significant alternatives were overlooked, general satellite configurations which would be necessary to support various position locations schemes were postulated and investigated on the basis of the impact on attendant communications requirements. Collected in this single report is a uniform evaluation of major design alternatives pertinent to communications performance, namely,

1) The polling technique
2) The multiple access technique
3) The range measurement technique
4) The modulation technique.

As was indicated in the text, perhaps the most fundamental trade-off exists between the selection of polling/multiple access pairs. This design decision has the most significant effect on the utilization of the basic resources of spectrum bandwidth, uses transmitter power, and required processing gain. In those configurations requiring range measurements to support position location, it was shown that considerable design flexibility in supporting the surveillance function is lost, when compared with system design in which the functions of position location and reporting are independent.

In the course of the study, a figure-of-merit, Q, was defined as a means of indicating the utilization of transmitter power, bandwidth, and processing gain. Additionally a uniform analytical procedure ensures that all candidates are evaluated equally. On this basis, general approaches to satellite ATC systems have been selected for further study. For comparison, the well-known concepts of LIT (location identification transmitter) and Woodford have also been analyzed for Q performance.

The chief benefits of the study lie not only in the identification of promising candidates but in the interpretation of the results and the observation of general trends accompanying design alternatives illustrated, e.g., in subsection 2.4.1 Noting that Q varies as N^2 (N equals the total number of users to be supported by the system) for

all candidates excepting those that employ frequency division multiplex, which vary only as N, is a strong indication that this conventional approach to channelization for tactical systems, may yet be valid. As a summary to this section we will conclude by presenting those basic system approaches which merit further consideration. A brief summary description of the LIT and Woodford approaches will be presented first.

2.8.1 IDENTIFICATION AND DESCRIPTION OF PREVIOUSLY PUBLISHED TECHNIQUES

2.8.1.1 Woodford (Reference 11)

The Woodford system uses three satellites in inclined synchronous orbits. It is essentially a scheme for surveillance by two-way ranging. The ground control center transmits continuous data and common-timing waveform interrogation signals through the three satellites to the users. A separate 1-Mb/s data stream is sent through each satellite, thus a total of 3 Mb/s is sent. The binary data in each signal is modulated onto a 10-megachip/s pseudo-random sequence. Since 10^5 users are serviced, 30 bits/s is transmitted from the ground to each user.

Each user receives and demodulates all the data from one of the satellites. All data except that addressed to him is discarded. In addition to data reception, the received signal is used to time-synchronize a 10-megachip/s pseudo-random sequence which is generated by the user and returned through all three satellites to ground. This roundtrip synchronization permits two-way range measurements to be made by the ground station.

All the users transmit continuously through all three satellites. The separation of these signals at the ground station is done by a combination of space division (multiple antenna beams), frequency division, and code division. Each satellite receives user signals on three separate antenna beams and on four frequency channels in each beam. With 10^5 users, this arrangement provides 12 separate channels each of which is used simultaneously by about 10^4 users. Within each channel signal separation is by code division with an integration time of 0.1 second, giving a signal processing gain of 10^6. A 20-dB signal to interference ratio is thus theoretically achieved.

The Woodford system provides surveillance position fixed with an rms error of about 100 ft from all error sources. The position update rate is once per second in high-density areas and one per 3 seconds, otherwise. Velocity measurements are made by Doppler techniques to an accuracy of about 1 ft/s. The bandwidth requirements is about 10 MHz at L-band for the user to satellite uplink signaling.

This system is essentially a Configuration III elicited-response polled system using hybrid FDMA/CDMA multiple access and common timing waveform interrogation. As mentioned in Subsection 2.6.4, the multiple access analysis is the same as that for a Configuration II system, and is given by the data of Table E-5, Appendix E, with appropriate modification to account both for Woodford's use of three antenna beams and for the allowance for a 10 bit/s user-to-satellite data transmission rate.

As has been discussed in Subsection 2.7, this communication method is not a recommended candidate because of the 60 dB of processing gain that must be achieved by the ground receiver.

2.8.1.2 LIT (Location Identification Transmitter) Surveillance

The LIT surveillance concept is based upon the idea of minimizing the cost of the user equipment. The user instrumented only for surveillance carries a transmitter, but no receiver. The transmitter sends a pulsed, periodic signal through four satellites to the control center, where the time-of-arrival differences are used for hyperbolic position location. These signals are generated autonomously by each user.

All the users transmit in a common frequency channel, with multiple access by code division and time division. LIT is a Configuration II system with autonomous reporting and CDMA/TDMA multiple access. To serve 10^5 users with a signal-to-clutter ratio of 13 dB, the required processing gain is given by (see Table E-6, Appendix E)

$$PG = (SNR)_C \times 3 \times \frac{N}{R_T}$$

Since the LIT transmission uses a 51.1-μs pulse,

$$R_T = 20 \times 10^3, \quad \frac{N}{R_T} = 5,$$

and

$$PG = 25 \text{ dB}$$

We have made the assumption that the number of simultaneous users to be overcome by code division is three times the number expected on the basis of random distribution.

The LIT system designers have recognized the difficulty of assigning a different orthogonal 511 bit code to each of 10^5 users. To solve this problem, the number of users is divided into a number of groups (15-20). All the users in a group transmit the same code, but each transmits with a slightly different pulse period. The assignment periods range in 10-μs increments from 1.0 to 1.1 seconds. From the multiple outputs of each code matched filter, the individual user signals are identified by synchronizing with each pulse repetition rate.

By extrapolation of the data in Table E-6, Appendix E, it can be seen that for $R_T = 20 \times 10^3$ the required user transmitted power, $T_{xp} = 500$ W for the postulated link. (The LIT design actually provides about 2 kW of pulse power as a result of slightly more stringent assumptions about the link parameters, and the provision of operating margin).

2.8.2 RECOMMENDED COMMUNICATION TECHNIQUES FOR FURTHER STUDY

The systematic approach taken to the analysis of candidate communication techniques in this section has been comprehensive in the sense that all possible approaches to multiple-access and polling have been considered, given the framework of the four basic satellite configurations. The intention has not been to select a single technique as having overall superiority, but to gain sufficient insight to make a first-level selection, from all the techniques considered, of those which are clearly unreasonable in the demands that they make upon the basic system resources of power, bandwidth, and signal processing gain. Those candidates that remain are considered suitable for further study as part of an overall satellite-based ATC system. To summarize the results, these selected candidates will be listed and briefly discussed.

2.8.2.1 Configuration I

The principal feature of Configuration I is its ability to use narrowband signals. This is because the satellite-to-ground link carries only data, rather than signals on which time-of-arrival measurements are to be made. Of the 12 candidates considered, two are considered suitable. These are elicited-response TDMA/FDMA, (E-TDMA/FDMA) and FDMA, both autonomous signaling and elicited-responses (E&A FDMA).

2.8.2.1.1 E&A FDMA

Each user in this system is assigned a separate narrowband channel over which he continuously transmits binary data representing the processed satellite navigation signals. The total user bandwidth requirement for transmission of this data is 100 Hz. Thus, the total system bandwidth is 10 MHz for 10^5 users. The feasibility of this approach depends upon the correction for Doppler frequency uncertaintly, which is in the 6 kHz range. If Doppler correction cannot reasonably be applied, the required system bandwidth goes up by a factor of 60, which exceeds the bandwidth that can be considered available for the system. A second possible drawback is the requirement to implement 10^5 separate ground receivers.

2.8.2.1.2 E-TDMA/FDMA

The difficulties encountered in implementing the pure FDMA approach in Configuration I can be alleviated by the introduction of an element of time-division into the multiple access. Range-ordered polling using discrete address interrogation is used to elicit responses sequentially from groups of users in separate frequency channels. The time-sharing of channels permits a more coarse channelization than in pure FDMA, and removes the stability problem of very narrowband signaling. The number of ground receivers is reduced. The user set must, however, incorporate a receiver with address-recognition ability so that the response can be made to the interrogation waveform.

A general conclusion regarding Configuration I communication techniques is that when narrowband signaling is possible, it results in higher bandwidth efficiency than code division for multiple-access, as is clear from the tables of Appendix A.

2.8.2.2 Configuration II

The principal feature distinguishing Configurations II and III from Configuration I is that time-of-arrival measurements must be made on the transmitted signal, which must therefore be relatively wideband. This requirement eliminates the advantage gained by narrowband signaling in Configuration I, and CDMA becomes preferred over FDMA in hybrids with TDMA.

2.8.2.1.3 A-TDMA/CDMA

Of all techniques considered under Configuration II, this technique proves to be the only one which is reasonable in its demand upon system resources. It is typified by the LIT surveillance system, and features autonomous pulsed signaling by all users in the same frequency band, with signal separation by code division.

Operationally, a significant advantage of this approach is that the user requires no receiver, and only an inexpensive transmitter. The autonomy of operation imposes the requirement for hyperbolic position location, with its GDOP deterioration relative to trilateration.

2.8.2.3 Configuration III

2.8.2.3.1 E-TDMA/CDMA

The elicited responses of Configuration III are limited in pure TDMA by the polling restrictions discussed in Subsection 2.3. A single frequency channel cannot be fully utilized with TDMA, and additional users are added by code division to increase the bandwidth efficiency of the system. A pure TDMA system of this general type is described in Reference 12, Appendix V, although the polling limitations were not at that time systematically explored and the potential bandwidth efficiency of the hybrid approach was not realized.

The range-cell polling approach, which was first described in Reference 12, gives this system considerable flexibility as shown by the three approaches described in Subsection 2.3. Operational desirability is further enhanced by its use of trilateration for position location.

2.8.2.4 Configuration IV

Surveillance systems using a single-satellite (interferometer) position location differ fundamentally from multisatellite systems in (1) being unable to locate the user in three dimensions, hence being dependent upon pressure altimeter data, and (2) being restricted in accuracy to the order of 1 km, rather than the 100 ft range achieved by multisatellite position location.

The single-satellite signaling path bears strong similarities with Configuration I in allowing range-ordered polling and narrowband signaling. FDMA systems are feasible, with the most desirable multiple access approach being TDMA/FDMA hybrid. CDMA signaling was not investigated for this configuration, but the same arguments that lead to its rejection in Configuration I can in general be applied. Further study of interferometer signaling methods is needed.

2.8.3 COMPARISON OF RECOMMENDED SYSTEMS

In this subsection we present and discuss comparative data on the five recommended polling and multiple-access techniques. The comparison is relative to the following set of primary criteria:

1) Bandwidth efficiency (users/MHz)
2) User transmitted power
3) Satellite power for polling
4) Signal processing gain required.

The comparison data assumes 10^5 simultaneous users for each system, and makes certain other assumptions regarding the specific configurations of each system. These assumptions are listed below with pertinent discussions. The basic comparison data is given in Table 2-8. This table also includes the same data for the surveillance portion of the LIT and Woodford systems. They are assumed to be operating with the same communication link and signal-to-noise margins in order to provide a common basis for comparison.

2.8.3.1 Configuration I — A-FDMA

As has been mentioned previously, the principal difficulty with realizing pure FDMA in Configuration I is that each user must occupy a band of only 100 Hz. This requires continuous Doppler correction, and may be difficult to implement economically. In Table 2-8 two figures are given for bandwidth efficiency. The larger number assumes that the 100-Hz-per-user bandwidth is realized, and the smaller assumes that each user is allotted 6 kHz of bandwidth to allow for Doppler uncertainty and oscillator instability. The reduction in efficiency is sufficient to eliminate the second case from serious consideration. An attractive feature of this basic approach is the low peak power requirement and relatively simple user sets.

Table 2-8

COMPARISON DATA FOR SURVEILLANCE COMMUNICATION TECHNIQUES

Method	Bandwidth Efficiency	T_{xp} (W)		P_{sat} (W)	PG (dB)	Q
		Peak	Avg.			
CI A-FDMA	10^4 assuming Doppler correction 168 otherwise	0.5	0.5	0	0	5×10^6 3×10^8
CI E-TDMA FDMA (R_F = 1000)	10^4	50	0.5	15	0	5×10^8
CII A = TDMA CDMA (R_T = 20,000)	10^4	500	0.025	0	25	1.5×10^{12}
LIT	10^4	500	0.025	0	25	1.5×10^{12}
CIII E-TDMA CDMA 1. ($T_i = 10^{-5}$ s)	8350	2500	0.025	200	28	1.8×10^{12}
CIII E-TDMA CDMA 2.	8150	2500	0.025	200	28	1.86×10^{12}
CIII E-TDMA CDMA 3.	16,650	2500	0.025	200	22	0.9×10^{12}
Woodford	2.5×10^3	0.25	0.25	5000	60	2×10^{17}
CIV E-FDMA TDMA R_F = 1000)	10^4	100	10	15	0	10^9

2.8.3.2 Configuration I-E-TDMA/FDMA

Channelization of the spectrum and the use of TDMA with elicited responses within each channel eases the difficulties associated with very narrowband signaling. The figures shown assume 1000 frequency channels, each supporting 100 users operating in a TDMA mode. The satellite power given assumes that discrete-address range-ordered polling is used. This is a worst-case, since there are several approaches that can be used to simplify the polling procedure. First, the use of a coarse range-cell configuration (see Subsection 2.3) with perhaps six cells permits nonrange-ordered polling within each cell with about 5 ms guard time. Each user transmission takes 10 ms, thus the efficiency is reduced by 50%. This reduction is the cost of simplifying the ground processing by eliminating the need for range-ordering the users at every scan.

A second simplification results from noting that users in different frequency channels can have the same address. Each interrogation address can therefore key responses from up to 1000 users, with a corresponding reduction in satellite power.

Finally, we note that the basic channel bandwidth in this case is 10 kHz. The reduction in capacity incurred by allowing a margin for Doppler is much less severe than in pure FDMA.

2.8.3.3 CII A-TDMA/CDMA

The basic configuration of this system is similar to that of the LIT system. Twenty-thousand time slots are assumed, (i.e., a 50 μs pulse length). The processing gain required assumes that three times the average number of overlapping pulses are allowed for, assuming random user distribution.

It is noted that although the transmission time per user is reduced by a factor of 200 from the CI TDMA/FDMA system, the required pulse power only increases by a factor of ten because this system sends only one bit of data per transmission.

2.8.3.4 CIII E-TDMA/CDMA, 1, 2, and 3

The basic assumptions for these three methods is a 10^{-5} second response pulse and one bit of information per transmission. These approaches have been discussed and compared in subsection 2.6.7. They differ primarily in the polling method used. In general they have, relative to the others, considered lower bandwidth efficiency and higher user pulse power requirements, because of the short pulse length. The pulse can be lengthened only at a reduction in bandwidth efficiency. They use higher satellite polling power to allow for the interrogation point updates which are required with range cell polling.

2.8.3.5 CIV E-TDMA/FDMA

The system evaluated assumes 1000 channels of 10 kHz bandwidth. This approach combines high bandwidth efficiency with moderate user power and low-satellite polling power. The same polling simplifications discussed above under CI-TDMA (FDMA) can be applied. The advantages of this system are purchased at a cost in position location accuracy relative to the multisatellite configuration.

2.8.4 OPERATIONAL FACTORS

In addition to the strictly technical criteria of Table 2-8, comparison of the recommended approaches should also consider certain operational factors.

An important point is the essential difference between autonomous and elicited systems. An elicited system has the intrinsic ability to return data to any user by

way of the polling waveform. In an autonomous system such a data path must be provided separately if collision avoidance is to be implemented for all users, and the additional cost to the user for this communication capability offsets the principal advantage of an autonomous system, which is low cost to the user. Elicited systems, while inherently more flexible, demand considerable total satellite-to-user data capacity depending upon the information content of the polling message. Hybrid autonomous/elicited systems may provide a viable compromise wherein elicited responses are used only in conflict situations.

Configuration I implies that the user is performing at least some processing and storage of the navigation data received from the navigation satellites, or other source (e.g., OMEGA).

This further implies some additional cost to the user although the polling and response function which take place through the response satellite can be implemented using relatively unsophisticated narrowband user hardware. The cost of processing and storage of time-of-arrival data could offset the advantage of user set simplicity obtained by narrowband signaling.

Except for Configuration IV, the position location accuracy performance of all configurations is roughly equivalent. Section 3 of this report analyzes this aspect of system capability in detail.

The question of the desirability of a single central control center compared to a decentralized system with a number of control centers controlling various sectors of the country is not one that is specifically addressed by this report. It seems apparent, however, that autonomous reporting lends itself to a central control, whereas elicited-response systems are more adaptible to the requirements of multiple sectors. This is particularly true of Configuration III, in which (see subsection 2.4) the flexibility of range-cell polling, together with CDMA, permits the simulation of a multiple-beam sector system using a simple CONUS Beam antenna.

2.8.5 DISCUSSION

Table 2-8 gives the basic trade-off data for the surveillance communication techniques selected from the wide range of possible techniques considered. The selection was based upon the achievement of reasonable values in each of the comparison criteria when implemented with 10^5 simultaneous users. Although the number of candidates was thereby significantly reduced, those remaining represent a broad spectrum of possibilities for specific systems.

The figure-of-merit, Q, is a convenient measure of overall use of the basic system resources of power, bandwidth, and signal processing gain, all of which have bounds which cannot reasonably be exceeded. This measure clearly shows the desirability of

the narrowband techniques that are possible in Configurations I and IV. The need for additional bandwidth to transmit ranging signals in Configurations II and III is the principal factor which causes Q to increase for these techniques. The signal-processing gain required by the Woodford system results in a Q four orders of magnitude greater than the worst of the recommended alternatives.

To pursue the development of satellite-based surveillance, future effort should concentrate upon further evaluation and comparison of the candidate systems represented by Table 2-8. Several specific steps should be taken, such as

1) Detailed design of a specific system representative of each candidate

2) Evaluation of the resulting systems relative both to the criteria of Table 2-8 and such additional operational criteria as necessary. Specific additional criteria of prime importance are user hardware requirements, satellite design requirements, position location performance, relative weighting factors, and additional consideration of the satellite to user link design.

3) Merging the surveillance communication system with an area navigation system to provide full capability.

Section 3

SURVEILLANCE/NAVIGATION ACCURACY PARAMETRIC ANALYSIS

Section 3

SURVEILLANCE/NAVIGATION ACCURACY PARAMETRIC ANALYSIS

3.1 INTRODUCTION

The purpose of this section is to provide a parametric error analysis of the four surveillance/navigation concepts given in Table 3-1.

Table 3-1

SURVEILLANCE/NAVIGATION CONCEPTS

Name	Description	Representative System
3P	Three range difference	621B
2P+H	Two range difference plus Altitude	—
3R	Three range	IBM (Fourth generation ATC proposed)
2R+H	Two range plus altitude	PLACE

P is defined as the range difference between two known points and an unknown (the navigator); i.e., $P = R_1 - R_0$. One possible implementation is to measure R_1 and R_0 separately via one way transmission. However, by doing so, a false geometric range is embedded in the measurement which is caused by a difference in the time reference between the transmitting and receiving systems. Since the false geometric range is common to both R_1 and R_0, the differencing operation removes this false range. However, it can be shown that instead of differencing R_1 and R_0, a different algorithm can be written which not only solves for the navigator's position but also for the false range, which is equivalent to solving for the reference time difference. The navigator's position accuracy is not affected by the choice of algorithm. Therefore, though referred to in this report as the 3P concept, the reader should understand that there are two choices of implementing the 3P system depending primarily on whether there is any advantage to solving for the time bias between transmitter and receiver.

The sources of error affecting the accuracy of these concepts include

1) Random errors — range, range difference, and altitude
2) Bias errors — range, range rate, and altitude rates

3) Ionospheric refraction — time and space correlations modeled

4) Satellite ephemeris — position and velocity with spatial and time correlations.

The following three types of positions fix accuracy were investigated (see Figure 3-1):

1) Absolute — position fix relative to the satellite support system

2) Relative — position fix relative to a local earth surface system; e.g., an airport

3) Resolution — distance between two aircraft in close proximity; i.e., less than 10 miles.

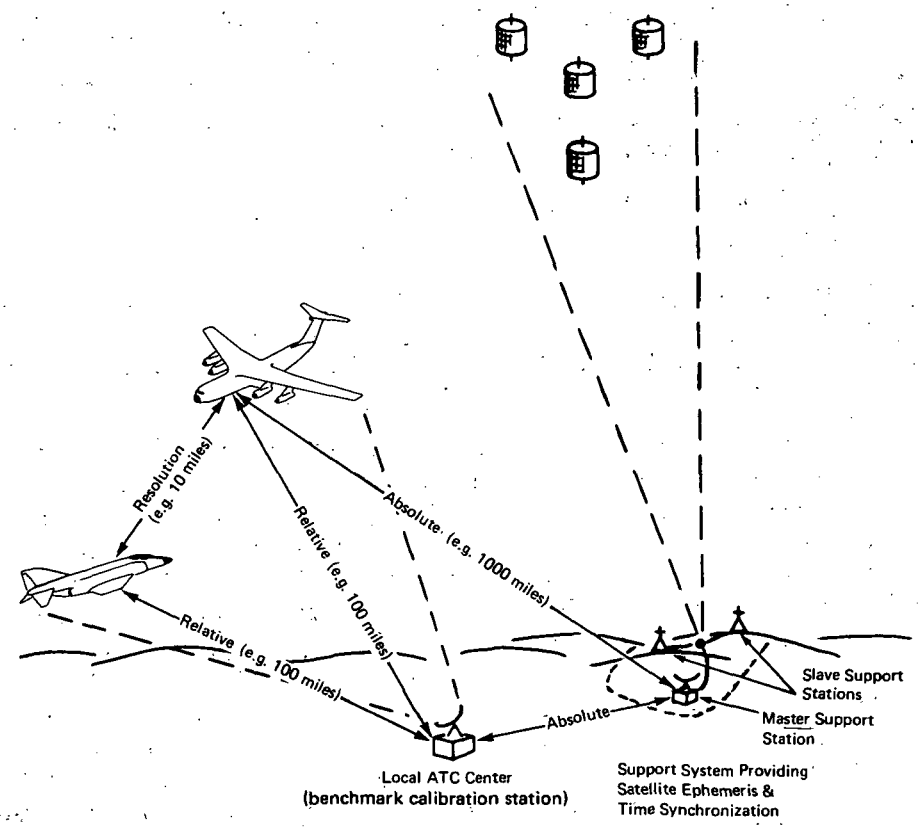

Figure 3-1. Pictorial Representation of Absolute, Relative, and Resolution Frames of Reference

The accuracy of all concepts is highly geometry dependent; that is, for a fixed range measurement error the accuracy of the position fix varies with the location of the user with respect to the satellites. Some concepts are more susceptible to this variation in geometry than others. This geometrical effect is often referred to as geometrical dilution of precision (GDOP). However GDOP is but a small part of the total problem. GDOP gives the effect on each component of the users position, (i.e., east, north, and vertical), to each and every source of error listed above. Even if all errors could be treated as either statistically independent or perfectly correlated a myriad of numbers would be needed to provide a complete error analysis. When compounded with the added dimension of correlated error sources, a direct assault on the problem would produce an unwieldy and impractial result.

Therefore, a practical and meaningful condensation was required which did not compromise the primary objective of presenting the results parametrically. In particular, the relative performance of concepts subjected to similar geometries and error models was considered essential.

The presentation of the results is structured to emphasize the relative performances among concepts. For example, the reader can compare the performance of the 3P and 3R systems due to an ionospheric ranging error of 1 ft and that due to an ephemeris error in the same figure. For example, if the ionosphere were a truly homogeneous stationary phenomena one might expect the ionosphere to affect the 3P system less than the 3R system because in the 3P system ranging errors (in this case the ionospheric range errors) common to all transmission paths cancel. However, the ionosphere is not uniform nor stationary and the GDOP is typically several times more for the 3P system than the 3R system. The net result is that the 3P system performance with respect to ionospheric effects is inferior to the 3R system and this will be evident from data presented in the same figure.

All results have been normalized; no judgements or conclusions have been reached with regards to the magnitude of each error source because this would necessarily imply a certain bandwidth, transmission frequency, etc. Rather, the reader may select the proper normalized results, apply the proper magnitude of error his design warrants and then combine everything for a total system error.

3.2 DEFINITION AND GENERAL EXPLANATION OF TERMS FOUND IN RESULTS

Due to the rather extensive amount of curves and bargraphs it is impractical to discuss each figure individually. Therefore, at the outset, the background information necessary for a proper interpretation will be given. Detailed mathematical explanations have been intentionally avoided in favor of verbal descriptions. Those readers interested in a complete mathematical development are referred to Appendix G.

3.2.1 OUTPUT COORDINATES, TYPES OF ACCURACY (ABSOLUTE, RELATIVE RESOLUTION)

All results are expressed in terms of the user's horizontal position/velocity errors and his vertical position/velocity errors. This reference frame seemed most appropriate in the context of an Air Traffic Control (ATC) system where, on the average, there is no preference for accuracy in a north/south (NS) or east/west (EW) direction. The horizontal error is a composite of the EW and NS components. This combination of EW and NS components also condenses the output; i.e., number of graphs by 30%.

The horizontal error could have been expressed as the rms of the EW and NS components, or as a circular error probable (CEP). CEP was not chosen because when the ratio of the major to the minor axes of the error ellipse exceeds 3 to 1, the CEP indicates a value much smaller than the major axis. For example, let the ratio of the major to minor axes be 10 to 1, with the major axis equal to 1, a very likely condition with some concepts in certain geometries. Then, CEP = 0.68 and rms = 1.005. The rms is always an excellent measure of the major axis (the largest error) whereas the CEP is not. Thus in the context of an ATC system evaluation, the rms must be considered more suitable.

The results may be interpreted in three reference coordinate frames; the absolute, the relative, and the resolution. Figure 3-1 illustrates these three frames pictorially. A complex of ground stations (the support system) locates, time synchronizes, and controls all of the satellites. This function may be a service to the ATC system and not inherently part of it, or it may be an integral part. In either case, all aircraft and local ground stations initially determine their positions with respect to the support system. This position fix is absolute and all errors made by the support system are passed along to all users. The distance between the support system and users may be on the order of several thousand miles, although it could be less. When two users are within several hundred miles there is a tendency to have not only the same errors affecting the position fix but also the same geometry between user and satellites. The position fixes of the two users would tend to be nearly the same under these conditions. A cancellation of the common sources of error is therefore anticipated. The distinction between relative accuracy and resolution is not as well defined. The distinction intended is that, for resolution, all the position errors cancel except those due to purely random errors. When the separation distance is but a few miles; e.g., 10; the resolution value probably applies. At greater distances there are incomplete cancellations because the errors are not exactly the same and the GDOP is somewhat different. Under these conditions the idea of relative accuracy is perhaps most appropriate.

To avoid any confusion in the interpretation, the results are not referred to by frame of reference but rather by error source and whether a benchmark calibration is, or is not, assumed. The final interpretation, based on the separation distance of interest, is left to the reader.

3.2.2 INTERPRETATION OF BENCHMARK CALIBRATION RESULTS

No attempt was made to prejudge the results by assuming that certain error sources had cancelling effects. For example, the ionospheric errors were not assumed to have complete cancellation due to the close proximity of two users, be they two aircraft or an aircraft and a ground control center; i.e., a benchmark calibration station.

The essence of the benchmark calibration is that two users in close proximity are affected by the same error sources, in the same way, and in a similar geometry situation. However, one of the users; i.e., the control center; knows of its location by other means. After computing its position via radio signals any difference between the computed and known positions is attributed to a composite affect of the many error sources and that unique geometry between user and satellites. This difference (a vector) is considered valid over some specified area and any other user in that area is assumed to have been affected in exactly the same way; i.e., the same vector error applies. Therefore the position fixes via radio signals are corrected by the correction vector of the benchmark station. In reality this correction vector is composed of many error sources but to present the results parametrically the composite is broken down into individual sources of error. This approach permits an evaluation of the benchmark calibration technique by error source, and indicates that some error sources may not be as amenable to benchmark calibration as others.

3.2.3 ALTERNATE CALIBRATION TECHNIQUES

Benchmark calibration is not the only practical means of calibration. In fact, a potential weakness to the benchmark calibration is that the benchmark correction vector must closely match the correction vector of any other user. Figure 3-2 is an example which illustrates the potential weakness of benchmark calibration. Here $\overline{D}_{co}$ and $\overline{D}_{ca}$ are of the same magnitude but of different orientation. The result is a sizeable residual calibration error. The reader may visualize a situation where $-\overline{D}_{co}$ is colinear with D_{ca}, in which case the calibration adds twice the position error instead of removing it. The possibility also exists that the benchmark calibration could work better with one error source than another. For example, the ephemeris errors may well be removed by the benchmark calibration, whereas the ionospheric errors may not. If a certain error source; e.g., the ionospheric error; does not respond well to the benchmark correction, an alternative is for the user to make an ionospheric range correction via a model of the ionosphere for each and every transmission path. This correction would eliminate approximately 90% of the ionospheric range error. Then, when the benchmark correction is applied, the ionospheric error effects have been reduced to 10% of their original levels; e.g., in Figure 3-2, the magnitude of $\overline{D}_{co}$ and $\overline{D}_{ca}$ have been reduced 10 times, and hence D_c is also 10 times less.

This calibration technique uses a model of the ionosphere which may require considerable software. For the surveillance function this would appear to be very practical since the model could be shared by thousands of users. However for navigation, the technique may be impractical.

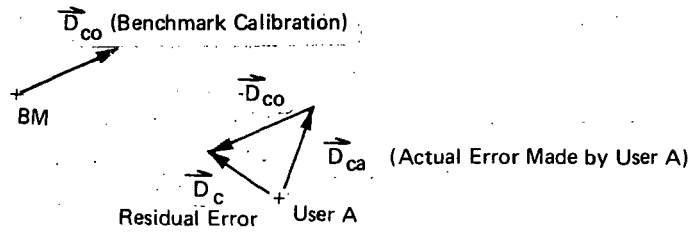

Figure 3-2. Benchmark Calibration Techniques

Another possibility is that employed by the TRANSIT navigation system which uses two carrier frequencies and the fact that ionospheric refraction is inversely proportioned to frequency squared. By measuring the range difference at these two frequencies and using the refraction-frequency relationship the refractive effect is computed and therefore available as a correction. The disadvantage of such an approach in an ATC system is the wider transmission bandwidth required.

3.2.4 DESCRIPTION AND DISCUSSION OF EACH CONCEPT

The discussion thus far applies to all concepts, but before discussing error sources, it might be well to first discuss the position location concepts.

3.2.4.1 3P Concept

Position location is derived from the mutual intersection of three hyperboloids. The foci of these hyperboloids are at the satellites. Figure 3-3 shows a two dimensional representation.

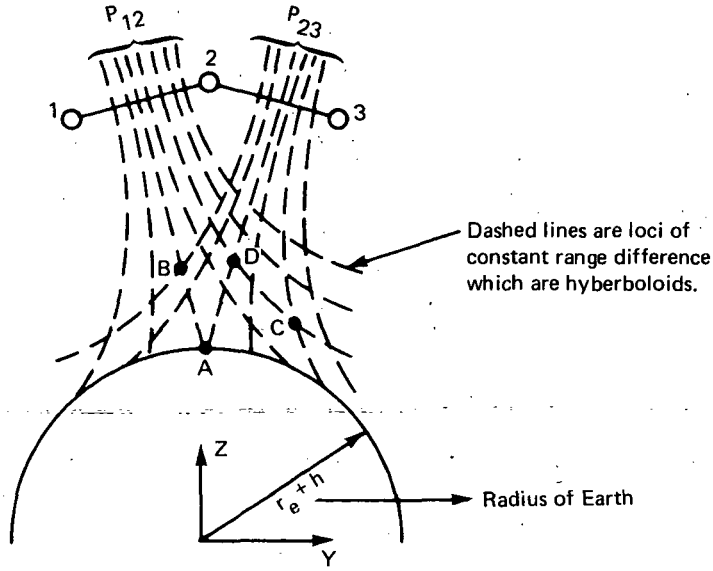

Figure 3-3. Two-Dimensional Pictorial Representation of 3P System

Point A in Figure 3-3 is at the intersection of the two range difference contours that are equal and zero; i.e., point A is equally distant from the three satellites. Point B is at the intersection of two unequal range difference contours. Each intersection defines a unique yz position which is equivalent to a horizontal and vertical position fix. Position errors can occur because

1) The measurement of a range difference yields the wrong contour.

2) The contours are misplaced due to an error in specifying the location of the foci.

Though Figure 3-3 is not drawn to scale the dependence of position error on geometry can be demonstrated. Assume that the contours shown are increments of 1 ft. Further, assume the true position is at A such that $P_{12} = P_{23} = 0$. However, the user measures $P_{23} = -2$ and $P_{12} = 0$. (P being the symbol for range difference.) The user computes his position at B. Notice that most of the error is in the z direction. As another example, assume the true position is at C. The true Ps and $P_{12} = 2$ and $P_{23} = 2$. If the same P error is made the same as the previous example, the measured Ps would be $P_{12} = 2+0 = 2$ and $P_{23} = 2-2 = 0$. The indicated position is at D. Notice that though the vector magnitude of the error is about the same there is considerably more error in the Y direction.

Errors in the location of the foci can be considered as the combination of two effects:

1) If a consistent or systematic error is made in specifying the location of all three foci, the net effect is a translation of the hyperbolas with respect to the earth. This does not change the shape of nor distort the hyperbolas. Nevertheless, this systematic error causes a user's position error. Ephemeris errors of this kind are said to be perfectly correlated and could be caused by errors in the support system which are common to all satellite ephemerides; e.g., location of slave stations with respect to the master.

2) The other extreme, error wise, is if estimates of the satellite locations are randomly errored. This causes a distortion of the hyperbolas. Figure 3-4 illustrates this possibility. The distortion in this case is caused by a spreading or tilting of the baselines.

The user assumes the foci, which are derived from the ephemeris (satellites), to be at 1 and 2 which uniquely specifies the location of all range difference contours on the users map. However, the satellite is actually at 2'. Therefore, when the user measures P = 0 he places himself on the P = 0 contour shown by the solid vertical line. However, to have measured P = 0 the user must have been on the P = 0 contour shown by the dashed vertical line. The important point here is that the location of the foci is critical to the establishment of the correct range difference contours, and hence the users position.

If the foci were in error such that satellite 2 was really at 2" the hyperbolas would be distorted and rotated as shown by the dotted contours.

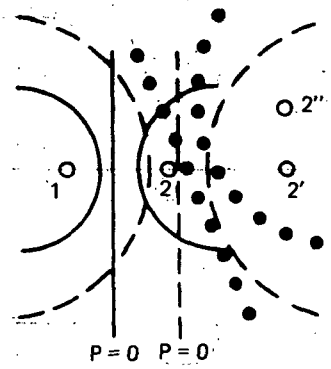

Figure 3-4. Geometrical Description of Ephemeris Error on 3P Position Location

In general case, all three effects may be present; translation, spreading, and rotation. These three effects are statistically embodied in the covariance matrix of satellite ephemeris errors, a $3n \times 3n$ matrix (n = number of satellites).

The reader can visualize the complex interaction of ephemeris errors on position location. More specifically, if four satellites are involved, a complete description of the ephemeris position errors is a 12×12 matrix which has 78 entries (accounts for the symmetry of the covariance matrix and ignores the velocity terms and their interaction with position). The 78 terms are the position variances of each component of each satellite (12 terms) and the covariances of all components with each other (66 terms). A term-by-term breakdown would yield unwieldy results of doubtful value. Nevertheless, the number of terms must be reduced for practical reasons, whereas for the completeness of the analyses all terms should be considered. The problem was resolved as follows:

1) An error ellipsoid is assumed which has the same shape, size, and orientation for all satellites. The ellipsoid can be circular, pancake, or cigar shaped. The choice of shape would depend on how the support system determines the ephemeris. Figure 3-5 shows some typical ellipsoids that could be specified. The assumption of same shape and size stems from an assumption that all satellite ephemerides are determined by a common support system.

2) Each ellipsoid can, in a broad sense, be related to the kind of satellite tracking system used by the support system. For example, the pancake shape ($T = 1$, $k_1 = 0.1$, $k_2 = 1$) could be representative of a trilateration system. The radial axis (R) is about equal to the range accuracy and, with reasonable placing of the ground stations, the accuracy of the T and N axes would be about equal, and considerably greater than the R axis due to the GDOP. Furthermore the size, shape, and orientation of all satellites should be approximately the same because the satellite ephemerides are being determined by a common system.

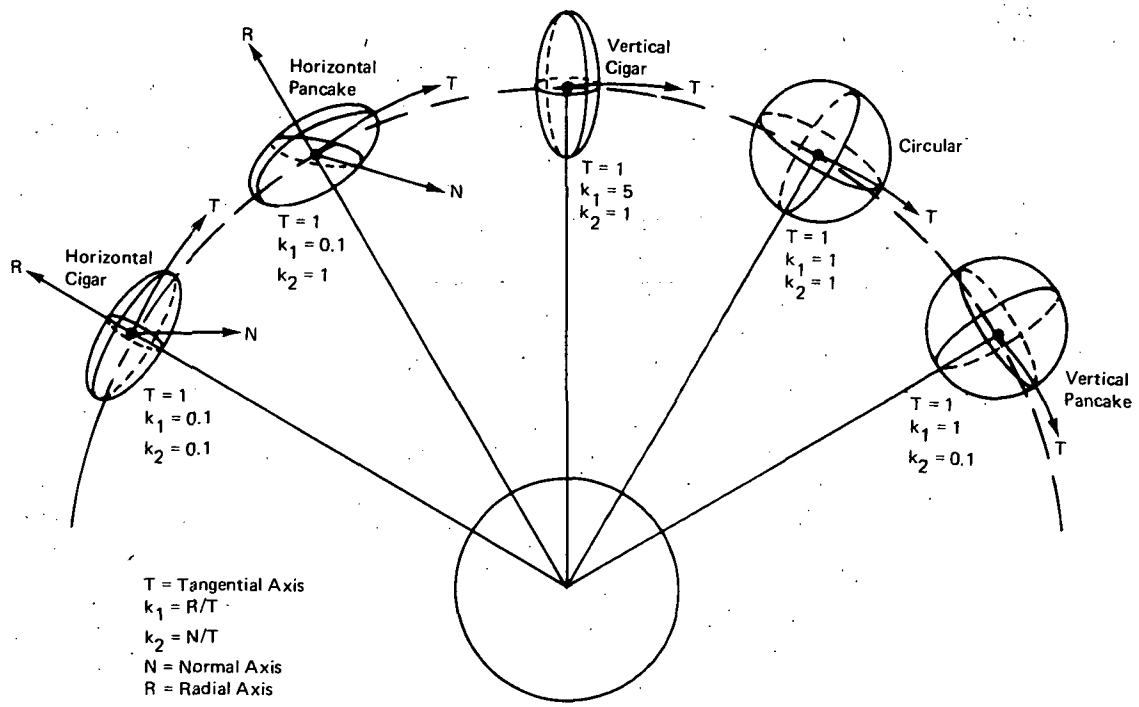

Figure 3-5. Specification of Satellite Error Ellipsoids

The T (tangential) axis is assumed to be in the plane of motion and orthogonal to the radius vector, R, (radial axis) which is parallel to the geocentric radius vector, and the N (normal axis) is assumed to be normal to the plane of motion and forms an orthogonal triad. Thus the error ellipsoid is specified by the size of the R, T and N axes (refer to Figure 3-5). However, the size of the T axis is, by definition, unity and the relative size of the R axis and T axis, k_1 and k_2 units, respectively. In other words, the ellipsoid is normalized to the size of the T axis. It is also assumed that the principal axes of the ellipsoid are aligned with the RTN axes. This is equivalent to assuming zero cross correlations among the R, T, and N components. The shape and orientation of the ellipsoid is specified by k_1 and k_2.

The cross correlation (ρ) among ellipsoids is accommodated by assuming the R axis error of satellite 1 is correlated with the R axis error of satellite 2 but not with the T and N axes of satellite 2; similarly, the T axis and of satellite 1 is correlated with the T axis of satellite 2 but not with the R and N axes, etc. The correlations among satellites is assumed to be equal; but the degree of correlation can be varied from -1 to +1.

The specification of the four satellite ephemeris errors has been reduced from 78 terms to 3 terms while retaining the essential features. For example, if $\rho = 0$, the ephemeris errors are uncorrelated and the random effects are emphasized. If $\rho = 1$

the ephemeris errors are perfectly correlated and the systematic effects are emphasized. By normalizing to the T axis the parametric form of the analyses is retained and by varying k_1 and k_2 the shape and orientation is varied.

Each range difference error is composed of two sources of error: (1) a random range error, and (2) an ionospheric range error.* Each source in turn consists of two errors introduced on the two transmission links. In mathematical terms,

$$\text{Range difference} = P_j = R_j - R_0 \qquad j=1,2,3 \tag{3-1}$$

$$\text{Error in range difference} = \Delta P_j = \Delta R_j - \Delta R_0 \quad j=1,2,3 \tag{3-2}$$

where

$$\Delta R_j = \Delta R_j(\text{NOISE}) + \Delta R_j\,(\text{REFRACTION}) + \Delta R_{BIAS} \tag{3-3a}$$

$$\Delta R_0 = \Delta R_0(\text{NOISE}) + \Delta R_0\,(\text{REFRACTION}) + \Delta R_{BIAS} \tag{3-3b}$$

The noise term (the random error) poses no particular analytical difficulty because ΔR_j is statistically independent of ΔR_i, which is independent of ΔR_0. The assumption is made that the variance of this random error is the same for all transmission paths. This assumption is reasonably valid because the dominant effect on the range variance is the SNR which is inversely proportional to the range between transmitter and receiver. The range variations among all signal paths is small. The following abbreviated analysis supports this assumption:

$$\sigma^2_{R(\text{NOISE})} = \frac{K_1}{SNR} = \frac{K_1}{SNR} \tag{3-4}$$

where K_1 is a constant related to the range resolution. However, from the one-way radar range equation

$$SNR = \frac{K_2}{R^2} \tag{3-5}$$

*Tropospheric effects were not considered per se. This is not necessarily to imply that tropospheric effects are negligible. However, the work scope had to be restricted to some level due to limited funding. The ionospheric model, modified for its effective altitude and time and space correlation, could represent a facsimile troposphere. However, no analyses were made based on this assumption.

where K_2 is another constant depending primarily on carrier frequency, power, and antenna gains. Thus,

$$\sigma^2_{R(NOISE)} = \frac{K_1}{K_4} R^2 \equiv AR^2 \qquad (3\text{-}6)$$

The variances for range 1 and 2 are

$$\sigma R_1^2 = A \quad R_1^2 \qquad (3\text{-}7)$$

$$\sigma R_2^2 = A \quad R_2^2$$

The ratio of $\sigma_{R_1}/\sigma_{R_2}$ is

$$\sigma_{R_1}/\sigma_{R_2} = R_1/R_2 \qquad (3\text{-}8)$$

The maximum range difference that can reasonably be expected for the COLM geometry is about 10^7 ft. The average range is about 10^8 ft. Thus,

$$\sigma_{R_1}/\sigma_{R_2} \approx \frac{10^8 + 10^7}{10^8} = 1.1 \qquad (3\text{-}9)$$

Generally, this ratio will be less, especially for those satellite constellations (see Section 4) with small inclination angles which give relatively close satellite spacing.

The refraction error poses an analysis problem because (1) the ionospheric range error depends on the angle at which the ray enters the ionosphere, and (2) the range error for path 1 is correlated to some degree with the range error for path 2. From Equations 3-2, 3-3a, and 3-3b, the reader can see that if the two ionospheric range errors were perfectly correlated and had the same entry angle $\Delta R_j = \Delta R_0$, the result would be a cancellation of the ionospheric range error.

Rather than assume this condition the ionospheric error model provided for

1) Time and space correlation
2) Entry angle effect
3) Latitude dependency (the ionosphere is known to produce less refraction at higher latitudes).

This model was derived directly from Reference 1.

The variance of the ionospheric error is defined as σ^2_{IONO} at the equator, and $\sigma^2_{IONO}\, e^{-a\phi}$ at latitude ϕ. "a" is constant which makes $e^{-a\phi} = 0.5$ when $\phi = 45°$. The range variance of any ray passing through the ionosphere at any angle other than perpendicular is $\sigma^2_{IONO}\, e^{-a\phi}$ (Q(E). Q(E) equals unity when E = 90°, and about 2.5 when E = 20°. Q is sometimes referred to as the obliquity factor.

The covariance of ionospheric range errors 1 and 2 is $\sigma^2_{IONO}\, e^{a\phi_1}\, Q(E_1)\, e^{a\phi_2}\, Q(E_2)\, \rho(S)\, \rho(t)$ where $\rho(S)$ is the space correlation and $\rho(t)$ is the time correlation. The correlation models used (taken from reference 1) are shown by Figure 3-6 and 3-7.

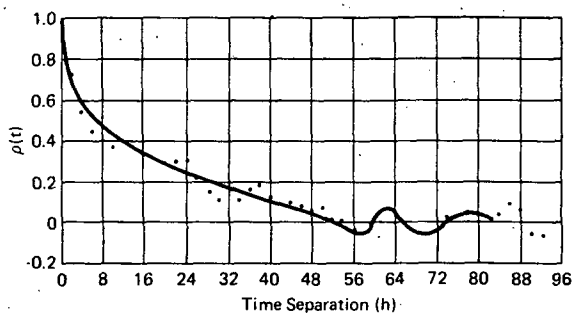

Figure 3-6. Ionospheric Time Correlation

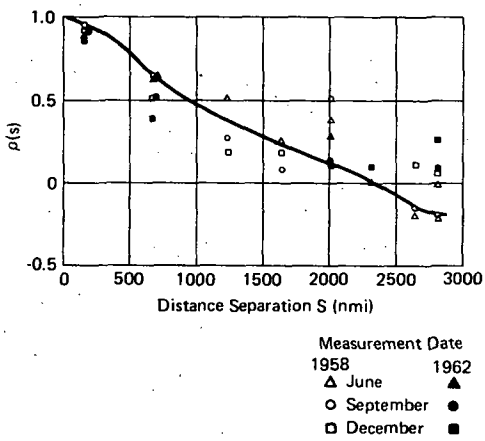

Figure 3-7. Ionospheric Space Correlation

The separation distance S of Figure 3-7 is illustrated by Figure 3-8. Since S depends on H_{IONO} (Reference 1 gives $H_{IONO} \approx 200$ nmi miles) and $\rho(S)$ in turn depends on S, H_{IONO} should be treated as a parameter, because for any given geometry of satellites and aircraft lowering H_{IONO} should make S smaller, thereby increasing the space correlation $\rho(S)$. It can be shown that increasing the space correlation causes more of the ionospheric range error to cancel.

Since the ionosphere constitutes a relatively thick shell about the earth ranging from an altitude of 50 mi (D layer) to an altitude of 500 mi (F_2 layers), H_{IONO} was varied between 50 and 400 nmi.

Reference 1. C. C. Chen, Range Difference Error Due to the Presence of Ionospheric Electrons, TRW Systems Group.

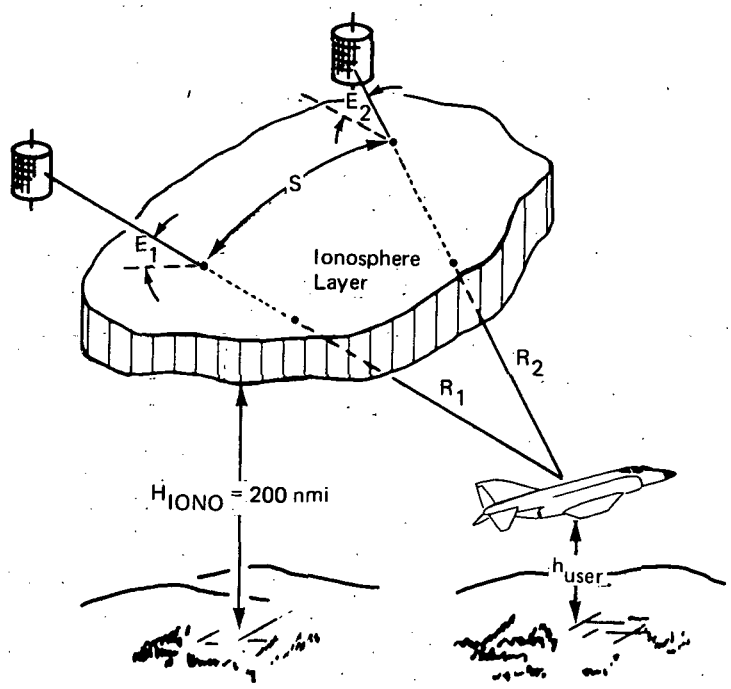

Figure 3-8. Pictorial Model of Ionosphere

3.2.4.2 2P+H Concept

The significant difference between the 3P and 2P+H concepts is that the 2P+H concept uses the earth radius whose locus is a sphere in lieu of the third hyperboloid. Figure 3-3 may again be used to visualize the concept. Point A is the intersection of P_{12} (or P_{23}) with a sphere-of-radius (r_e + h). An r_e is assumed, and h is provided by some form of altimeter. Point B is the intersection of P_{12} with a radius of h plus Δ h. If the user makes an altitude error, Δ h, it may produce a horizontal error, but the vertical error is always equal to the altitude error. Therefore, the 2P+H results do not show any vertical error results. The sensitivity of horizontal position errors to both P and H errors is also geometry sensitive.

In general, the comments on the 3P system with regards to random errors, ephemeris errors, and ionosphere errors are applicable to the 2P+H system. One less satellite is involved which means one less signal path, but this is properly accounted for in the results.

3.2.4.3 3R Concept

A position fix with the 3R concept involves the intersection of three spheres whose centers are located at each satellite respectively. A two dimensional representation is shown by Figure 3-9.

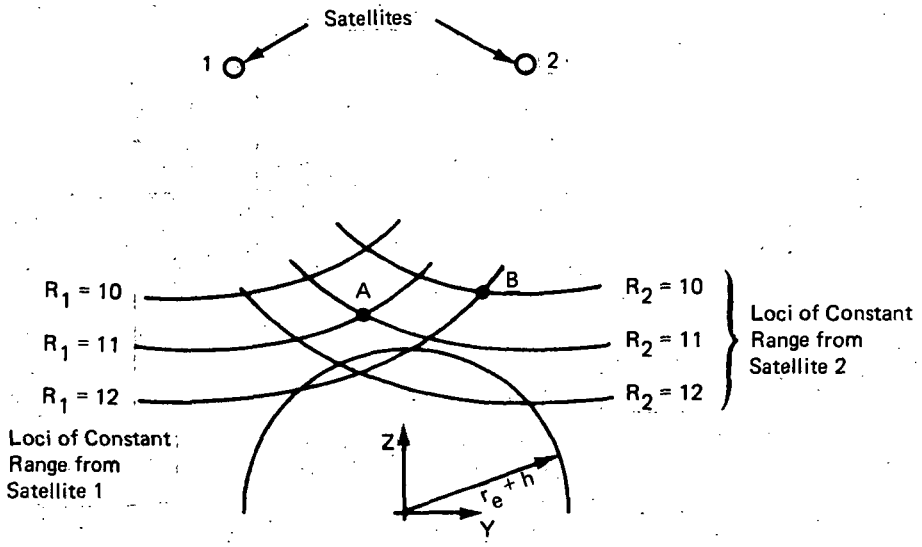

Figure 3-9. Two-Dimensional Pictorial Representation of 3R System

Point A is the intersection of $R_1 = 11$ and $R_2 = 11$. If, in the measurement of R_2, an error of minus 1 ft were made, then R_2 (measured) = 10 and the estimated position would be at B. Note that both horizontal and vertical errors result.

The sensitivity of position errors due to range errors is again geometry dependent, as will be shown, but not to the extent of the 3P concept. This is because the range loci of the 3R concept are spheres which have a uniform curvature whereas the 3P concept loci are hyperboloids which have a variable curvature.

Furthermore, the sensitivity is proportional to the angle of intersection of the two loci. A right angle intersection is best; i.e., least error magnification or GDOP. Though the reader should not draw too quantitative a conclusion from Figures 3-3 and 3-9, it is fair to say that, in general, the 3R concept will generally have intersections closer to right angles than the 3P concept. Based on these simple observations one would expect the 3R concept to be more accurate on the average, and also to have less variation in accuracy than the 3P concept.

In other words, if all other things were equal, and a histogram were prepared of all the sensitivities for all possible geometries, one could conceivably generate a plot similar to that shown in Figure 3-10.

Though the preparation of the complete histogram would have been prohibitively expensive for this study, there are two parameters which can be used to quantitatively characterize the histogram. These two parameters are mean and standard deviation. The mean deviation gives the average sensitivity (or accuracy) over the geographic region of interest while the standard deviation shows how much the sensitivity might vary within the region. A small mean deviation implies an accurate system and a small standard deviation implies a dependable accuracy.

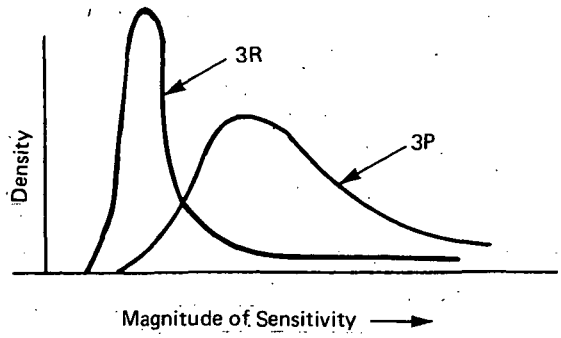

Figure 3-10. Typical Histogram of Error Sensitivities for 3P and 3R Concepts

Therefore the mean and standard deviation are provided for each concept and for each source of error. The reader should find them useful in making comparisons of concepts and how those concepts behave to the different sources of error. In addition, results are provided which show in detail how the concepts behave as a function of geometry and source of error.

The 3R concept is sensitive to all error sources identified for the 3P system plus one — the range bias. It may be seen from Figure 3-9 that a range bias causes, primarily, an altitude error with no horizontal error when directly under the satellites. As the user moves away from a point directly under the satellites the horizontal error due to a range bias increase.

3.2.4.4 2R+H Concept

The 2R+H concept is very similar to the 3R concept with the one exception, that, in effect, the third satellite is located at the earth's center, and in lieu of the third range an altitude measurement is substituted. In general, the 2R+H concept is sensitive to all error sources identified for the 3R concept. However, the vertical error always equals the altimeter error.

3.2.5 SOME ADDITIONAL EFFECTS RELATING TO EPHEMERIS AND IONOSPHERIC ERRORS WITH BENCHMARK CALIBRATION

This subsection has been reserved until the background information related to the ephemeris and ionospheric errors and the benchmark calibration was presented.

As discussed in Subsection 3.2.1 the relative accuracy is based on a correction vector from a local ATC center. If the total system were time stationary the correction would be valid over an indefinite time period. However, there are three things which negate the idea of a time stationary system:

1) The satellites are not truly stationary with respect to the earth (see Section 4), which causes the GDOP to vary with time.

2) The satellite error ellipsoids are not time stationary. It can be shown theoretically, that in an energy conservation system the uncertainty of the total state vector is time invariant; but the position and velocity uncertainty grows. Thus while the position ellipsoid and velocity ellipsoids constantly change their shape and orientation the correlations between position and velocity change accordingly so that the total state uncertainty is time invariant.

3) The ionosphere as shown by Figure 3-7 is nonstationary.

The first item above is treated by providing results for different satellite positions. The different satellite positions are dictated from an initial choice of constellations (see Section 4) and the time of day. The second item is treated in the results as follows: the user does not move after the calibration; however, the calibration vector should be recomputed continually. However, if only updated periodically, the effect of time correlation on the ephemeris error should be considered. Due to the limited funding it was practical to consider only two cases which are the extremes of correlation. In the first case, the satellite ephemeris error is assumed to be uncorrelated after some time (unspecified in this report), and in the second, the ephemeris is assumed to be perfectly correlated. The actual degree of correlation depends on how the support system estimates the ephemeris. This aspect was beyond the scope of this study. In a practical sense the updating interval could be sufficiently short so that the perfectly correlated results are probably closer to realism.

The third item has been treated much like the second except that the time correlation of the ionosphere has been varied from zero to one. The reader can interpret these results by considering a user initially calibrated while waiting at the end of the runway prior to takeoff. After takeoff the aircraft circles the airfield (so as not to affect the GDOP) using the satellite radio signals for navigation and the correction vector registered at takeoff. However, because the ionosphere is not stationary, the correction vector changes but the user is unaware of the change, or at least incapable of compensating for the change. The error analysis then shows how the relative accuracy varies with time variations in the ionosphere.

3.2.6 ANALYSIS OF DETERMINATION OF AIRCRAFT VELOCITY FROM DOPPLER MEASUREMENTS

Appendix G gives a mathematical development showing how the error in measuring Doppler affects the determination of aircraft velocity. For the 3P and 2P+H concepts the Doppler measurement is actually a Doppler difference measurement:

$$\dot{P}_j = \dot{R}_j - \dot{R}_0 \qquad (3\text{-}10)$$

where $\dot{R}_j = \dot{R}_{true} + \dot{R}_{BIAS}$

$\dot{R}_{BIAS}$ is, in a way, one transmission, due to unknown unequal LO frequencies in the transmitter and receiver. As seen from Equation 10, the bias in the 3P and 2P+H concept cancel. This bias does not cancel in the 3R and 2R+H concepts. (Like the position algorithm if desired, the $\dot{R}_{BIAS}$ may be solved for which would then allow the user to synchronize his LO with the satellite LO.)

The derivations in Appendix G show that the propagation of Doppler or Doppler difference errors into velocity errors is exactly the same as for the propagation of range or range difference errors into position errors, with one addition. The error in range (or range difference) which produces a position error also produces a velocity error.

This effect in a well engineered design is usually not dominant, but if precise Doppler is to be measured and very inaccurate ranges are measured because the primary intent was to have a highly accurate estimate of velocity, the velocity error could be dominated by the position error. Thus, the effect of range (or range difference) errors on velocity have been investigated and are on the order of 10^{-3} to 10^{-5} ft/s/ft of range error.

3.3 RESULTS

3.3.1 COMPARISON OF 3P, 3R, 2P+H and 2R+H CONCEPTS VERSUS ERROR SOURCES AND BENCHMARK CALIBRATION

Figures 3-11, 3-12, 3-13, and 3-14 provide a summary comparison of the four surveillance/navigation concepts employing multiple satellites. The reader is referred to subsection 3.2.4 for a description of each source of errors. The solid bars give the mean (average) accuracies over the surveillance region and the white bars give the standard deviations.

Three satellite constellations are given for each concept corresponding to the midnight Y constellation (see Figure 6-a) with inclinations of 10°, 20°, and 30°. Other figures will give comparable results for the Y, 4 A.M. constellation.

The ordinates of all graphs are in dimensionless units (ft/ft). If a satellite to user radio link were designed to provide a range standard deviation of x ft, the users position error would be the value of the ordinate times x. Note also that the normalization has been reduced to one radio link. In some concepts 2, 3 or 4 satellites may be involved; however, the curves properly account for the number of satellites by a statistical combination of the errors on all of the necessary radio links.

For example, consider the 3P case, i = 10°. Four satellite radio links are required. Assume each link was contaminated with 10 ft of range jitter (a random type error). Then, on the average, the horizontal position error will be 460 ft and the variation from this average (mean) depending on where the user is in region of interest, will be 108 ft. (For Figures 3-11 through 3-14, the region of interest is defined by Region 2, Figure 4-1.) In other words, the position error could vary from 460 - 2(108) ft. = 244 ft to 460 + 2(108) ft = 676 ft. Since the complete histogram has not been computed, there is no quantitative correlation of probability with standard deviation; i.e., 3 σ does not imply 99.7%. The standard deviation given should be considered more in the context of how much the position error is likely to vary from the mean at any given location.

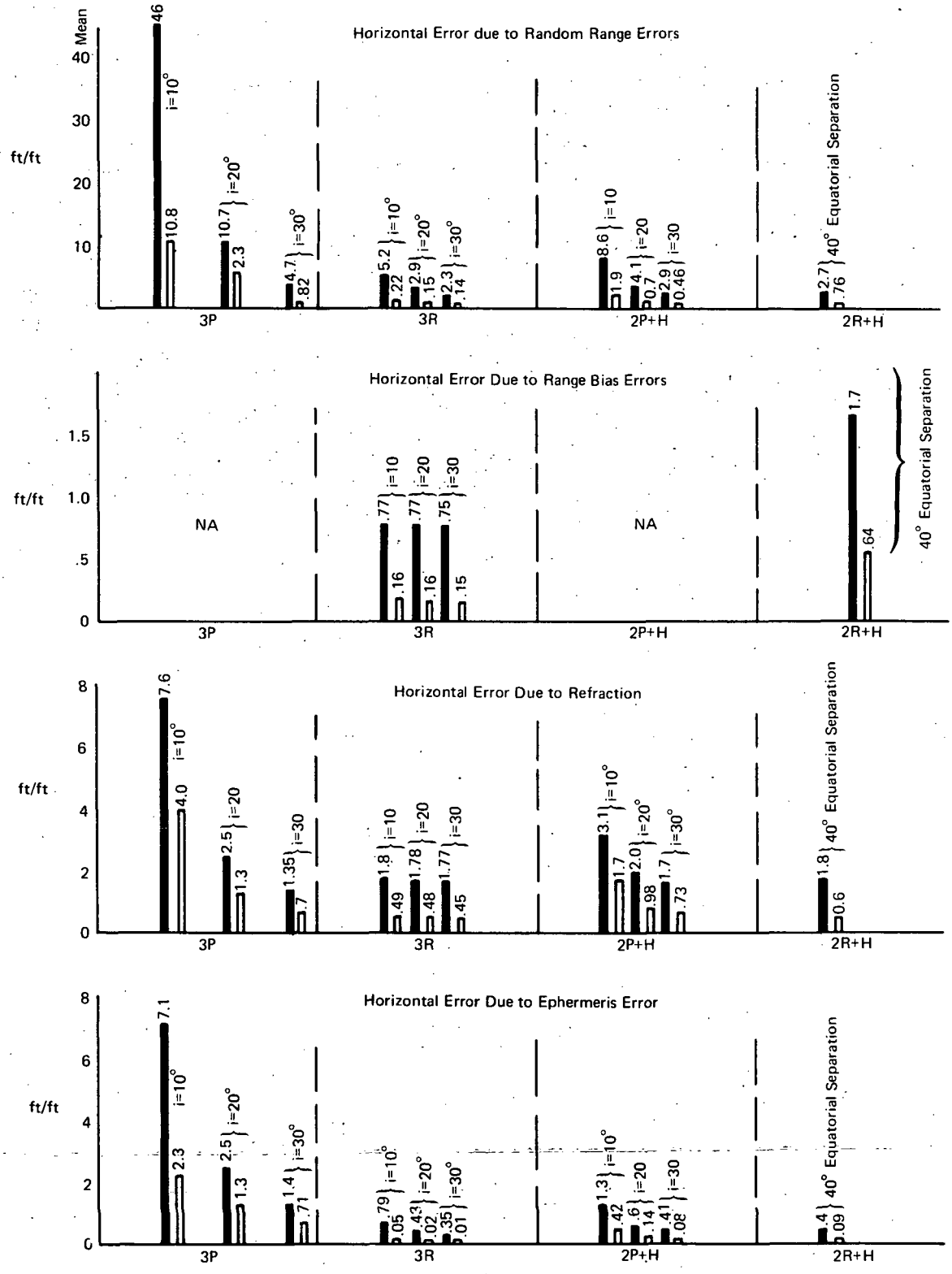

Figure 3-11. Comparison of 3P, 3R, 2P+H and 2R+H Concepts vs Error Source without Calibration/Horizontal Position, CONUS, Midnight Y, $k_1 = .1$, $k_2 = 1$

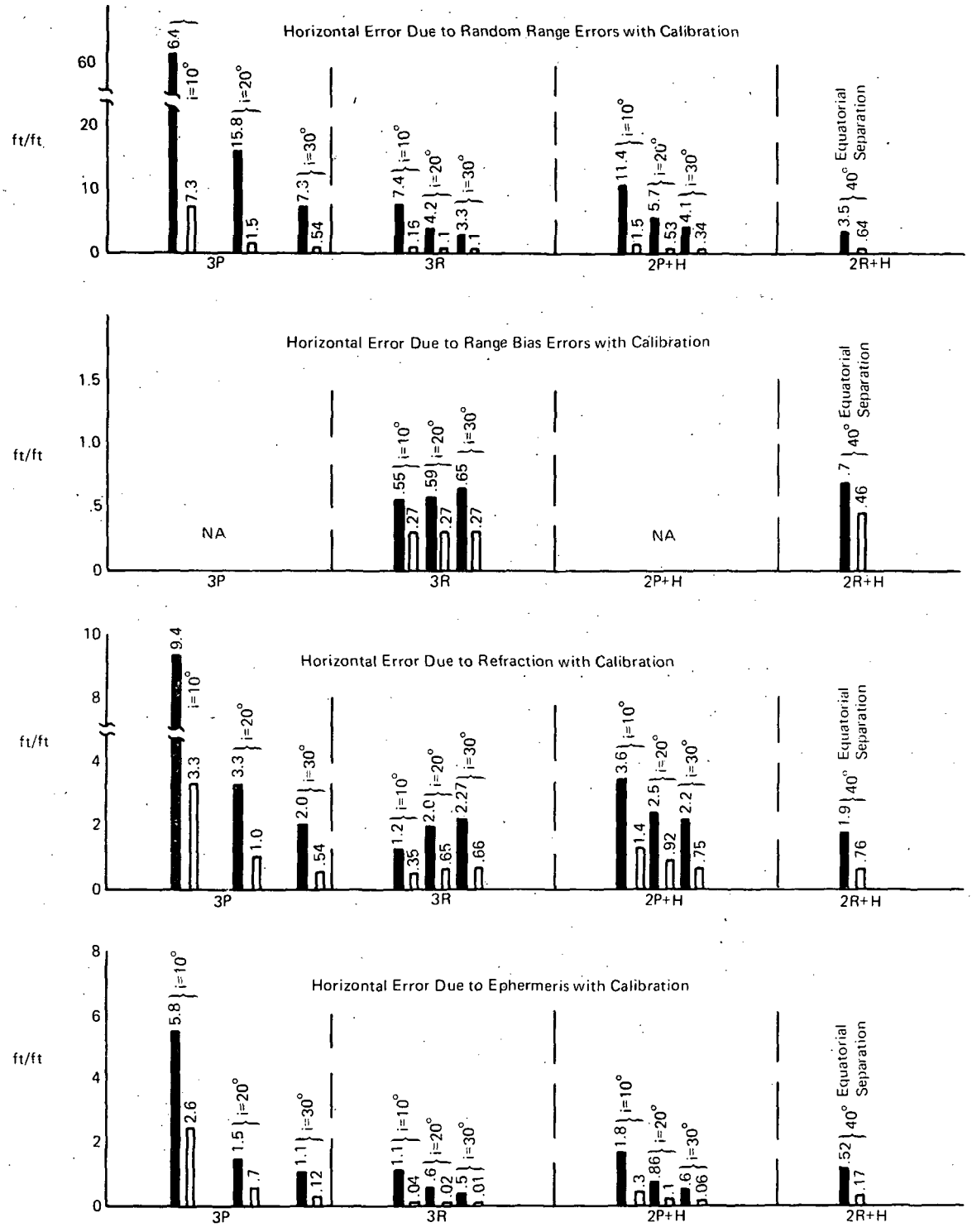

Figure 3-12. Comparison of 3P, 3R, 2P+H, 2R+H Concepts vs Error Source with Calibration/Horizontal Position, CONUS, Midnight Y, $k_1 = .1$, $k_2 = 1$

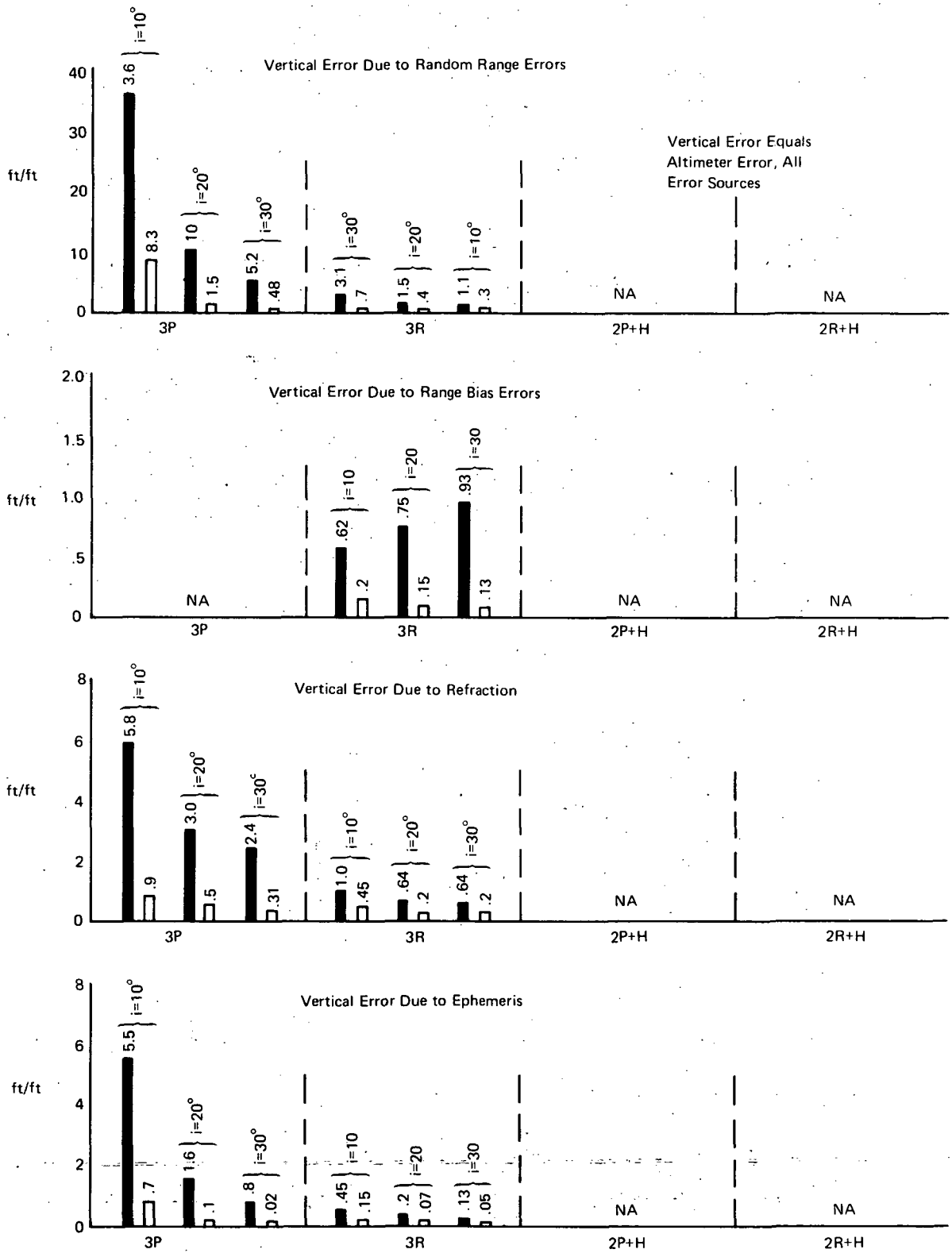

Figure 3-13. Comparison of 3P, 3R, 2P+H, and 2R+H Concepts vs Error Source without Calibration; Vertical Position, CONUS, Midnight Y, $k_1 = .1$, $k_2 = 1$

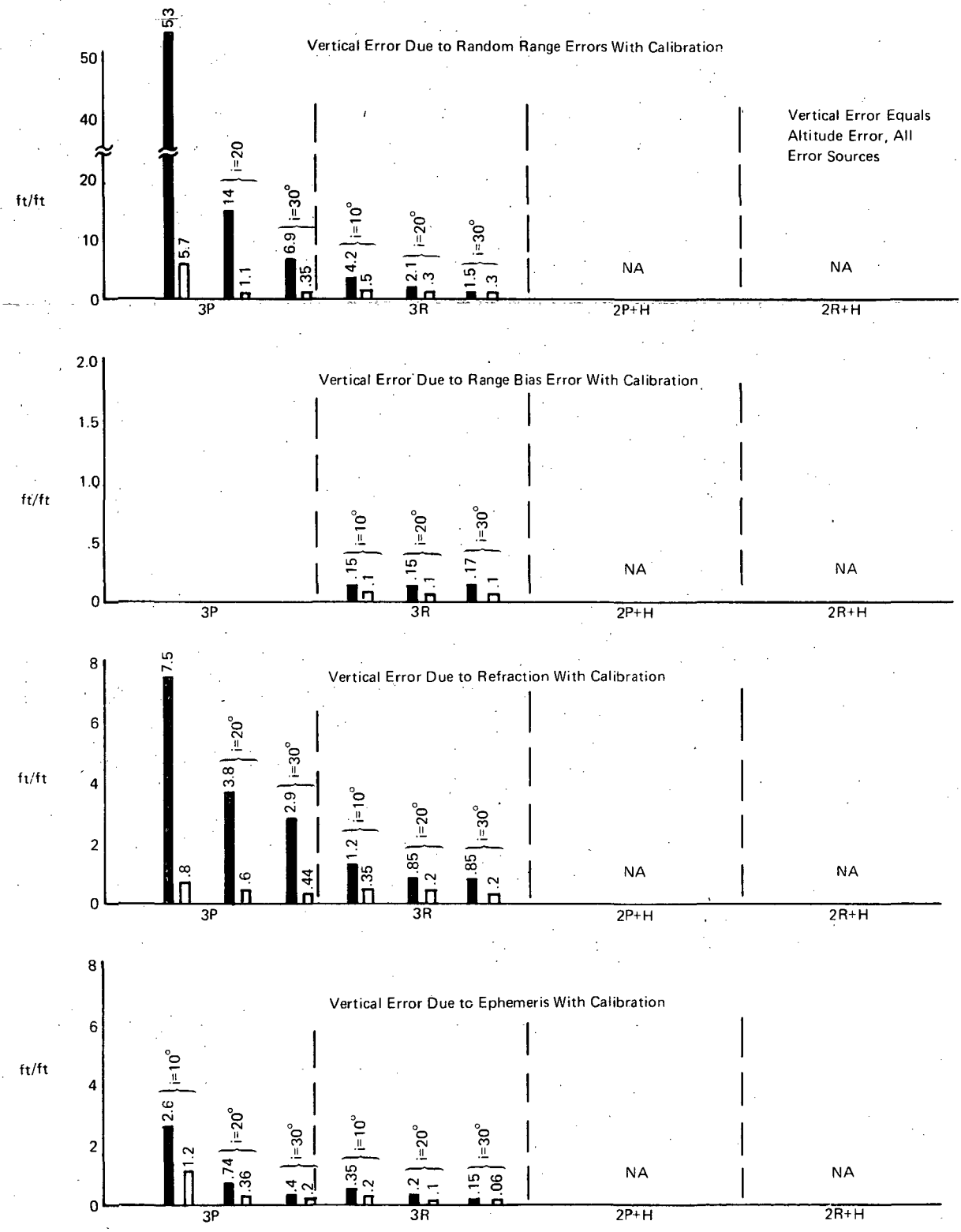

Figure 3-14. Comparison of 3P, 3R, 2P+H, and 2R+H Concepts vs Error Source with Calibration; Vertical Position, CONUS, Midnight Y, $k_1 = .1$, $k_2 = 1$

Assuming the same radio link design, if applied to the 3R concept, the average horizontal position error would be 52 ft with a 2.2-ft variation. The ionospheric range error results have been normalized to 1 ft. The actual ionospheric range error is inversely proportional to the carrier frequency squared. At 1.6 GHz, the ionospheric ranging error is between 10 and 100 ft.

3.3.2 COMPARISON OF 3P, 3R, 2P+H, AND 2R+H CONCEPTS VERSUS VALUE OF BENCHMARK CALIBRATION AND SIZE OF AREA TO BE SERVICED BY CALIBRATION

Based on these first four figures the benchmark calibration appears to be of little value. However, only one benchmark was assumed for the entire region (region 2, Figure 4-1) which may be too large an area. Therefore the region was reduced to a 300 × 300-nmi square (a 5° × 5° grid). The center of the 5° × 5° grid is at the center of the larger grid (CONUS) and approximates the area about Chicago. The results are shown in Figure 3-15. The solid bars are for the 5° × 5° grid and the white bars are for the area given by region 2. In most cases the value of benchmark calibration is doubtful even for the 5° × 5° region. The increase for random errors closely approximates $\sqrt{2}$ because of the RSSing of the user and benchmark errors. However, the results for the ephemeris and refraction are somewhat surprising and the reasons for the rather poor improvements will be investigated in subsequent figures and discussion.

In the case of the ephemeris error the results have been presented for a worst-case. The results assume that the correlation of the current correction vector is uncorrelated with the one made at the time of the benchmark calibration. In practice the correlation is determined from the type of satellite location system employed, the length of the filter span in the orbit determination algorithm, and the time from calibration. Hence these results could be loosely interpreted as a long time (i.e., several hours) between benchmark calibrations as opposed to a continuous type of benchmark calibration.

3.3.3 EFFECTS OF EPHEMERIS ERROR ON HORIZONTAL POSITION

Figure 3-16 shows the effects of ephemeris error on horizontal position assuming (1) no calibration, (2) calibration with zero correlation, and (3) calibration with perfect correlation. Figure 3-16 thus presents the effects of the ephemeris error three different ways: (1) the top bar graph represents the effects of the ephemeris error assuming no calibration; i.e., the user position error is in an absolute frame; (2) the middle bar graph represents the effects of the ephemeris error for the previously described situation; i.e., calibrated but the correlation has gone to zero; and (3) the bottom bar graph represents the effects of the ephemeris error with calibration and where the correlation is unity; i.e., equivalent to a frequent updating of the benchmark calibration.

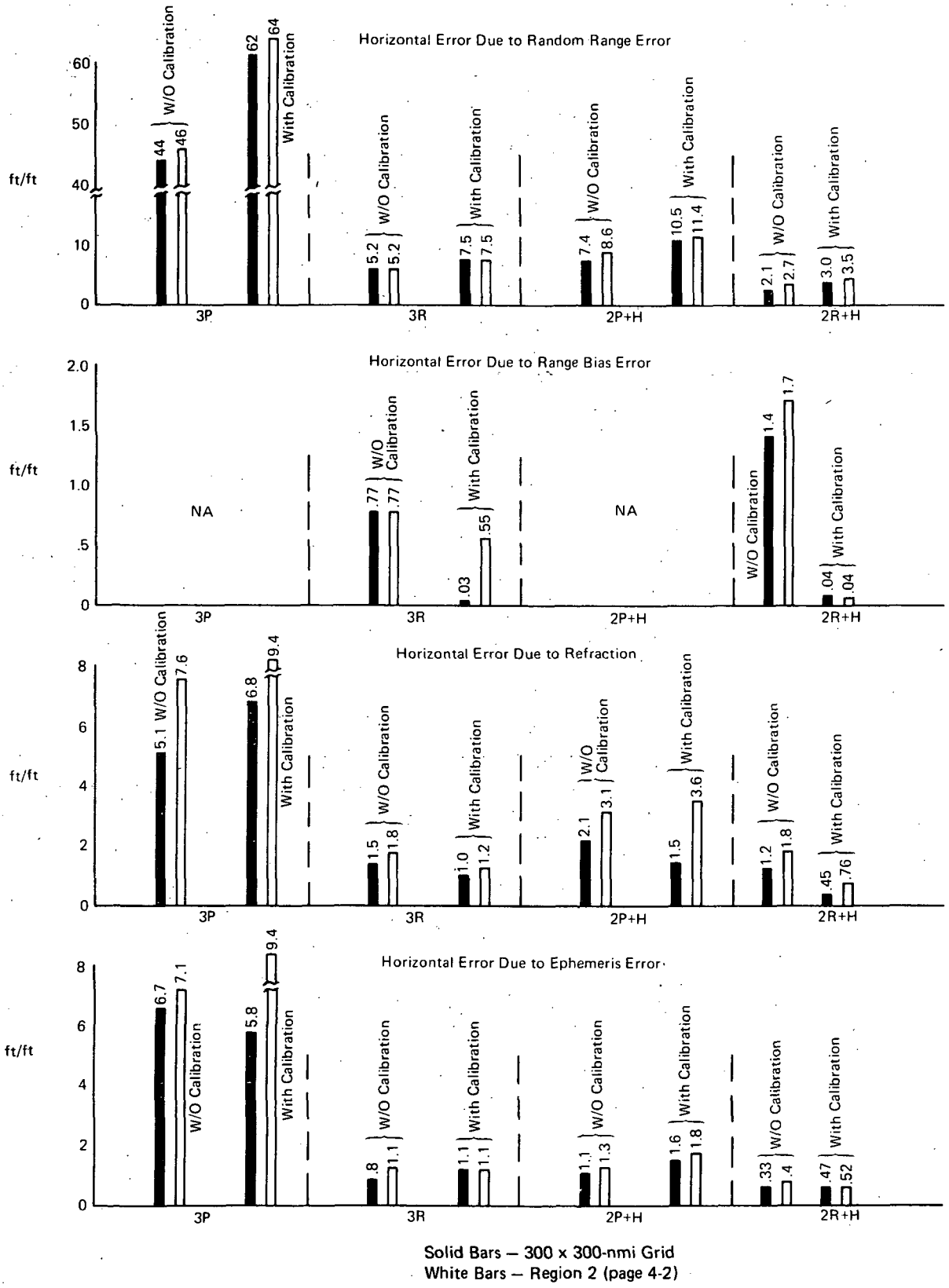

Figure 3-15. Comparison of 3P, 3R, 2P+H, 2R+H Concepts vs Value of Benchmark Calibration and Size of Area to be Serviced by Calibration

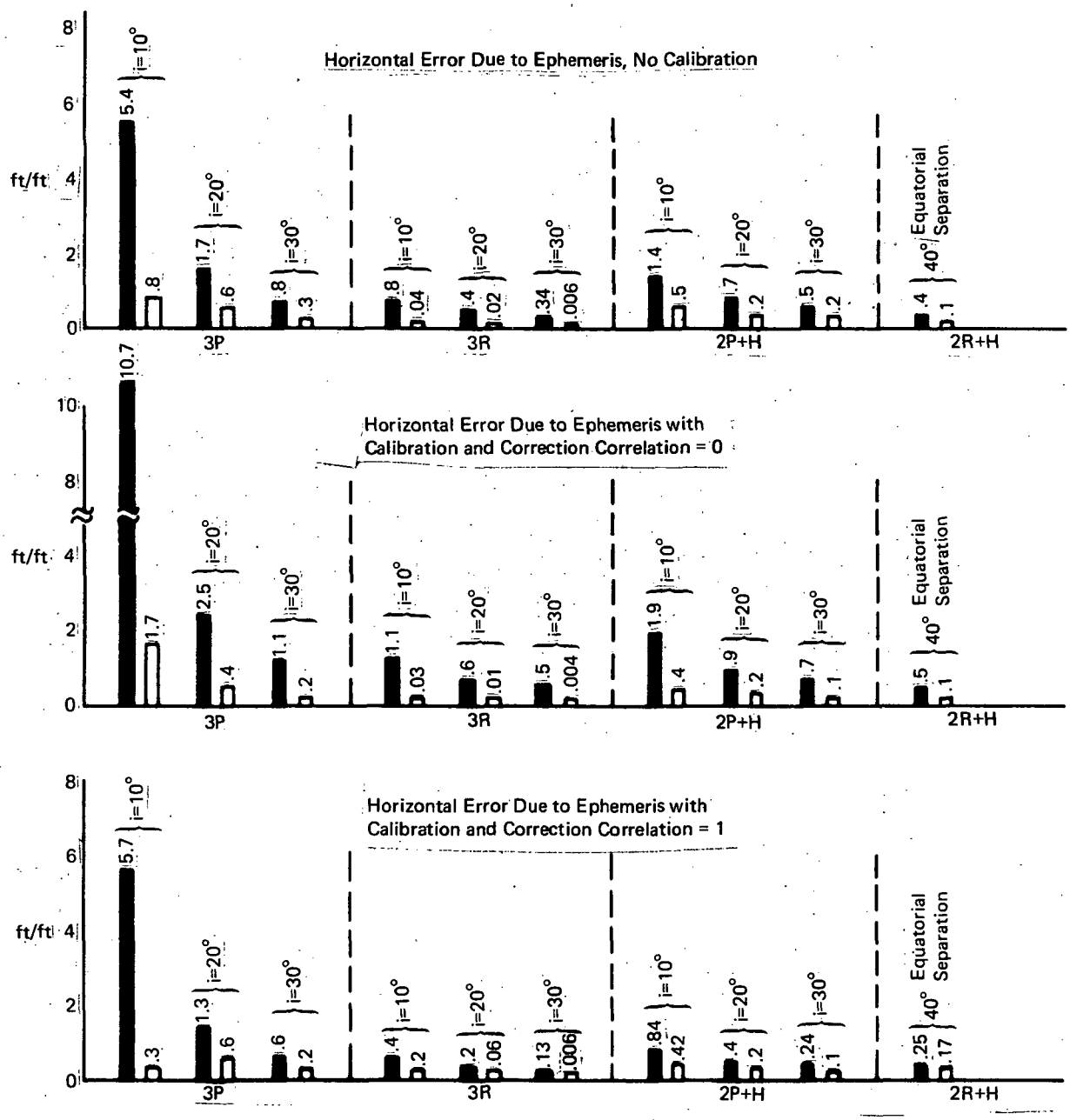

Figure 3-16. Effects of Ephemeris Error on Horizontal Position, Region 2

The bottom bar graph indicates that the benchmark calibration is almost always beneficial when the correlation is high or equivalently when the benchmark calibration is performed frequently. Figure 3-16 also assumes a single calibration station for the entire Region 2 (see Figure 4-1).

3.3.4 HORIZONTAL ERROR DUE TO EPHEMERIS

Figure 3-17 shows the horizontal error due to ephemeris within a 300 x 300 nmi grid versus time from calibration and presents the effects of the ephemeris error for

a smaller region (5° × 5°) with correction correlation equal to one. A somewhat different aspect of the calibration update interval is apparent. In Figure 3-16, the correlation of the benchmark calibration is based on the correlation of the ephemeris errors themselves, but the movement of the satellites was not factored into the results. In Figure 3-17, the movement of the satellites is emphasized. The movement of the satellites is shown by Figure 4-2. As the satellites move, even if the ephemeris errors are perfectly correlated, the correction vector of the benchmark calibration will change. This is due strictly to a change in the relative geometry among satellites and users. If this correction vector is not updated frequently, even with perfectly correlated ephemeris errors, there will be an error introduced in the presently computed position. Figure 3-17 shows the value of the benchmark calibration when used over a 5° × 5° region. The degradation of the correction is only moderate over a 3-hour interval. The time span was chosen where the relative satellite motions would be greatest; i.e., the midnight constellation.

3.3.5 EFFECT OF CHOICE OF SATELLITE ERROR ELLIPSOID ON THE HORIZONTAL ERROR

Another consideration affecting the ephemeris error results is the choice of error ellipsoid (see Figure 3-5). The results shown thus far assume the error ellipsoid second from the left in Figure 3-5. It is the pancake shape with the radial error 10 times smaller than the tangential and normal errors. Figure 3-18 compares the results of the pancake shape ellipsoid with the cigar shape (first figure on the left in Figure 3-5) ellipsoid. In Figure 3-18, the solid bar represents the pancake shape and the white bar represents the cigar shape. The differences are seen to be small even though the normal error has been reduced by 10 to 1; i.e., the volume of uncertainty of the pancake shape is greater than for the cigar shape.

3.3.6 EFFECTS OF IONOSPHERE RANGE ERROR AND MODEL ON POSITION LOCATION

Figure 3-19 shows the effects of the ionospheric refraction on the four position location concepts. The results are presented in the context of mean and standard deviations discussed previously. The region of calibration is a 5° × 5° grid (300 × 300 nmi). Figure 3-19 indicates that the 3P system accuracy is actually degraded when the calibration is applied, and that the improvement for the 3R, 2P+H and 2R+H concepts is marginal. The variation in accuracy is due to the time correlation of the ionosphere and the movement of the satellites with respect to the earth.

A simplified mathematical explanation of why the calibration does not improve the accuracy is given below. Consider first the range difference error due to refraction:

$$\Delta P_1 = \Delta R_1 - \Delta R_0 \tag{3-11}$$

(3-12)

$$\sigma^2_{P_1} = \sigma^2_{R_1} + \sigma^2_{R_0} - 2\sigma_{R_1}\sigma_{R_0}\rho(s) \tag{3-13}$$

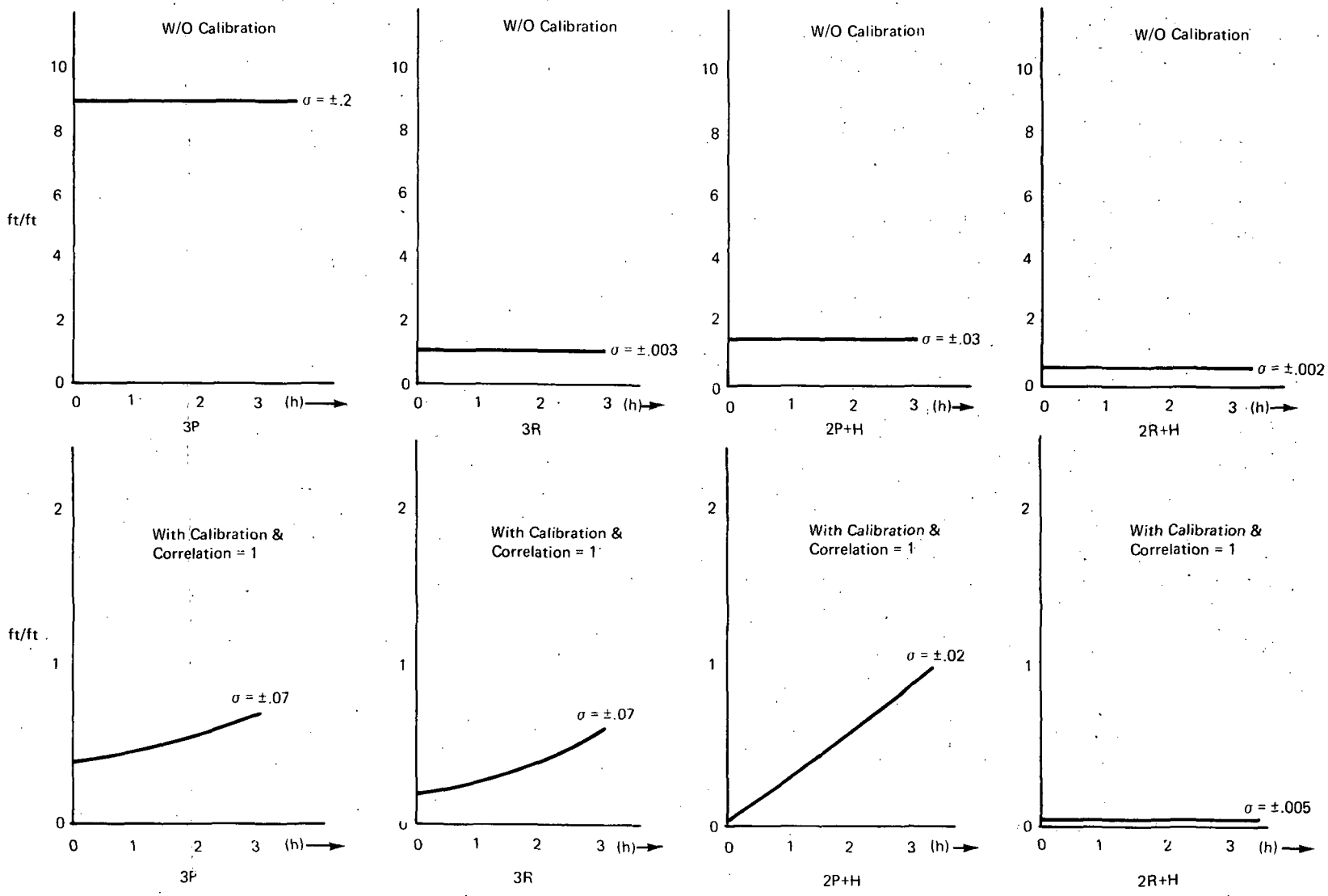

Figure 3-17. Horizontal Error Due to Ephemeris (300 × 300-nmi Grid) vs Time from Calibration

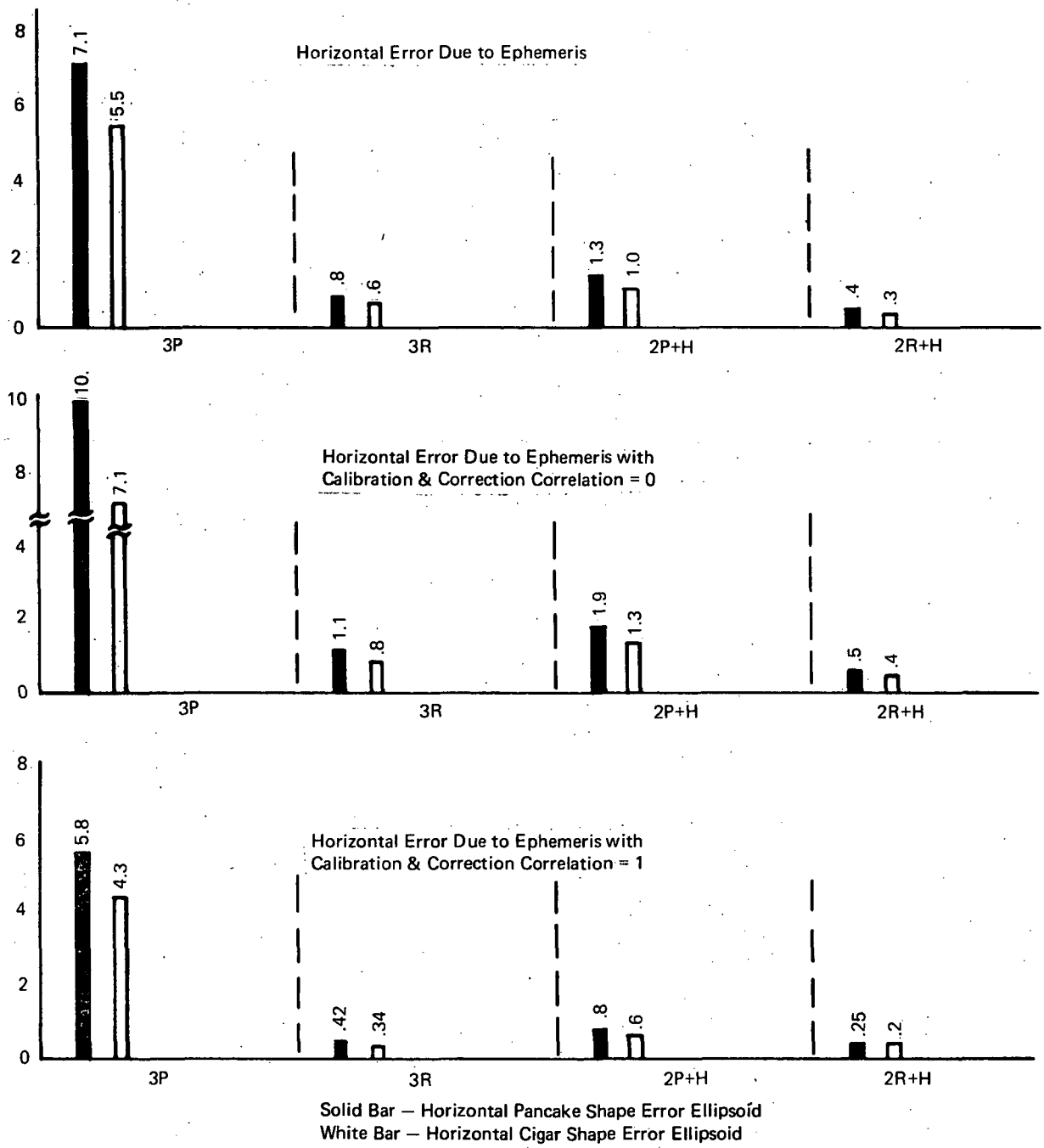

Figure 3-18. Effect of Satellite Error Ellipsoid on the Horizontal Error

Equation 3-11 is a simple statement of the range difference error; Equation 3-12 is the ensemble average of ΔP^2 and Equation 3-13 is but a redefinition of terms in Equation 3-12. $\sigma^2_{R_1}$ and $\sigma^2_{R_0}$ are the variances due to the ionospheric refraction and $\rho(S)$ is the correlation distance (see Figures 3-7 and 3-8). Neglect the effect of latitude on the ionosphere and assume the obliquity factor is the same for paths 1 and 0. Then,

$$\sigma R_1 = \sigma R_0$$

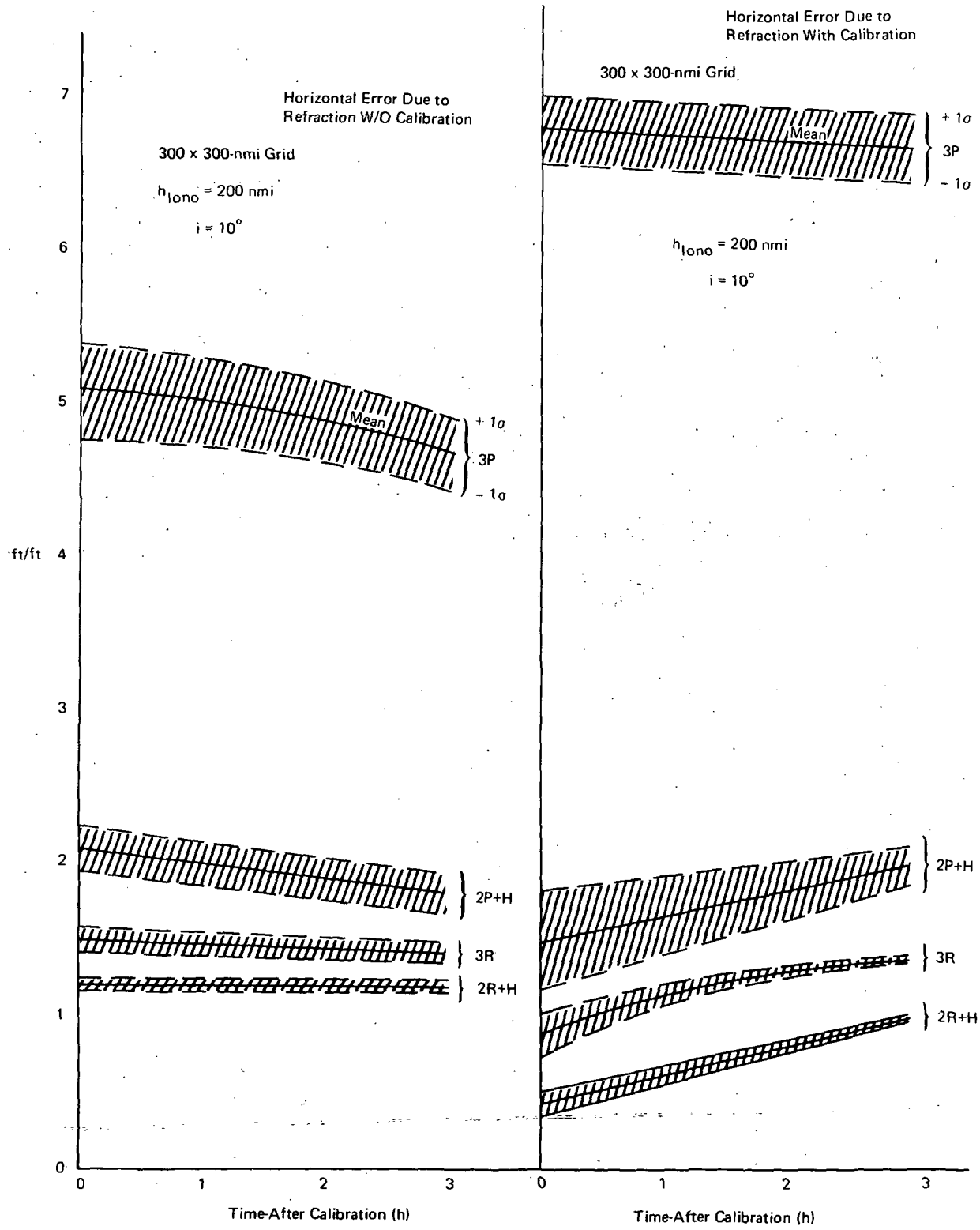

Figure 3-19. Comparison of 3P, 3R, 2P+H and 2R+H Concepts due to Refraction with and without Calibration/Vertical Position, 300 x 300-nmi Region, Midnight Y, $k_1 = k_2 = .1$

Under this assumption Equation 13 becomes

$$\sigma_p^2 = 2\sigma_R^2 \left[1 - \rho(s)\right] \tag{3-14}$$

$\rho(S)$ is determined from the relative positions of the user, the satellites and the ionosphere. Figure 3-20 gives a simplified geometrical picture.

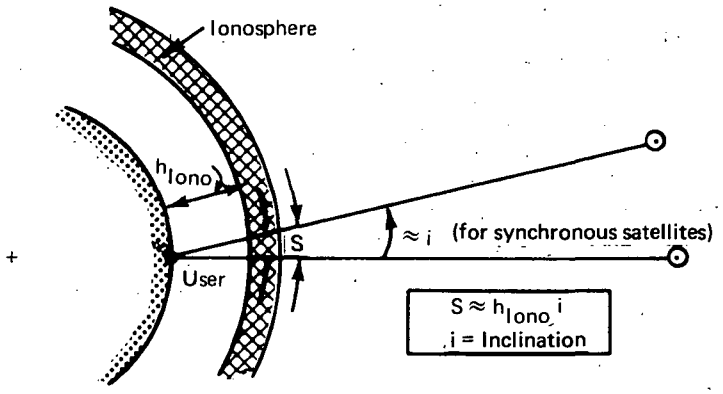

Figure 3-20. Simplified Diagram Illustrating Correlation Distance

Applying a straight line fit to Figure 3-7 gives

$$\rho(s) = 1 - \frac{S}{2400} \tag{3-15}$$

and substituting Equation 15 into 14 gives

$$\sigma_P^2 = 2\sigma_R^2 \left[\frac{S}{2400}\right] = \frac{h_{IONO}\, i}{1200}\ \sigma \frac{2}{R} \tag{3-16}$$

with

h_{IONO} in nmi

i in radians

Given $h_{IONO} = 200$ nmi, $i = 10°$

$$\sigma_P^2 = \sigma_R^2 \left[0.03\right] \tag{3-17}$$

whence

$$\sigma_P = \sigma_R\ (0.17)$$

In other words about 17% of the refraction error remains in σ_P^2. However, the GDOP (defined in Subsection 3.1) is very nearly the same as the sensitivity of the random error. From Figure 3-11, we have GDOP = 46. Therefore, the horizontal position error would be 46 (0.17) = 7.8 which agrees quite well with the value given in Figure 3-11; i.e., 7.6.

When i = 30°, $\sigma_p^2 = \sigma_R^2 [0.09]$ and $\sigma_p = 0.3\sigma_R$. The GDOP for i = 30 is seen to be 4.7 and hence the position error due to refraction is (4.7) (0.3) = 1.4 which again agrees closely with the result given in Figure 3-11; i.e., 1.77.

When i = 10°, S $\approx 200 \left(\frac{10}{57.4}\right)$, which is about 35 miles. Apparently the error cancellation property of range differencing does not counterbalance the loss in accuracy due to GDOP. In other words, to have good ionospheric error cancellation characteristics the satellite spacing must be very close which imposes a severe GDOP penalty. A similar argument can be applied to explain why the calibration is not too effective even for short distances. The calibration depends on a very high correlation of the range difference error to be effective because, due to the large GDOP, any residual refraction errors are multiplied by the large GDOP to yield a large position error. The severity of the effect is shown in Figure 3-21. This figure shows the growth of the position error as the user moves away from the calibration point.

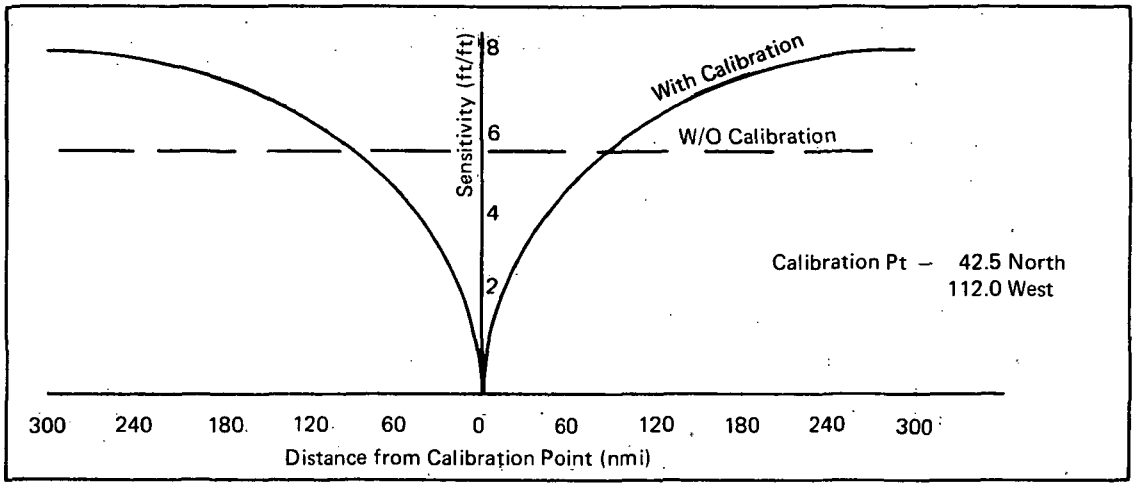

Figure 3-21. Effect of Refraction Error on Horizontal Position with and without Calibration as a Function of Distance from Calibration Point

Figures 3-22, 3-23, and 3-24 explore another aspect of the refraction problem. From the previous discussions and results, the impact on error sensitivities due to S has been established. One of the parameters directly influencing S is the height of the ionosphere, h_{IONO}. Since there is no clearly defined altitude at which the refraction takes place, h_{IONO} was varied.

The results of this parametric analysis are summarized in Figures 3-22, 3-23, and 3-24 with good agreement with the previous results; the 3P concept is very sensitive to anything that changes $P(S)$. Furthermore, the lower h_{IONO} is, the less change there is in $P(S)$ and the 3P system should indicate better performance. The figures are in agreement.

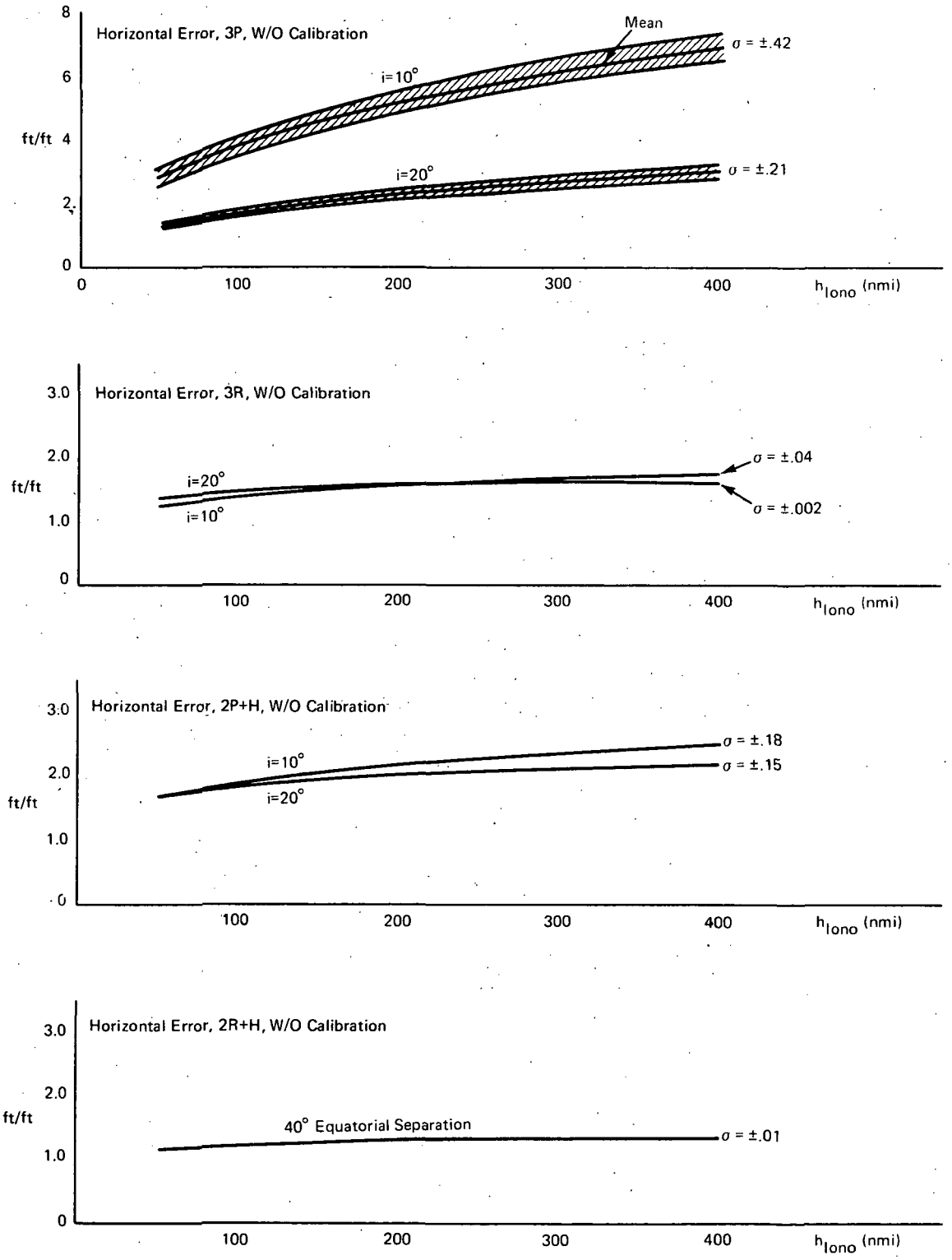

Figure 3-22. Effect of Height of Ionosphere on Horizontal Error without Calibration

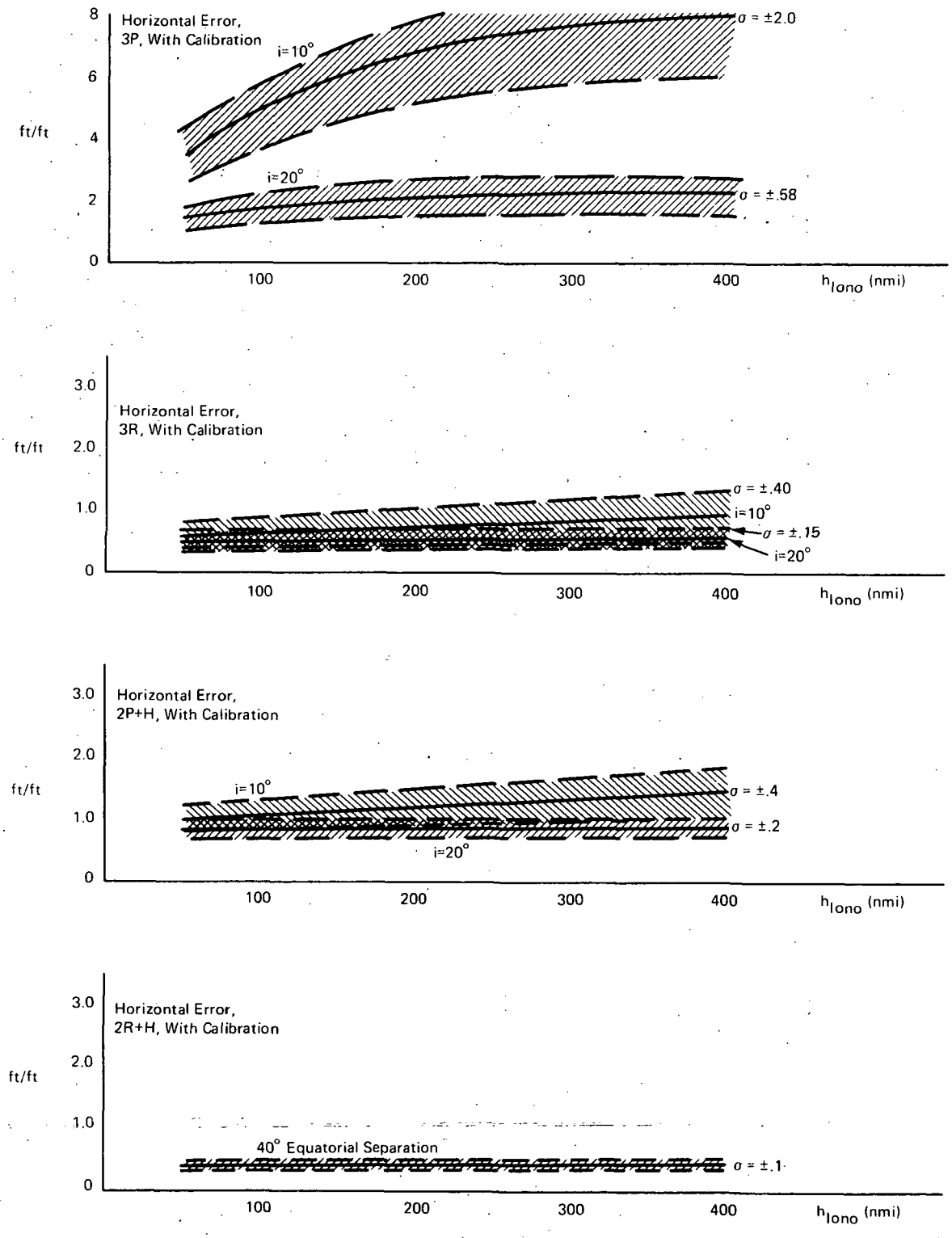

Figure 3-23. Effect of Height of Ionosphere on Horizontal Error with Calibration

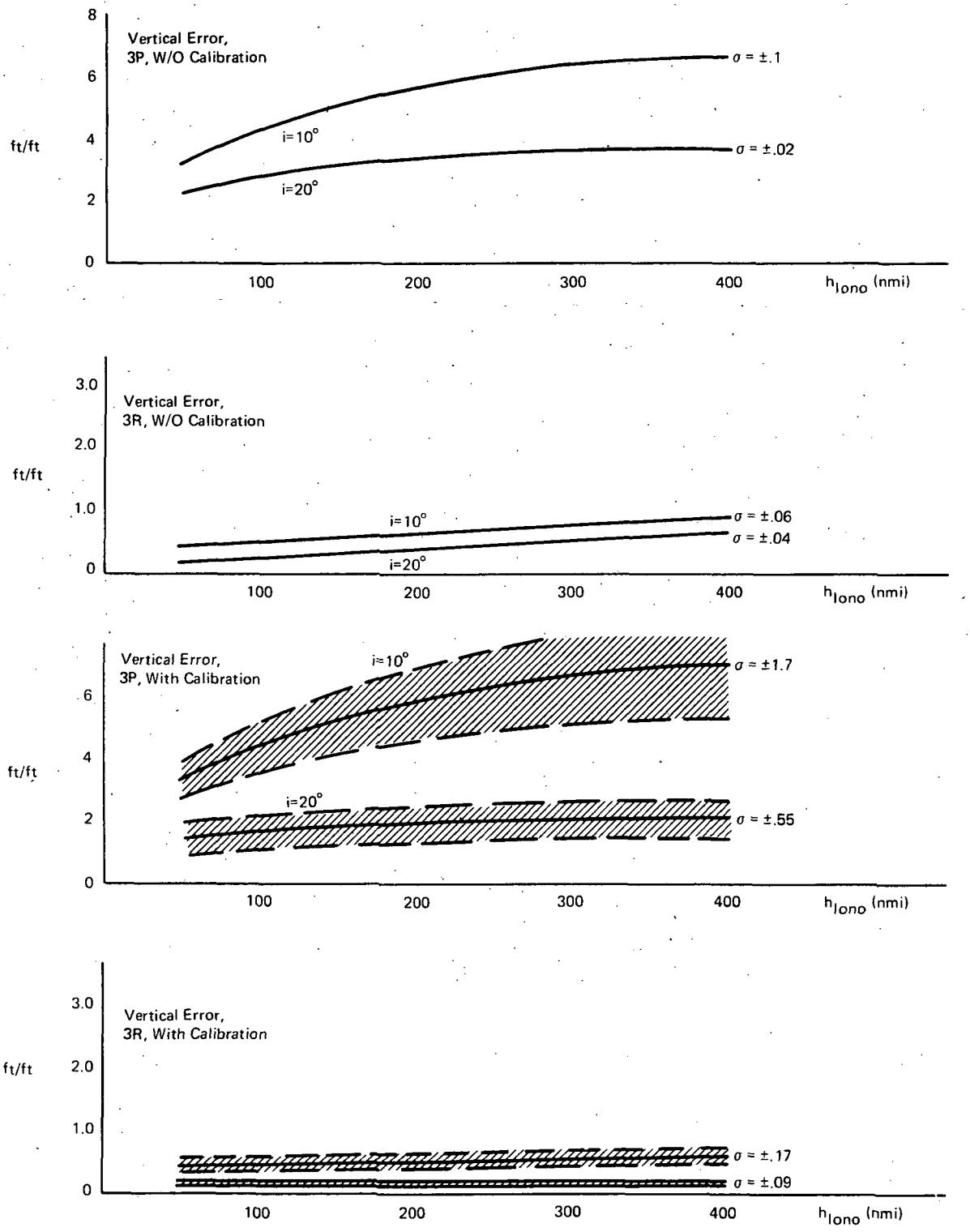

Figure 3-24. Effect of Height of Ionosphere on Vertical Error with and without Calibration

3.3.7 EFFECT ON HORIZONTAL ERROR DUE TO ROTATION OF SATELLITES IN THE Y CONSTELLATION

Figures 3-11, 3-12, 3-13 and 3-14 assumed a midnight Y constellation. Figure 3-25 and 3-26 assume exactly the same conditions except that four hours have passed and the Y constellation has moved from its midnight to its 4 AM configuration, (see Figure 4-2a). The results are very nearly the same for i = 10° but show some differences for i = 30°. The explanation lies in noting from Figure 4-2a that for i = 10° the Y shape is maintained throughout a 24 hour period whereas for i = 30°, the Y shape is transformed into an inverted T after 4 hours. The change from the Y to the T shape is very likely the major reason for the differences. If the horizontal errors were broken into two parts; i.e., EW and NS; there would be a noticeable shift in the accuracy of the EW and NS components with time. But since the EW and NS components are RMSed, the rotation of the Y shape (i = 10°) does not have a major influence. The shift would be most noticeable in areas of low elevation angle where there is a tendency for the EW and NS errors to be unequal.

3.3.8 HORIZONTAL ERROR DUE TO ALTIMETER ERROR WITH AND WITHOUT CALIBRATION

The 2P+H and 2R+H concepts use an altitude measurement in lieu of a P or R measurement. An error in the altitude measurement produces an error in the horizontal measurement (see Subsection 3.2.4.2). Figure 3-27 addresses this aspect considering both the 2P+H and 2R+H concepts with and without calibration. The results show a nearly one to one effect; that is, 100 ft of altitude error causes 100 ft of horizontal error. The value of the calibration is marginal, but there was only one calibration station assumed for the entire Region 2. Considerably better results are possible when the serviced region is substantially reduced. The black bars represent the mean deviation and the white bars the standard deviation.

3.3.9 MISCELLANY

3.3.9.1 3P Performance With Box Constellations

The 3P concept can, for certain satellite constellations, yield accuracies which are much worse than those indicated thus far. In particular, the box constellation as its name implies arranges the satellite into a box pattern. In Figure 4-26, the 3 AM or 3 PM constellation with the center satellite removed is one example of a box constellation. In Figure 4-8, 12 midnight case, if satellite 4 (or 5) were located at the bottom of the figure 8, a box constellation would result.

Figure 3-28 illustrates quantitatively how disastrous the consequences are when a box constellation occurs. The top figure should be compared with the two bottom figures. All things are equal except for the arrangement of the satellites.

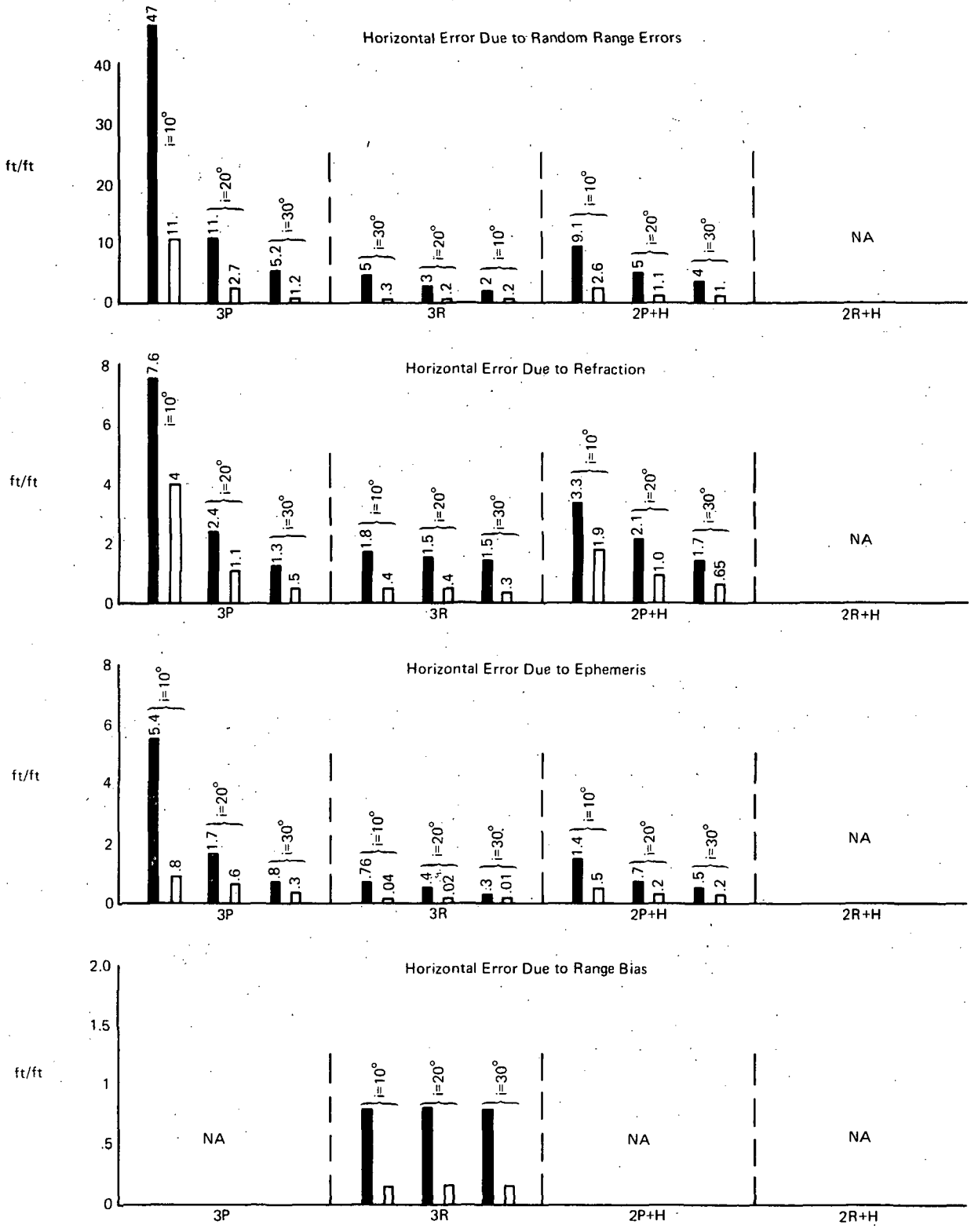

Figure 3-25. Comparison of 3P, 3R, 2P+H, and 2R+H Concepts Versus Error Source without Calibration, 4 AM Y Constellation

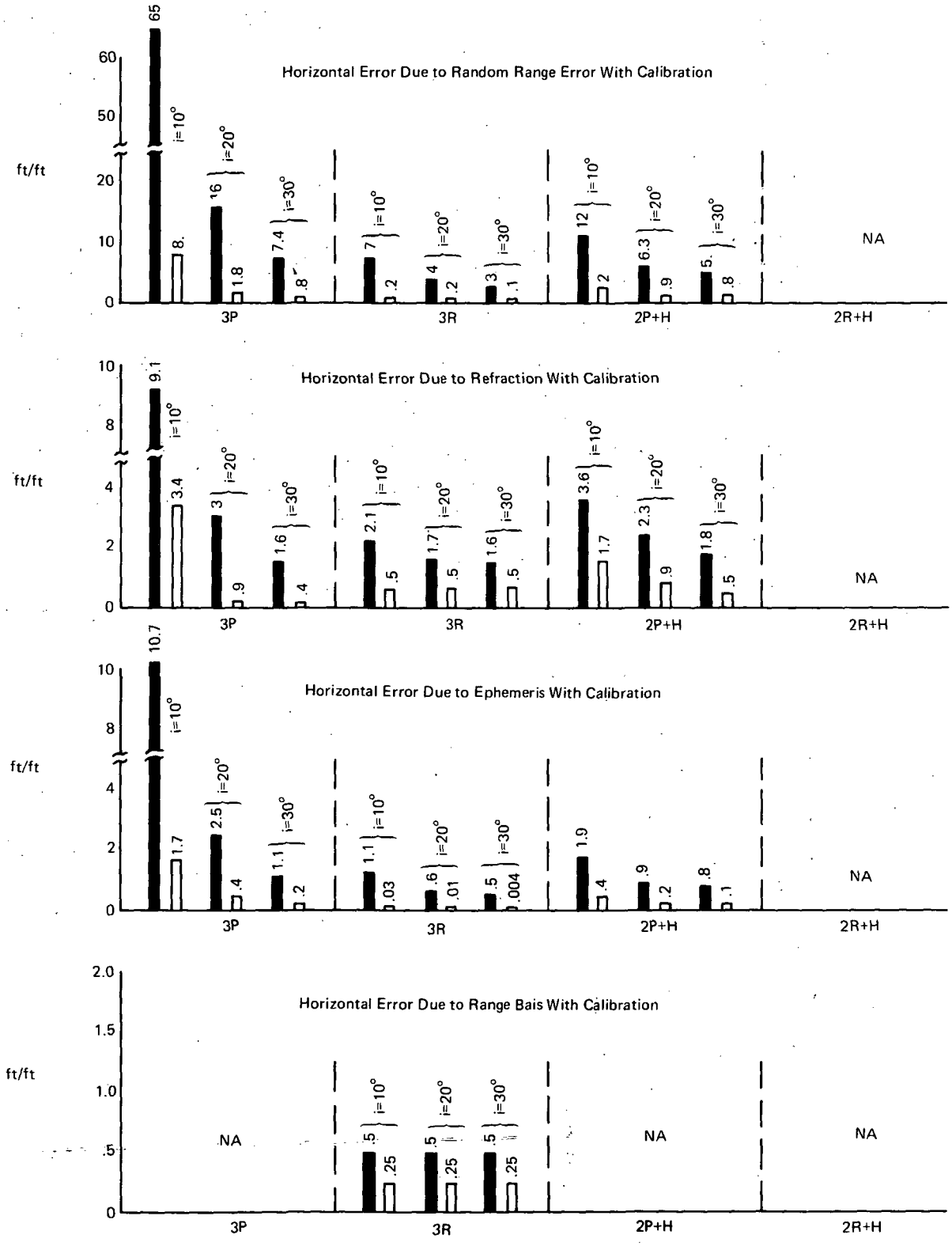

Figure 3-26. Comparison of 3P, 3R, 2P+H and 2R+H Concepts vs Error Source with Calibration, 4 AM Y Constellation

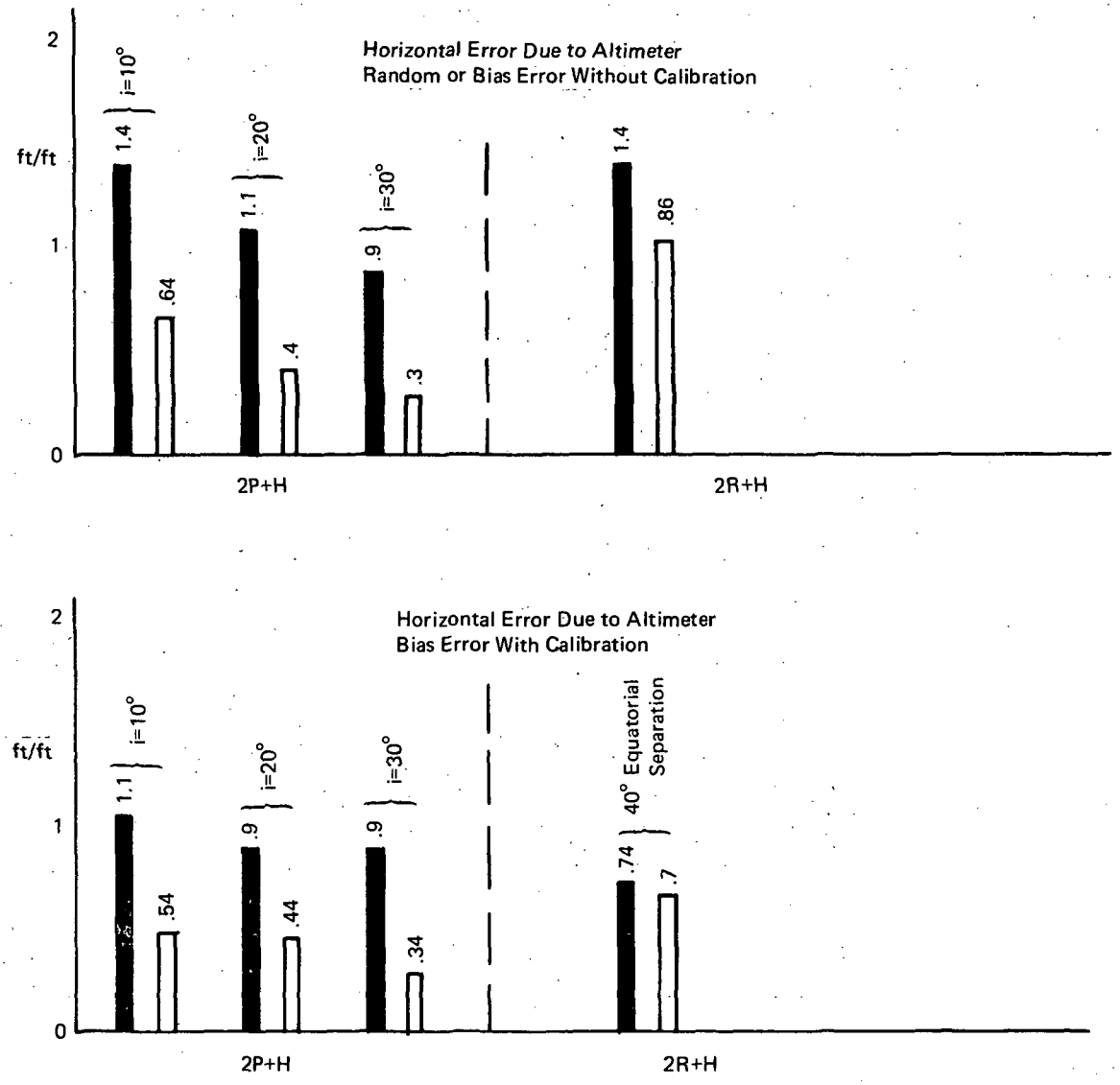

Figure 3-27. Horizontal Error due to Altimeter Error with and without Calibration

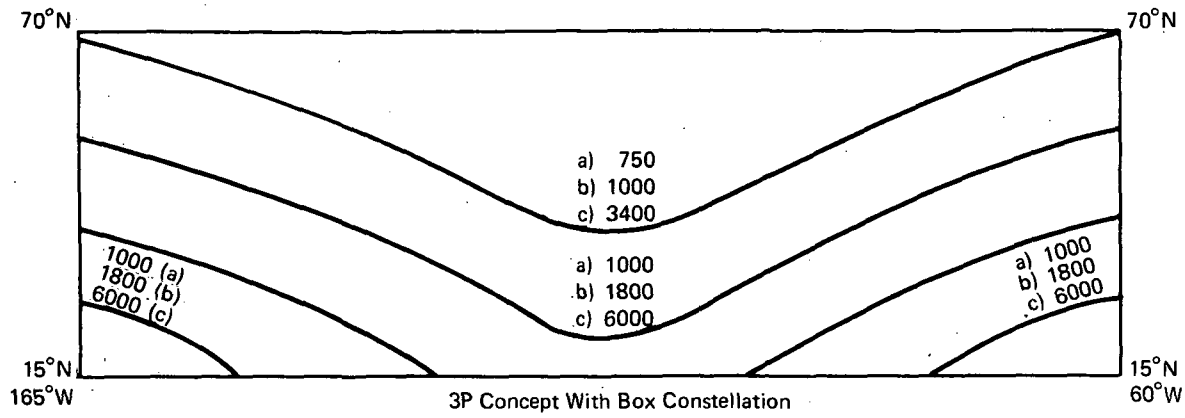

a) 30° Inclination
b) 20° Inclination
c) 10° Inclination

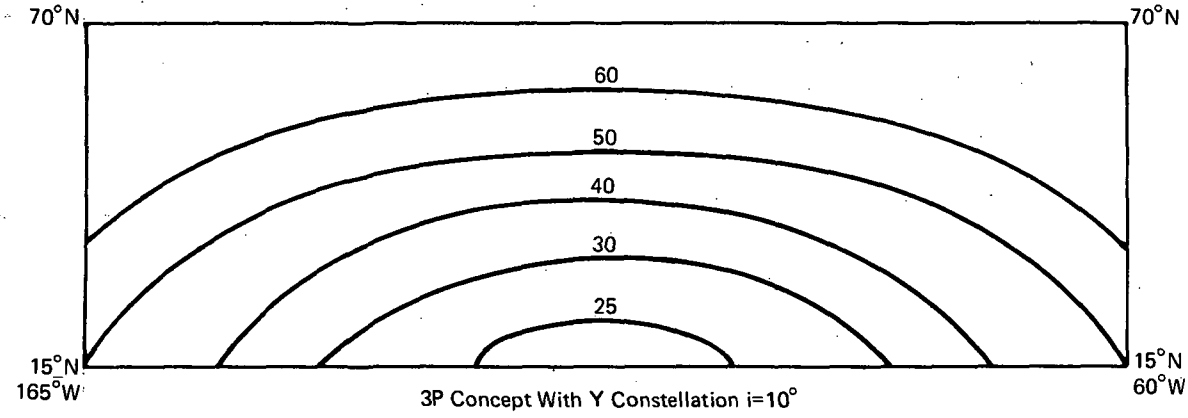

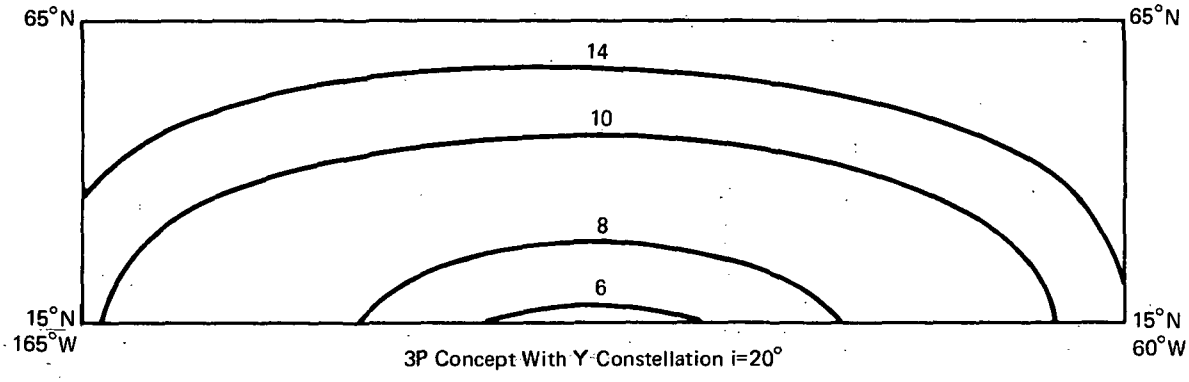

Contours in feet of Horizontal Error
per foot of Random Range Error

Figure 3-28. Horizontal Error due to Random Range Error for Box and Y Constellations

It is important to realize that, though the satellites are arranged as the corners of a rectangle, the baselines upon which the 3P concept derives its range differences and hence its hyperboloids are as shown in Figure 3-29.

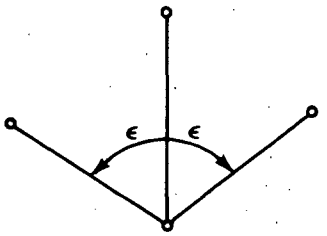

Figure 3-29. Baselines Formed from Box Constellation for 3P Concept

When ϵ is about 120°, we have the midnight Y configuration and when ϵ is about 90° we have the 3 AM configuration (see Figure 4-20). From this, one could infer that the overall performance of the 3P concept is strongly related to ϵ. Figure 3-30 has been constructed to show this relationship.

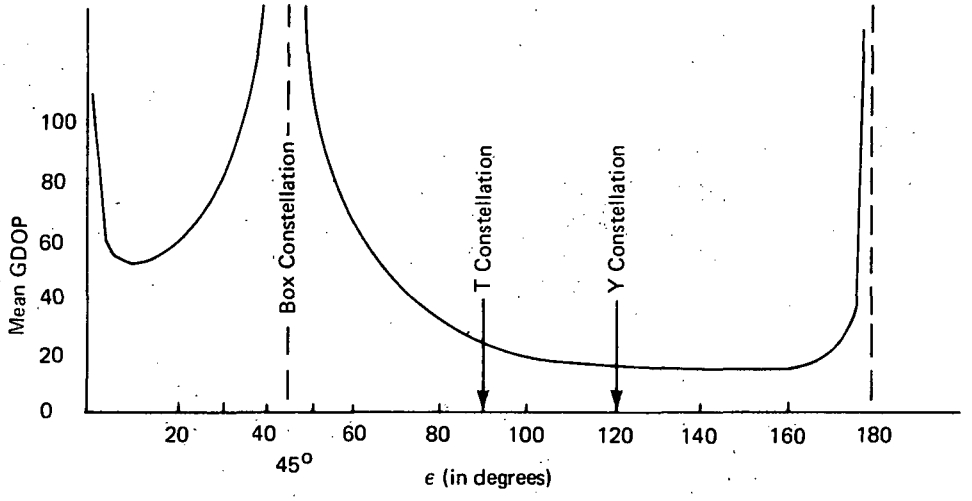

Figure 3-30. Effect of 3P Performance vs the Angle between the Three Baselines

At zero and 180° the baselines are parallel, which explains the shape of the curve there. The flatness of the curve between 90° and 170° is somewhat surprising but indicates a very uniform performance of the 3P concept for that range of ϵ. Certainly $\epsilon < 60°$ should be avoided. There is no known simplified explanation for the performance singularity at $\epsilon = 45°$. An isolated case can be constructed which shows graphically that when $\epsilon = 45°$ and the user is at the center of the box there is no vertical information, i.e., the intersection of three hyperboloids is a vertical line. This isolated case also helps to explain why the 2P+H concept does not have a singularity, the H provides the vertical information.

Section 4

SATELLITE COVERAGE

Section 4

SATELLITE COVERAGE

4.1 INTRODUCTION

All the surveillance/navigation systems that have been investigated, require simultaneous visibility to two, three, or four satellites (more than four is always redundant). A problem exists in how to deploy the least number of satellites to provide visibility over the largest desired area of the globe. There are two classic approaches to this problem: (1) combinations of 24-hour period satellites in geostationary and inclined/elliptical orbits which form stationary constellations over a fixed geographic region, and (2) less than 24-hour period satellites in inclined, near circular orbits with uniformly spaced orbit planes. The latter produces a nongeostationary pattern of satellites over any geographic region and, in fact, tends to provide global coverage though not perhaps on a continuous basis.

Many investigations have been performed for Defense Navigation Satellite Systems (DNSS) with regards to the satellite coverage problem and both the stationary and nonstationary cases have been investigated in depth[1]. However, these studies have had global coverage as the principal requirement. In this study we were interested primarily in coverage for a specified and limited region of the globe: i.e., the 49 continental United States, Puerto Rico, and Hawaii.

Three test cases, or geographic regions were established (see Figure 4.1). Region 1 covers CONUS and southern Canada. Region 2 extends the boundaries of Region 1 to include most of Alaska, Puerto Rico, and Hawaii. Region 3 covers CONUS, Hawaii, Puerto Rico and a very narrow strip of Canada along our border, but not Alaska.

Initially, it was throught that the stationary constellations would prove superior for the limited coverage problem primarily because (from the DNSS studies) it was known that global coverage requires about 20 satellites and the total number of satellites was about the same for either the stationary or nonstationary constellations. The stationary constellation, on the other hand, requires only four to six satellites. Therefore, based solely on the number of satellites in orbit, the stationary constellation appeared more attractive.

However, since the objective of this study was to perform a parametric treatment of all aspects of the COLM/ATC problem, the nonstationary constellations were also investigated.

---

[1] "621B Geometric Performance for a 20 Satellite Global Deployment," Aerospace Report No. TR-0172 (2521-01)-1; November 5, 1971.

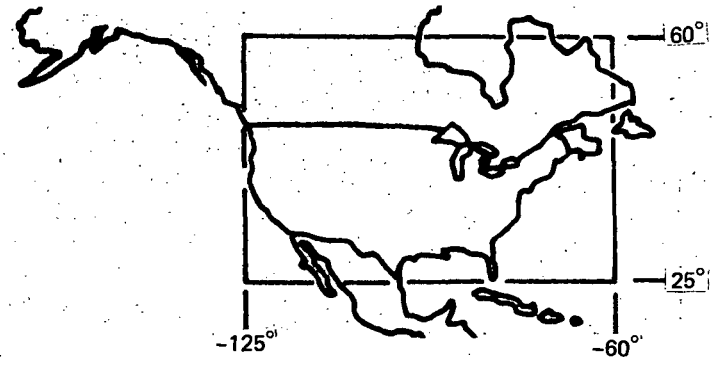

Region 1

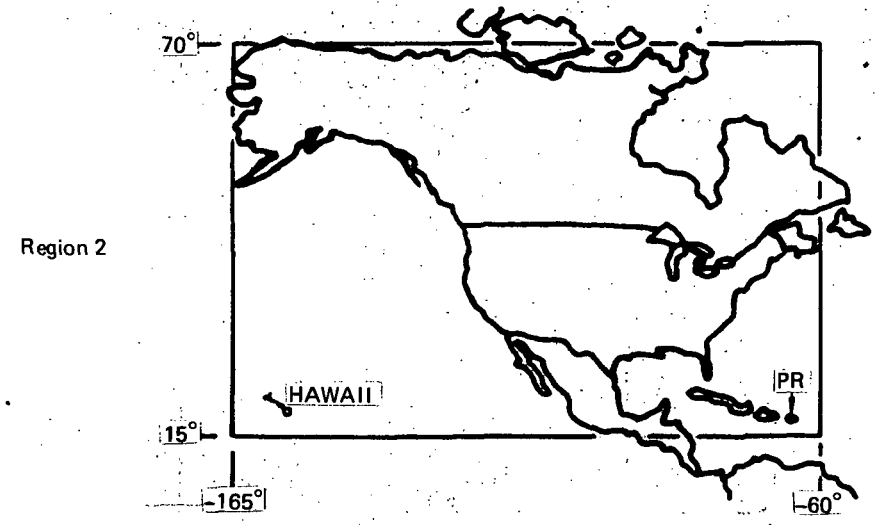

Region 2

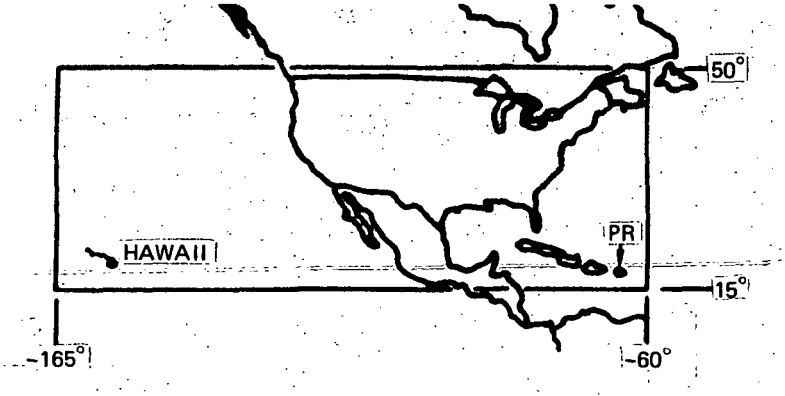

Region 3

Figure 4-1. Selected Geographic Regions

4.2 RESULTS

4.2.1 STATIONARY CONSTELLATIONS

Coverage for two types of stationary constellations are presented in this subsection. The first type is the so called "pin wheel" constellation which has a geostationary satellite in the center and three or four 24-hour period, inclined, and eccentric satellites which appear to an earth observer to produce a nearly circular pattern about the geostationary satellite (see Figures 4-2, 4-3 and 4-4). The satellite movement in 1-hour increments shows the effect of the eccentricity of the orbit which varies as $e = \tan i/2$ in order to produce the circular ground trace. Notice that the Y or X formations are retained for all time for $i = 10°$, whereas there is considerable change for $i = 30°$. The change is caused by the eccentricity which causes a speeding up in the southern hemisphere and a slowing down in the northern hemisphere.

The second type is a variation of the pinwheel, which uses two geostationary satellites and three or four elliptical/inclined satellites, the latter of which appear to an earth observer as an egg-shaped pattern about the two geostationary satellites.

The pin wheel constellation has two parameters to be varied: (1) the longitude of the geostationary satellite, and (2) the inclination of the satellites in the ring. The longitude of the geostationary satellite was chosen to provide maximum coverage of CONUS. The inclination was then varied and the contours of visibility were established. The contours are defined as the locus of points where the earth observer can see the required number of satellites, and where at least one of the satellites is at an elevation of 10°, which is generally accepted as a practical radio navigation horizon. These contours establish the boundaries of multiple satellite visibility. The results for the four satellite pinwheel constellations are shown in Figure 4-5. The contours are shown for the worst case; i.e., when one of the satellites is at perigee or at the point of maximum southern latitude. This condition occurs three times daily. Otherwise, the visibility contours would extend farther north. However, since an ATC system must function continuously, the extended coverage is only of secondary value.

From Figure 4-5, it can be concluded that for CONUS coverage, with any position location system using four satellites, the inclination must be less than 20°, whereas to provide coverage for CONUS, Hawaii, and Puerto Rico the inclination should be about 10°. For position location systems using only three satellites there is considerably more coverage in the northern latitudes, but still not adequate for coverage of both CONUS and Alaska (see Figure 4-6). Figure 4-6 is shown for the 12 noon configuration (Figure 4-3) using satellites 2, 3, and 4, which provide the best accuracy but least coverage.

For all other time configurations, the three-satellite visibility contours are essentially that for the geostationary satellites because, as seen from Figure 4-3, the satellite south of the equator would not necessarily be used.

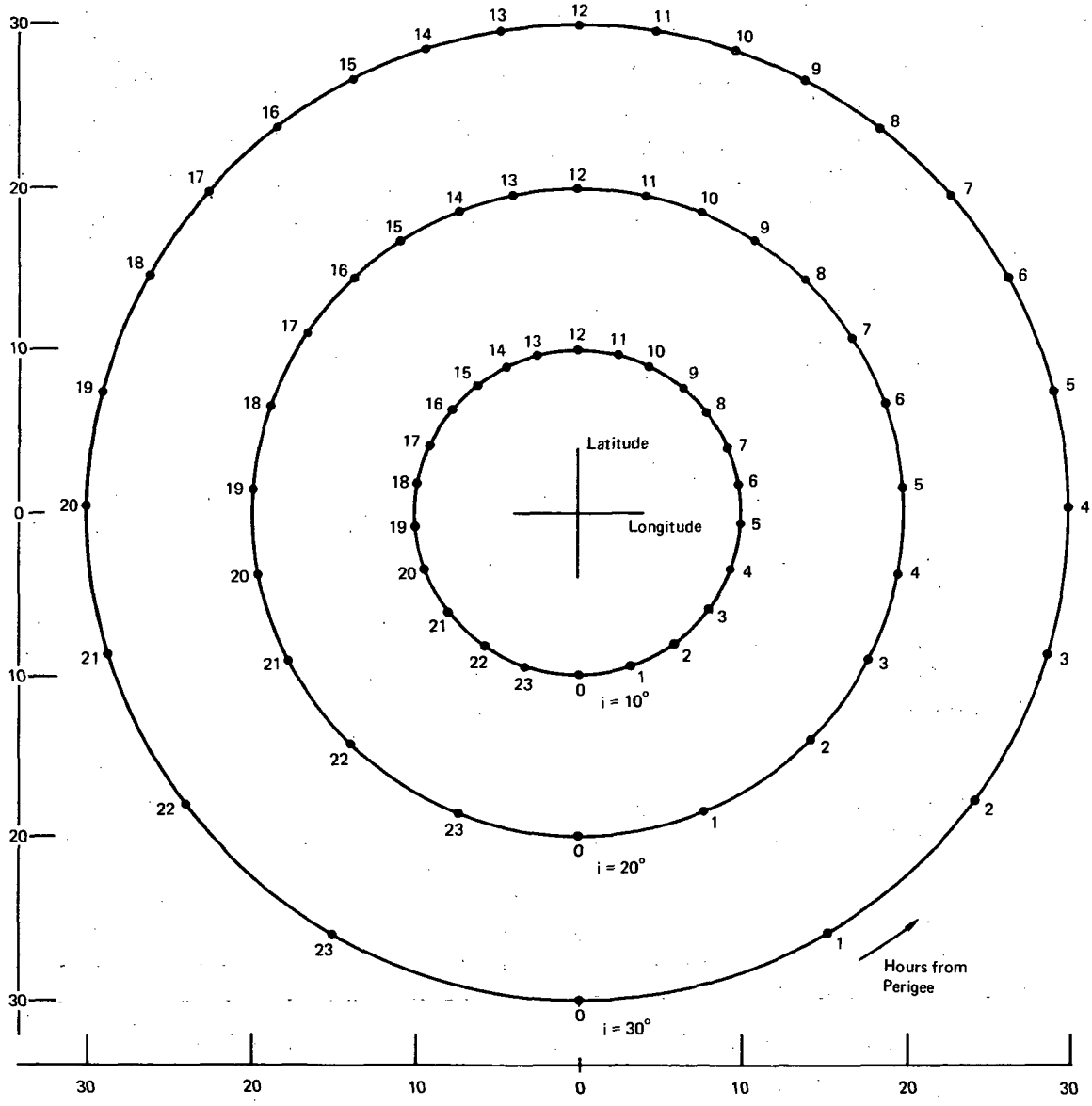

Figure 4-2. Ground Trace of Pinwheel Constellation with Hours from Perigee

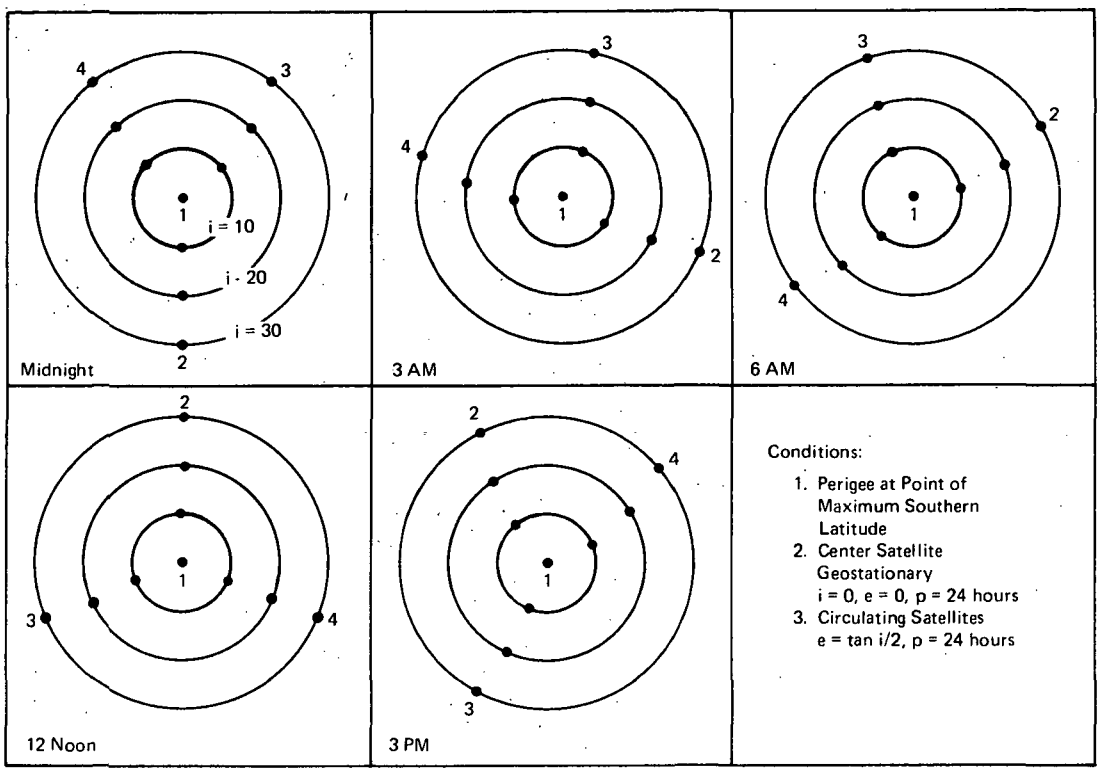

Figure 4-3. Four-Satellite Pinwheel Constellation

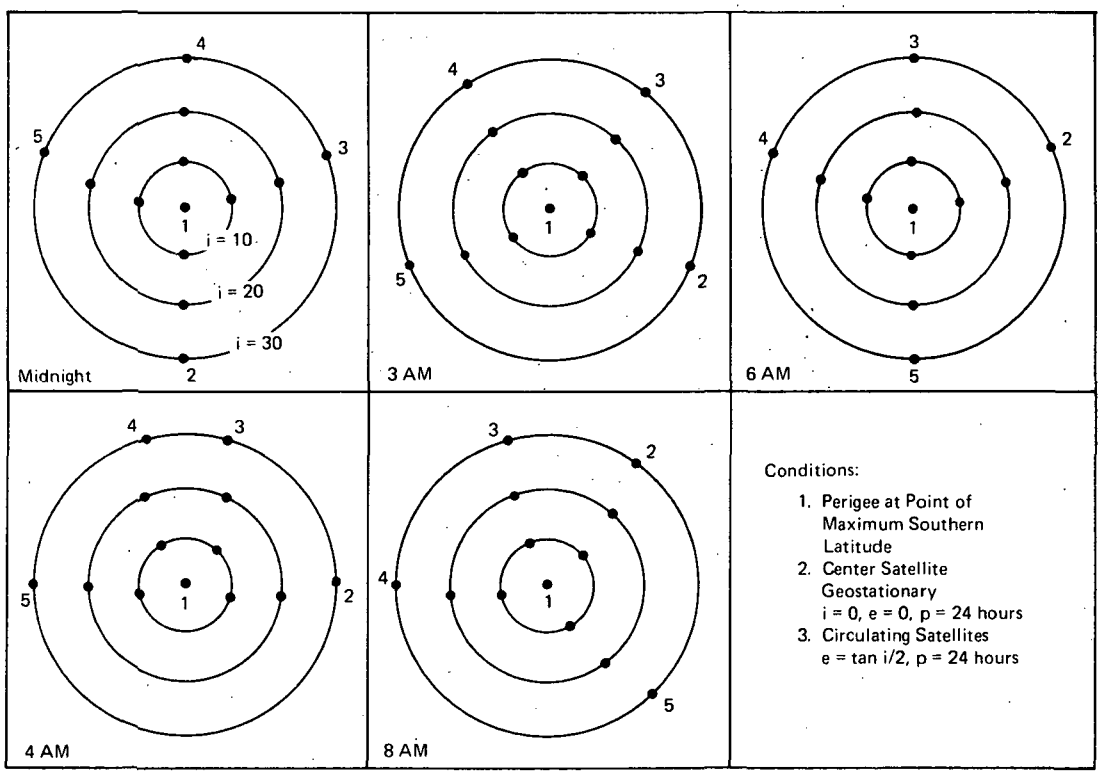

Figure 4-4. Five-Satellite Pinwheel Constellation

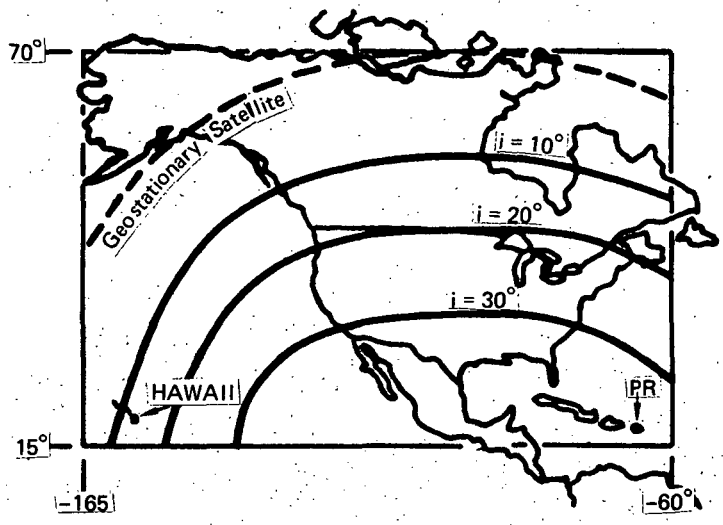

Figure 4-5. Four-Satellite Pinwheel Constellation, Four-Satellite Visibility Contours

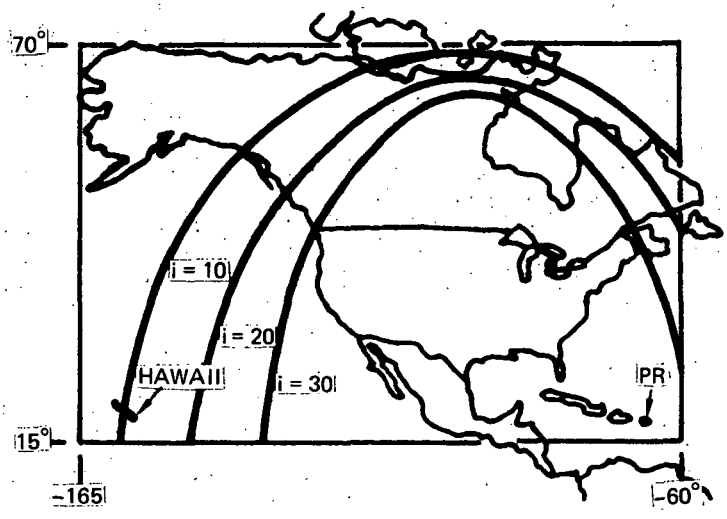

Figure 4-6. Four-Satellite Pinwheel Constellation, Three-Satellite Visibility Contours

If a fifth satellite is added to the pinwheel constellation, there is an improvement in the coverage, particularly in the northern latitudes. This configuration is shown in Figure 4-7.

Figure 4-7 assumes the 3 AM configuration (see Figure 4-4), and the position fix would be derived from satellites 1, 3, 4, and 5 when west of satellite 1, and from satellites 1, 2, 3, and 4 when east of satellite 1. The midnight and 4 AM, 6 AM, and 8 AM configurations will provide slightly more coverage at higher latitudes. However, Figure 4-7 is based on the premise that 100% visibility is required, at all times.

Three satellite visibility contours are essentially the same as for the geostationary satellite since the satellite in the southern hemisphere is not visible at the northern latitudes. Note, however, that at 4 AM and 4 PM, satellites 3 and 4 are quite close, which affects the position accuracy.

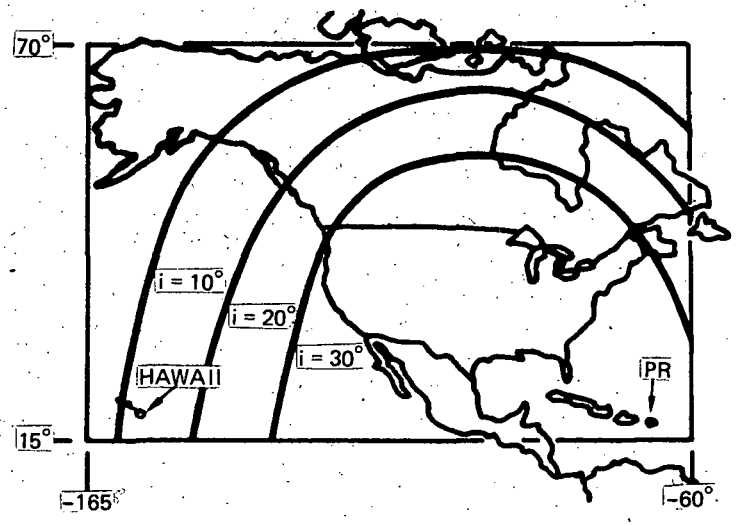

Figure 4-7. Five-Satellite Pinwheel Constellation, Four-Satellite Visibility Contours

Figure 4-8 shows another variation of the stationary satellite constellation wherein the inclination is very high (60°) and two geostationary satellites are placed inside the ring. The eccentricity for this constellation exceeds 0.5. Consequently, perigee altitude is only about 7000 miles which results in some loss of visibility and higher Doppler rates when viewing those satellites during their passage in the southern hemisphere. However, as Figure 4-8 shows, it is never necessary to use a satellite south of the equator for position fixing.

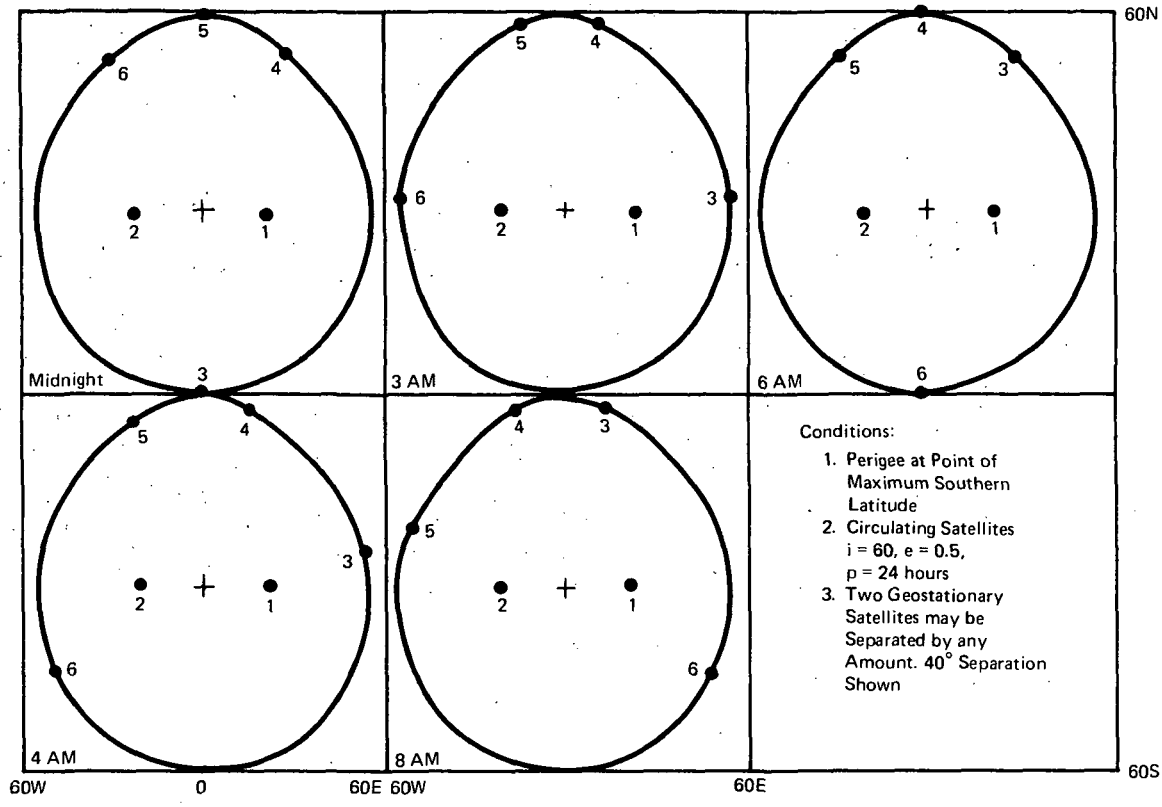

Figure 4-8. Six-Satellite Constellation with Large Inclination and Eccentricity

Figure 4-9 shows the coverage for six-satellite constellations. The 3 AM configuration was selected because it has the largest spread, thereby providing the least amount of coverage but the best position accuracy. Figure 4-9 also assumes that aircraft west of the center of the geographic coverage use satellites 1, 2, 5, and 6, whereas those east of center use satellites 1, 2, 3, and 4. Combinations like 1, 2, 4, and 5 provide very poor accuracy (see Figure 3-30).

Another stationary constellation is shown by Figure 4-10. This constellation uses two geostationary satellites and three others in inclined circular 24-hour orbits. The equatorial spacing of the geostationary satellites should be about equal to the inclination angle so as to provide an equal position accuracy in the EW and NS directions.

The augmented Figure 8 five-satellite constellation has a noticeable disadvantage in that the 4 AM and 4 PM configurations have no satellite well north of the equator. Therefore, during these two times each day, the NS position accuracy will be from two to three times worse than the EW position error. At other times, the EW and NS position errors will be about equal.

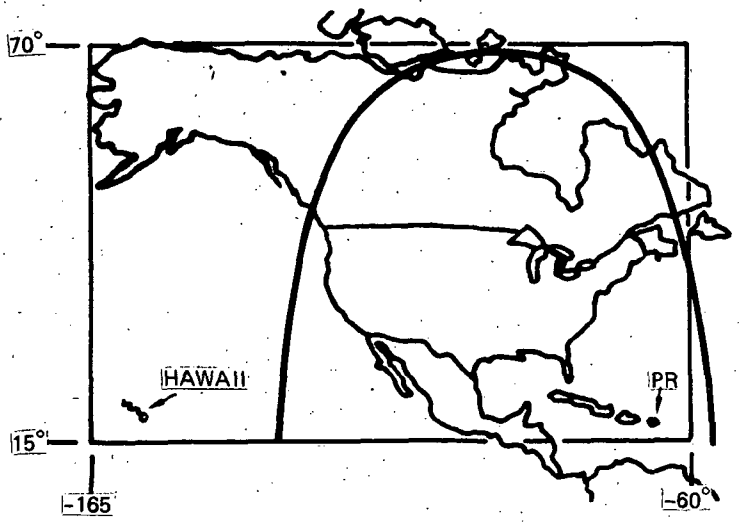

Figure 4-9. Six-Satellite Constellation with
Large Inclination and Eccentricity, Visibility Contours

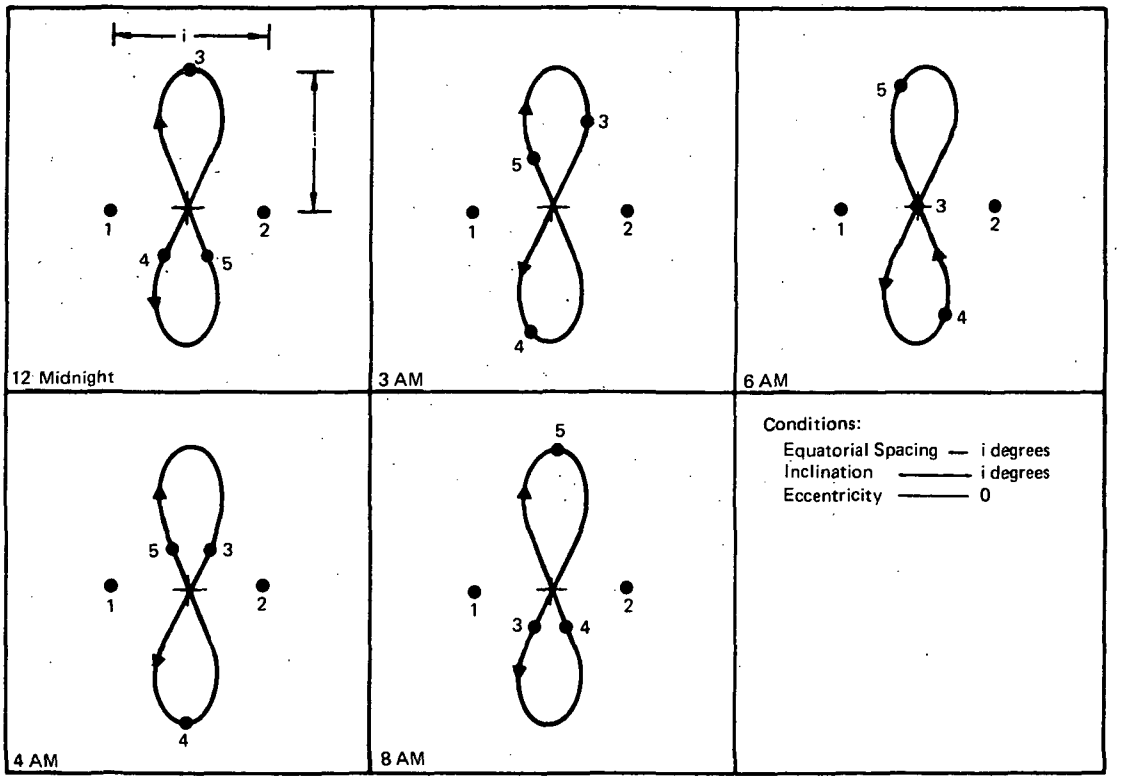

Figure 4-10. Augmented Figure 8 Five-Satellite Constellation

The coverage and effect of varying the inclination angle of the Figure 8 five-satellite constellation is shown in Figure 4-11.

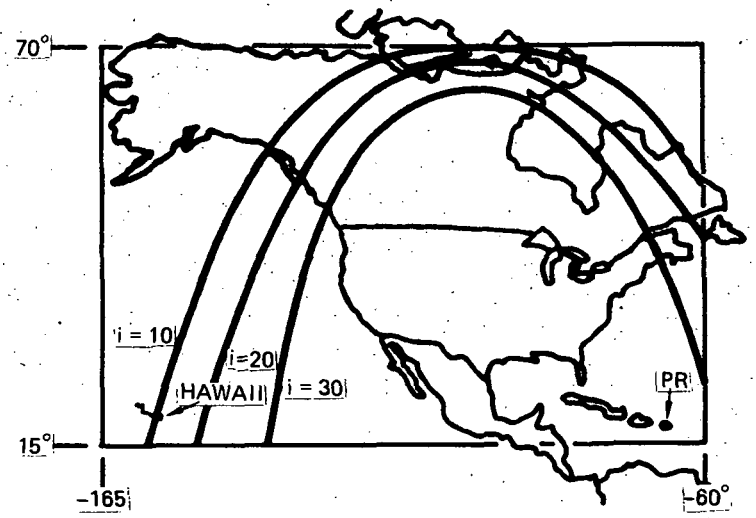

Figure 4-11. Figure 8 Five-Satellite Constellation Visibility Contours

Comparison with Figure 4-7 (five-satellite pinwheel constellations) shows very comparable coverage characteristics.

In summary, all of the stationary constellations considered exhibit similar coverage characteristics for the same number of satellites. The fifth and sixth satellites provide additional coverage especially in the northern latitudes. However, no single stationary constellation provided coverage for CONUS, Puerto Rico, Hawaii, and Alaska simultaneously.

The reader can visualize sliding the coverage plots in a longitudal direction from whence it can be seen that Alaska and Puerto Rico can never be covered with a single stationary constellation.

4.2.2 NONSTATIONARY CONSTELLATIONS

Since these constellations are not stationary, they tend to provide coverage of the entire globe. Therefore, to provide 100% coverage over any given area is almost equivalent to providing coverage for the entire globe. Since this requires more than five or six satellites, why consider the nonstationary cases?

Besides the reason of performing a parametric study, there are such reasons as (1) a single stationary constellation could not provide coverage for CONUS, Puerto Rico, Hawaii, and Alaska; (2) the nonstationary constellation will have the satellites at less than synchronous (24 hours) altitudes thereby having potential benefits in terms of launch costs and less free space radio propagation loss; (3) the nonstationary case will have a very soft degradation as the failure of any given satellite produces only intermittent coverage problems; (4) each satellite can be independently commanded ON or OFF which implies the potential of increasing coverage when and where necessary or desired without a marked increase in system costs. The satellite would be commanded ON when entering the desired coverage area and OFF when leaving. This feature is particularly easily implemented with polar orbits where a single station at Fairbanks or Thule can "see" each satellite once every orbit. Simple timing mechanisms reset at each north polar passage would provide the OFF command for the south going passes. Increased coverage would be provided by altering the ON/OFF commands; e.g., a longer On time on the south-going pass would provide coverage for many Latin American countries.

As was shown in Subsection 4.2.1, the stationary constellation coverage deficiency was decidedly in the northern latitudes. Therefore, the choice of nonstationary constellations focused on correcting this deficiency. This was done by concentrating on polar orbits, though orbits with 40° inclinations were also briefly investigated. The polar orbit grossly "over covers" the polar regions at some expense to the equatorial regions. The 40° inclination restores some of the unbalance. However, the inclined orbits are not visible from the same ground station; e.g. Fairbanks; on every pass, which would complicate the Satellite control by requiring several control stations.

A computer program was developed to study the nonstationary constellations and a description may be found in Appendix G. Basically, the program distributes the satellites about the world in a uniform manner, restricted only by the number of orbit planes and the total number of satellites. The orbital altitude and inclination are free variables but must be the same for all satellites. A region is specified and the program computes the number of satellites visible in that region. For large regions; e.g., like those shown in Figure 4-1; the program generates a raster within the region; and at each point in the raster, computes the number of satellites visible. The program then determines the number of raster points where either three or four satellites were visible. Time is then advanced and new positions of the satellites relative to the earth are computed, and the sequence of determining the number of raster points where with three or four satellites were visible is repeated and at the completion of some time (24 hours) the program computes the total number of raster points satisfying the visibility criterion and divides by the total number of raster points. This result is defined as the percent visibility.

The results of this investigation are summarized by Figures 4-12 and 4-13. Figure 4-12 is for 100% coverage, and Figure 4-13 is for 90% coverage. Comparison of Figures 4-12 and 4-13 tend to show the soft degradation of the nonstationary constellations. For example, in Region 3, with a period of 8 hours, four satellite visibility requires 23 satellites for 100% coverage and 18 satellites for 90% coverage. Therefore, if 23 satellites were initially deployed and five failed, there would be long term outage of only 10%.

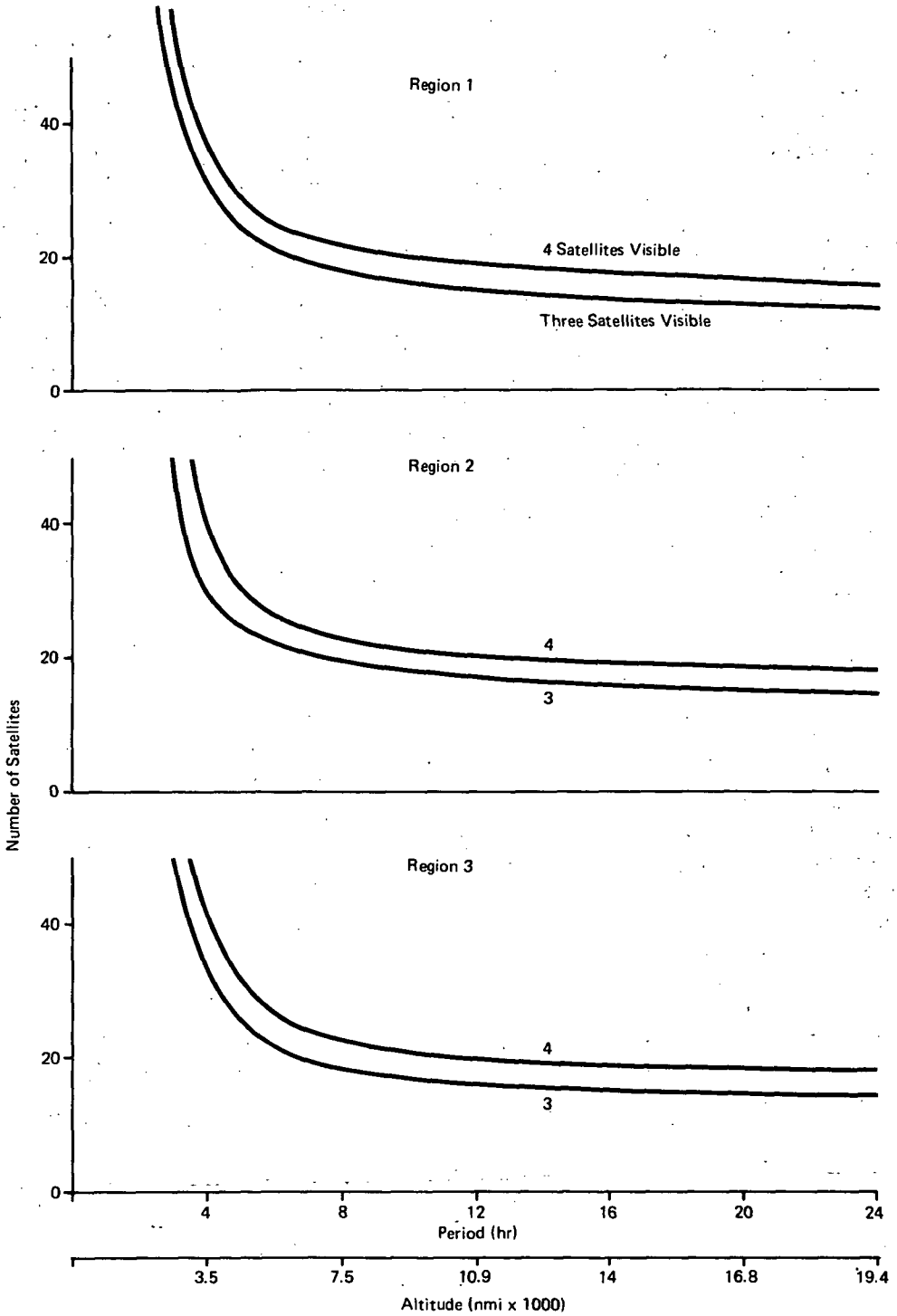

Figure 4-12. Number of Satellites for 100% Coverage

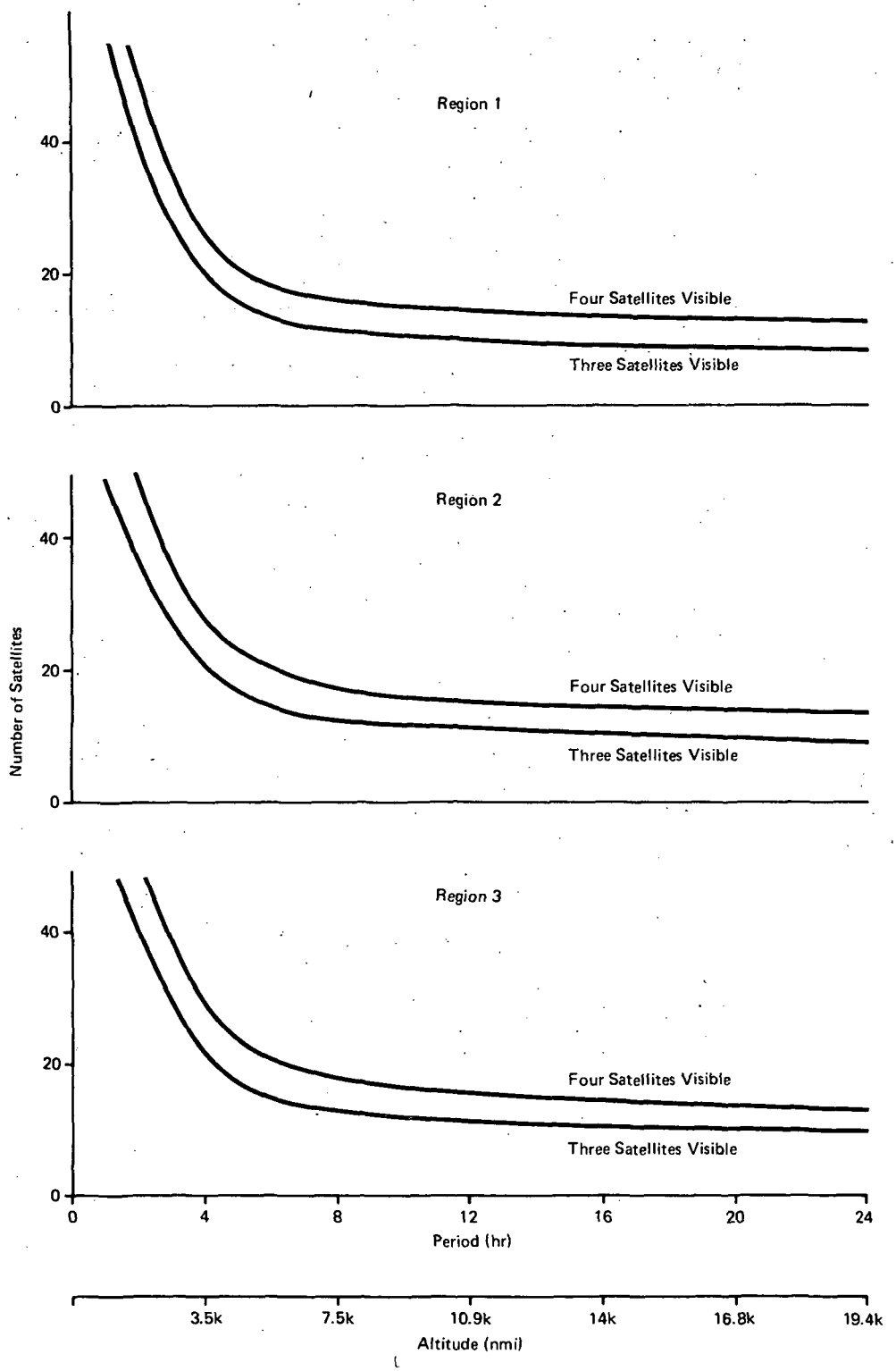

Figure 4-13. Number of Satellites for 90% Coverage

Notice the knee of the curves is around 6000 nmi which corresponds closely to the knee of the single satellite visibility curve (see Figure 4-14).

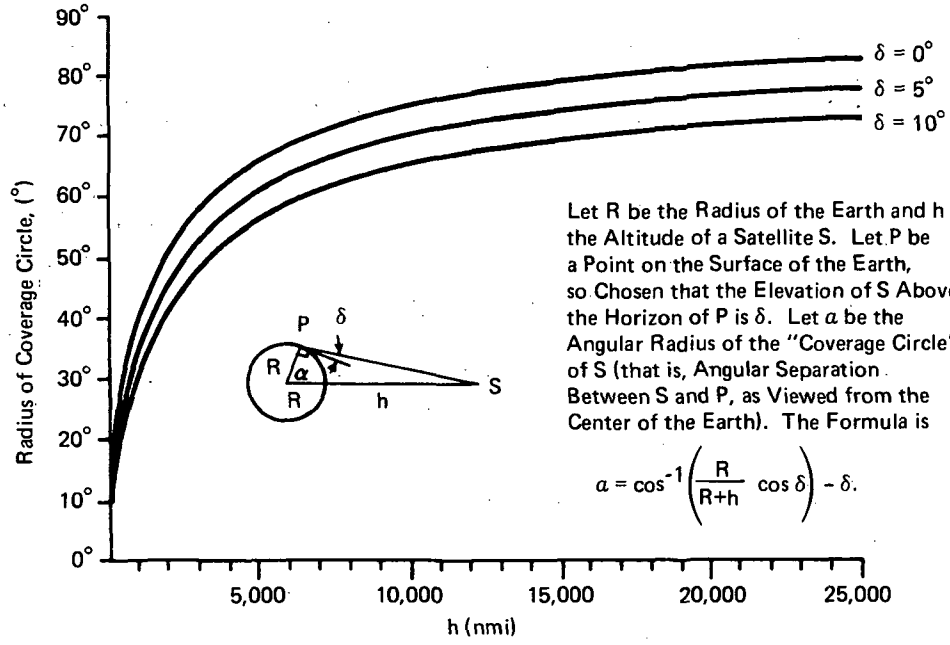

Figure 4-14. Single Satellite Earth Coverage

Figure 4-12 and 4-13 show that very attractive constellations exist with periods between 6 and 12 hours. Consider Tables 4-1 and 4-2, which were constructed from Figures 4-12 and 4-13.

Table 4-1

SUMMARY COMPARISON OF NUMBER OF SATELLITES REQUIRED VS ORBITAL PERIOD FOR REGION 2 AND FOUR-SATELLITE VISIBILITY

Period (h)	100% Coverage	90% Coverage
6	26	20
8	23	17
10	21	16
12	20	15
24	18	14

TABLE 4-2

SUMMARY COMPARISON OF NUMBER OF SATELLITES REQUIRED VS ORBITAL ALTITUDE FOR REGION 2 AND THREE-SATELLITE VISIBILITY

Period (h)	100% Coverage	90% Coverage
6	22	14
8	19	12
10	18	12
12	17	11
24	14	9

The 10-hour period constellation with its 21 satellites could be deployed in three equally spaced orbit planes with seven equally spaced satellites in each plane. The 24-hour period with its 18 satellites could be deployed in three equally spaced orbit planes with six satellites in each plane. The difference between six and seven satellites per launch vehicle could be more than offset by the almost 2 to 1 reduction in orbital altitude; i.e., the seven-satellite launch may require a smaller booster than the six-satellite launch. A failure of one satellite in each launch would mean 21 - 3 = 18 operating satellites for the 10-hour period, and 18 - 3 = 15 operating satellites for the 24-hour period. Either would provide more than 90% coverage on the whole.

Table 4-3 summarizes the effect on the number of required satellites vs region 1, 2, and 3.

Table 4-3

EFFECT ON THE NUMBER OF SATELLITES REQUIRED VS REGIONS 1, 2, OR 3

Period (h)	Region		
	1	2	3
6	24	26	26
8	21	23	23
10	20	21	21
12	18	20	20
24	16	18	18

By comparing Table 4-3 and Figure 4-1, it may be concluded that the reason for the additional satellites is because Regions 2 and 3 extend into more southernly latitudes. In other words, expansion of Region 1 in a northward or east/west direction does not create the need for additional satellites, whereas expansion southward does.

Figures 4-15 through 4-25 provide additional details. In particular Figure 4-16 indicates that with orbital periods of less than 4 hours the increase in the required number of satellites is very rapid. For example, a 2-hour period requires about 100 satellites for four satellite visibility which is about 4 to 5 times that required for 6-hour orbits.

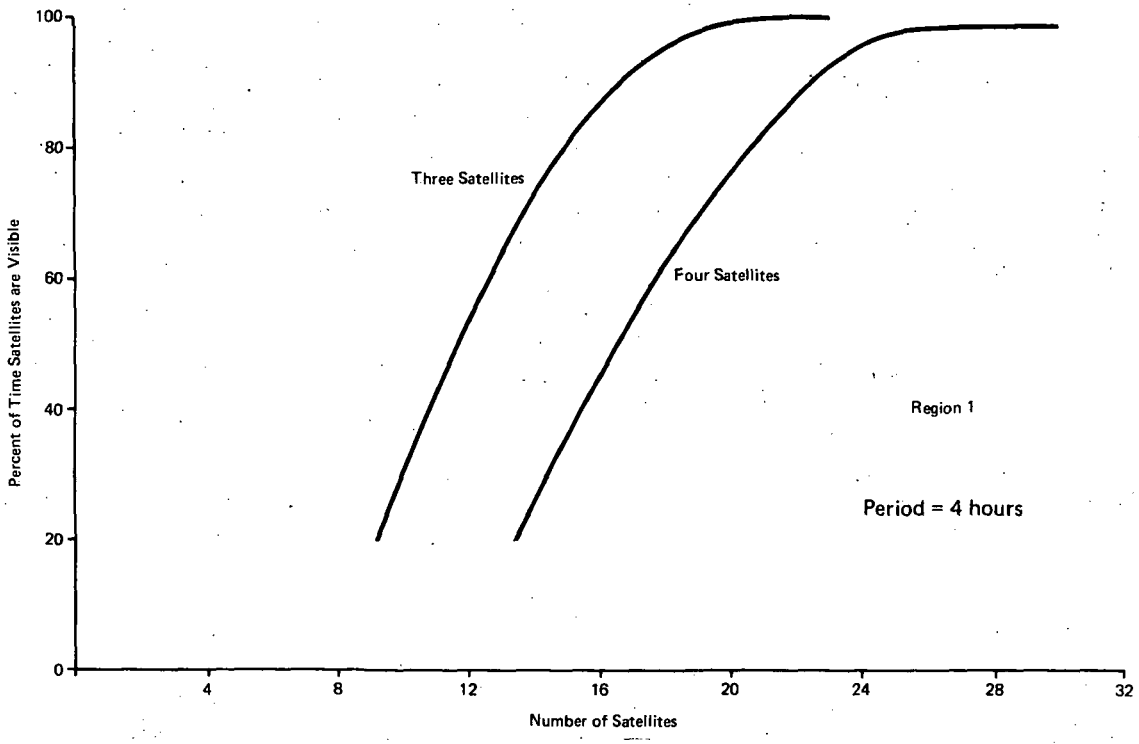

Figure 4-15. Percent Coverage vs Number of Satellites, Region 1

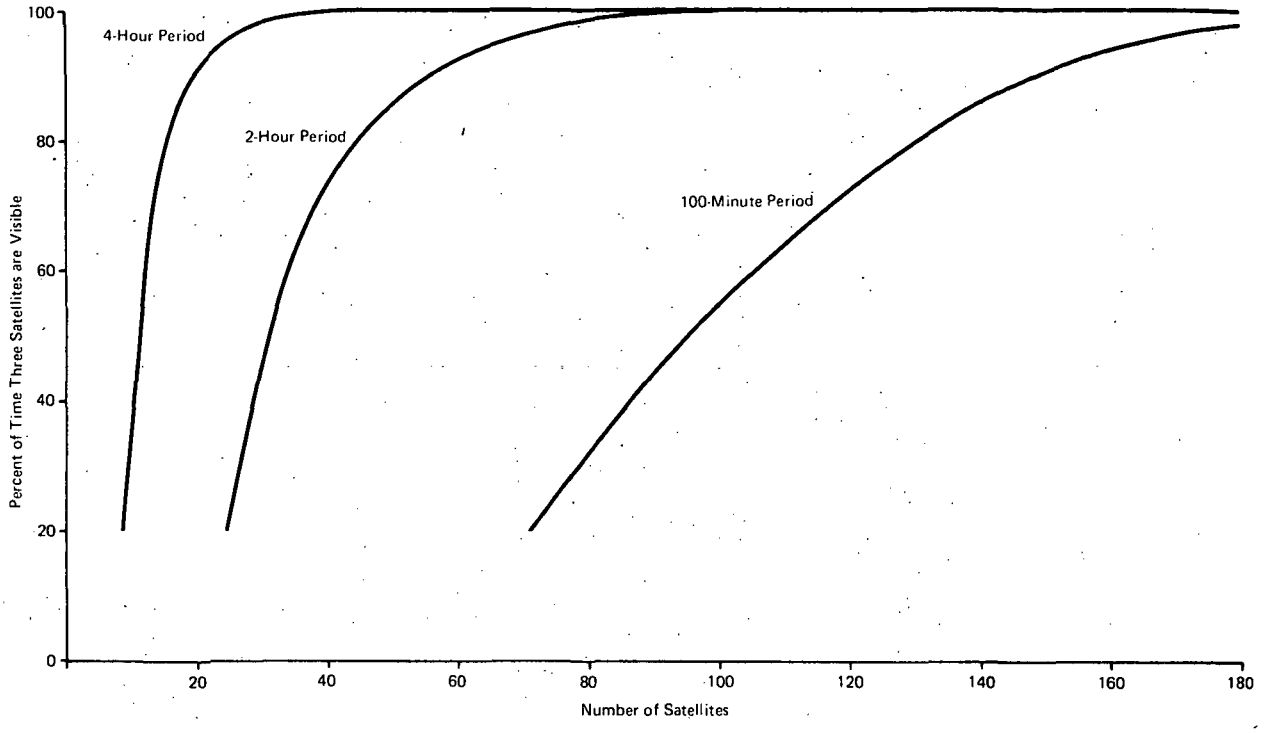

Figure 4-16. Three-Satellite Visibility in Region 1

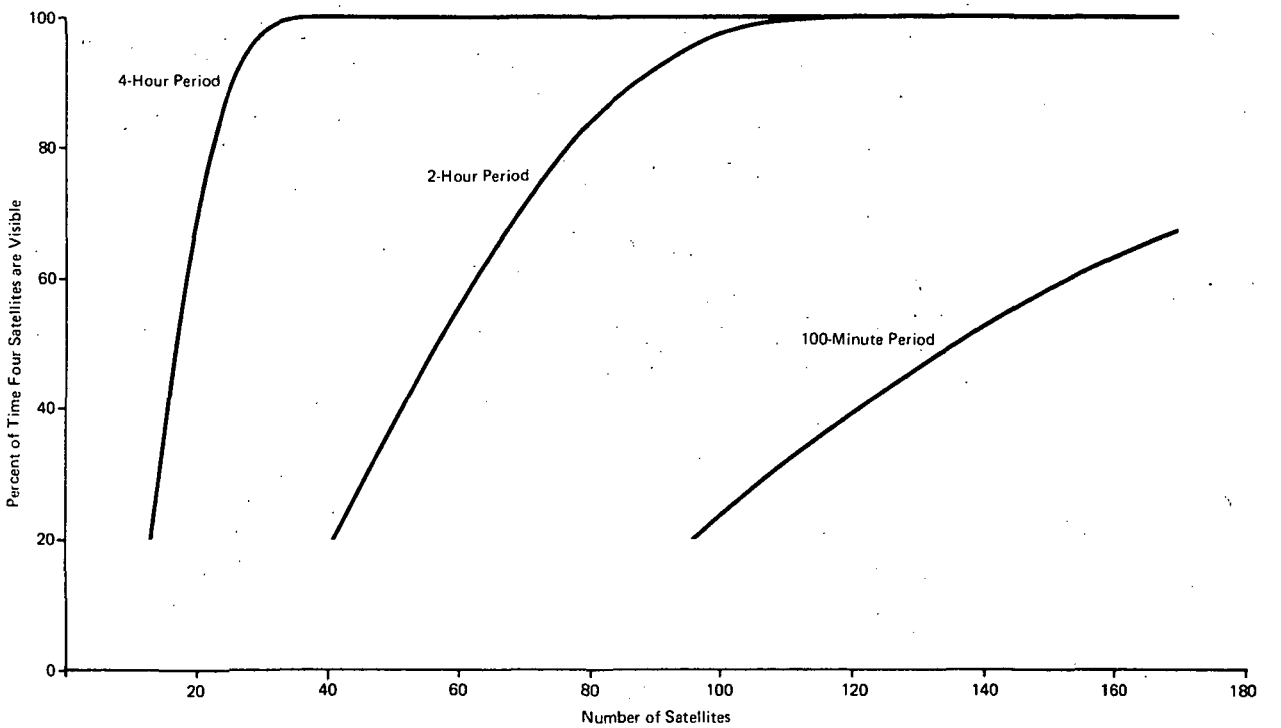

Figure 4-17. Four-Satellite Visibility in Region 1

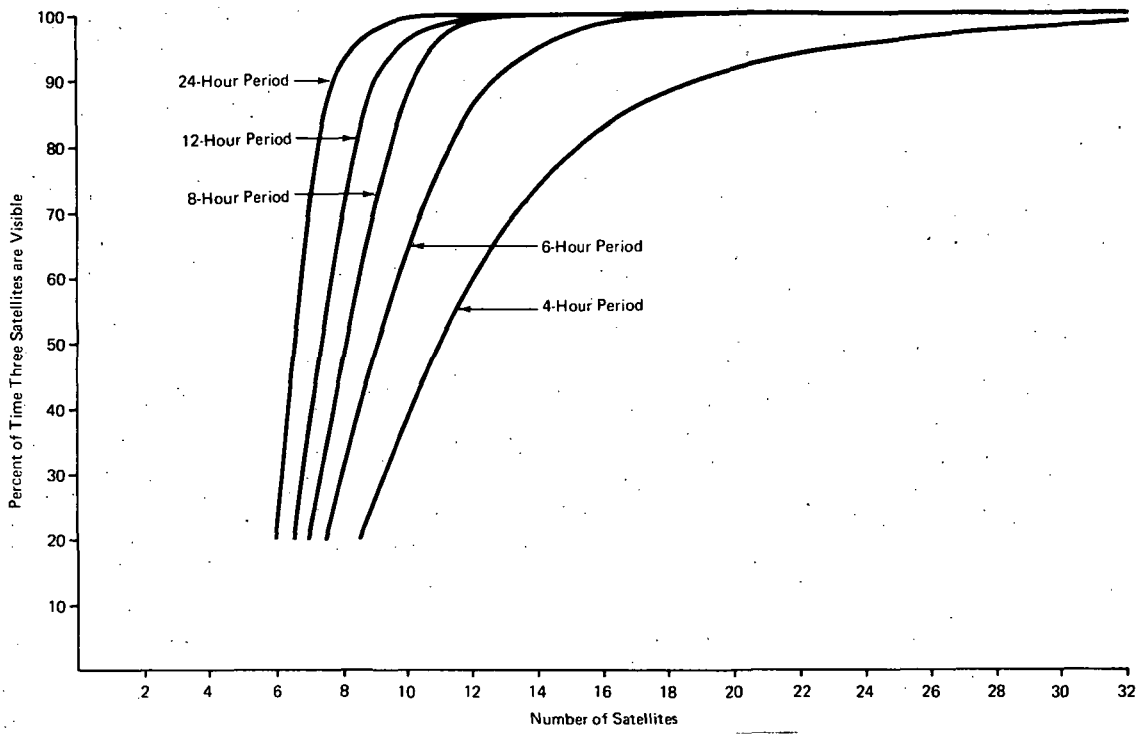

Figure 4-18. Three-Satellite Visibility in Region 1

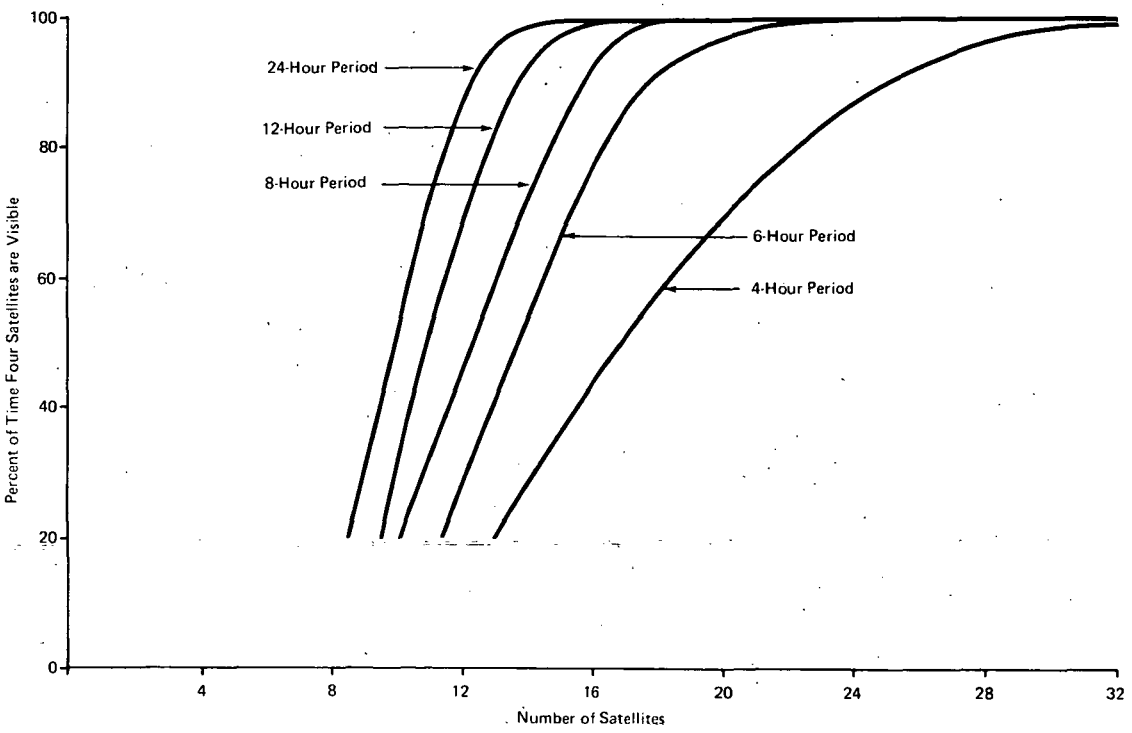

Figure 4-19. Four-Satellite Visibility in Region 1

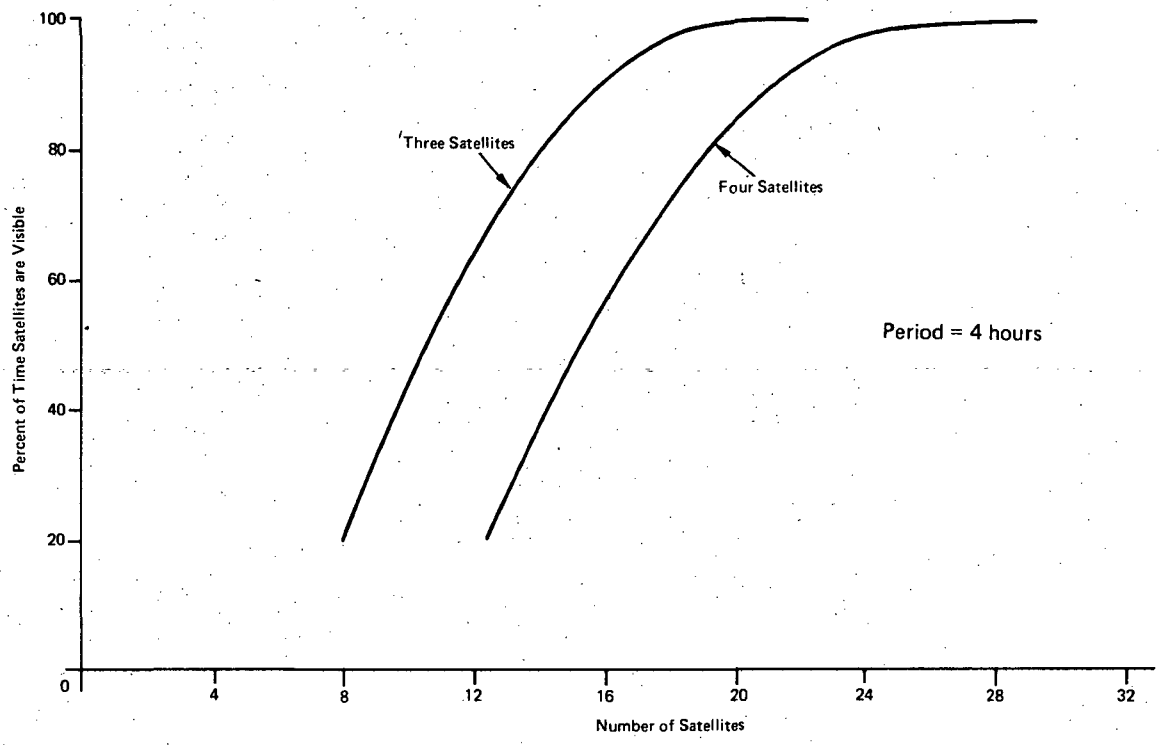

Figure 4-20. Percent Coverage vs Number of Satellites, Region 2

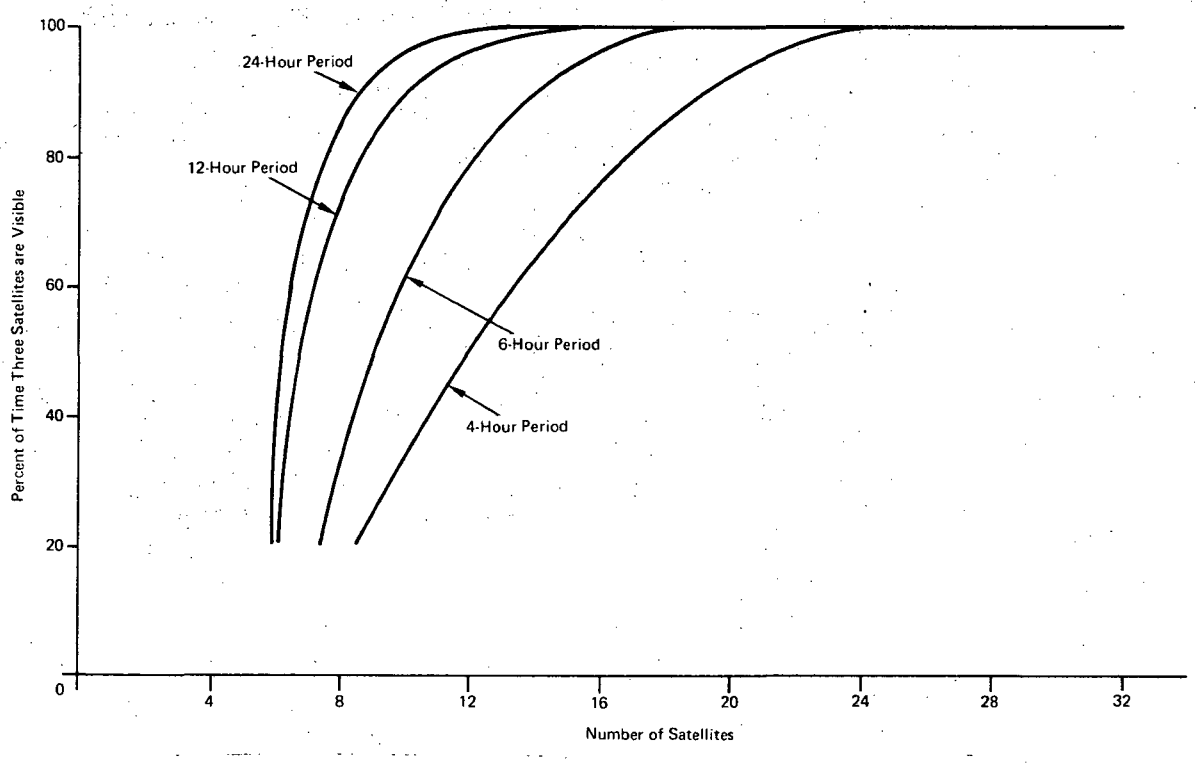

Figure 4-21. Three-Satellite Visibility for Region 2

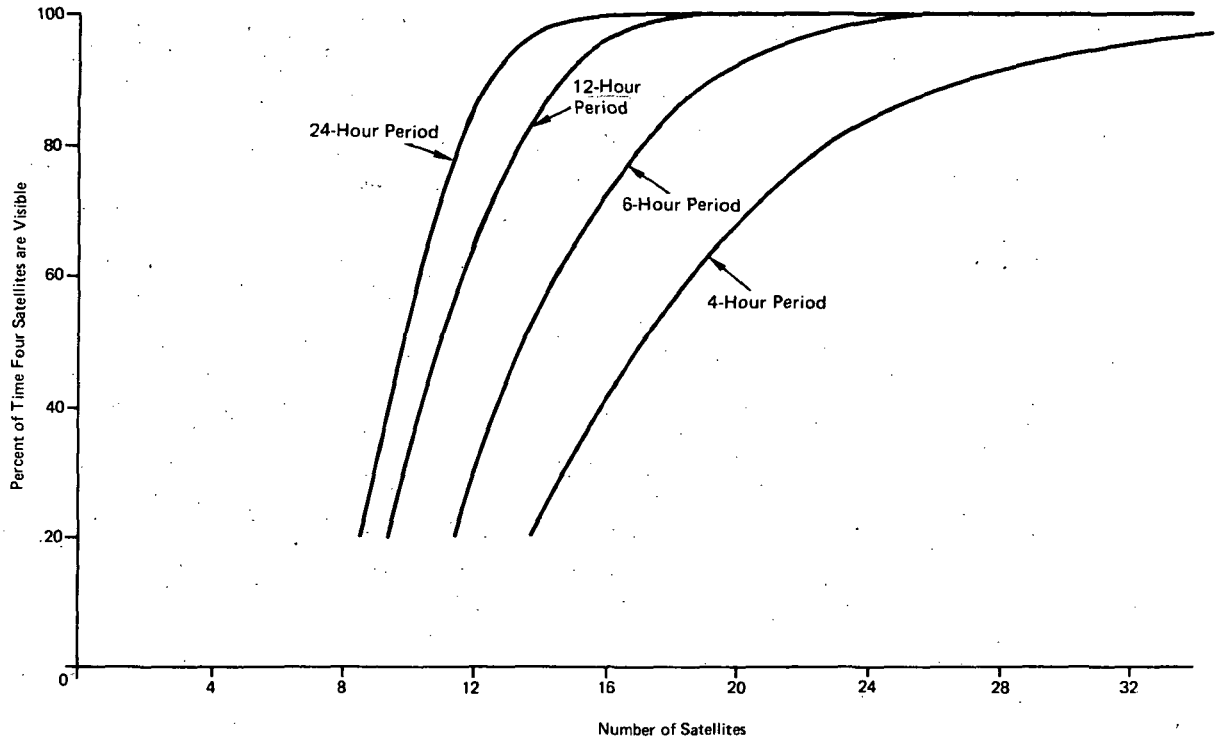

Figure 4-22. Four-Satellite Visibility for Region 2

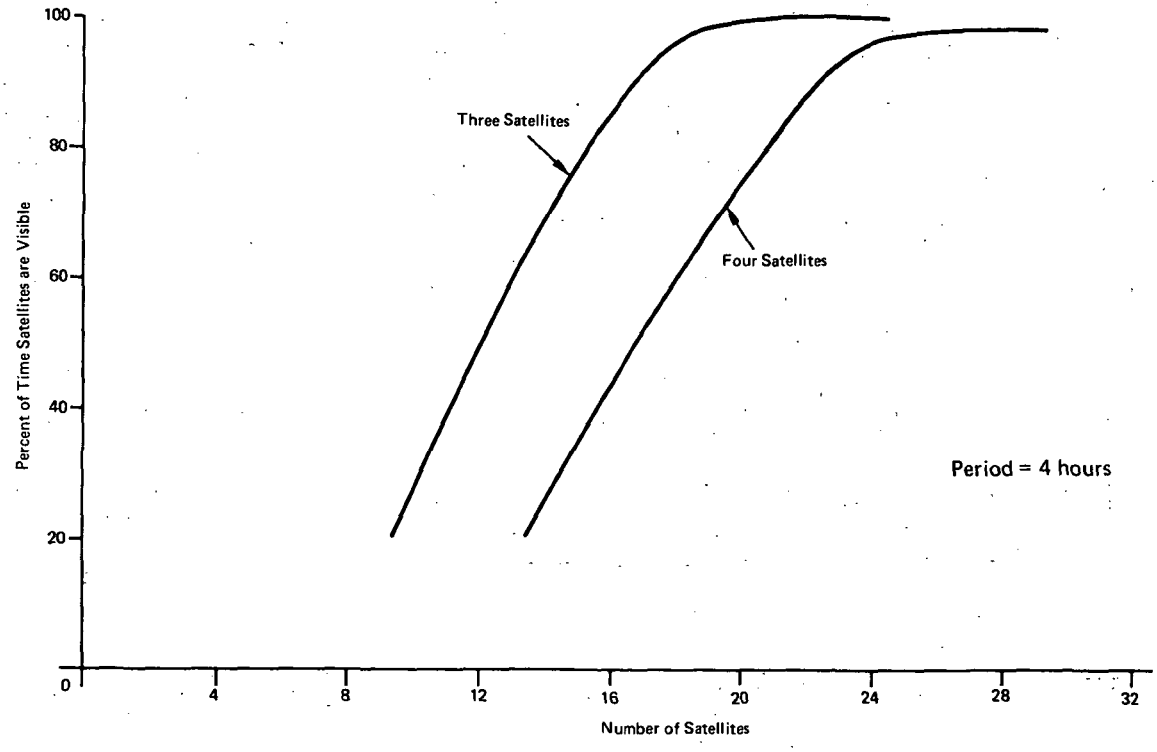

Figure 4-23. Percent Coverage vs Number of Satellites, Region 3

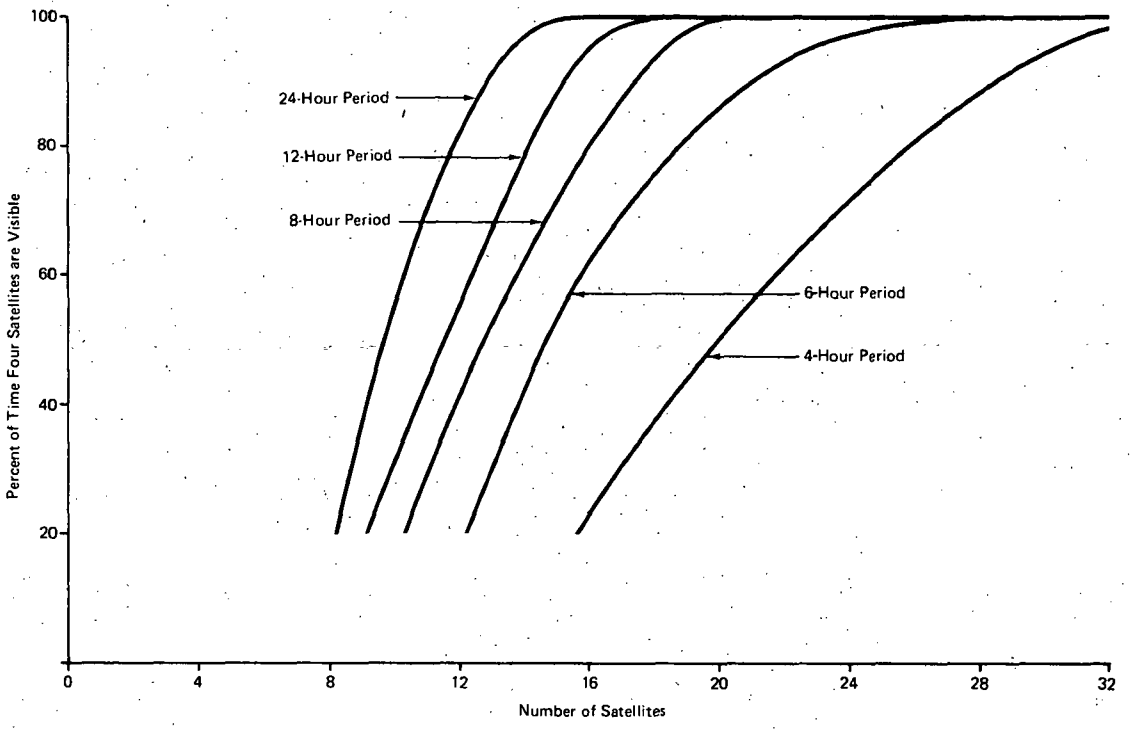

Figure 4-24. Three-Satellite Visibility for Region 3

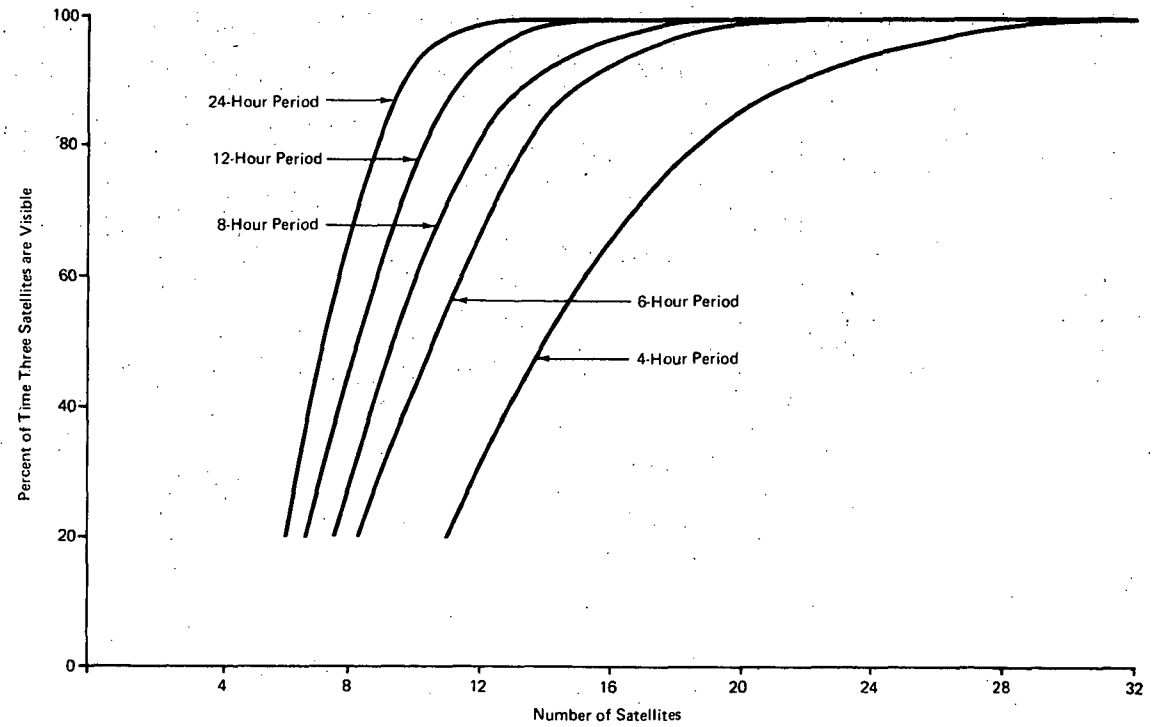

Figure 4-25. Four-Satellite Visibility for Region 3

It is possible that there are several combinations of the number of orbit planes, and satellites within a plane, which will yield the same coverage. Therefore, though the coverage curves are plotted as if all total number of satellites were possible, the reader should recognize that some totals are impractical. Therefore the next higher number, which provides a rational choice of orbit planes and satellites in a plane, should be selected.

Certain total numbers have several possible combinations. For example, 24 satellites can be arranged into eight planes, three satellites in each plane, or three planes and eight satellites in each plane; or four planes and six satellites in each plane, or six planes and four satellites in each plane. The percent of coverage depends to some extent on which combination is used. However, reasonable selections; e.g., three planes and eight satellites in each plane, or four planes and six satellites in each plane; provide about the same percentage coverage. Less reasonable selections, as 12 satellites in each plane and two planes, provide less coverage.

Basically uniform coverage in an EW direction is obtained by a uniform spacing of orbit planes, whereas uniform coverage in a NS direction is achieved by a uniform spacing within an orbit plane. These comments are made for guidance and should not be taken too literally. However, in the equatorial regions, the reader can see the logic of the statement. The reader is cautioned that the curves generated herein are for trade-off purposes, and for optimization detailed investigations should be undertaken with regards to booster costs, in orbit maintenance, and booster failure rates.

As mentioned previously, the lower altitude satellites have less free space loss which may have advantages relative to the accuracy of the position fix; i.e., for a given ERP, the accuracy of the range or range difference improves as the range decreases. However, the free space loss gain is offset somewhat by the fact that as the altitude increases the satellite antenna gain increases because the beamwidth necessary for earth coverage (horizon to horizon) is less.

The net loss is really the significant factor. Figures 4-28, 4-29, and 4-30 show the free space loss, the earth coverage antenna gain, and the net loss (free space loss minus antenna gain) respectively for three frequencies, 400 MHz, 1GHz, and 6GHz. Above 6000 nmi, the net loss is about 1/7 dB per 1000 miles. Below 6000, nmi the net loss decreases rapidly with altitude.

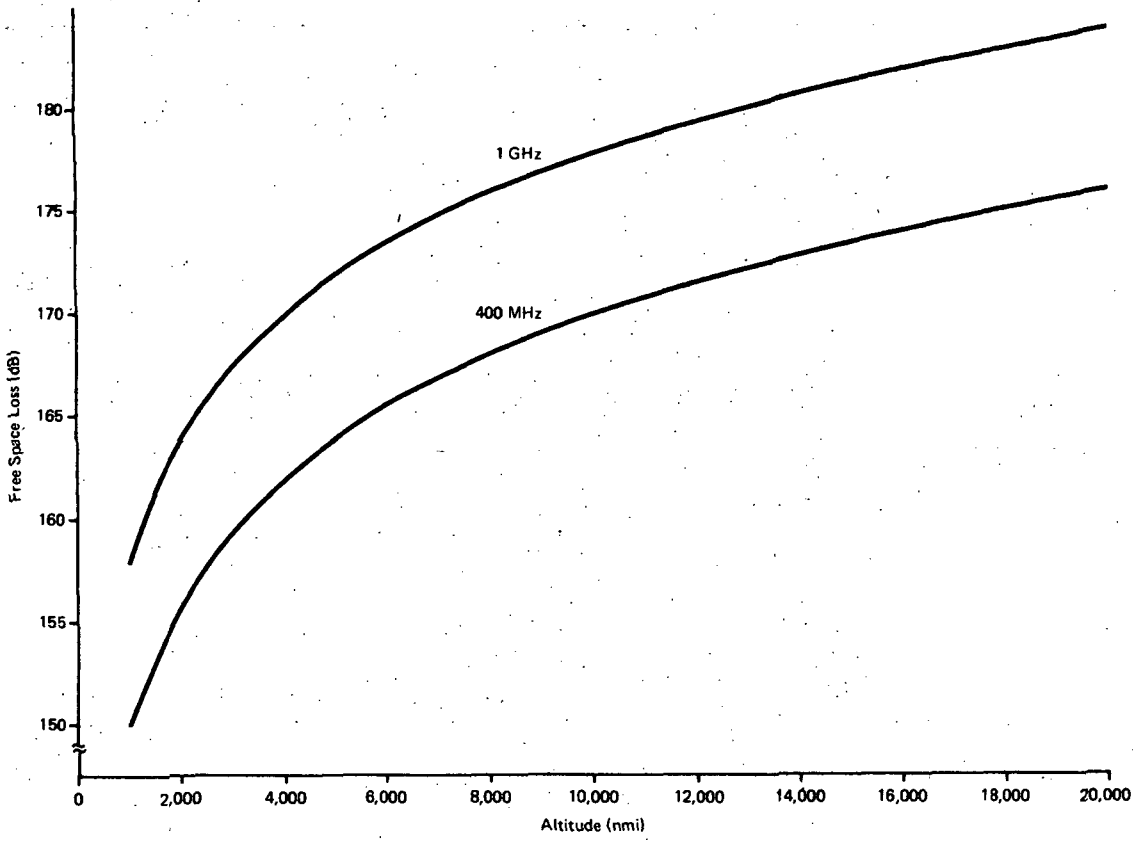

Figure 4-26. Free Space Loss vs Altitude for 1GHz and 400 MHz

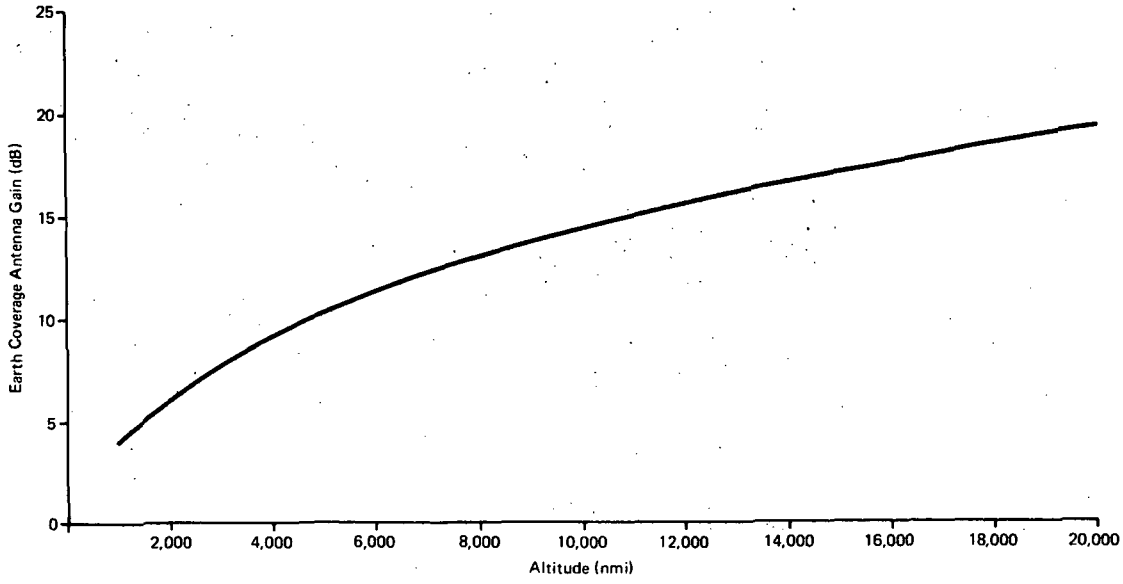

Figure 4-27. Earth Coverage Antenna Gain vs Altitude

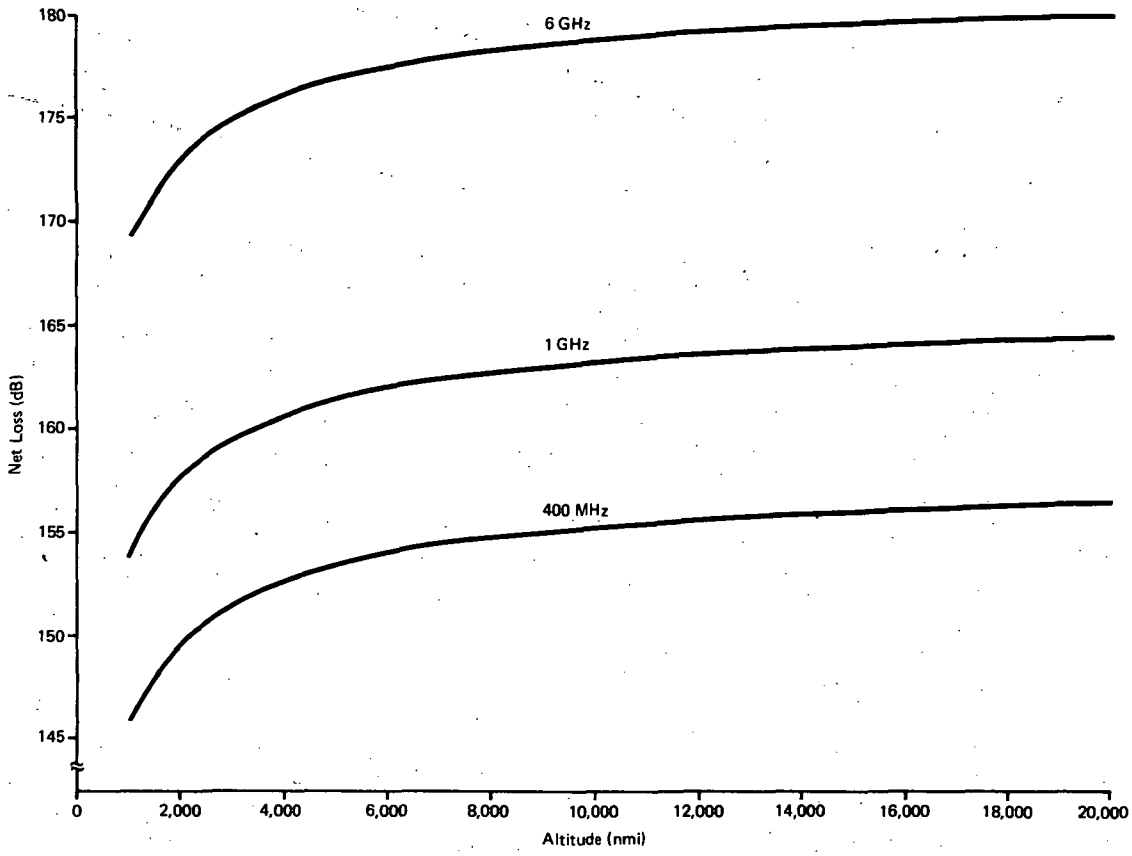

Figure 4-28. Net Loss vs Altitude for 400 MHz, 1 GHz, and 6 GHz

Appendix A

DERIVATION OF RESOURCE PARAMETERS FOR MULTIPLE ACCESS TECHNIQUES

Appendix A

DERIVATION OF RESOURCE PARAMETERS FOR MULTIPLE ACCESS TECHNIQUES

The ensuing subsections briefly describe the prime performance derivations of resource parameters for multiple access techniques.

A.1 AUTONOMOUS TDM

PG = 1, since all system users utilize the same code. Then the transmit time T_i available for each message is $T_i = T_u/N$. However, since the transmissions are randomly generated, this transmit time must either be shortened or more time slots allocated to ensure an acceptable probability of a clear channel. The probability of a clear channel can be calculated as follows. Assuming the probability of a user occupying any interval, T_i, is uniformly distributed, then the probability of a user selecting a particular slot is T_i/T_u, where T_u is a 1-second frame interval to provide adequate data refresh.

Then, probability of clear channel, P_c, is

$$P_c = \left(1 - \frac{T_i}{T_u}\right)^{N-1}$$

for large N and for $\frac{T_i}{T_u} <<< 1$

$$P_c = \exp - (N - 1)\frac{T_i}{T_u}$$

or

$$P_c = 1 - (N - 1)\frac{T_i}{T_u} + \ldots\ldots$$

Now probability of error, P_e, caused by message overlap, e.g., two users in same slot; is

$$P_e = (N - 1)\frac{T_i}{T_u} \text{ and } P_e = 10^{-5} \text{ is assumed which yields one overlap per } 10^5 \text{ messages}$$

Then,

$$T_i = \frac{T_u \, 10^{-5}}{N}$$

The total bandwidth required can now be expressed as

$$B_T = \frac{M}{T_i} = \frac{MN}{T_u P_e} = 10^7 \, N$$

where M = number of bits/message = 100

The peak user transmitter power is expressed in terms of the desired output or detected signal-to-noise ratio. This is given as

$$\frac{P_r T_D}{N_o} = \frac{T_{xp} \, L_{fs} \, G_{ac} \, G_{sc}}{KT \, B_i}$$

where

T_D = one bit interval

B_i = detection bandwidth

L_{fs} = free space loss

G_{ac} = gain of aircraft antenna

G_{sc} = gain of spacecraft antenna

KT = Johnson noise in 1-Hz bandwidth

From this relation

$$T_{xp} = \frac{P_r T_D}{N_o} \cdot \frac{KT \, B_i}{L_{fs} \, G_{ac} \, G_{sc}}$$

This expression can be restated as

$$36 + 10 \log T_{xp} - 10 \log B_i = 13$$

for the assumed system parameters and link power budget. Solving for T_{xp} yields

$$10 \log T_{xp} = -23 + 10 \log B_i$$

or

$$T_{xp} = \text{antilog} \left[\frac{-23 + 10 \log \frac{M}{T_i}}{10} \right]$$

A.2 ELICITED TDM

For elicited TDM,

$$T_i = \frac{T_u}{R_T}$$

where

R_T = the number of time slot assignments = N

As with autonomous TDM, PG = 1; therefore, B_T becomes

$$B_T = \frac{M}{T_i} C_T = \frac{MN}{T_u} = 10^2 NC_T$$

where

C_T = the guard spaces between time slots and is set equal to one for purposes of system comparison

Similarly,

$$T_{xp} = \text{antilog} \left[\frac{-23 + 10 \log \frac{M}{T_i}}{10} \right]$$

A.3 AUTONOMOUS OR ELICITED FDM

For autonomous or elicited FDM, PG = 1, and $T_i = T_u = 1$. Then, each channel bandwidth equals $B_i = M/T_i$, and the total bandwidth becomes

$$B_T = N B_i = N \frac{M}{T_i} = NMC_F$$

where

C_F = guard space between channels = 1.

and

$$T_{xp} = \text{antilog} \left[\frac{-23 + 10 \log \frac{M}{T_i}}{10} \right]$$

A.4 AUTONOMOUS AND ELECITED CDM

For autonomous and elicited CDM,

1) The number of time slots, $R_T = 1$

2) The number of frequency slots, $R_F = 1$

3) The number of code users, $R_C = N$

4) The transmit time per message, $T_i = T_u$

5) A signal-to-clutter ratio, SNR_c, of 20 is assumed necessary to achieve $P_e = 10^{-5}$.

Then the processing gain PG may be expressed as

$$PG = SNR_c N$$

and the bandwidth expression is

$$B_T = PG \frac{M}{T_i} = SNR_c \frac{NM}{T_u} \Bigg|_{N>2}$$

An additional expression is introduced into the user transmitter power expression to ensure that the thermal noise is much less than the signal-to-clutter factor. A signal-to-thermal noise ratio, $SNR_T = 20 \times 5$ is assumed for CDM to ensure that thermal noise is negligible when referenced to the above clutter noise.

The corrective factor of 5 shows up in the T_{xp} formula as follows:

$$T_{xp} = \text{antilog}\left[\frac{-23 + 10 \log \frac{M}{T_i}}{10} + \log 5\right]$$

A.5 AUTONOMOUS TDM/FDM

For A-TDM/FDM, the processing gain = 1, and the message transmit time is

$$T_i = \frac{T_u}{R_T}$$

where

R_T = number of time slots per frequency slot

However, to ensure a probability of an error of 10^{-5} for random overlapping messages, the expression must be modified as follows:

$$T_i = \frac{T_u P_e}{R_T}$$

Then,

$$B_T = \left.\frac{M}{T_i} \cdot R_F \right| N > R_F = \frac{M}{T_u P_e} \cdot R_T R_F = \frac{MN}{T_u P_e} \quad N > R_F \Bigg|$$

or when $N \leq R_F$, $T_i = T_u$, i.e., all users are accommodated via FDM;

$$B_T = \frac{M}{T_i} N \Big| \; N \leq R_F = \frac{M}{T_u} N \Big| \; N \leq R_F$$

Then,

$$T_{xp} = \text{antilog}\left[\frac{-23 + 10 \log \frac{M}{T_i}}{10}\right] = \text{antilog}\left[\frac{-23 + 10 \log \frac{M}{T_i}}{10}\right]\Bigg|_{N \leq R_F}$$

or

$$T_{xp} = \text{antilog}\left[\frac{-23 + 10 \log \frac{MR_t}{T_u}}{10}\right]\Bigg|_{N > R_F}$$

A.6 AUTONOMOUS AND ELICITED FDM/CDM

For A-FDM/CDM and E-FDM/CDM,

$$T_i = T_u$$

and the number of coded subscribers per FDM channel is

$$N_s = \frac{N}{R_F}$$

Then,

$$PG = SNR_c \, N_s = SNR_c \, \frac{N}{R_F}$$

and

$$B_T = PG \, \frac{M}{T_i} \, R_F = SNR_c \, N \cdot \frac{M}{T_u} = SNR_c \, \frac{NM}{T_u}$$

User transmitter power is identical to FDM when $2 \geq N < R_T$ and identical to CDM when $N > R_F$.

$$T_{xp} = \text{antilog} \left[\frac{-23 + 10 \log \frac{M}{T_i}}{10} \right] \quad 2 \geq N < R_F$$

$$T_{xp} = \text{antilog} \left[\frac{-23 + 10 \log \frac{M}{T_i}}{10} + \log 5 \right] \quad N > R_F$$

A.7 AUTONOMOUS TDM/CDM

The conditions for autonomous TDM/CDM are similar to elicited TDM/CDM except that the random nature of the technique causes overlap between time slots. This random overlap distribution has been assumed to be binomial, therefore, to ensure sufficient signal process gain for simultaneous users of time slots N_s is redefined as

N_s = Three times the average numbers of simultaneous users per time slot.

In a binomial distribution, the average number users per slot is given as

$$N_s = N \frac{1}{R_T}$$

where

R_T = number of equally probable slots.

Since the variance is also given as N/R_T letting $N_S = 3\ N/R_T$ means that the probability of a greater number of simultaneous users is equal to that probability beyond the 3σ point on the binomial distribution. Then,

$$PG = SNR_c \cdot 3 \cdot \frac{N}{R_T} = SNR_c\ 3\ \frac{NT_i}{T_u}$$

and

$$B_T = PG \left.\frac{M}{T_i}\right|_{N \geq 2} = SNR_c\ 3\ \frac{T_i N}{T_u}\left(\frac{M}{T_i}\right)\Bigg|_{N \geq 2} = SNR_c\ 3\ \left.\frac{NM}{T_u}\right|_{N \geq 2}$$

Similar to elicited TDM/CDM

$$T_{xp} = \text{antilog}\left[\frac{-23 + 10 \log \frac{M}{T_i}}{10} + \log 5\right]$$

A.8 ELICITED TDM/CDM

For elicited TDM/CDM, the number of code users within a time slot may be expressed as

$$N_s = \frac{N}{R_T}$$

where R_T the number of time slots and

$$T_i = \frac{T_u}{R_T}$$

As before, the processing gain may be expressed as

$$PG = SNR_c N_s = SNR_c \frac{N}{R_T}$$

Then, the bandwidth becomes

$$B_T = PG\,\frac{M}{T_i} = SNR_c\,\frac{N}{R_T}\cdot\frac{M}{T_u}\,R_T\Bigg|_{N\geq 2} = SNR_c\,\frac{NM}{T_u}\Bigg|_{N\geq 2}$$

Now, the expression for the user transmitter power is identical to the pure TDM case when the number of users $N < R_T$ and identical to the CDM case when $N \geq R_T$:

$$T_{xp} = \text{antilog}\left[\frac{-23 + 10\log\frac{M}{T_i}}{10}\right] \quad 2 \geq N < R_T$$

$$T_{xp} = \text{antilog}\left[\frac{-23 + 10\log\frac{M}{T_i}}{10} + \log 5\right] \quad N > R_T$$

Appendix B

DETAILED DATA SHEETS FOR MULTIPLE ACCESS TECHNIQUES

Table B-1

AUTONOMOUS OR ELICITED FDM

Concept: Autonomous or Elicited FDM

Basic Parameters: $T_u = 1$ s; M = 100 Bits; $P_E = 10^{-5}$

Parameter	Expression	Comment														
R_{CDM} R_T R_F	$R_C = 1$ $R_T = 1$ $R_F = N$	Number of Coded Users per FDM Channel Number of Time Slots per FDM Channels Number of FDM Channels														
Calculated Parameter	Expression	for N = Number of Users														
		$R_F = N$					$R_T =$					$R_T =$				
		10	10^2	10^3	10^4	10^5	10	10^2	10^3	10^4	10^5	10	10^2	10^3	10^4	10^5
Processing Gain (dB)	$PG = 1$	1	1	1	1	1										
Transmit Time (s)	$T_i = T_u = 1$															
Real Time Data Rate (bps)	$D = \frac{M}{T_u}$	100	100	100	100	100										
Message Bandwidth (Hz)	$B_i = D$	100	100	100	100	100										
Probability of Clear Channel	$P_c = 1$	1	1	1	1	1										
Total Bandwidth (Hz)	$B_T = N\frac{M}{T_u}$ (Hz)	10^3	10^4	10^5	10^6	10^7										
User Transmit Power (W)	$T_{xp} \cong \text{antilog}\left[\frac{-23 + 10\log\frac{M}{T_u}}{10}\right]$	0.5	0.5	0.5	0.5	0.5										
Number of Users/MHz	$\frac{N}{B_T} \times 10^6$	10^4	10^4	10^4	10^4	10^4										
Timing Accuracy (s)	$A \cong \frac{1}{D}$															
Parallel Receiver Signal Processor	$\cong N$	10	10^2	10^3	10^4	10^5										

Table B-2

AUTONOMOUS AND ELICITED CDM

Concept: Autonomous and Elicited CDM

Basic Parameters: $T_u = 1$ s; M = 100 Bits; $P_E = 10^{-5}$

Parameter	Expression	Comment														
R_T	$R_T = 1$	Number of Time Slots per FDM Channel														
R_F	$R_F = 1$	Number of FDM Channels														
R_c	$R_c = N$	Number of Orthogonally Coded Users														
SNR_c	$SNR_c = 20$; (13 dB)	Signal-to-Clutter Ratio Necessary for $P_E = 10^{-5}$														
Calculated Parameter	Expression	for N = Number of Users														
		$R_c = N$					$R_T =$					$R_T =$				
		10	10^2	10^3	10^4	10^5	10	10^2	10^3	10^4	10^5	10	10^2	10^3	10^4	10^5
Processing Gain (dB)	$PG = SNR_c\ N$	23	33	43	53	63										
Transmit Time (s)	$T_i = T_u$	1	1	1	1	1	1									
Real Time Data Rate (bps)	$D = \frac{M}{T_u}$	100	100	100	100	100										
Message Bandwidth	$B_i = D$	100	100	100	100	100										
Probability of Clear Channel	$P_c = 1$ for $P_E = 10^{-5}, SNR_c = 20$	1	1	1	1	1										
Total Bandwidth (Hz)	$B_T = SNR_c\ N \frac{M}{T_u} \quad N_s \geq 2$	2×10^4	2×10^5	2×10^6	2×10^7	2×10^8										
User Transmit Power (W)	$T_{xp} \cong \text{antilog}\left[\frac{-23 + 10 \log \frac{M}{T_i}}{10} + \log 5\right]$	2.5	2.5	2.5	2.5	2.5										
Number of Users/MHz	$\frac{N}{B_T} \times 10^6$	500	500	500	500	500										
Timing Accuracy	$A \cong \frac{1}{D}$															
Parallel Receiver Signal Processor	$\cong N^*$	10	10^2	10^3	10^4	10^5										

*Reduced by a factor, F, due to adaptive elicited polling techniques

Table B-3

AUTONOMOUS TDM – EACH USER ASYNCHRONOUSLY BURST TRANSMITS HIS POSITION MESSAGE

Concept: Autonomous TDM — Each User Asynchronously Burst Transmits His Position Message

Basic Parameters: $T_u = 1$ s; $M = 100$ bits; $P_E = 10^{-5}$

Parameter	Expression	Comment
R_F	$R_F = 1$	Number of FDM Channels
R_c	$R_c = 1$	Number of Coded Users per Time Slot
R_T	$R_T = \frac{T_u}{T_i}$	Number of Time Slots
P_c	$P_c = 1 - P_E \leq \left(1 - \frac{T_i}{T_u}\right)^{N-1}$ or $\frac{1}{N} 10^5 \geq \frac{M}{B_T T_u}$	Probability of an Interference Free or Clear Channel for $P_E = 10^{-5}$

Calculated Parameter	Expression	for N = Number of Users														
		$R_T = N$					$R_T =$					$R_T =$				
		10	10^2	10^3	10^4	10^5	10	10^2	10^3	10^4	10^5	10	10^2	10^3	10^4	10^5
Processing Gain (dB)	$PG = \cong 1$	1	1	1	1	1										
Transmit Time (s)	$T_i = \frac{T_u P_E}{N-1}$ | $N > 1$	10^{-6}	10^{-7}	10^{-8}	10^{-9}	10^{-10}										
Real Time Data Rate (bps)	$D = \frac{M}{T_i}$ (BPS)	10^8	10^9	10^{10}	10^{11}	10^{12}										
Message Bandwidth (Hz)	$B_i = D$	10^8	10^9	10^{10}	10^{11}	10^{12}										
Probability of Clear Channel	$P_c = 1 - 10^{-5}$ for $P_E = 10^{-5}$	.99999	.99999	.99999	.99999	.99999										
Total Bandwidth (Hz)	$B_T \cong \frac{M N}{T_u 10^{-5}}$	10^8	10^9	10^{10}	10^{11}	10^{12}										
User Transmit Power (W)	$T_{xp} \cong \text{antilog}\left[\frac{-23 + 10 \log \frac{M}{T_i}}{10}\right]$	5×10^5	5×10^6	5×10^7	5×10^8	5×10^9										
Number of Users/MHz	$\frac{N}{B_T} \times 10^6$	.1	.1	.1	.1	.1										
Timing Accuracy	$A \cong \frac{1}{D}$	10^{-3}	10^{-4}	10^{-5}	10^{-6}	10^{-7}										
Parallel Receiver Signal Processor	$\cong 1 - 10$	1	1	3	5	10										

Table B-4

ELICITED TDM – USERS BURST TRANSMIT WITHIN A *SPECIFIED TIME SLOT CONTROLLED BY COMMAND*

Concept: Elicited TDM — Users Burst Transmit Within a Specified Time Slot Controlled by Command

Basic Parameters: $T_u = 1$ s; M = 100 Bits; $P_E = 10^{-5}$

Parameter	Expression	Comment														
R_F R_c R_T	$R_F = 1$ $R_c = 1$ $R_T = N$	Number of FDM Channels Number of Coded Users/Time or Frequencies Slot Number of Time Slots														
Calculated Parameter	Expression	for N = Number of Users														
		$R_T = N$					$R_T =$					$R_T =$				
		10	10^2	10^3	10^4	10^5	10	10^2	10^3	10^4	10^5	10	10^2	10^3	10^4	10^5
Processing Gain (dB)	PG = ≅1; (0 dB)	1	1	1	1	1										
Transmit Time (s)	$T_i = \frac{T_u}{R_T}$ (s)	10^{-1}	10^{-2}	10^{-3}	10^{-4}	10^{-5}										
Real Time Data Rate (bps)	$D = \frac{M}{T_i}$ (bps)	10^3	10^4	10^5	10^6	10^7										
Message Bandwidth (Hz)	$B_i = B_T$	10^3	10^4	10^5	10^6	10^7										
Probability of Clear Channel	$P_c = 1$ for Elicited	1	1	1	1	1										
Total Bandwidth (Hz)	$B_T = \frac{M}{T_i}$ (Hz)	10^3	10^4	10^5	10^6	10^7										
User Transmit Power (W)	$T_{xp} \cong \text{antilog}\left[\frac{-23 + 10 \log \frac{M}{T_i}}{10}\right]$	5	5×10^1	5×10^2	5×10^3	5×10^4										
Number of Users / MHz	$\frac{N}{B_T} \times 10^6$	10^4	10^4	10^4	10^4	10^4										
Timing Accuracy	$A \cong \frac{1}{D}$	10^{-3}	10^{-4}	10^{-5}	10^{-6}	10^{-7}										
Parallel Receiver Signal Processor																

Table B-5

ELICITED TDM/CDM – GROUPS OR ORTHOGONALLY CODED USERS RESPOND SIMULTANEOUSLY ON COMMAND

Concept: Elicited TDM/CDM — Groups of Orthogonally Coded Users Respond Simultaneously on Command

Basic Parameters: $T_u = 1$ s; M = 100 Bits; $P_E = 10^{-5}$

Parameter	Expression	Comment														
N_s	$N_s = \frac{N}{R_T}$	Number of Coded Users in a Time Slot														
R_T	R_T = Variable	Number of Time Slots (Limited by max Data Rate)														
R_F	$R_F = 1$	Number of FDM Channels														
SNR_c	$SNR_c = 20$; (13 dB)	Signal-to-Clutter Ratio Necessary for $P_E = 10^{-5}$														
P_E	$P_E = 10^{-5}$	Probability of Message Error														
		for N = Number of Users														
Calculated Parameter	Expression	$R_T = 10$					$R_T = 100$					$R_T = 1000$				
Total Number of Users	N = Variable	10	10^2	10^3	10^4	10^5	10	10^2	10^3	10^4	10^5	10	10^2	10^3	10^4	10^5
Processing Gain (dB)	$PG = SNR_c N_s = \frac{B_T T_i}{M}$	0	23	33	43	53		0	23	33	43		0	0	23	33
Transmit Time (s)	$T_i = \frac{T_u}{R_T}$	10^{-1}	10^{-1}	10^{-1}	10^{-1}	10^{-1}		10^{-2}	10^{-2}	10^{-2}	10^{-2}		10^{-3}	10^{-3}	10^{-3}	10^{-3}
Real Time Data Rate (bps)	$D = \frac{M}{T_i}$	10^3	10^3	10^3	10^3	10^3		10^4	10^4	10^4	10^4		10^5	10^5	10^5	10^5
Message Bandwidth (Hz)	$B_i = D$															
Probability of Clear Channel	$P_c = 1$ for Elicited	1	1	1	1	1		1	1	1	1		1	1	1	1
Total Bandwidth (Hz)	$B_T = SNR_c \frac{N M}{T_i}\Big\vert_{N_s \geq 2}$ or	10^3	2×10^5	2×10^6	2×10^7	2×10^8		10^4	2×10^6	2×10^7	2×10^8		10^5	10^5	2×10^7	2×10^8
	$B_T = \frac{M}{T_i}\Big\vert_{N_s = 1}$															
User Transmit Power (W)	$T_{xp} \cong \text{antilog}\left[\frac{-23 + 10 \log \frac{M}{T_i}}{10}\right]_{N<R_T}$	5	10	10	10	10		50	250	250	250		500	500	2500	2500
	$T_{xp} = \text{antilog}\left[\frac{23 + 10 \log \frac{M}{T_i}}{10} + \log 5\right]_{N>R_T}$															
Number of Users/MHz	$\frac{N}{B_T} \times 10^6$	10^4	500	500	500	500		10^4	500	500	500		10^3	10^4	500	500
Timing Accuracy	$A \cong \frac{1}{D}$	10^{-3}	10^{-3}	10^{-3}	10^{-3}	10^{-3}		10^{-4}	10^{-4}	10^{-4}	10^{-4}		10^{-5}	10^{-5}	10^{-5}	10^{-5}
Parallel Receiver Signal Processor																

Table B-6

AUTONOMOUS TDM/FDM

Concept: Autonomous TDM/FDM

Basic Parameters: $T_u = 1$ s; M = 100 Bits; $P_E = 10^{-5}$

Parameter	Expression	Comment
R_T	$R_T = \frac{N}{R_F}$	Number of Time Slots per FDM Channel
R_c	$R_c = 1$	Number of Code Users per Time/Frequency Slot
R_F	R_F = Variable	Number of FDM Channels
P_c	$P_c = 1 - P_E \leq \left(1 - \frac{T_i}{T_u}\right)^{N-1}$ or $\frac{1}{N} 10^5 \geq \frac{M}{B_T T_u}$	Probability of Interference Free or Clear Time Slot for $P_E = 10^{-5}$

Calculated Parameter	Expression	for N = Number of Users														
		$R_F = 10$					$R_F = 100$					$R_F = 1000$				
Total Number of Users	N = Variable	10	10^2	10^3	10^4	10^5	10	10^2	10^3	10^4	10^5	10	10^2	10^3	10^4	10^5
Processing Gain (dB)	$PG = \cong 1$	1	1	1	1	1		1	1	1	1			1	1	1
Transmit Time (s)	$T_i = \frac{T_u P_E}{R_T}$ $N > R_F$ $T_u = \frac{T_u}{R_T} N_s R_F$	1	10^{-6}	10^{-7}	10^{-8}	10^{-9}		1	10^{-6}	10^{-7}	10^{-8}			1	10^{-6}	10^{-7}
Real Time Data Rate (bps)	$D = \frac{M}{T_i}$	10^2	10^8	10^9	10^{10}	10^{11}		10^2	10^8	10^9	10^{10}			10^2	10^8	10^9
Message Bandwidth (Hz)	$B_i = D$															
Probability of Clear Channel	$P_c = 1 - P_E$	.99999	.99999	.99999	.99999	.99999		.99999	.99999	.99999	.99999			.99999	.99999	.99999
Total Bandwidth (Hz)	$B_T = \frac{M}{T_i} R_F = \frac{M N}{T_u} 10^5$ $N > R$ $B_T = \frac{M}{T_i} N$ $N < R_F$	10^4	10^9	10^{10}	10^{11}	10^{12}		10^5	10^6	10^{11}	10^{12}			10^{10}	10^{11}	10^{12}
User Transmit Power (W)	$T_{xp} \cong \text{antilog}\left[\frac{-23 + 10 \log \frac{M}{T_i}}{10}\right]$	5	5×10^5	5×10^6	5×10^7	5×10^8		50	5×10^5	5×10^6	5×10^7			50	5×10^5	5×10^6
Number of Users/MHz	$\frac{N}{B_T} \times 10^6$	0.1	0.1	0.1	0.1	0.1		0.1	0.1	0.1	0.1			0.1	0.1	0.1
Timing Accuracy	$A \cong \frac{1}{D}$	10	10^{-3}	10^{-3}	10^{-3}	10^{-3}		10^{-4}	10^{-4}	10^{-4}	10^{-4}			10^{-5}	10^{-5}	10^{-5}
Parallel Receiver Signal Processor	$\cong R_F$	10^1	10^1	10^1	10^1	10^1		10^2	10^2	10^2	10^2			10^3	10^3	10^3

Table B-7

ELICITED TDM/FDM

Concept: Elicited TDM/FDM

Basic Parameters: $T_u = 1$ s; M = 100 Bits; $P_E = 10^{-5}$

Parameter	Expression	Comment														
R_T	R_T = Variable	Number of Time Slots per FDM Channel														
R_C	$R_C = 1$	Number of Coded Users per Time Slot														
R_F	$R_F = \frac{N}{R_T}$	Number of FDM Channels														
		for N = Number of Users														
Calculated Parameter	Expression	$R_T = 10$					$R_T = 100$					$R_T = 1000$				
Total Number of Users	N = Variable	10	10^2	10^3	10^4	10^5	10	10^2	10^3	10^4	10^5	10	10^2	10^3	10^4	10^5
Processing Gain	PG = $\cong$ 1; (0 dB)	1	1	1	1	1		1	1	1	1			1	1	1
Transmit Time	$T_i = \frac{T_u}{R_T}$	10^{-1}	10^{-1}	10^{-1}	10^{-1}	10^{-1}		10^{-2}	10^{-2}	10^{-2}	10^{-2}			10^{-3}	10^{-3}	10^{-3}
Real Time Data Rate	$D = \frac{M}{T_i}$	10^3	10^3	10^3	10^3	10^3		10^4	10^4	10^4	10^4			10^5	10^5	10^5
Message Bandwidth	$B_i = \frac{M}{T_i}$	10^3	10^3	10^3	10^3	10^3		10^4	10^4	10^4	10^4			10^5	10^5	10^5
Probability of Clear Channel	$P_C = 1$ for Elicited TDM/FDM	1	1	1	1	1		1	1	1	1			1	1	1
Total Bandwidth	$B_T = \frac{M}{T_i} R_F$	10^3	10^4	10^5	10^6	10^7		10^4	10^5	10^6	10^7			10^5	10^6	10^7
User Transmit Power (W)	$T_{xp} \cong \text{antilog}\left[\frac{-23 + 10 \log \frac{M}{T_i}}{10}\right]$	5	5	5	5	5		50	50	50	50			500	500	500
Number of Users/MHz	$\frac{N}{B_T} \times 10^6$	10^4	10^4	10^4	10^4	10^4		10^4	10^4	10^4	10^4			10^4	10^4	10^4
Timing Accuracy	$A \cong \frac{1}{D}$	10^{-3}	10^{-3}	10^{-3}	10^{-3}	10^{-3}		10^{-4}	10^{-4}	10^{-4}	10^{-4}			10^{-5}	10^{-5}	10^{-5}
Parallel Receiver Signal Processor																

Table B-8

AUTONOMOUS OR ELICITED FDM/CDM

Concept: Autonomous or Elicited FDM/CDM

Basic Parameters: $T_u = 1$ s; M = 100 Bits; $P_E = 10^{-5}$

Parameter	Expression	Comment														
N_s	$N_s = \frac{N}{R_F}$	Number of Coded Users per FDM Channel														
R_F	R_F = Variable	Number of Frequency Channels														
R_T	$R_T = 1$	R_T = Number of Time Slots per FDM Channel														
SNR_C	$SNR_C = 20$ (13 dB)	Signal-to-Clutter Ratio Necessary for $P_E = 10^{-5}$														
SNR_T	$SNR_T = 5$ (7 dB)	Signal to Thermal Noise Ratio														
		for N = Number of Users														
Calculated Parameter	Expression	$R_F = 10$					$R_F = 100$					$R_F = 1000$				
Total Number of Users	N = Variable	10	10^2	10^3	10^4	10^5	10	10^2	10^3	10^4	10^5	10	10^2	10^3	10^4	10^5
Processing Gain (dB)	$PG = SNR_C N_s$ (dB)	0	23	33	43	53		0	23	33	43			0	23	33
Transmit Time (s)	$T_i = T_u$ (s)	1	1	1	1	1		1	1	1	1			1	1	1
Real Time Data Rate (bps)	$D = \frac{M}{T_u}$ (bps)	100	100	100	100	100		100	100	100	100			100	100	100
Message Bandwidth (Hz)	$B_i = SNR_C N_s \frac{M}{T_u}\Big\|_{N_s \geq 2}$ or $B_i = \frac{M}{T_u}\Big\|_{N_s = 1}$	100	2×10^4	2×10^5	2×10^6	2×10^7		100	2×10^4	2×10^5	2×10^6			100	2×10^4	2×10^5
Probability of Clear Channel	$P_c = 1$ for FDM	1	1	1	1	1		1	1	1	1			1	1	1
Total Bandwidth (Hz)	$B_T = N \frac{M}{T_u} SNR_C\Big\|_{N_s \geq 2}$ or $B_T = N \frac{M}{T_u}\Big\|_{N_s = 1}$	10^3	2×10^5	2×10^6	2×10^7	2×10^8		10^4	2×10^6	2×10^7	2×10^8			10^5	2×10^7	2×10^8
User Transmit Power (W)	$T_{xp} \cong \text{antilog} \simeq \left[\frac{-23 + 10 \log \frac{M}{T_i}}{10} + \log 5\right]$	.5	2.5	2.5	2.5	2.5		.5	2.5	2.5	2.5			.5	2.5	2.5
Number of Users/MHz	$\frac{N}{B_T} \times 10^6$	10^4	500	500	500	500		10^4	500	500	500			10^4	500	500
Timing Accuracy	$A \cong \frac{1}{D}$	10^{-2}	10^{-2}	10^{-2}	10^{-2}	10^{-2}		10^{-2}	10^{-2}	10^{-2}	10^{-2}			10^{-2}	10^{-2}	10^{-2}
Parallel Receiver Signal Processor																

Table B-9

AUTONOMOUS TDM/CDM

Concept: Autonomous TDM/CDM

Basic Parameters: $T_u = 1$ s; M = 100 Bits; $P_E = 10^{-5}$

Parameter	Expression	Comment
R_F	$R_F = 1$	Number of FDM Channels
R_T	R_T = Variable	Number of Time Slots per FDM Channel
R_c	$R_c = \frac{N}{R_T}$	Number of Coded Users per Time Slot
SNR_c	SNR_c = 20 (13 dB)	Signal-to-Clutter Ratio Necessary for $P_E = 10^{-5}$
N_s	$N_s = 3\frac{N}{R_T}$	Three Sigma Average Number of Simultaneous Users per Time Slot

Calculated Parameter	Expression	for N = Number of Users														
		$R_T = 10$					$R_T = 100$					$R_T = 1000$				
Total Number of Users N = Variable	N = Variable	10	10^2	10^3	10^4	10^5	10	10^2	10^3	10^4	10^5	10	10^2	10^3	10^4	10^5
Processing Gain	$PG = SNR_c\, 3\frac{NT_i}{T_u} = B_T\frac{T_i}{M}$	0	28	38	48	58		0	28	38	48		0	0	28	38
Transmit Time	$T_i = \frac{T_u}{R_T}$	10^{-1}	10^{-1}	10^{-1}	10^{-1}	10^{-1}		10^{-2}	10^{-2}	10^{-2}	10^{-2}		10^{-3}	10^{-3}	10^{-3}	10^{-3}
Real Time Data Rate	$D = \frac{M}{T_i}$	10^3	10^3	10^3	10^3	10^3		10^4	10^4	10^4	10^4		10^5	10^5	10^5	10^5
Message Bandwidth	$B_i = D$															
Probability of Clear Channel	$P_c = 1$	1	1	1	1	1		1	1	1	1		1	1	1	1
Total Bandwidth (Hz)	$B_T = 3\frac{(SNR_c)\,M\,N}{T_u}\Big\vert_{N_s \geq 2}$ or $B_T = \frac{M}{T_i}\Big\vert_{N_s = 1}$	10^3	6×10^5	6×10^6	6×10^7	6×10^8		10^4	6×10^6	6×10^7	6×10^8		10^5	10^5	6×10^7	6×10^8
User Transmit Power (W)	$T_{xp} \cong \text{antilog}\left[\frac{-23 + 10\log\frac{M}{T_i}}{10} + \log 5\right]$	25	25	25	25	25		50	250	250	250		500	2500	2500	2500
Number of Users/MHz	$\frac{N}{B_T}\times 10^6$	10^4	166	166	166	166		10^4	166	166	166		10^5	10^5	166	166
Timing Accuracy	$A \cong \frac{1}{D}$	10^{-3}	10^{-3}	10^{-3}	10^{-3}	10^{-3}		10^{-4}	10^{-4}	10^{-4}	10^{-4}		10^{-5}	10^{-5}	10^{-5}	10^{-5}
Parallel Receiver Signal Processor																

T_{xp} Calculation No CDMA $SNR_o = \frac{1\,W\,L_{FS}}{K_T}\cdot\frac{T_{xp}}{B_i} = 20 \rightarrow 36 + 10\log T_{xp} - 10\log B_i = 13$

$T_{xp} = \text{antilog}\left[\frac{-23 + 10\log\frac{M}{T_i}}{10}\right]$ for CDMA $SNR_o = 100$ $T_{xp} = \text{anti}\left[\frac{-23 + 10\log\frac{M}{T_i}}{10} + \log 5\right]$

Appendix C

GRAPHICAL PRESENTATION OF NORMALIZED BANDWIDTH VERSUS NUMBER OF USERS

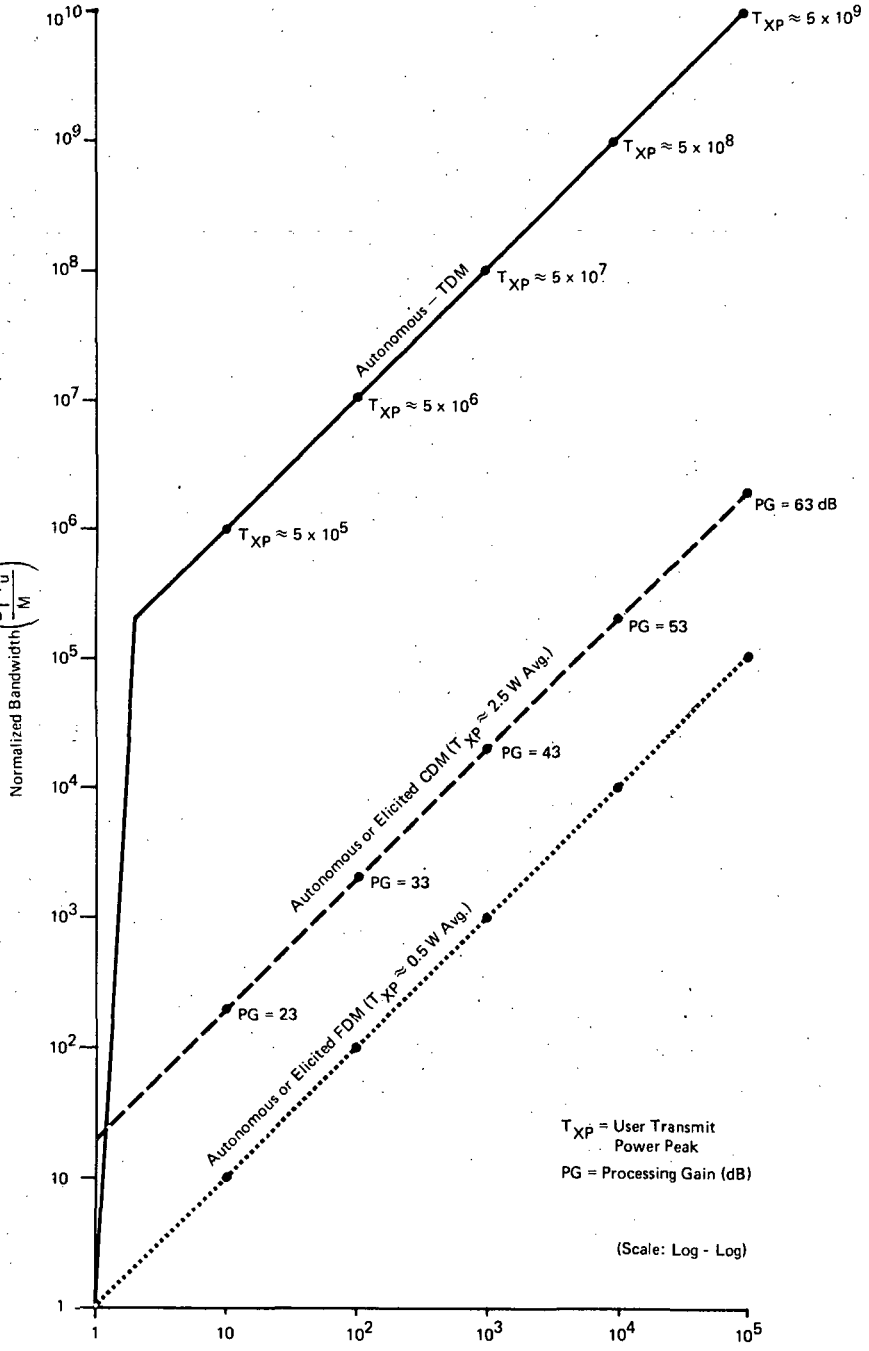

Figure C-1. Number of Users vs Normalized Bandwidth for Autonomous and Elicited FDM, TDM, and CDM

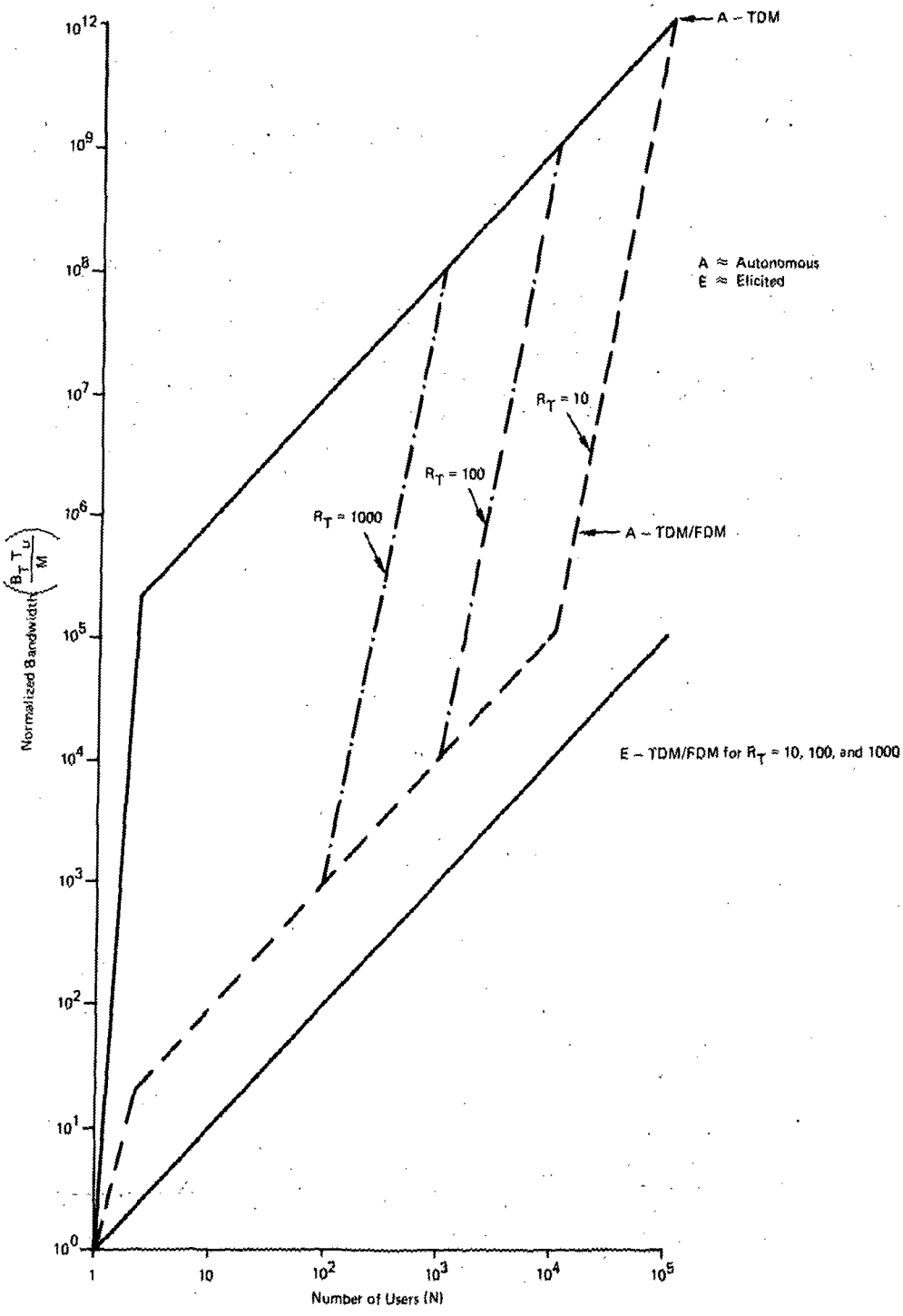

Figure C-2. Number of Users vs Normalized Bandwidth for Autonomous and Elicited TDM/FDM

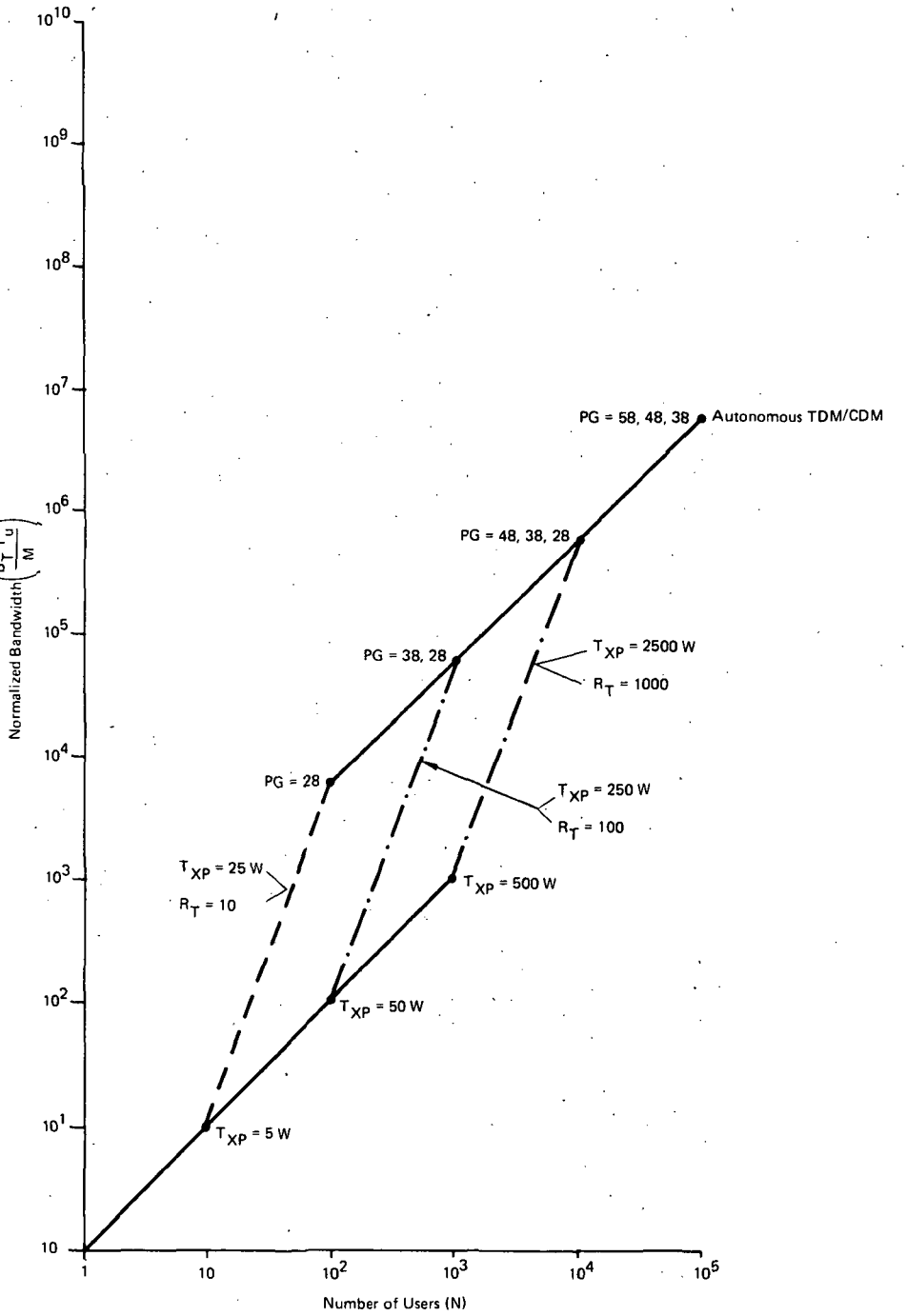

Figure C-3. Number of Users vs Normalized Bandwidth for Autonomous TDM/CDM

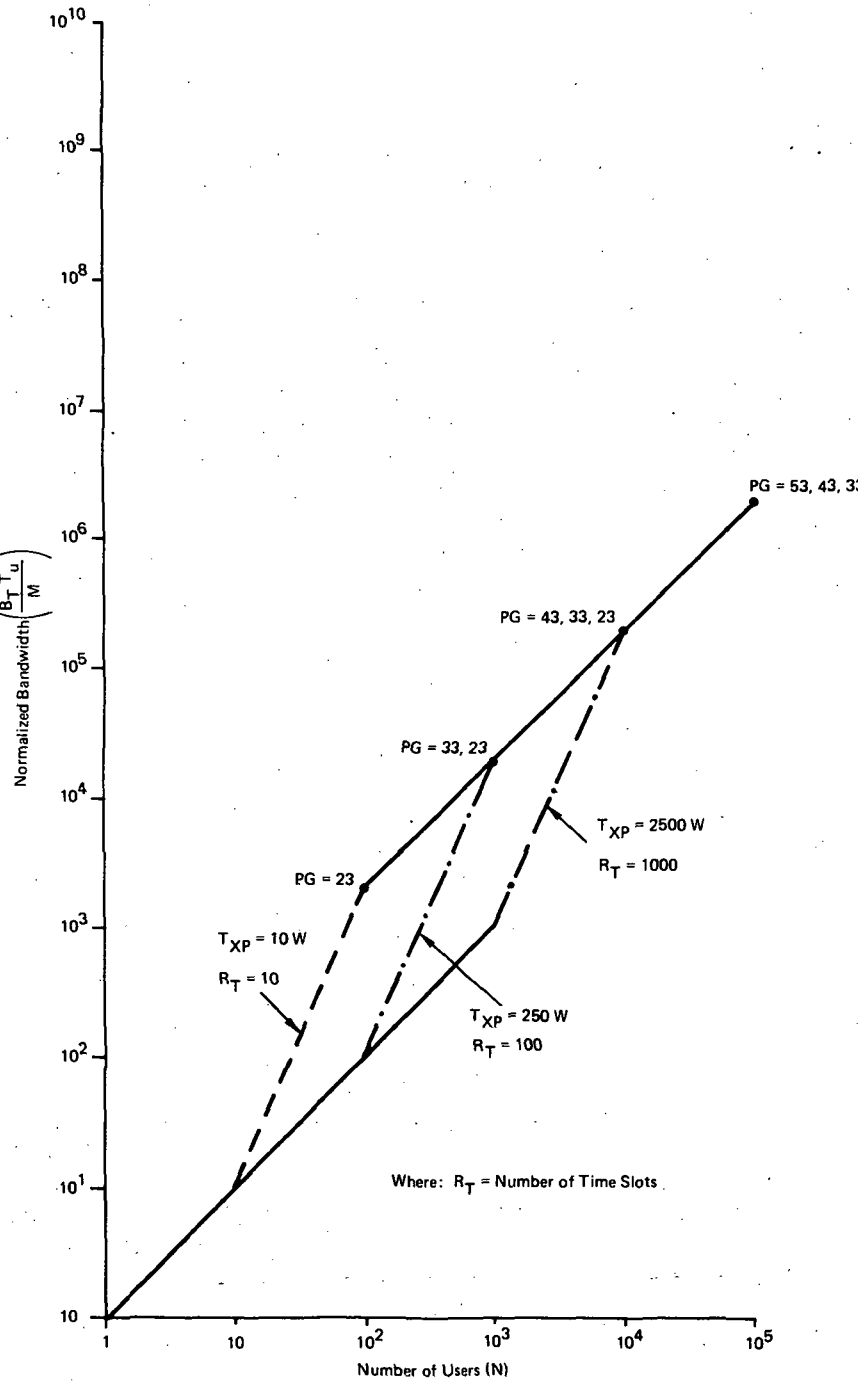

Figure C-4. Number of Users vs Normalized Bandwidth for Elicited TDM/CDM

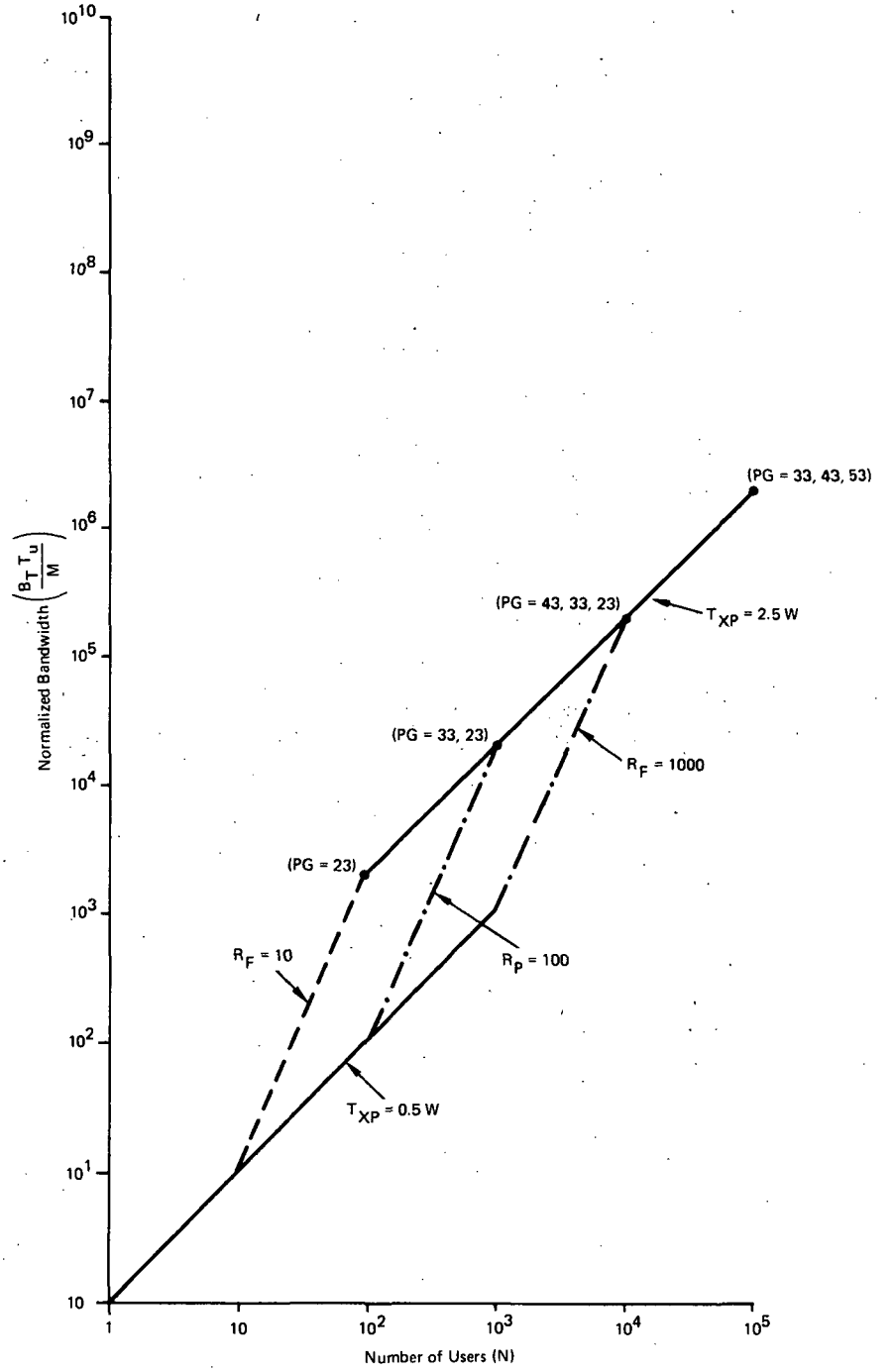

Figure C-5. Number of Users vs Normalized Bandwidth for Autonomous or Elicited FDM/CDM

Appendix D

MISCELLANEOUS POWER AND CODE GRAPHS

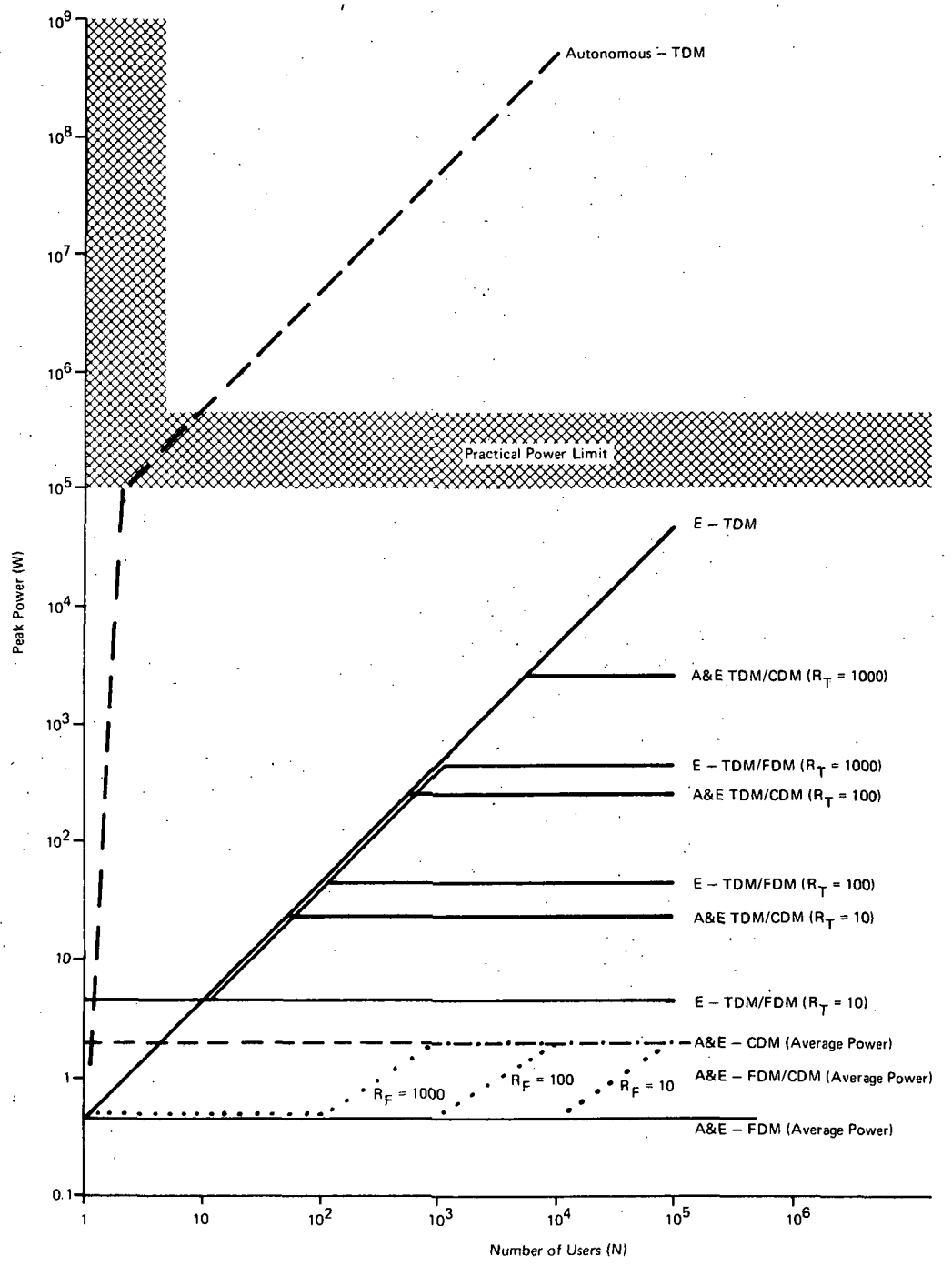

Figure D-1. Number of Users vs User Transmitter Power for Competitive Techniques

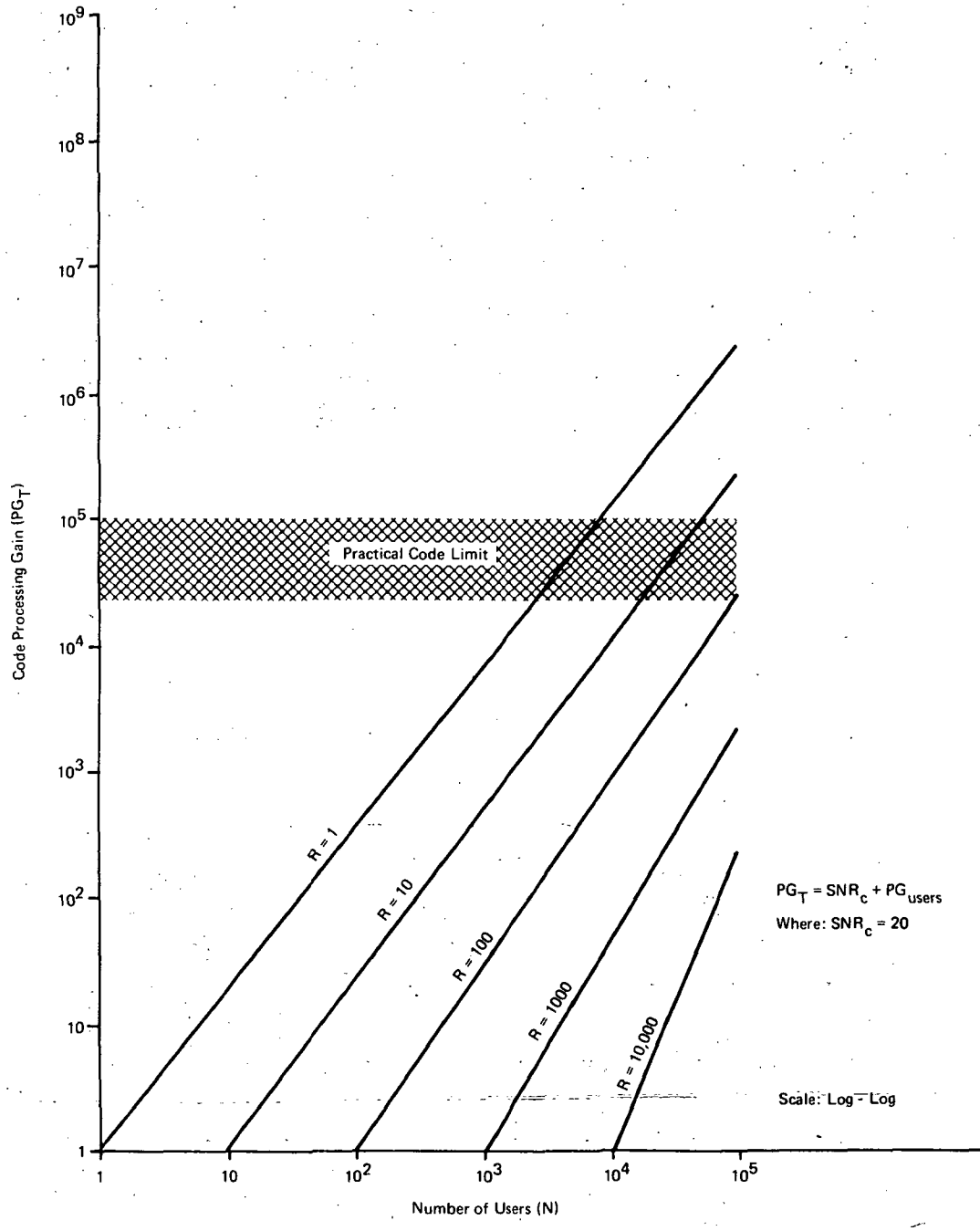

Figure D-2. Number of Users vs Code Process Gain for a Various Number of Time or Frequency Slots

Appendix E

DETAILED DATA SHEETS FOR MULTIPLE ACCESS TECHNIQUES, C II

Table E-1

AUTONOMOUS TDM CONFIGURATION II

Parameter	Expression	Comment
	$R_F = 1$	Number of FDM Channels
	$R_c = 1$	Number of Coded Users per Time Slot
	$R_T = \frac{T_u}{T_i}$	Number of Time Slots
	$B_c = 10^7$	Minimum Bandwidth for Ranging Signal

		for N = Number of Users														
Calculated Parameter	Expression	N														
		10	10^2	10^3	10^4	10^5	10	10^2	10^3	10^4	10^5	10	10^2	10^3	10^4	10^5
Process Gain	PG = 1															
Transmit Time	$T_i = \frac{T_u \times 10^{-5}}{N} \Big\vert N > 1$	10^{-6}	10^{-7}	10^{-8}	10^{-9}	10^{-10}										
Burst Data Rate	$D = \frac{M}{T_i}$	0.2×10^8	0.2×10^9	0.2×10^{10}	0.2×10^{11}	0.2×10^{12}										
Probability of Clear Channel	$P_c = 1\text{-}10^{-5} = 0.9999$															
Total Bandwidth	$B_T = D$	0.2×10^8	0.2×10^9	0.2×10^{10}	0.2×10^{11}	0.2×10^{12}										
Transmitted Power	$T_{xp} = \log^{-1}\left[\frac{-23 + 10 \log D}{10}\right]$	10^5	10^6	10^7	10^8	10^9										
Users/MHz	$\frac{N}{B_T} \times 10^6 = 0.5$															

Table E-2

AUTONOMOUS FDM CONFIGURATION II

Parameter	Expression	Comment														
	$R_c = 1$ $R_T = 1$ $R_F = N$ $B_s = 10^7$	Number of Coded Users per Channels Number of Time Slots per Channel Number of FDM Channels Minimum Bandwidth for Ranging Signal														
Calculated Parameter	Expression	for N = Number of Users														
		N														
		10	10^2	10^3	10^4	10^5	10	10^2	10^3	10^4	10^5	10	10^2	10^3	10^4	10^5
Processing Gain (dB)	$PG = 1$															
Transmit Time (s)	$T_i = T_u = 1$ s															
Data Rate	$D = 1$ bit/s															
Signal Bandwidth	$B_i = B_s = 10^7$															
Probability of Clear Channel	$P_E = 1$															
Total Bandwidth	$B_T = NB_s$	10^8	10^9	10^{10}	10^{11}	10^{12}										
User Power	$T_{xp} = \log^{-1}\left[\frac{-23 + 10 \log D}{10}\right]$ $= 0.005$ W															
Users/MHz	$\frac{N}{B_T} \times 10^6 = 0.5$															

Table E-3

AUTONOMOUS CDM CONFIGURATION II

Parameter	Expression	Comment														
	$R_T = 1$ $R_F = 1$ $R_c = N$ $SNR_T = 20$ dh $SNR_c = 13$ dB $B_s = 10^7$	Number of Time Slots per FDM Channel Number of FDM Channels Number of Coded Users Signal-to-Thermal-Noise Ratio Signal-to-Clutter Ratio for $P_E = 10^{-5}$ Minimum Bandwidth for Ranging Signal													
Calculated Parameter	Expression	for N = Number of Users														
		N														
		10	10^2	10^3	10^4	10^5	10	10^2	10^3	10^4	10^5	10	10^2	10^3	10^4	10^5
Processing Gain (Required)	$PG = SNR_c + R_c$	23	33	43	53	63										
Transmit Time	$T_i = T_u = 1$ s															
Data Rate	$D = 1$ bit/s															
Signal Bandwidth	$B_s = 10^7$															
Probability of Clear Channel	$P_c = 1$															
Total Bandwidth	$B_T = B_s = 10^7$															
User Power	$T_{xp} = \log^{-1}\left[\frac{-14 + 10 \log D}{10}\right]$ $= 0.025$ W															
Users/MHz	$\frac{N}{B_T} \times 10^6$	1	10	10^2	10^3	10^4										

Table E-4

AUTONOMOUS TDM/FDM CONFIGURATION II

Parameter	Expression	Comment														
	$R_T = \frac{N}{R_F} \times 10^5$	Number of Time Slots per FDM Channel														
	$R_c = 1$	Number of Coded Users														
	R_F	Number of FDM Channels														
	$P_c = \left(1 - \frac{T_i}{T_u}\right)^N$	Probability of Clear Channel														
	$B_s = 10^7$	Minimum Bandwidth for Ranging Signal														
		for N = Number of Users														
Calculated Parameter	Expression	$R_F = 10$					$R_F = 100$					$R_F = 1000$				
Total Number of Users	N = Variable	10	10^2	10^3	10^4	10^5	10	10^2	10^3	10^4	10^5	10	10^2	10^3	10^4	10^5
Processing Gain	PG = 1															
Transmit Time	$T_i = \frac{T_u}{R_T}$		10^{-6}	10^{-7}	10^{-8}	10^{-9}		10^{-6}	10^{-7}	10^{-8}					10^{-6}	10^{-7}
Data Rate	$D = \frac{M}{T_i}$		2×10^7	2×10^8	2×10^9	2×10^{10}		2×10^7	2×10^8	2×10^9					2×10^7	2×10^8
Signal Bandwidth	$B_i = D$															
Probability of Clear Channel	$P_c = 0.9999$															
Total Bandwidth	$B_T = R_F D$		2×10^8	2×10^9	2×10^{10}	2×10^{12}		2×10^9	2×10^{10}	2×10^{11}					2×10^{10}	2×10^{11}
User Power	$T_{xp} = \log^{-1}\left[\frac{-23 + 10 \log \frac{M}{T_i}}{10}\right]$		10^5	10^6	10^7	10^8		10^5	10^6	10^7					10^5	10^6
Users/MHz	$\frac{N}{B_T} \times 10^6 = 0.5$															

Table E-5

AUTONOMOUS FDM/CDM CONFIGURATION II

Parameter	Expression	Comment														
	$N_s = \frac{N}{R_F}$	Number of Users per FDM Channel														
	R_F	Number of Frequency Channels														
	$B_s = 10^7$	Minimum Bandwidth for Ranging Signal														
	$R_T = 1$	Signal-to-Clutter Ratio														
	$SNR_C = 13$ dB	Signal-to-Thermal-Noise Ratio														
		for N = Number of Users														
Calculated Parameter	Expression	$R_F = 10$					$R_F = 100$					$R_F = 1000$				
Total Number of Users	N = Variable	10	10^2	10^3	10^4	10^5	10	10^2	10^3	10^4	10^5	10	10^2	10^3	10^4	10^5
Processing Gain (Required)	$PG = SNR_C \times N_s$	0	23	33	43	53		0	23	33	43			0	23	33
Transmit Time	$T_i = T_u$															
Data Rate	$D = \frac{M}{T_u} = 1$ bps															
Signal Bandwidth	$B_i = B_s = 10^7$															
Probability of Clear Channel	$P_c = 1$															
Total Bandwidth	$B_T = B_s R_F = 10^7 R_F$	10^8	10^8	10^8	10^8	10^8	10^9	10^9	10^9	10^9	10^9	10^{10}	10^{10}	10^{10}	10^{10}	10^{10}
User Power	$T_{xp} = \log^{-1}\left[\frac{-14 + 10 \log D}{10}\right]$ $= 0.025$ W															
Users/MHz	$\frac{N}{B_T} \times 10^6 = \frac{N}{R_F} \times 10^{-1}$	10^{-1}	1	10	10^2	10^2		10^{-1}	1	10	10^2			10^{-1}	1	10

Table E-6

AUTONOMOUS TDM/CDM CONFIGURATION II

Parameter	Expression	Comment
	$R_F = 1$	Number of FDM Channels
	R_T	Number of Time Slots
	$R_c = \frac{N}{R_T}$	Number of Users per Time Slot
	$SNR_T = 20$ dB	Signal-to-Thermal-Noise Ratio
	$SNR_C = 13$ dB	Signal-to-Clutter Ratio for $P_E = 10^{-5}$
	$N_S = 3R_c$	Number of Users Allowed per Time Slot
	$B_S = 10^7$	Minimum Bandwidth for Ranging Signal

Calculated Parameter	Expression	for N = Number of Users														
		$R_T = 10$					$R_T = 100$					$R_T = 1000$				
Total Number of Users	N = Variable	10	10^2	10^3	10^4	10^5	10	10^2	10^3	10^4	10^5	10	10^2	10^3	10^4	10^5
Processing Gain (Required)	$PG = N_s \times SNR_c$	0	28	38	48	58		0	28	38	48			0	28	38
Transmit Time	$T_i = \frac{T_u}{R_T}$	10^{-1}	10^{-1}	10^{-1}	10^{-1}	10^{-1}		10^{-2}	10^{-2}	10^{-2}	10^{-2}			10^{-3}	10^{-3}	10^{-3}
Data Rate	$D = \frac{1}{T_i}$	10	10	10	10	10		10^2	10^2	10^2	10^2			10^3	10^3	10^3
Signal Bandwidth	$B_i = B_s = 10^7$															
Probability of Clear Channel	$P_c = 1$															
Total Bandwidth	$B_T = B_s = 10^7$															
Transmit Power	$T_{xp} = \log^{-1}\left[\frac{-14 + 10 \log D}{10}\right]$	.25	.25	.25	.25	.25		2.5	2.5	2.5	2.5			25	25	25
Users/MHz	$\frac{N}{B_T} \times 10^6$	1	10	10^2	10^3	10^4		10	10^2	10^3	10^4			10^2	10^3	10^4

Appendix F

DETAILED DATA SHEETS FOR MULTIPLE ACCESS TECHNIQUES, C IV

Table F-1

E-TDMA, CONFIGURATION IV

$T_u = 1$ s M = 40 Bits

Parameter	Expression	Comment														
	$R_T = \frac{T_u}{T_i}$	Number of Time Slots														
	$SNR_P = 36$ dB	SNR Required for 1 km Accuracy ($\sigma\rho = 1°$)														
		Number of Users														
Calculated Parameter	Expression															
	$N = R_T$ = Variable	10	10^2	10^3	10^4	10^5	10	10^2	10^3	10^4	10^5	10	10^2	10^3	10^4	10^5
Processing Gain	PG = 1															
Transmit Time	$T_i = \frac{T_u}{N}$	10^{-1}	10^{-2}	10^{-3}	10^{-4}	10^{-5}										
Data Rate	$D = \frac{M}{T_i}$	4×10^2	4×10^3	4×10^4	4×10^5	4×10^6										
Signal Bandwidth	$B_i = D$															
Total Bandwidth	$B_T = B_i$															
Transmit Power	$T_{xp} = \log^{-1}\left[\log T_i^{-1}\right]$ $= T_i^{-1}$ W	10	10^2	10^3	10^4	10^5										
Users/MHz	$\frac{N}{B_T} \times 10^6 = 25 \times 10^3$															

Table F-2

A&E FDMA - CONFIGURATION IV

T_u = 1 s M = 40 Bits

Parameter	Expression	Comment														
	$R_F = N$ $R_T = 1$ $R_c = 1$ SNR_P = 36 dB B_D = 6 kHz	Number of Frequency Channels Number of Coded Users/Channel Number of Time Slots per Channel SNR Required for 1 km PL Error Bandwidth Due to Doppler and Oscillator Instability														
Calculated Parameter	Expression	Number of Users N														
	$N = R_F$ = Variable	10	10^2	10^3	10^4	10^5	10	10^2	10^3	10^4	10^5	10	10^2	10^3	10^4	10^5
Processing Gain	PG = 1															
Transmit Time	$T_i = T_u$ = 1 s															
Data Rate	$D = \frac{M}{T_u}$ = 40 bps															
Signal Bandwidth	$B_i = D$ = 40 bps															
Total Bandwidth	$B_T = N(B_i + B_D)$	6040 × 10	6040 × 10^2	6040 × 10^3	6040 × 10^4	6040 × 10^5										
Transmit Power	$T_{xp} = \log^{-1}\left[\log T_i^{-1}\right] = T_i^{-1}$ W															
Users/MHz	$\frac{N}{B_T} \times 10^6 = 164$															

Table F-3

A-TDMA - CONFIGURATION IV

$T_u = 1$ s M = 40 Bits

Parameter	Expression	Comment														
	$R_T = \frac{T_u}{T_i}$	Number of Time Slots														
	$SNR_p = 36$ dB	SNR Required for 1 km Accuracy														
Calculated Parameter	Expression	Number of Users														
	$N = R_T$ = Variable	10	10^2	10^3	10^4	10^5	10	10^2	10^3	10^4	10^5	10	10^2	10^3	10^4	10^5
Processing Gain	PG = 1															
Transmit Time	$T_i = \frac{T_u}{N} \times 10^{-5}$	10^{-6}	10^{-7}	10^{-8}	10^{-9}	10^{-10}										
Data Rate	$D = \frac{M}{T_i}$	4×10^7	4×10^8	4×10^9	4×10^{10}	4×10^{11}										
Signal Bandwidth	$B_i = D$															
Total Bandwidth	$B_T = B_i$															
Transmit Power	$T_{xp} = \log^{-1}\left[\log T_i^{-1}\right]$	10^6	10^7	10^8	10^9	10^{10}										
Users/MHz	$\frac{N}{B_T} = 10^6 = 0.25$															

Table F-4

A-FDMA/TDMA CONFIGURATION IV

$T_u = 1$ s M = 40 Bits $P_e = 10^{-5}$

Parameter	Expression	Comment														
	R_F	Number of Frequency Channels														
	$R_T = \frac{T_u}{T_i}$	Number of Time Slots per Channel														
	$SNR_p = 36$ dB	SNR Required for 1 km Accuracy														
Calculated Parameter	B_D = 6 kHz Doppler & Oscillator Drift Bandwidth	Number of Users														
	Expression	$R_F = 10$					$R_F = 100$					$R_F = 1000$				
	N = Variable.	10	10^2	10^3	10^4	10^5	10	10^2	10^3	10^4	10^5	10	10^2	10^3	10^4	10^5
Processing Gain	PG = 1															
Transmit Time	$T_i = \frac{T_u R_F}{N} P_e$	10^{-5}	10^{-6}	10^{-7}	10^{-8}	10^{-9}		10^{-5}	10^{-6}	10^{-7}	10^{-8}			10^{-5}	10^{-6}	10^{-8}
Data Rate	$D = \frac{M}{T_i}$	4×10^6	4×10^7	4×10^8	4×10^9	4×10^{10}		4×10^6	4×10^7	4×10^8	4×10^9			4×10^6	4×10^7	4×10^8
Signal Bandwidth	$B_i = D$															
Total Bandwidth	$B_T = R_F (B_i + B_D)$	4×10^7	4×10^8	4×10^9	4×10^{10}	4×10^{11}		4×10^8	4×10^9	4×10^{10}	4×10^{11}			4×10^7	4×10^{10}	4×10^{11}
Transmit Power	$T_{xp} = \log^{-1} \log T^{-1}$ $= T^{-1}$ W	10^5	10^6	10^7	10^8	10^9		10^5	10^6	10^7	10^8			10^5	10^6	10^7
Users/MHz	$\frac{N}{B_T} \times 10^6 = 0.25$															

Table F-5

E-FDMA/TDMA CONFIGURATION IV

T_u = 1 s M = 40 Bits

Parameter	Expression	Comment														
	R_F	Number of Frequency Channels														
	$R_T = \frac{T_u}{T_i}$	Number of Time Slots per Channel														
	SNR_P = 36 dB	SNR Required for 1 km Accuracy														
	B_D = 6 kHz	Bandwidth for Doppler and Oscillator Instability														
Calculated Parameter	Expression	Number of Users														
		R_F = 10					R_F = 100					R_F = 1000				
	N = Variable	10	10^2	10^3	10^4	10^5	10	10^2	10^3	10^4	10^5	10	10^2	10^3	10^4	10^5
Processing Gain	PG = 1															
Transmit Time	$T_i = \frac{T_u R_F}{N}$	1	10^{-1}	10^{-2}	10^{-3}	10^{-4}		1	10^{-1}	10^{-2}	10^{-3}			1	10^{-1}	10^{-2}
Data Rate	$D = \frac{M}{T_i}$	40	400	4000	4×10^4	4×10^5		40	400	4000	4×10^4			40	400	4000
Signal Bandwidth	$B_i = D$															
Total Bandwidth	$B_T = R_F (B_i + B_D)$	6.04×10^4	6.4×10^4	10^5	4.6×10^5	4×10^6		6.04×10^5	6.4×10^5	10^6	46×10^6			6.04×10^6	6.4×10^6	10^7
Transmit Power	$T_{xp} = \log^{-1}\left[\log T_i^{+1}\right] = T_i$	1	10	10^2	10^3	10^4		1	10	10^2	10^3			1	10	10^2
Users/MHz	$\frac{N}{B_T}\times10^6$	164	1570	10^4	21,800	25×10^3		164	1570	10^4	2.18×10^4			164	1570	10^4

REFERENCES

1. "Study of a Navigation and Traffic Control Technique Employing Satellites," Interim Report, Contract Number NAS 12-539, TRW Systems Group, Volumes I and III, December 1967.

2. Gill, W. J., "A Comparison of Binary Delay-Lock Tracking-Loop Implementations, "IEEE Transactions, Aerospace and Electronic Systems, AES-2, Number 4, July 1966.

3. "Integrated Function Waveform Design," Final Report, Contract Number F30602-69-C-0185, prepared for RADC C&N Division, Griffis AFB by IBM Corporation, Volume III, December 1969.

4. Gold, R., "A Study of Correlation Properties of Binary Sequencies", Tech. Report, AFAL TR 67 311, November, 1967.

5. Stiffler, J. J., "Rapid Acquisition Sequences", IEE Transaction Information Theory, IT-14, Number 2, March 1968.

6. "PLACE Experiment Ground Equipment Study, " Final Report, Contract Number NAS-5-21103, prepared by IBM Corporation, June 1970.

7. Skolnik, M. I., Introduction to Radar Systems, McGraw-Hill, New York, 1962.

8. Reed, I. S., and Blasbalg, H., "Multipath Tolerant Ranging and Data Transfer Techniques", Proc. IEEE, Volume 58, No. 2, March, 1970.

9. "The Applications of Satellites to Communications, Navigation, and Surveillance", FTR, Contract No. NAS-5-21535 by TRW Systems for NASA-GSFC, December, 1970.

10. "Interferometer Position Location Concept," FTR, Contract No. NAS-5-21043, prepared by IBM Corp. for NASA-GSFC, June, 1970.

11. Woodford, J. B., and Dutcher, R. L., "A Satellite System to Support an Advanced ATC Concept," Proc. IEEE, Vol. 5B No. 3, March 1970.

12. "A Study and Concept Formulation for a Fourth Generation ATCS," Technical Proposal No. 18037.0000, Prepared by TRW Systems for DOT, Appendix V, October, 1970.

Appendix G

PROGRAMMING CONSIDERATIONS

Appendix G

PROGRAMMING CONSIDERATIONS

G.1 ERROR ANALYSIS PROGRAM

The program first computes the satellite position, velocity, and the RTN to ECFC transformation matrix. The satellite computations are done in an inertial frame (assummed to be coincident with the ECFC frame at t = 0).

The input parameters (for each satellite) are

θ_N Inertial longitude of ascending node

i Inclination of orbit plane ($0 \leq i \leq 180°$)

ζ_p Argument of perigee

t_p Time of perigee

e Eccentricity

T Period.

The computations (for the jth satellite) are (reference Figure G-1)

$$n_j = 2\pi/T_j, \text{ mean rate} \tag{G-1}$$

$$a_j = \left(\mu/n_j^2\right)^{1/3}, \text{ semimajor axis} \tag{G-2}$$

where

$\mu = 1.40765 \times 10^{16}\ ft^3/s^2$

$$M_j = n_j (t - t_{pj}), \text{ mean anomaly} \tag{G-3}$$

$$E_j = M_j = e_j \sin E_j, \text{ eccentric anomaly} \tag{G-4}$$

$$\zeta_j = 2\tan^{-1}\left(\sqrt{\frac{1+e_j}{1-e_j}}\tan\frac{E_j}{2}\right), \text{ true anomaly} \tag{G-5}$$

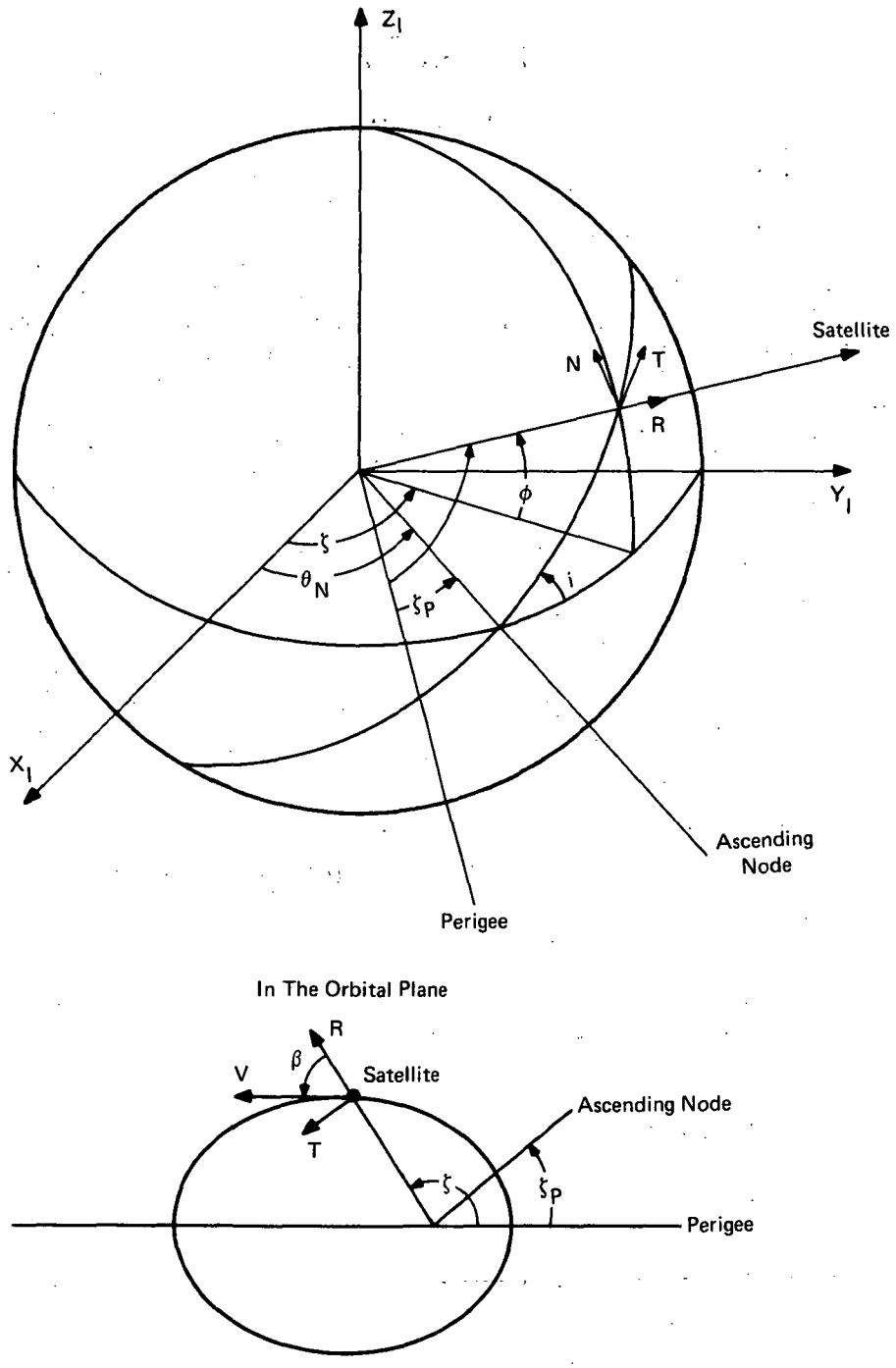

Figure G-1. Orbital Parameters

$$R_{gj} = a_j (1 - e_j^2)/(1 + e_j \cos \zeta_j), \text{ geocentric radius} \tag{G-6}$$

$$V_j = \left[\mu\left(\frac{2}{R_{gj}} - \frac{1}{a_j}\right)\right]^{1/2}, \text{ speed} \tag{G-7}$$

$$\beta_i = \cos^{-1}\left[\frac{e_j \sin \zeta_j}{(1 + 2 e_j \cos \zeta_j + e_j^2)^{1/2}}\right], \text{ flight path angle} \tag{G-8}$$

$$\phi_j = \sin^{-1}\left[\sin i_j \sin (\zeta_j - \zeta_{pj})\right], \text{ latitude} \tag{G-9}$$

$$\xi_j = \theta_{Nj} + \sin^{-1}\left(\frac{\sin (\zeta_j - \zeta_{pj}) \cos i_j}{\cos \phi_j}\right), \text{ inertial longitude} \tag{G-10}$$

$$\theta_j = \xi_j - \omega_e t, \text{ ECF longitude (Earth Centered Fixed)} \tag{G-11}$$

where

$$\omega_e = 7.27221 \times 10^{-5} \text{ rad/s}$$

Define $W_j + W_j$ so that

$$\overline{P}_{ECFC} \equiv W_j \overline{P}_{ECRTj} \tag{G-12}$$

and

$$\dot{\overline{P}}_{ECFC} \equiv W_j \overline{P}_{ECRTNj} + W_j \dot{\overline{P}}_{ECRTNj} \tag{G-13}$$

Then,

$$W_j = \begin{bmatrix} \cos(\theta_{N_j} - \omega_e t) & -\sin(\theta_{N_j} - \omega_e t) & 0 \\ \sin(\theta_{N_j} - \omega_e t) & \cos(\theta_{N_j} - \omega_e t) & 0 \\ 0 & 0 & 1 \end{bmatrix} \begin{bmatrix} 1 & 0 & 0 \\ 0 & \cos i_j & -\sin i_j \\ 0 & \sin i_j & \cos i_j \end{bmatrix} \begin{bmatrix} \cos(\zeta_j - \zeta_{pj}) & -\sin(\zeta_j - \zeta_{pj}) & 0 \\ \sin(\zeta_j - \zeta_{pj}) & \cos(\zeta_j - \zeta_{pj}) & 0 \\ 0 & 0 & 1 \end{bmatrix} \tag{G-14}$$

and

$$\dot{W}_j = \omega_e \begin{bmatrix} \sin(\theta_{N_j} - \omega_e t) & \cos(\theta_{N_j} - \omega_e t) & 0 \\ -\cos(\theta_{N_j} - \omega_e t) & \sin(\theta_{N_j} - \omega_e t) & 0 \\ 0 & 0 & 0 \end{bmatrix} \begin{bmatrix} 1 & 0 & 0 \\ 0 & \cos i_j & -\sin i_j \\ 0 & \sin i_j & \cos i_j \end{bmatrix} \begin{bmatrix} \cos(\zeta_j - \zeta_{pj}) & -\sin(\zeta_j - \zeta_{pj}) & 0 \\ \sin(\zeta_j - \zeta_{pj}) & \cos(\zeta_j - \zeta_{pj}) & 0 \\ 0 & 0 & 1 \end{bmatrix} \tag{G-15}$$

The position ($\overline{P}_{sj}$) and the velocity ($\dot{\overline{P}}_{sj}$) of the jth satellite in ECFC are computed by

$$\overline{P}_{sj} \equiv \begin{bmatrix} X_j \\ Y_j \\ Z_j \end{bmatrix} = W_j \begin{bmatrix} R_{gj} \\ 0 \\ 0 \end{bmatrix} \tag{G-16}$$

$$\dot{\overline{P}}_{sj} \equiv \begin{bmatrix} \dot{X}_j \\ \dot{Y}_j \\ \dot{Z}_j \end{bmatrix} = \dot{W}_j \begin{bmatrix} R_{gj} \\ 0 \\ 0 \end{bmatrix} + W_j \begin{bmatrix} V_j \cos \beta_j \\ V_j \sin \beta_j \\ 0 \end{bmatrix} \tag{G-17}$$

The Navigator's position, $\overline{P}_N$, and velocity, $\dot{\overline{P}}_N$, in ECFC are computed as

$$\dot{\overline{P}}_N \equiv \begin{bmatrix} X_N \\ Y_N \\ Z_N \end{bmatrix} = (R_e + h) \begin{bmatrix} \cos L_a \cos L_o \\ \cos L_a \sin L_o \\ \sin L_a \end{bmatrix} \tag{G-18}$$

and

$$\dot{\overline{P}}_N \equiv \begin{bmatrix} \dot{X}_N \\ \dot{Y}_N \\ \dot{Z}_N \end{bmatrix} = V_N \begin{bmatrix} -\sin n \sin L_o - \cos n \sin L_a \cos L_o \\ \sin n \cos L_o - \cos n \sin L_a \sin L_o \\ \cos n \cos L_a \end{bmatrix} \tag{G-19}$$

where

L_a, L_o is the ECFC latitude and longitude of the navigator

$R_e = 2.092567 \times 10^7$ ft

h, V_N, n are input quantities

h = altitude of the navigator

V_N = navigators speed relative to earth

n = the ECFC heading angle from north.

(Note: The navigators flight path angle is defined to be zero which is equivalent to flying horizontal)

The range, R_j, and the range rate, $\dot{R}_j$, to the jth satellite are

$$R_j = \left[(X_N - X_j)^2 + (Y_N - Y_j)^2 + (Z_N - Z_j)^2 \right]^{1/2} \qquad j = 1, 2, 3 \qquad \text{(G-20)}$$

$$\dot{R}_j = \frac{1}{R_j} \left[(\dot{X}_N - \dot{X}_j)(X_N - X_j) + (\dot{Y}_N - \dot{Y}_j)(Y_N - Y_j) + (\dot{Z}_N - \dot{Z}_j)(Z_N - Z_j) \right] \qquad \text{(G-21)}$$

For the range difference navigation schemes, the jth range difference, P_j, and range rate difference, $\dot{P}_j$, are

$$P_j = R_{j+1} - R_1 \qquad \text{(G-22)}$$

$$\dot{P}_j = \dot{R}_{j+1} - \dot{R}_1 \qquad \text{(G-23)}$$

The error equations (by navigation type) are

$$\begin{bmatrix} \Delta P_1 \\ \Delta P_2 \\ \Delta P_3 \\ \Delta \dot{P}_1 \\ \Delta \dot{P}_2 \\ \Delta \dot{P}_3 \end{bmatrix} = M_T \begin{bmatrix} \Delta \bar{P}_N \\ \hline \Delta \dot{\bar{P}}_N \end{bmatrix} + N_T \begin{bmatrix} \Delta \bar{P}_{S1} \\ \hline \Delta \bar{P}_{S2} \\ \hline \Delta \bar{P}_{S3} \\ \hline \Delta \bar{P}_{S4} \\ \hline \Delta \dot{\bar{P}}_{S1} \\ \hline \Delta \dot{\bar{P}}_{S2} \\ \hline \Delta \dot{\bar{P}}_{S3} \\ \hline \Delta \dot{\bar{P}}_{S4} \end{bmatrix} \qquad \text{(G-24}_{3P}\text{)}$$

$$\begin{bmatrix} \Delta P_1 \\ \Delta P_2 \\ \Delta h \\ \Delta \dot{P}_1 \\ \Delta \dot{P}_2 \\ \Delta \dot{h} \end{bmatrix} = M_T \begin{bmatrix} \Delta \bar{P}_N \\ \hline \Delta \dot{P}_N \end{bmatrix} + N_T \begin{bmatrix} \Delta \bar{P}_{S1} \\ \hline \Delta \bar{P}_{S2} \\ \hline \Delta \bar{P}_{S3} \\ \hline \Delta \dot{\bar{P}}_{S1} \\ \hline \Delta \dot{\bar{P}}_{S2} \\ \hline \Delta \dot{\bar{P}}_{S3} \end{bmatrix} \qquad \text{(G-24}_{2P+H}\text{)}$$

$$\begin{bmatrix} \Delta R_1 \\ \Delta R_2 \\ \Delta R_3 \\ \Delta \dot{R}_1 \\ \Delta \dot{R}_2 \\ \Delta \dot{R}_3 \end{bmatrix} = M_T \begin{bmatrix} \Delta \bar{P}_N \\ \hline \Delta \dot{\bar{P}}_N \end{bmatrix} + N_T \begin{bmatrix} \Delta \bar{P}_{S1} \\ \hline \Delta \bar{P}_{S2} \\ \hline \Delta \bar{P}_{S3} \\ \hline \Delta \dot{\bar{P}}_{S1} \\ \hline \Delta \dot{\bar{P}}_{S2} \\ \hline \Delta \dot{\bar{P}}_{S3} \end{bmatrix} \qquad (G\text{-}24_{3R})$$

$$\begin{bmatrix} \Delta R_1 \\ \Delta R_2 \\ \Delta h \\ \Delta \dot{R}_1 \\ \Delta \dot{R}_2 \\ \Delta \dot{h} \end{bmatrix} = M_T \begin{bmatrix} \Delta \bar{P}_N \\ \hline \Delta \dot{\bar{P}}_N \end{bmatrix} + N_T \begin{bmatrix} \Delta \bar{P}_{S1} \\ \hline \Delta \bar{P}_{S2} \\ \hline \Delta \dot{\bar{P}}_{S1} \\ \hline \Delta \dot{\bar{P}}_{S2} \end{bmatrix} \qquad (G\text{-}24_{2R+H})$$

A condensed notation for the error equation for all navigation schemes is

$$\begin{bmatrix} \Delta \bar{P} \\ \hline \Delta \dot{\bar{P}} \end{bmatrix} = M_T \begin{bmatrix} \Delta \bar{P}_N \\ \hline \Delta \dot{\bar{P}}_N \end{bmatrix} + N_T \begin{bmatrix} \Delta \bar{P}_S \\ \hline \Delta \dot{\bar{P}}_S \end{bmatrix} \qquad (G\text{-}24_{GENERAL})$$

The matrix, M_T, is

$$M_T = \left[\begin{array}{c|c} M & O \\ \hline \dot{M} & M \end{array}\right] \left(\text{since } \frac{\partial R_j}{\partial X_N} = \frac{\partial \dot{R}_j}{\partial \dot{X}_N}, \text{ etc.} \right) \qquad (G\text{-}25)$$

Where

$$M = \begin{bmatrix} \frac{\partial R_2}{\partial X_N} & \frac{\partial R_2}{\partial Y_N} & \frac{\partial R_2}{\partial Z_N} \\ \frac{\partial R_3}{\partial X_N} & \frac{\partial R_3}{\partial Y_N} & \frac{\partial R_3}{\partial Z_N} \\ \frac{\partial R_4}{\partial X_N} & \frac{\partial R_4}{\partial Y_N} & \frac{\partial R_4}{\partial Z_N} \end{bmatrix} - \begin{bmatrix} \frac{\partial R_1}{\partial X_N} & \frac{\partial R_1}{\partial Y_N} & \frac{\partial R_1}{\partial Z_N} \\ \frac{\partial R_1}{\partial X_N} & \frac{\partial R_1}{\partial Y_N} & \frac{\partial R_1}{\partial Z_N} \\ \frac{\partial R_1}{\partial X_N} & \frac{\partial R_1}{\partial Y_N} & \frac{\partial R_1}{\partial Z_N} \end{bmatrix}$$

$$\dot{M} = \begin{bmatrix} \frac{\partial \dot{R}_2}{\partial X_N} & \frac{\partial \dot{R}_2}{\partial Y_N} & \frac{\partial \dot{R}_2}{\partial Z_N} \\ \frac{\partial \dot{R}_3}{\partial X_N} & \frac{\partial \dot{R}_3}{\partial Y_N} & \frac{\partial \dot{R}_3}{\partial Z_N} \\ \frac{\partial \dot{R}_4}{\partial X_N} & \frac{\partial \dot{R}_4}{\partial Y_N} & \frac{\partial \dot{R}_4}{\partial Z_N} \end{bmatrix} - \begin{bmatrix} \frac{\partial \dot{R}_1}{\partial X_N} & \frac{\partial \dot{R}_1}{\partial Y_N} & \frac{\partial \dot{R}_1}{\partial Z_N} \\ \frac{\partial \dot{R}_1}{\partial X_N} & \frac{\partial \dot{R}_1}{\partial Y_N} & \frac{\partial \dot{R}_1}{\partial Z_N} \\ \frac{\partial \dot{R}_1}{\partial X_N} & \frac{\partial \dot{R}_1}{\partial Y_N} & \frac{\partial \dot{R}_1}{\partial Z_N} \end{bmatrix} \qquad (G\text{-}26_{3P})$$

or

$$M = \begin{bmatrix} \frac{\partial R_2}{\partial X_N} & \frac{\partial R_2}{\partial Y_N} & \frac{\partial R_2}{\partial Z_N} \\ \frac{\partial R_3}{\partial X_N} & \frac{\partial R_3}{\partial Y_N} & \frac{\partial R_3}{\partial Z_N} \\ \frac{\partial R_4}{\partial X_N} & \frac{\partial R_4}{\partial Y_N} & \frac{\partial R_4}{\partial Z_N} \end{bmatrix} - \begin{bmatrix} \frac{\partial R_1}{\partial X_N} & \frac{\partial R_1}{\partial Y_N} & \frac{\partial R_1}{\partial Z_N} \\ \frac{\partial R_1}{\partial X_N} & \frac{\partial R_1}{\partial Y_N} & \frac{\partial R_1}{\partial Z_N} \\ 0 & 0 & 0 \end{bmatrix}$$

$$\dot{M} = \begin{bmatrix} \frac{\partial \dot{R}_2}{\partial X_N} & \frac{\partial \dot{R}_2}{\partial Y_N} & \frac{\partial \dot{R}_2}{\partial Z_N} \\ \frac{\partial \dot{R}_3}{\partial X_N} & \frac{\partial \dot{R}_3}{\partial Y_N} & \frac{\partial \dot{R}_3}{\partial Z_N} \\ \frac{\partial \dot{R}_4}{\partial X_N} & \frac{\partial \dot{R}_4}{\partial Y_N} & \frac{\partial \dot{R}_4}{\partial Z_N} \end{bmatrix} - \begin{bmatrix} \frac{\partial \dot{R}_1}{\partial X_N} & \frac{\partial \dot{R}_1}{\partial Y_N} & \frac{\partial \dot{R}_1}{\partial Z_N} \\ \frac{\partial \dot{R}_1}{\partial X_N} & \frac{\partial \dot{R}_1}{\partial Y_N} & \frac{\partial \dot{R}_1}{\partial Z_N} \\ 0 & 0 & 0 \end{bmatrix} \qquad (G\text{-}26_{3P+H})$$

with $X_4 = Y_4 = Z_4 = \dot{X}_4 = \dot{Y}_4 = \dot{Z}_4 = 0$

when evaluating R_4, $\dot{R}_4$, $\frac{\partial R_4}{\partial}$, $\frac{\partial \dot{R}_4}{\partial}$

or

$$M = \begin{bmatrix} \frac{\partial R_1}{\partial X_N} & \frac{\partial R_1}{\partial Y_N} & \frac{\partial R_1}{\partial Z_N} \\ \frac{\partial R_2}{\partial X_N} & \frac{\partial R_2}{\partial Y_N} & \frac{\partial R_3}{\partial Z_N} \\ \frac{\partial R_3}{\partial X_N} & \frac{\partial R_3}{\partial Y_N} & \frac{\partial R_3}{\partial Z_N} \end{bmatrix}$$

$$\dot{M} = \begin{bmatrix} \frac{\partial \dot{R}_1}{\partial X_N} & \frac{\partial \dot{R}_1}{\partial X_N} & \frac{\partial \dot{R}_1}{\partial X_N} \\ \frac{\partial \dot{R}_2}{\partial X_N} & \frac{\partial \dot{R}_2}{\partial Y_N} & \frac{\partial \dot{R}_2}{\partial Z_N} \\ \frac{\partial \dot{R}_3}{\partial X_N} & \frac{\partial \dot{R}_3}{\partial Y_N} & \frac{\partial \dot{R}_3}{\partial Z_N} \end{bmatrix} \quad \left.\vphantom{\begin{bmatrix} a \\ b \\ c \end{bmatrix}}\right\} (G\text{-}26_{3R})$$

or

$$M = \begin{bmatrix} \frac{\partial R_1}{\partial X_N} & \frac{\partial R_1}{\partial Y_N} & \frac{\partial R_1}{\partial Z_N} \\ \frac{\partial R_2}{\partial X_N} & \frac{\partial R_2}{\partial Y_N} & \frac{\partial R_2}{\partial Z_N} \\ \frac{\partial R_3}{\partial X_N} & \frac{\partial R_3}{\partial Y_N} & \frac{\partial R_3}{\partial Z_N} \end{bmatrix} \quad \left.\vphantom{\begin{bmatrix} a \\ b \\ c \end{bmatrix}}\right\} (G\text{-}26_{2R+H})$$

(cont)

$$\dot{M} = \begin{bmatrix} \frac{\partial \dot{R}_1}{\partial X_N} & \frac{\partial \dot{R}_1}{\partial Y_N} & \frac{\partial \dot{R}_1}{\partial Z_N} \\ \frac{\partial \dot{R}_2}{\partial X_N} & \frac{\partial \dot{R}_2}{\partial Y_N} & \frac{\partial \dot{R}_2}{\partial Z_N} \\ \frac{\partial \dot{R}_3}{\partial X_N} & \frac{\partial \dot{R}_3}{\partial Y_N} & \frac{\partial \dot{R}_3}{\partial Z_N} \end{bmatrix}$$

with $X_3 = Y_3 = Z_3 = \dot{X}_3 = \dot{Y}_3 = \dot{Z}_3 = 0$

when evaluating R_3, $\dot{R}_3$, $\frac{\partial R_3}{\partial}$, $\frac{\partial \dot{R}_3}{\partial}$ (G-26$_{2R+H}$) (cont)

The matrix N_T is

$$N_T = \left[\begin{array}{c|c} N & 0 \\ \hline \dot{N} & N \end{array}\right] \qquad \text{(G-27)}$$

where

$$N = \begin{bmatrix} -\frac{\partial R_1}{\partial X_1} & -\frac{\partial R_1}{\partial Y_1} & -\frac{\partial R_1}{\partial Z_1} & \frac{\partial R_2}{\partial X_2} & \frac{\partial R_2}{\partial Y_2} & \frac{\partial R_2}{\partial Z_2} & 0 & 0 & 0 & 0 & 0 & 0 \\ -\frac{\partial R_1}{\partial X_1} & -\frac{\partial R_1}{\partial Y_1} & -\frac{\partial R_1}{\partial Z_1} & 0 & 0 & 0 & \frac{\partial R_3}{\partial X_3} & \frac{\partial R_3}{\partial Y_3} & \frac{\partial R_3}{\partial Z_3} & 0 & 0 & 0 \\ -\frac{\partial R_1}{\partial X_1} & -\frac{\partial R_1}{\partial Y_1} & -\frac{\partial R_1}{\partial Z_1} & 0 & 0 & 0 & 0 & 0 & 0 & \frac{\partial R_4}{\partial X_4} & \frac{\partial R_4}{\partial Y_4} & \frac{\partial R_4}{\partial Z_4} \end{bmatrix}$$

$$\dot{N} = \begin{bmatrix} -\frac{\partial \dot{R}_1}{\partial X_1} & -\frac{\partial \dot{R}_1}{\partial Y_1} & -\frac{\partial \dot{R}_1}{\partial Z_1} & \frac{\partial \dot{R}_2}{\partial X_2} & \frac{\partial \dot{R}_2}{\partial Y_2} & \frac{\partial \dot{R}_2}{\partial Z_2} & 0 & 0 & 0 & 0 & 0 & 0 \\ -\frac{\partial \dot{R}_1}{\partial X_1} & -\frac{\partial \dot{R}_1}{\partial Y_1} & -\frac{\partial \dot{R}_1}{\partial Z_1} & 0 & 0 & 0 & \frac{\partial \dot{R}_3}{\partial X_3} & \frac{\partial \dot{R}_3}{\partial Y_3} & \frac{\partial \dot{R}_3}{\partial Z_3} & 0 & 0 & 0 \\ -\frac{\partial \dot{R}_1}{\partial X_1} & -\frac{\partial \dot{R}_1}{\partial Y_1} & -\frac{\partial \dot{R}_1}{\partial Z_1} & 0 & 0 & 0 & 0 & 0 & 0 & \frac{\partial \dot{R}_4}{\partial X_4} & \frac{\partial \dot{R}_4}{\partial Y_4} & \frac{\partial \dot{R}_4}{\partial Z_4} \end{bmatrix}$$

(G-28$_{3P}$)

or

$$N = \begin{bmatrix} -\frac{\partial R_1}{\partial X_1} & -\frac{\partial R_1}{\partial Y_1} & -\frac{\partial R_1}{\partial Z_1} & \frac{\partial R_2}{\partial X_2} & \frac{\partial R_2}{\partial Y_2} & \frac{\partial R_2}{\partial Z_2} & 0 & 0 & 0 \\ -\frac{\partial R_1}{\partial X_1} & -\frac{\partial R_1}{\partial Y_1} & -\frac{\partial R_1}{\partial Z_1} & 0 & 0 & 0 & \frac{\partial R_3}{\partial X_3} & \frac{\partial R_3}{\partial Y_3} & \frac{\partial R_3}{\partial Z_3} \\ 0 & 0 & 0 & 0 & 0 & 0 & 0 & 0 & 0 \end{bmatrix}$$

$$\dot{N} = \begin{bmatrix} -\frac{\partial \dot{R}_1}{\partial X_1} & -\frac{\partial \dot{R}_1}{\partial Y_1} & -\frac{\partial \dot{R}_1}{\partial Z_1} & \frac{\partial \dot{R}_2}{\partial X_2} & \frac{\partial \dot{R}_2}{\partial Y_2} & \frac{\partial \dot{R}_2}{\partial Z_2} & 0 & 0 & 0 \\ -\frac{\partial \dot{R}_1}{\partial X_1} & -\frac{\partial \dot{R}_1}{\partial Y_1} & -\frac{\partial \dot{R}_1}{\partial Z_1} & 0 & 0 & 0 & \frac{\partial \dot{R}_3}{\partial X_3} & \frac{\partial \dot{R}_3}{\partial Y_3} & \frac{\partial \dot{R}_3}{\partial Z_3} \\ 0 & 0 & 0 & 0 & 0 & 0 & 0 & 0 & 0 \end{bmatrix}$$

$(G28_{2P+H})$

or

$$N = \begin{bmatrix} \frac{\partial R_1}{\partial X_1} & \frac{\partial R_1}{\partial Y_1} & \frac{\partial R_1}{\partial Z_1} & 0 & 0 & 0 & 0 & 0 & 0 \\ 0 & 0 & 0 & \frac{\partial R_2}{\partial X_2} & \frac{\partial R_2}{\partial Y_2} & \frac{\partial R_2}{\partial Z_2} & 0 & 0 & 0 \\ 0 & 0 & 0 & 0 & 0 & 0 & \frac{\partial R_3}{\partial X_3} & \frac{\partial R_3}{\partial Y_3} & \frac{\partial R_3}{\partial Z_3} \end{bmatrix}$$

$$\dot{N} = \begin{bmatrix} \frac{\partial \dot{R}_1}{\partial X_1} & \frac{\partial \dot{R}_1}{\partial Y_1} & \frac{\partial \dot{R}_1}{\partial Z_1} & 0 & 0 & 0 & 0 & 0 & 0 \\ 0 & 0 & 0 & \frac{\partial \dot{R}_2}{\partial X_2} & \frac{\partial \dot{R}_2}{\partial Y_2} & \frac{\partial \dot{R}_2}{\partial Z_2} & 0 & 0 & 0 \\ 0 & 0 & 0 & 0 & 0 & 0 & \frac{\partial \dot{R}_3}{\partial X_3} & \frac{\partial \dot{R}_3}{\partial Y_3} & \frac{\partial \dot{R}_3}{\partial Z_3} \end{bmatrix}$$

$(G-28_{3R})$

or

$$N = \begin{bmatrix} \frac{\partial R_1}{\partial X_1} & \frac{\partial R_1}{\partial Y_1} & \frac{\partial R_1}{\partial Z_1} & 0 & 0 & 0 \\ 0 & 0 & 0 & \frac{\partial R_2}{\partial X_2} & \frac{\partial R_2}{\partial Y_2} & \frac{\partial R_2}{\partial Z_2} \\ 0 & 0 & 0 & 0 & 0 & 0 \end{bmatrix}$$

$$\dot{N} = \begin{bmatrix} \frac{\partial \dot{R}_1}{\partial X_1} & \frac{\partial \dot{R}_1}{\partial Y_1} & \frac{\partial \dot{R}_1}{\partial Z_1} & 0 & 0 & 0 \\ 0 & 0 & 0 & \frac{\partial \dot{R}_2}{\partial X_2} & \frac{\partial \dot{R}_2}{\partial Y_2} & \frac{\partial \dot{R}_2}{\partial Z_2} \\ 0 & 0 & 0 & 0 & 0 & 0 \end{bmatrix} \qquad (G\text{-}28_{2R+H})$$

For evaluating the partial derivatives

$$-\frac{\partial R_j}{\partial X_j} = \frac{\partial R_j}{\partial X_N} = \frac{1}{R_j}(X_N - X_j)$$

$$-\frac{\partial R_j}{\partial Y_j} = \frac{\partial R_j}{\partial Y_N} = \frac{1}{R_j}(Y_N - Y_j)$$

$$-\frac{\partial R_j}{\partial Z_j} = \frac{\partial R_j}{\partial Z_N} = \frac{1}{R_j}(Z_N - Z_j)$$

$$-\frac{\partial \dot{R}_j}{\partial X_j} = \frac{\partial \dot{R}_j}{\partial X_N} = \frac{R_j(\dot{X}_N - \dot{X}_j) - \dot{R}_j(X_N - X_j)}{R_j^2}$$

$$-\frac{\partial \dot{R}_j}{\partial Y_j} = \frac{\partial \dot{R}_j}{\partial Y_N} = \frac{R_j(\dot{Y}_N - \dot{Y}_j) - \dot{R}_j(Y_N - Y_j)}{R_j^2}$$

$$-\frac{\partial \dot{R}_j}{\partial Z_j} = \frac{\partial \dot{R}_j}{\partial Z_N} = \frac{R_j(\dot{Z}_N - \dot{Z}_j) - \dot{R}_j(Z_N - Z_j)}{R_j^2} \qquad (G\text{-}29)$$

The error Equation G-24$_{GENERAL}$ can be solved for navigation errors:

$$\begin{bmatrix} \Delta\bar{P}_N \\ \hline \Delta\dot{\bar{P}}_N \end{bmatrix} = M_T^{-1} \begin{bmatrix} \Delta\bar{P} \\ \hline \Delta\dot{\bar{P}} \end{bmatrix} - M_T^{-1} N_T \begin{bmatrix} \Delta\bar{P}_S \\ \hline \Delta\dot{\bar{P}}_S \end{bmatrix} \tag{G-30}$$

where

$$M_T^{-1} = \left[\begin{array}{c|c} M & 0 \\ \hline \dot{M} & M \end{array}\right]^{-1} = \left[\begin{array}{c|c} M^{-1} & 0 \\ \hline -M^{-1}\dot{M}M^{-1} & M^{-1} \end{array}\right] \equiv \left[\begin{array}{c|c} A & 0 \\ \hline \dot{A} & A \end{array}\right] \equiv A_T \tag{G-31}$$

A more relevant coordinate system for the navigation errors is an earth surfaced tangential (ESTC) frame located at the navigator. Define Q such that

$$Q\,\Delta\bar{P}_{N_{ECFC}} = \begin{bmatrix} \text{East component of } \Delta\bar{P}_N \\ \text{North component of } \Delta\bar{P}_N \\ \text{Up component of } \Delta\bar{P}_N \end{bmatrix}_{ESTC} \quad \text{(at the navigator)} \tag{G-32}$$

Then,

$$Q = \begin{bmatrix} -\sin L_o & \cos L_o & 0 \\ -\cos L_o \sin L_a & -\sin L_o \sin L_a & \cos L_a \\ \cos L_o \cos L_a & \sin L_o \cos L_a & \sin L_a \end{bmatrix} \tag{G-33}$$

and

$$\dot{Q} = \dot{L}_o \begin{bmatrix} -\cos L_o & -\sin L_o & 0 \\ \sin L_o \sin L_a & -\cos L_o \sin L_a & 0 \\ -\sin L_o \cos L_a & \cos L_o \cos L_a & 0 \end{bmatrix} + \dot{L}_a \begin{bmatrix} 0 & 0 & 0 \\ -\cos L_o \cos L_a & -\sin L_o \cos L_a & -\sin L_a \\ -\cos L_o \sin L_a & -\sin L_o \sin L_a & \cos L_a \end{bmatrix} \tag{G-34}$$

where

$$\dot{L}_a = \frac{V_N}{R_e + h} \cos n \tag{G-35}$$

$$\dot{L}_o = \frac{V_N \sin n}{(R_e + h) \cos L_a} \tag{G-36}$$

Defining Q_T

$$Q_T \equiv \left[\begin{array}{c|c} Q & 0 \\ \hline \dot{Q} & Q \end{array}\right] \tag{G-37}$$

the navigation errors can be transformed to

$$\left[\begin{array}{c} \Delta\bar{P}_{Ng} \\ \hline \Delta\dot{\bar{P}}_{Ng} \end{array}\right] \equiv Q_T \left[\begin{array}{c} \Delta\bar{P}_N \\ \hline \Delta\dot{\bar{P}}_N \end{array}\right] = Q_T A_T \left[\begin{array}{c} \Delta\bar{P} \\ \hline \Delta\dot{\bar{P}} \end{array}\right] - Q_T A_T N_T \left[\begin{array}{c} \Delta\bar{P}_S \\ \hline \Delta\dot{\bar{P}}_S \end{array}\right] \tag{G-38}$$

where the subscript g indicates ESTC frame, and the covariance matrix of navigator errors is

$$E\left\{\left[\begin{array}{c} \Delta\bar{P}_{Ng} \\ \hline \Delta\dot{\bar{P}}_{Ng} \end{array}\right]\left[\begin{array}{c} \Delta\bar{P}_{Ng} \\ \hline \Delta\dot{\bar{P}}_{Ng} \end{array}\right]^T\right\} = Q_T A_T E\left\{\left[\begin{array}{c} \Delta\bar{P} \\ \hline \Delta\dot{\bar{P}} \end{array}\right]\left[\begin{array}{c} \Delta\bar{P} \\ \hline \Delta\dot{\bar{P}} \end{array}\right]^T\right\}(Q_T A_T)^T$$
$$+ Q_T A_T N_T E\left\{\left[\begin{array}{c} \Delta\bar{P}_S \\ \hline \Delta\dot{\bar{P}}_S \end{array}\right]\left[\begin{array}{c} \Delta\bar{P}_S \\ \hline \Delta\dot{\bar{P}}_S \end{array}\right]^T\right\}(Q_T A_T N_T)^T \tag{G-39}$$

Designating

$$E\left\{\left[\begin{array}{c} \Delta\bar{P}_{Ng} \\ \hline \Delta\dot{\bar{P}}_{Ng} \end{array}\right]\left[\begin{array}{c} \Delta\bar{P}_{Ng} \\ \hline \Delta\dot{\bar{P}}_{Ng} \end{array}\right]^T\right\} \equiv \tau^2_{NAV} \tag{G-40}$$

and

$$E\left\{\begin{bmatrix}\Delta\bar{P}\\ \dot{\Delta\bar{P}}\end{bmatrix}\begin{bmatrix}\Delta\bar{P}\\ \dot{\Delta\bar{P}}\end{bmatrix}^T\right\} \equiv \left[\begin{array}{c|c}\tau_{pp}^2 & 0\\ \hline 0 & \dot{\tau}_{pp}^2\end{array}\right] \tag{G-41}$$

and

$$E\left\{\begin{bmatrix}\Delta\bar{P}_s\\ \dot{\Delta\bar{P}}_s\end{bmatrix}\begin{bmatrix}\Delta\bar{P}_s\\ \dot{\Delta\bar{P}}_s\end{bmatrix}^T\right\} \equiv \omega_T\, E\left\{\begin{bmatrix}\overline{\Delta S}\\ \dot{\overline{\Delta S}}\end{bmatrix}\begin{bmatrix}\overline{\Delta S}\\ \dot{\overline{\Delta S}}\end{bmatrix}\right\}\omega_T^T$$

$$\equiv \omega_T \left[\begin{array}{c|c}\tau_{ss}^2 & 0\\ \hline 0 & \dot{\tau}_{ss}^2\end{array}\right] \omega_T^T \tag{G-42}$$

where τ_{pp}^2, $\dot{\tau}_{pp}^2$, τ_{ss}^2, $\dot{\tau}_{ss}^2$ are defined in Subsection G. 2 and

$$\omega_T \equiv \left[\begin{array}{c|c}\omega & 0\\ \hline \dot{\omega} & \omega\end{array}\right] = \left[\begin{array}{c|c|c|c|c|c|c|c}\omega_1 & 0 & 0 & 0 & 0 & 0 & 0 & 0\\ \hline 0 & \omega_2 & 0 & 0 & 0 & 0 & 0 & 0\\ \hline 0 & 0 & \omega_3 & 0 & 0 & 0 & 0 & 0\\ \hline 0 & 0 & 0 & \omega_4 & 0 & 0 & 0 & 0\\ \hline \dot{\omega}_1 & 0 & 0 & 0 & \omega_1 & 0 & 0 & 0\\ \hline 0 & \dot{\omega}_2 & 0 & 0 & 0 & \omega_2 & 0 & 0\\ \hline 0 & 0 & \dot{\omega}_3 & 0 & 0 & 0 & \omega_3 & 0\\ \hline 0 & 0 & 0 & \dot{\omega}_4 & 0 & 0 & 0 & \omega_4\end{array}\right] \tag{G-43}$$

for the 3P navigation mode. ω_T is suitably reduced for navigation schemes using two or three satellites.

If $\dot{\overline{QA}}$ and $\dot{\overline{QANW}}$ are defined as

$$\dot{\overline{QA}} \equiv \dot{Q}A + Q\dot{A} \tag{G-44}$$

$$\dot{\overline{QANW}} \equiv \dot{Q}ANW + Q\dot{A}NW + QA\dot{N}W + QANW \tag{G-45}$$

then the equation producing the covariance matrix of the navigator errors, can be written as implemented:

$$\tau^2_{NAV} = \left[\begin{array}{c|c} QA\tau^2_{pp}(QA)^T & QA\tau^2_{pp}(\dot{\overline{QA}})^T \\ \hline \dot{\overline{QA}}\tau^2_{pp}(QA)^T & \dot{\overline{QA}}\tau^2_{pp}(\dot{\overline{QA}})^T \end{array}\right] + \left[\begin{array}{c|c} 0 & 0 \\ \hline 0 & QA\dot{\tau}^2_{pp}(QA)^T \end{array}\right]$$

$$+ \left[\begin{array}{c|c} QANW\tau^2_{ss}(QANW)^T & QANW\tau^2_{ss}(QANW)^T \\ \hline \dot{\overline{QANW}}\tau^2_{ss}(QANW)^T & \dot{\overline{QANW}}\tau^2_{ss}(\dot{\overline{QANW}})^T \end{array}\right] + \left[\begin{array}{c|c} 0 & 0 \\ \hline 0 & QANW\dot{\tau}^2_{ss}(QANW)^T \end{array}\right] \tag{G-46}$$

For the case where a reference station calibration is assumed, the navigator error Equation 38 becomes

$$\begin{bmatrix} \Delta\overline{P}_{Ng} \\ \hline \Delta\dot{\overline{P}}_{Ng} \end{bmatrix} = Q_T A_T \begin{bmatrix} \Delta\overline{P} \\ \hline \Delta\dot{\overline{P}} \end{bmatrix} - Q_T A_T N_T \begin{bmatrix} \Delta\overline{P}_s \\ \hline \Delta\dot{\overline{P}}_s \end{bmatrix}$$

$$- Q_{T_o} A_{T_o} \begin{bmatrix} \Delta\overline{P}_o \\ \hline \Delta\dot{\overline{P}}_o \end{bmatrix} + Q_{T_o} A_{T_o} N_{T_o} \begin{bmatrix} \Delta\overline{P}_{s_o} \\ \hline \Delta\dot{\overline{P}}_{s_o} \end{bmatrix} \tag{G-47}$$

where the subscript, o, indicates that the quantity is evaluated at the time of the calibration using the satellite/navigator geometry defined by placing the navigator at the reference station at the time of calibration.

Then the covariance matrix of the navigator errors (with reference station calibration) becomes

$$\tau^2_{REF} = \tau^2_{NAV} + \left(\tau^2_{NAV}\right)_o - \tau^2_{CROSS} - \left(\tau^2_{CROSS}\right)^T \tag{G-48}$$

where

$$\tau^2_{CROSS} = \left[\begin{array}{c|c} (QA)_o \tau^2_{p_o p} (QA)^T & (QA)_o \tau^2_{p_o p} (\dot{\overline{QA}})^T \\ \hline (\dot{\overline{QA}})_o \tau^2_{p_o p} (QA)^T & (\dot{\overline{QA}})_o \tau^2_{p_o p} (\dot{\overline{QA}})^T \end{array}\right] + \left[\begin{array}{c|c} 0 & 0 \\ \hline 0 & (QA)_o \dot{\tau}^2_{p_o p} (QA)^T \end{array}\right]$$

$$+ \left[\begin{array}{c|c} (QANW)_o \tau^2_{s_o s} (QANW)^T & (QANW)_o \tau^2_{s_o s} (\dot{\overline{QANW}})^T \\ \hline (\dot{\overline{QANW}})_o \tau^2_{s_o s} (QANW)^T & (\dot{\overline{QANW}})_o \tau^2_{s_o s} (\dot{\overline{QANW}})^T \end{array}\right] + \left[\begin{array}{c|c} 0 & \\ \hline 0 & (QANW)_o \dot{\tau}^2_{s_o s} (QANW)^T \end{array}\right] \qquad \text{(G-49)}$$

The terms $\tau^2_{p_o p}$, $\dot{\tau}^2_{p_o p}$, $\tau^2_{s_o s}$, $\dot{\tau}^2_{s_o s}$ (defined in Subsection G. 2) relate the source errors at calibration to the current source errors.

For example

$$\tau^2_{p_o p} = E\left\{\Delta\bar{P}_o \, \Delta\bar{P}^T\right\} \qquad \text{(G-50)}$$

The program computes the diagonal elements of

$$\tau^2_{NAV} \text{ and } \tau^2_{REF}$$

for each of the error sources defined in Subsection G. 2 and prepares the following quantities for output:

$$\left.\begin{array}{ll} \sqrt{\tau^2_{NAV_{1,1}} + \tau^2_{NAV_{2,2}}} & = \text{Horizontal Position Error} \\ \sqrt{\tau^2_{NAV_{3,3}}} & = \text{Vertical Position Error} \\ \sqrt{\tau^2_{NAV_{4,4}} + \tau^2_{NAV_{5,5}}} & = \text{Horizontal Rate Error} \\ \sqrt{\tau^2_{NAV_{6,6}}} & = \text{Vertical Rate Error} \end{array}\right\} \qquad \text{(G-51)}$$

Similar expressions using τ^2_{REF} are formed and output for the four components of error with reference station calibration.

G.2 ERROR SOURCES

G.2.1 3P NAVIGATION

$$\begin{bmatrix} \Delta\bar{P} \\ \hline \Delta\dot{\bar{P}} \end{bmatrix} = \begin{bmatrix} \Delta R_2 - \Delta R_1 \\ \Delta R_3 - \Delta R_1 \\ \Delta R_4 - \Delta R_1 \\ \Delta\dot{R}_2 - \Delta\dot{R}_1 \\ \Delta\dot{R}_3 - \Delta\dot{R}_1 \\ \Delta\dot{R}_4 - \Delta\dot{R}_1 \end{bmatrix} \tag{G-52}$$

The ij element of τ^2_{pp} is equal to

$$E(\Delta P_i \Delta P_j) = E(\Delta R_{i+1} \Delta R_{j+1}) + E(\Delta R_1 \Delta R_1) - E(\Delta R_{i+1} \Delta R_1) - E(\Delta R_1 \Delta R_{j+1}) \tag{G-53}$$

the ij element of $\tau^2_{p_o p}$ is

$$E(\Delta P_{i_o} \Delta P_j) = E(\Delta R_{i+1_o} \Delta R_{j+1}) + E(\Delta R_{1_o} \Delta R_1) - E(\Delta R_{i+1_o} \Delta R_1) - E(\Delta R_{1_o} \Delta R_{j+1}) \tag{G-54}$$

the ij element of $\dot{\tau}^2_{pp}$ is

$$E(\Delta\dot{P}_i \Delta\dot{P}_j) = E(\Delta\dot{R}_{i+1} \Delta\dot{R}_{j+1}) + E(\Delta\dot{R}_1 \Delta\dot{R}_1) - E(\Delta\dot{R}_{i+1} \Delta\dot{R}_1) - E(\Delta\dot{R}_1 \Delta\dot{R}_{j+1}) \tag{G-55}$$

and the i j element of $\dot{\tau}^2_{p_o p}$ is

$$E\left(\Delta\dot{P}_{i_o}\,\Delta\dot{P}_j\right) = E\left(\Delta\dot{R}_{i+1_o}\,\Delta\dot{R}_{j+1}\right) + E\left(\Delta\dot{R}_{1_o}\,\Delta\dot{R}_1\right) - E\left(\Delta\dot{R}_{i+1_o}\,\Delta\dot{R}_1\right) - E\left(\Delta\dot{R}_{1_o}\,\Delta\dot{R}_{j+1}\right) \tag{G-56}$$

G. 2. 1. 1 3P Navigation, Range (and Range Rate) Noise Errors

When normalized to a unit error, the expected values needed to evaluate Equations G-53 through G-56 are

$$E\left(\Delta R_{i+1}\,\Delta R_{j+1}\right) = E\left(\Delta\dot{R}_{i+1}\,\Delta\dot{R}_{j+1}\right) = \delta_{ij} \tag{G-57}$$

$$E\left(\Delta R_1\,\Delta R_1\right) = E\left(\Delta\dot{R}_1\,\Delta\dot{R}_1\right) = 1 \tag{G-58}$$

where δ_{ij} is the Kronecker delta function.

The remainder of the terms have the value zero. Therefore,

$$\tau^2_{pp} = \dot{\tau}^2_{pp} = \begin{bmatrix} 2 & 1 & 1 \\ 1 & 2 & 1 \\ 1 & 1 & 2 \end{bmatrix} \tag{G-59}$$

and

$$\tau^2_{p_o p} = \dot{\tau}^2_{p_o p} = [\,0\,] \tag{G-60}$$

G. 2. 1. 2 3P Navigation, Range (and Range Rate) Bias Errors

When normalized to a unit error, the expected values needed to evaluate Equations G-53 through G-56 are all equal to the value one.

Therefore,

$$\tau^2_{pp} = \dot{\tau}^2_{pp} = \tau^2_{p_o p} = \dot{\tau}^2_{p_o p} = [\,0\,] \tag{G-61}$$

G.2.1.3 3P Navigation, Refraction Errors

When normalized to a unit error,

$$E\,(\Delta R_i\ \Delta R_j) = \rho_{ij} \tag{G-62}$$

and

$$E\,(\Delta R_{i_o}\ \Delta R_j) = \rho_{i_o j} \tag{G-63}$$

for all where ρ_{ij} and $\rho_{i_o j}$ are defined in Subsection G.3.

Therefore,

$$\tau^2_{pp} = \begin{bmatrix} \rho_{22} & \rho_{23} & \rho_{24} \\ \rho_{32} & \rho_{33} & \rho_{34} \\ \rho_{42} & \rho_{43} & \rho_{44} \end{bmatrix} + \rho_{11} \begin{bmatrix} 1 & 1 & 1 \\ 1 & 1 & 1 \\ 1 & 1 & 1 \end{bmatrix} - \begin{bmatrix} \rho_{21} & \rho_{21} & \rho_{21} \\ \rho_{31} & \rho_{31} & \rho_{31} \\ \rho_{41} & \rho_{41} & \rho_{41} \end{bmatrix} - \begin{bmatrix} \rho_{12} & \rho_{13} & \rho_{14} \\ \rho_{12} & \rho_{13} & \rho_{14} \\ \rho_{12} & \rho_{13} & \rho_{14} \end{bmatrix} \tag{G-64}$$

$$\tau^2_{p_o p} = \begin{bmatrix} \rho_{2_o 2} & \rho_{2_o 3} & \rho_{2_o 4} \\ \rho_{3_o 2} & \rho_{3_o 3} & \rho_{3_o 4} \\ \rho_{4_o 2} & \rho_{4_o 3} & \rho_{4_o 4} \end{bmatrix} + \rho_{1_o 1} \begin{bmatrix} 1 & 1 & 1 \\ 1 & 1 & 1 \\ 1 & 1 & 1 \end{bmatrix} - \begin{bmatrix} \rho_{2_o 1} & \rho_{2_o 1} & \rho_{2_o 1} \\ \rho_{3_o 1} & \rho_{3_o 1} & \rho_{3_o 1} \\ \rho_{4_o 1} & \rho_{4_o 1} & \rho_{4_o 1} \end{bmatrix} - \begin{bmatrix} \rho_{1_o 2} & \rho_{1_o 3} & \rho_{1_o 4} \\ \rho_{1_o 2} & \rho_{1_o 3} & \rho_{1_o 4} \\ \rho_{1_o 2} & \rho_{1_o 3} & \rho_{1_o 4} \end{bmatrix} \tag{G-65}$$

$\dot{\tau}^2_{pp}$ and $\dot{\tau}^2_{p_o p}$ are not applicable for this error source.

G.2.1.4 3P Navigation, Satellite Position (and Rate) Errors

The ephemeris errors are normalized to the tangential axis. The radial and normal errors are related to the tangential error by the input factors k_1 and k_2. The ephemeris errors are assumed to be correlated over the four satellites by the input factor ρ_s. The source error covariance matrix is

$$\tau^2_{ss} = \dot{\tau}^2_{ss} = \left[\begin{array}{c|c|c|c} K & \rho_s K & \rho_s K & \rho_s K \\ \hline \rho_s K & K & \rho_s K & \rho_s K \\ \hline \rho_s K & \rho_s K & K & \rho_s K \\ \hline \rho_s K & \rho_s K & \rho_s K & K \end{array}\right] \qquad \text{(G-66)}$$

where

$$K = \begin{bmatrix} k_1^2 & 0 & 0 \\ 0 & 1 & 0 \\ 0 & 0 & k_s^2 \end{bmatrix} \qquad \text{(G-67)}$$

Two values of $\tau^2_{s_o s}$ and $\dot{\tau}^2_{s_o s}$ are used. These represent the limiting cases of temporal correlation, as follows:

$$\tau^2_{s_o s} = \dot{\tau}^2_{s_o s} = [\,0\,] \quad \text{(uncorrelated)} \qquad \text{(G-68)}$$

and

$$\tau^2_{s_o s} = \dot{\tau}^2_{s_o s} = \tau^2_{ss} \quad \text{(correlated)} \qquad \text{(G-69)}$$

G.2.2 2P+H NAVIGATION

$$\begin{bmatrix} \overline{\Delta P} \\ \hline \overline{\Delta \dot{P}} \end{bmatrix} \qquad \begin{bmatrix} \Delta R_2 - \Delta R_1 \\ \Delta R_3 - \Delta R_1 \\ \Delta h \\ \Delta \dot{R}_2 - \Delta \dot{R}_1 \\ \Delta \dot{R}_3 - \Delta \dot{R}_1 \\ \Delta \dot{h} \end{bmatrix} \tag{G-70}$$

For i and j both less than 3, the ij elements of τ^2_{pp}, $\dot{\tau}^2_{pp}$, $\tau^2_{p_o p}$, and $\dot{\tau}^2_{p_o p}$ are given by Equations G-53 through G-56, respectively.

For i or j equal to 3, the ij elements are

$$\tau^2_{pp}(ij) = E(\Delta P_i \Delta P_j) = \delta_{ij} E(\Delta h \Delta h) \tag{G-71}$$

$$\dot{\tau}^2_{pp}(ij) = E(\Delta \dot{P}_i \Delta \dot{P}_j) = \delta_{ij} E(\Delta \dot{h} \Delta \dot{h}) \tag{G-72}$$

$$\tau^2_{p_o p}(ij) = E(\Delta P_{i_o} \Delta P_j) = \delta_{ij} E(\Delta h_o \Delta h) \tag{G-73}$$

$$\dot{\tau}^2_{p_o p}(ij) = E(\Delta \dot{P}_{i_o} \Delta P_j) = \delta_{ij} E(\Delta h_o \Delta h) \tag{G-74}$$

where δ_{ij} is the Kroenecker delta function.

G.2.2.1 2P+H Navigation, Range (and Range Rate) Noise Errors

Using Equations G-57 and G-58 produces

$$\tau^2_{pp} = \dot{\tau}^2_{pp} = \begin{bmatrix} 2 & 1 & 0 \\ 1 & 2 & 0 \\ 0 & 0 & 0 \end{bmatrix} \tag{G-75}$$

and

$$\tau^2_{p_o p} = \dot{\tau}^2_{p_o p} = [0] \tag{G-76}$$

G.2.2.2 2P+H Navigation, Range (and Range Rate) Bias Errors

Similarly to the 3P case (G.2.1.2),

$$\tau^2_{pp} = \dot{\tau}^2_{pp} = \tau^2_{p_o p} = \dot{\tau}^2_{p_o p} = [0] \tag{G-77}$$

G.2.2.3 2P+H Navigation, Altitude (and Altitude Rate) Noise Errors

Normalizing to a unit error and using Equations G-71 through G-74, gives

$$\tau^2_{pp} = \dot{\tau}^2_{pp} = \begin{bmatrix} 0 & 0 & 0 \\ 0 & 0 & 0 \\ 0 & 0 & 1 \end{bmatrix} \tag{G-78}$$

and

$$\tau^2_{p_o p} = \dot{\tau}^2_{p_o p} = [0] \tag{G-79}$$

G.2.2.4 2ρ+H Navigation, Altitude (and Altitude Rate) Bias Errors

Normalized to a unit error,

$$\tau^2_{pp} = \dot{\tau}^2_{pp} = \tau^2_{p_o p} = \dot{\tau}^2_{p_o p} = \begin{bmatrix} 0 & 0 & 0 \\ 0 & 0 & 0 \\ 0 & 0 & 1 \end{bmatrix} \tag{G-80}$$

G. 2. 2. 5 2P+H Navigation, Refraction Errors

Similarly to the 3P case (G. 2. 1. 3),

$$\tau^2_{pp} = \begin{bmatrix} \rho_{22} & \rho_{23} & 0 \\ \rho_{32} & \rho_{33} & 0 \\ 0 & 0 & 0 \end{bmatrix} + \rho_{11} \begin{bmatrix} 1 & 1 & 0 \\ 1 & 1 & 0 \\ 0 & 0 & 0 \end{bmatrix} - \begin{bmatrix} \rho_{21} & \rho_{21} & 0 \\ \rho_{31} & \rho_{31} & 0 \\ 0 & 0 & 0 \end{bmatrix} \quad \text{(G-81)}$$

$$- \begin{bmatrix} \rho_{12} & \rho_{13} & 0 \\ \rho_{12} & \rho_{13} & 0 \\ 0 & 0 & 0 \end{bmatrix}$$

and

$$\tau^2_{p_o p} = \begin{bmatrix} \rho_{2_o 2} & \rho_{2_o 3} & 0 \\ \rho_{3_o 2} & \rho_{3_o 3} & 0 \\ 0 & 0 & 0 \end{bmatrix} + \rho_{1_o 1} \begin{bmatrix} 1 & 1 & 0 \\ 1 & 1 & 0 \\ 0 & 0 & 0 \end{bmatrix} \quad \text{(G-82)}$$

$$- \begin{bmatrix} \rho_{2_o 1} & \rho_{2_o 1} & 0 \\ \rho_{3_o 1} & \rho_{3_o 1} & 0 \\ 0 & 0 & 0 \end{bmatrix} - \begin{bmatrix} \rho_{1_o 2} & \rho_{1_o 3} & 0 \\ \rho_{1_o 2} & \rho_{1_o 3} & 0 \\ 0 & 0 & 0 \end{bmatrix}$$

$\dot{\tau}^2_{pp}$ and $\dot{\tau}^2_{p_o p}$ are not applicable for this error source.

G. 2. 2. 6 2P+H Navigation, Satellite Position (and Rate) Errors

$$\tau^2_{ss} = \dot{\tau}^2_{ss} = \left[\begin{array}{c|c|c} K & \rho_s K & \rho_s K \\ \hline \rho_s K & K & \rho_s K \\ \hline \rho_s K & \rho_s K & K \end{array}\right] \quad \text{(G-83)}$$

where K and ρ_s are defined in Subsection G. 2. 1. 4.

The two values of $\tau^2_{s_o s}$ and $\dot{\tau}^2_{s_o s}$ are given by Equations G-68 and G-69.

G. 2. 3 3R NAVIGATION

$$\begin{bmatrix} \Delta\bar{\bar{\rho}} \\ \hline \Delta\dot{\bar{\rho}} \end{bmatrix} = \begin{bmatrix} \Delta R_1 \\ \Delta R_2 \\ \Delta R_3 \\ \Delta \dot{R}_1 \\ \Delta \dot{R}_2 \\ \Delta \dot{R}_3 \end{bmatrix} \tag{G-84}$$

The ij element of τ^2_{pp} is

$$E\,(\Delta P_i\, \Delta P_j) = E\,(\Delta R_i\, \Delta R_j) \tag{G-85}$$

the ij element of $\dot{\tau}^2_{pp}$ is

$$E\,(\Delta \dot{P}_i\, \Delta \dot{P}_j) = E\,(\Delta \dot{R}_i\, \Delta \dot{R}_j) \tag{G-86}$$

the ij element of $\tau^2_{p_o p}$ is

$$E\,(\Delta P_{i_o}\, \Delta P_j) = E\,(\Delta R_{i_o}\, \Delta R_j) \tag{G-87}$$

and the ij element of $\dot{\tau}^2_{p_o p}$ is

$$E\,(\Delta \dot{P}_{i_o}\, \Delta \dot{P}_j) = E\,(\Delta \dot{R}_{i_o}\, \Delta \dot{R}_j) \tag{G-88}$$

G. 2. 3. 1 3R Navigation, Range (and Range Rate) Noise Errors

When normalized to a unit error,

$$E\,(\Delta R_i\, \Delta R_j) = E\,(\Delta \dot{R}_i\, \Delta \dot{R}_j) = \delta_{ij} \tag{G-89}$$

and

$$E\,(\Delta R_{i_o}\, \Delta R_j) = E\,(\Delta \dot{R}_{i_o}\, \Delta \dot{R}_j) = 0 \tag{G-90}$$

Therefore,

$$\tau^2_{pp} = \dot{\tau}^2_{pp} = \begin{bmatrix} 1 & 0 & 0 \\ 0 & 1 & 0 \\ 0 & 0 & 1 \end{bmatrix} \quad \text{(G-91)}$$

and

$$\tau^2_{p_o p} = \dot{\tau}^2_{p_o p} = [\,0\,] \quad \text{(G-92)}$$

G.2.3.2 3R Navigation, Range (and Range Rate) Bias Errors

When normalized to a unit error

$$E\,(\Delta R_i\ \Delta R_j) = E\,(\Delta \dot{R}_i\ \Delta \dot{R}_j) = E\,(\Delta R_{i_o}\ \Delta R_j) = E\,(\Delta \dot{R}_{i_o}\ \Delta \dot{R}_j) = 1 \quad \text{(G-93)}$$

and

$$\tau^2_{pp} = \dot{\tau}^2_{pp} = \tau^2_{p_o p} = \dot{\tau}^2_{p_o p} = \begin{bmatrix} 1 & 1 & 1 \\ 1 & 1 & 1 \\ 1 & 1 & 1 \end{bmatrix} \quad \text{(G-94)}$$

G.2.3.3 3R Navigation, Refraction Errors

Equations G-62 and G-63 hold; therefore,

$$\tau^2_{pp} = \begin{bmatrix} \rho_{11} & \rho_{12} & \rho_{13} \\ \rho_{21} & \rho_{22} & \rho_{23} \\ \rho_{31} & \rho_{32} & \rho_{33} \end{bmatrix} \quad \text{(G-95)}$$

and

$$\tau^2_{p_o p} = \begin{bmatrix} \rho_{1_o 1} & \rho_{1_o 2} & \rho_{1_o 3} \\ \rho_{2_o 1} & \rho_{2_o 2} & \rho_{2_o 3} \\ \rho_{3_o 1} & \rho_{3_o 2} & \rho_{3_o 3} \end{bmatrix} \quad \text{(G-96)}$$

$\dot{\tau}^2_{pp}$ and $\dot{\tau}^2_{p_o p}$ are not applicable for the error source.

G.2.3.4 3R Navigation, Satellite Position (and Rate) Errors

τ^2_{ss} and $\dot{\tau}^2_{ss}$ are given by Equation G-83. The two values of $\tau^2_{s_o s}$ and $\dot{\tau}^2_{s_o s}$ are given by Equations G-68 and G-69.

G.2.4 2R+H NAVIGATION

$$\begin{bmatrix} \Delta\bar{\rho} \\ \Delta\dot{\bar{P}} \end{bmatrix} = \begin{bmatrix} \Delta R_1 \\ \Delta R_2 \\ \Delta h \\ \Delta \dot{R}_1 \\ \Delta \dot{R}_2 \\ \Delta \dot{h} \end{bmatrix} \tag{G-97}$$

For i and j both less than 3, the ij elements of τ^2_{pp}, $\dot{\tau}^2_{pp}$, $\tau^2_{p_o p}$, $\dot{\tau}^2_{p_o p}$ are given by Equations G-85 through G-88, respectively.

For i or j equal to 3, the ij elements are given by Equations G-71 through G-74.

G.2.4.1 2R+H Navigation, Range (and Range Rate) Noise Errors

Using Equations G-89 and G-90 produces

$$\tau^2_{pp} = \dot{\tau}^2_{pp} = \begin{bmatrix} 1 & 0 & 0 \\ 0 & 1 & 0 \\ 0 & 0 & 0 \end{bmatrix} \tag{G-98}$$

and

$$\tau^2_{p_o p} = \dot{\tau}^2_{p_o p} = [0] \tag{G-99}$$

G.2.4.2 2R+H Navigation, Range (and Range Rate) Bias Errors

Equation G-93 holds, and

$$\tau^2_{pp} = \dot{\tau}^2_{pp} = \tau^2_{p_o p} = \dot{\tau}^2_{p_o p} = \begin{bmatrix} 1 & 1 & 0 \\ 1 & 1 & 0 \\ 0 & 0 & 0 \end{bmatrix} \quad \text{(G-100)}$$

G.2.4.3 2R+H Navigation, Altitude (and Altitude Rate) Noise Errors

τ^2_{pp}, $\dot{\tau}^2_{pp}$, $\tau^2_{p_o p}$, $\dot{\tau}^2_{p_o p}$ are given by Equations G-78 and G-79.

G.2.4.4 2R+H Navigation, Altitude (and Altitude Rate) Bias Errors

τ^2_{pp}, $\dot{\tau}^2_{pp}$, $\tau^2_{p_o p}$, $\dot{\tau}^2_{p_o p}$ are given by Equation G-80.

G.2.4.5 2R+H Navigation, Refraction Errors

Using Equations G-62 and G-63.

$$\tau^2_{pp} = \begin{bmatrix} \rho_{11} & \rho_{12} & 0 \\ \rho_{21} & \rho_{22} & 0 \\ 0 & 0 & 0 \end{bmatrix} \quad \text{(G-101)}$$

and

$$\tau^2_{p_o p} = \begin{bmatrix} \rho_{1_o 1} & \rho_{1_o 2} & 0 \\ \rho_{2_o 1} & \rho_{2_o 2} & 0 \\ 0 & 0 & 0 \end{bmatrix} \quad \text{(G-102)}$$

$\dot{\tau}^2_{pp}$ and $\dot{\tau}^2_{p_o p}$ are not applicable for this error source.

G.2.4.6 2R+H Navigation, Satellite Position (and Rate) Errors

$$\tau^2_{ss} = \dot{\tau}^2_{ss} = \left[\begin{array}{c|c} K & \rho_s K \\ \hline \rho_s K & K \end{array}\right] \quad \text{(G-103)}$$

where K and ρ_s are defined in Subsection G.2.1.4.

The two values of $\tau^2_{s_o s}$ and $\dot{\tau}^2_{s_o s}$ are given by Equations G-68 and G-69.

G.3 REFRACTION CORRELATION FACTORS

The term

$$\rho_{ij}$$

represents the correlation factor between the range measurement errors due to refraction effects along the two paths

$$\bar{R}_i \text{ and } \bar{R}_j,$$

the vectors between the navigator and the satellites i and j at the current time. From Chen's paper, "Range Difference Error due to the Presence of Ionospheric Electrons",

$$\rho_{ij} = G_i G_j (1 - 0.665 \times 10^{-7} S_{ij}) \tag{G-104}$$

where S_{ij} is the distance, at ionosphere altitude, between $\bar{R}_i$ and $\bar{R}_j$ in feet, and

$$G_k = e^{-0.883 L_a (\csc 0.03046) + E_k^2} \quad k = i, j \tag{G-105}$$

with

L_a, the latitude of the navigator in radians

E_k, the elevation angle of R_k in radians.

The term,

$$\rho_{i_o j}$$

represents the correlation factor between the measurement errors due to refraction effects along the two paths

$$\bar{R}_{i_o} \text{ and } \bar{R}_j,$$

where

$\bar{R}_{i_o}$ is the vector between the reference station and satellite i at $t = t_o$.

$\bar{R}_j$ is the vector between the navigator and satellite j at the current time.

Then,

$$\rho_{i_o j} = G_{i_o} G_j (1 - 0.665 \times 10^{-7} S_{i_o j}) \quad (1 - 0.1195656 \Delta T + 0.806205 \times 10^{-2} \Delta t^2 - 0.242344 \times 10^{-3} \Delta t^3 + 0.254357 \times 10^{-5} \Delta t^4) \tag{G-106}$$

where

$S_{i_o j}$ is the distance, at ionosphere altitude, between $\bar{R}_{i_o}$ and $\bar{R}_j$ in feet, and

$\Delta t = t - t_o$ in hours, and

$$G_{i_o} = e^{-0.833\, L_{a_o}} (\csc \quad 0.03046) + E_{i_o}^2)^{1/2} \tag{G-107}$$

with

L_{a_o}, the latitude of the reference station in radians

E_{i_o}, the elevation angle of $\bar{R}_{i_o}$ in radians.

Appendix H

MULTIPLE SATELLITE COVERAGE

Appendix H

MULTIPLE SATELLITE COVERAGE

This program is designed to provide coverage patterns for a specific number of satellites in a specified number of orbit planes. Distribution of the satellites takes place internal to the program and is based on the following input data:

1) Number of satellites - Maximum of 153
2) Number of orbits - Must be an integer factor of the above
3) Satellite period - T (minutes)
4) Eccentricity - e
5) Time of perigee for first satellite - T_p (1) (minutes)
6) Longitude of ascending node for first satellite - ξ_N (1) (degrees)
7) Angle of inclination - i (degrees)
8) Argument of perigee for first satellite - ζ_N (1) (degrees)

The intent is to provide uniform spacing of the satellites about the globe, initially and as the satellites move within their orbits.

The secular effects of oblateness, i.e., regression of the line of nodes and argument of perigee, are accounted for in the satellite motions. The following criteria have been used to properly space the satellites.

The space between orbital planes is equal to 180°/number of orbits. Start the first orbital plane off at the equator and Greenwich. Space the satellites uniformly within the orbit by changing the time of perigee (T_p). Delta T_p is equal to period/number of satellites per orbit.

Example 1 (Figure H-1)

8 satellites $\qquad i = 90^\circ$

2 orbital planes

4 satellites per orbit

2 hour satellite period

Delta $T_p = -T/4 = -30$ minutes

Delta $\xi = 180^\circ/2 = 90^\circ$

Thus, the second orbital plane will be spaced 90^{o} from the first

Delta ζ_p = Delta $\xi/2 = 90^{o}/2 = 45^{o}$

Plane 1

$\xi_N = 0.0$

$\zeta_p = 0.0$

$T_p = 0.0, -30.0, -60.0, -90.0$

Plane 2

$\xi_N = 90.0^{o}$

$\zeta_p = 45.0^{o}$

$T_p = 0.0, -30.0, -60.0, -90.0$

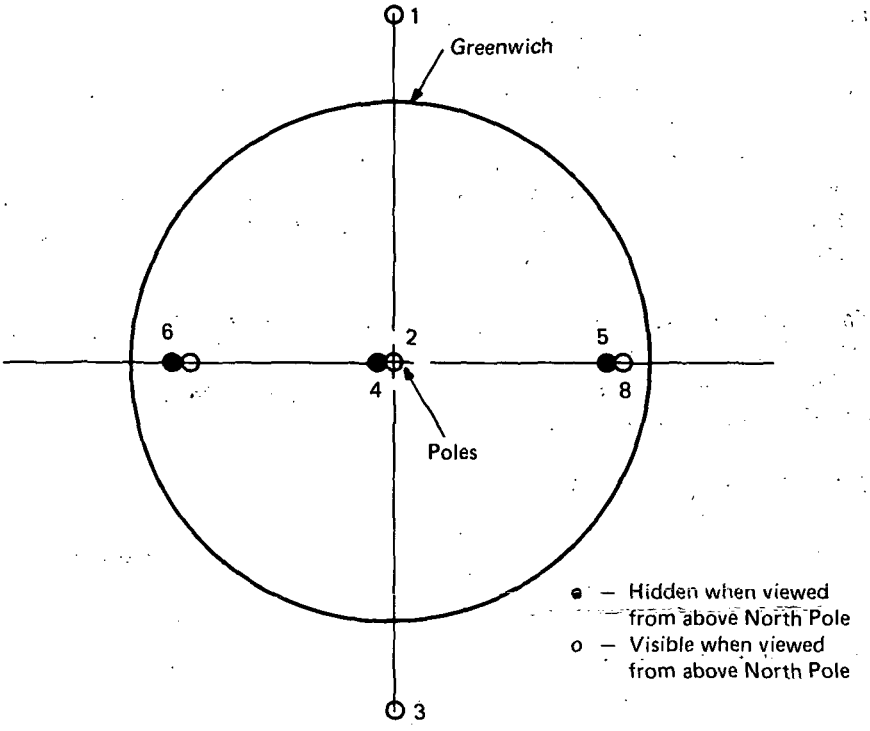

Figure H-1

Example 2 (Figure H-2)

15 satellites

3 orbital planes

5 satellites per plane

2 hour period

$i = 90^{o}$

Delta $T_p = 120/5 = 24$ minutes

Delta $\xi = 180^{o}/3 = 60^{o}$

Thus, the second and third orbital planes will be spaced 60^{o} and 120^{o} away from the first.

Delta $\zeta_p = 60^{o}/3 = 20^{o}$

Thus, the argument of perigee for the second and third orbital planes will be 20^{o} and 40^{o}, respectively.

Plane 1

$\xi_N = 0.0^{o}$

$\zeta_p = 0.0^{o}$

$T_p = 0.0, -24.0, -48.0, -72.0, -96.0$

Plane 2

$\xi_N = 60.0^{o}$

$\zeta_p = 20.0^{o}$

$T_p = 0.0, -24.0, -48.0, -72.0, -96.0$

Plane 3

$\xi_N = 120.0^{o}$

$\zeta_p = 40.0^{o}$

$T_p = 0.0, -24.0, -48.0, -72.0, -96.0$

Once the satellites have been spaced properly, it is possible, at any given time, to display a graphic representation of where all the satellites are located and how many can be seen from any point on the earth. At time t, the vector for each satellite

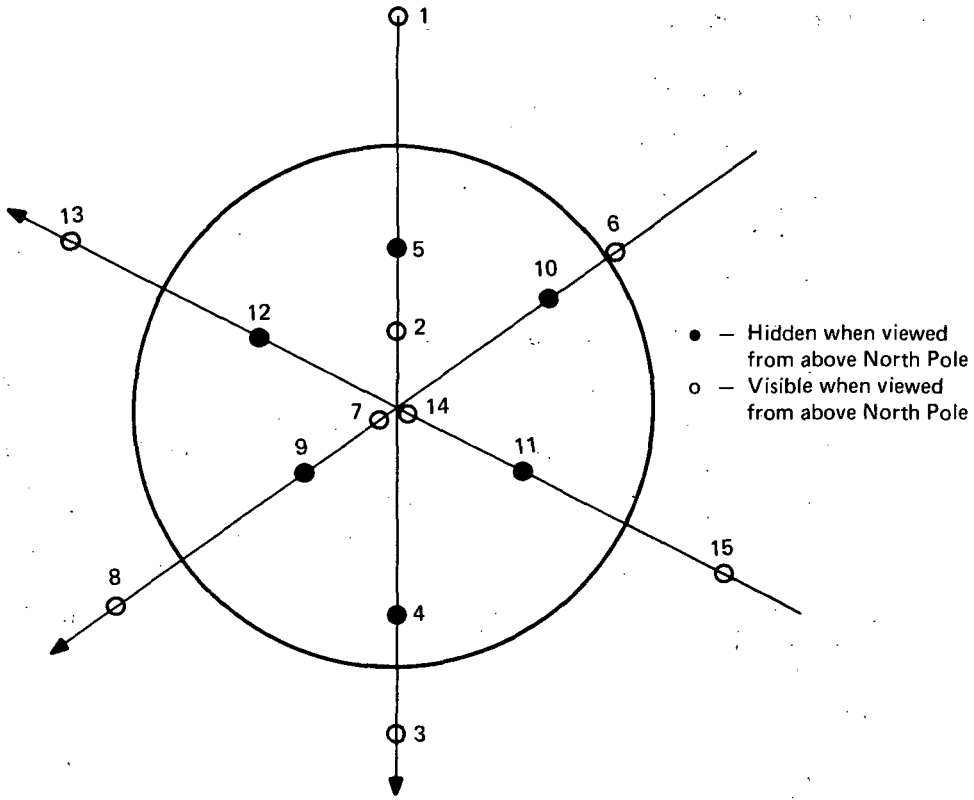

Figure H-2

is computed and stored. At every 5^{o} latitude and longitude, a test is made to determine how many satellites are visible, i.e., above 10^{o} elevation angle to meet navigational requirements.

Altitude (R_s), latitude (ϕ_s), and longitude (θ_s) of a satellite produces the vector $\overline{R}_s$ (see Figure H-3). See Program flow for equations deriving R_s, ϕ_s, and θ_s.

$$\overline{R}_s = R_s \begin{bmatrix} \cos \phi_s & \cos \theta_s \\ \cos \phi_s & \sin \theta_s \\ \sin \phi_s & \end{bmatrix}$$

Altitude (R_p = radius of earth), latitude (ϕ_p), and longitude (θ_p) of a position on the earth's surface gives the vector $\overline{R}_p$ (see Figure H-3).

$$\overline{R}_p = R_p \begin{bmatrix} \cos \phi_p & \cos \theta_p \\ \cos \phi_p & \sin \theta_p \\ \sin \phi_p & \end{bmatrix}$$

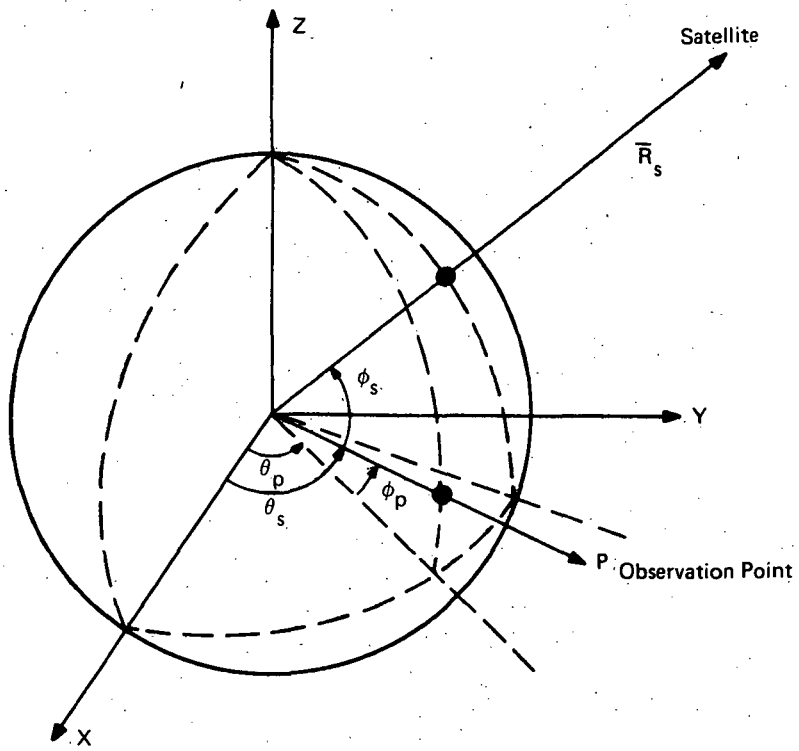

Figure H-3

A line (Rel) drawn from a satellite tangent to a point on the earth gives the maximum distance that satellite can be from the point on the earth (see Figure H-4). Thus,

$$Rel = R_s^2 - R_e^2 \quad \text{where, } R_e = \text{radius of earth}$$

The vector $\overline{R_{ps}}$ (point on the earth to satellite) is computed by:

$$\overline{R}_{ps} = \overline{R}_s - \overline{R}_p$$

(See Figure H-4.)

If $\overline{R_{ps}} >$ Rel, the satellite is not acceptable since it is beyond the horizon.

If not, the elevation angle of the satellite (ϵ) is computed as follows:

$$\cos \beta = \frac{\overline{R}_{ps} \bullet \overline{R}_p}{|R_{ps}| \quad |R_p|}$$

$$\epsilon = 90^o - \beta$$

If the elevation angle is above 10^o, the satellite is therefore acceptable for navigational purposes.

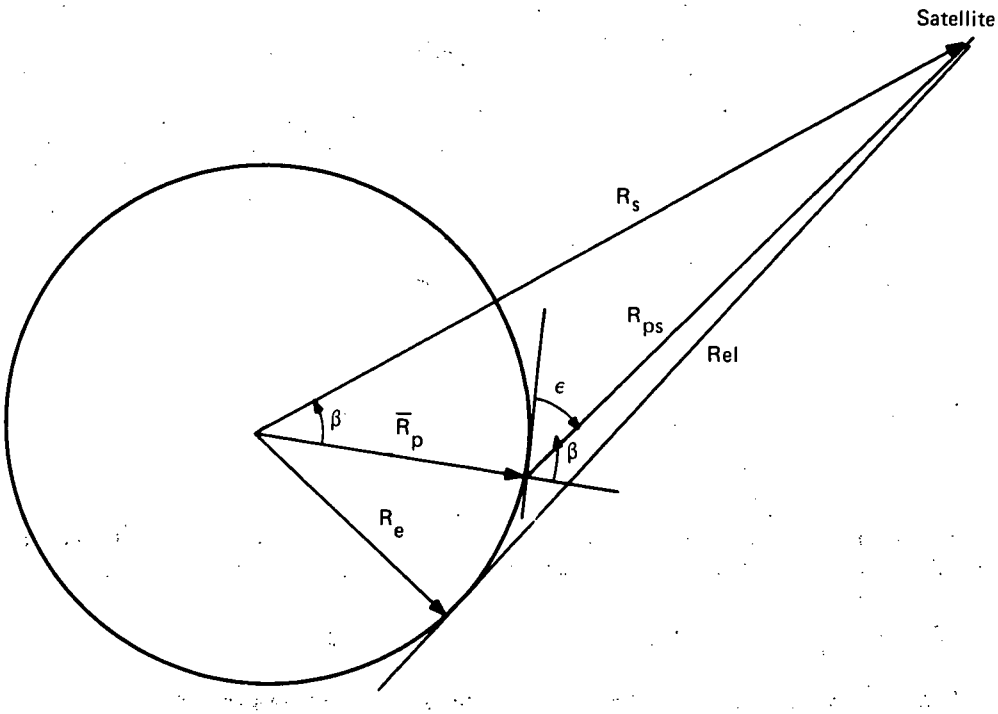

Figure H-4

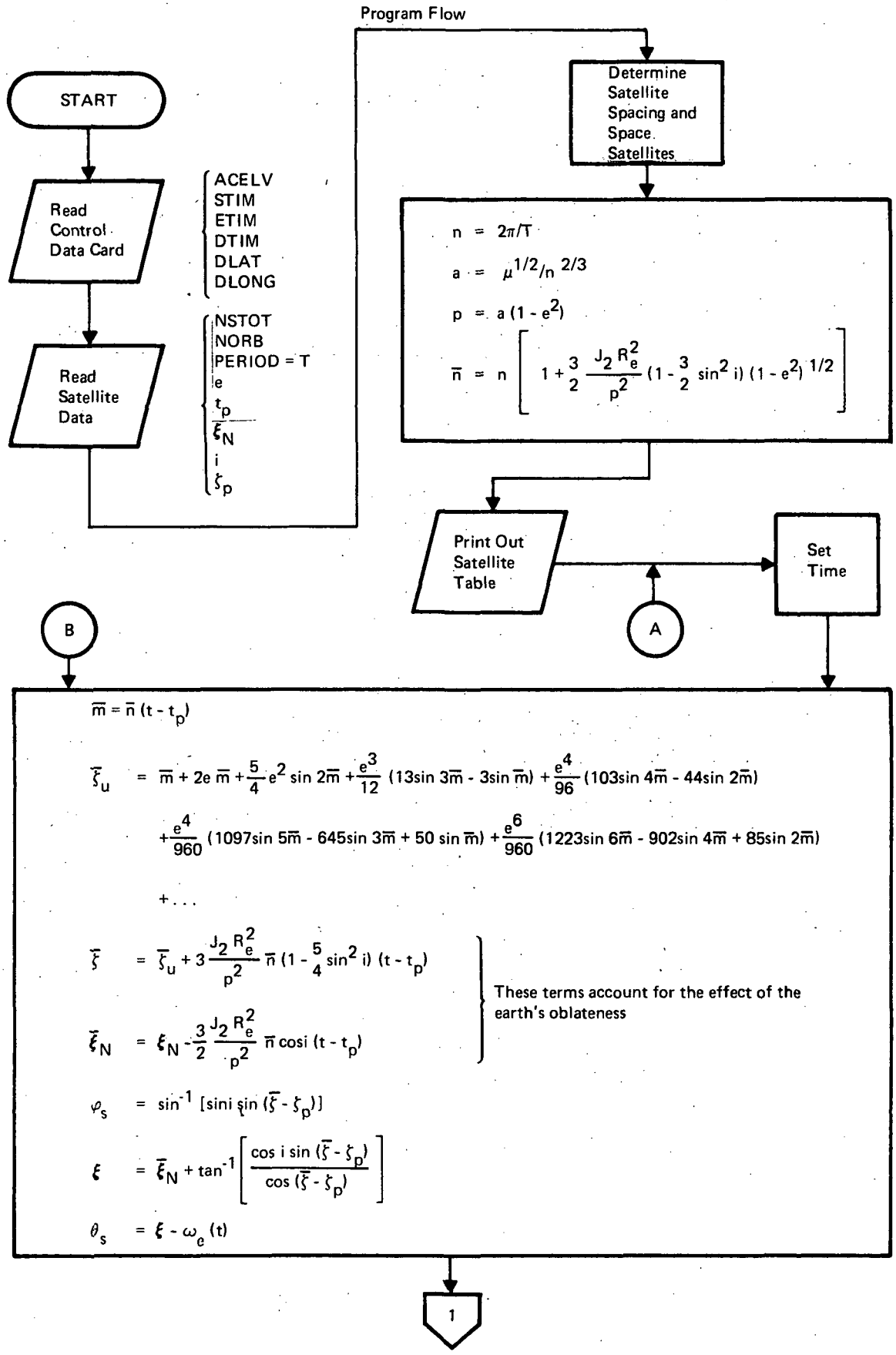
Program Flow
START
Read Control Data Card
ACELV
STIM
ETIM
DTIM
DLAT
DLONG
Read Satellite Data
NSTOT
NORB
PERIOD = T
e
t_p
ξ_N
i
ζ_p
Determine Satellite Spacing and Space Satellites
$n = 2\pi/T$
$a = \mu^{1/2}/n^{2/3}$
$p = a(1 - e^2)$
$\bar{n} = n\left[1 + \frac{3}{2}\frac{J_2 R_e^2}{p^2}(1 - \frac{3}{2}\sin^2 i)(1 - e^2)^{1/2}\right]$
Print Out Satellite Table
A
Set Time
B
$\bar{m} = \bar{n}(t - t_p)$
$\bar{\zeta}_u = \bar{m} + 2e\bar{m} + \frac{5}{4}e^2 \sin 2\bar{m} + \frac{e^3}{12}(13\sin 3\bar{m} - 3\sin \bar{m}) + \frac{e^4}{96}(103\sin 4\bar{m} - 44\sin 2\bar{m})$
$+\frac{e^4}{960}(1097\sin 5\bar{m} - 645\sin 3\bar{m} + 50\sin \bar{m}) + \frac{e^6}{960}(1223\sin 6\bar{m} - 902\sin 4\bar{m} + 85\sin 2\bar{m})$
$+ \ldots$
$\bar{\zeta} = \bar{\zeta}_u + 3\frac{J_2 R_e^2}{p^2}\bar{n}(1 - \frac{5}{4}\sin^2 i)(t - t_p)$
$\bar{\xi}_N = \xi_N - \frac{3}{2}\frac{J_2 R_e^2}{p^2}\bar{n}\cos i\,(t - t_p)$
These terms account for the effect of the earth's oblateness
$\varphi_s = \sin^{-1}[\sin i \sin(\bar{\zeta} - \zeta_p)]$
$\xi = \bar{\xi}_N + \tan^{-1}\left[\frac{\cos i \sin(\bar{\zeta} - \zeta_p)}{\cos(\bar{\zeta} - \zeta_p)}\right]$
$\theta_s = \xi - \omega_e(t)$
1

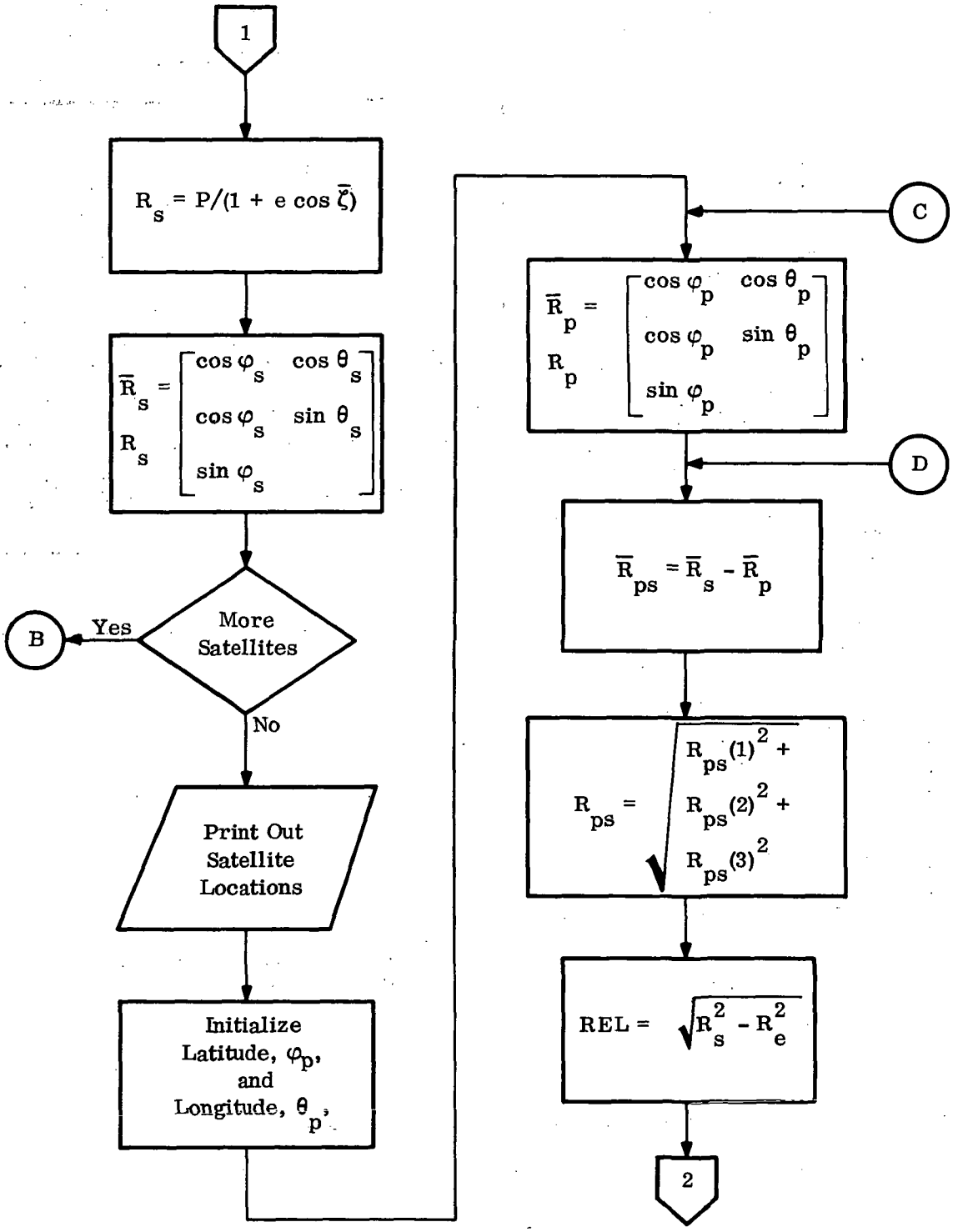
1
$R_s = P/(1 + e \cos \bar{\zeta})$
$\bar{R}_s = \begin{bmatrix} \cos\varphi_s & \cos\theta_s \\ \cos\varphi_s & \sin\theta_s \\ \sin\varphi_s & \end{bmatrix}$
R_s
More Satellites
Yes
B
No
Print Out Satellite Locations
Initialize Latitude, φ_p, and Longitude, θ_p,
C
$\bar{R}_p = \begin{bmatrix} \cos\varphi_p & \cos\theta_p \\ \cos\varphi_p & \sin\theta_p \\ \sin\varphi_p & \end{bmatrix}$
R_p
D
$\bar{R}_{ps} = \bar{R}_s - \bar{R}_p$
$R_{ps} = \sqrt{R_{ps}(1)^2 + R_{ps}(2)^2 + R_{ps}(3)^2}$
$REL = \sqrt{R_s^2 - R_e^2}$
2

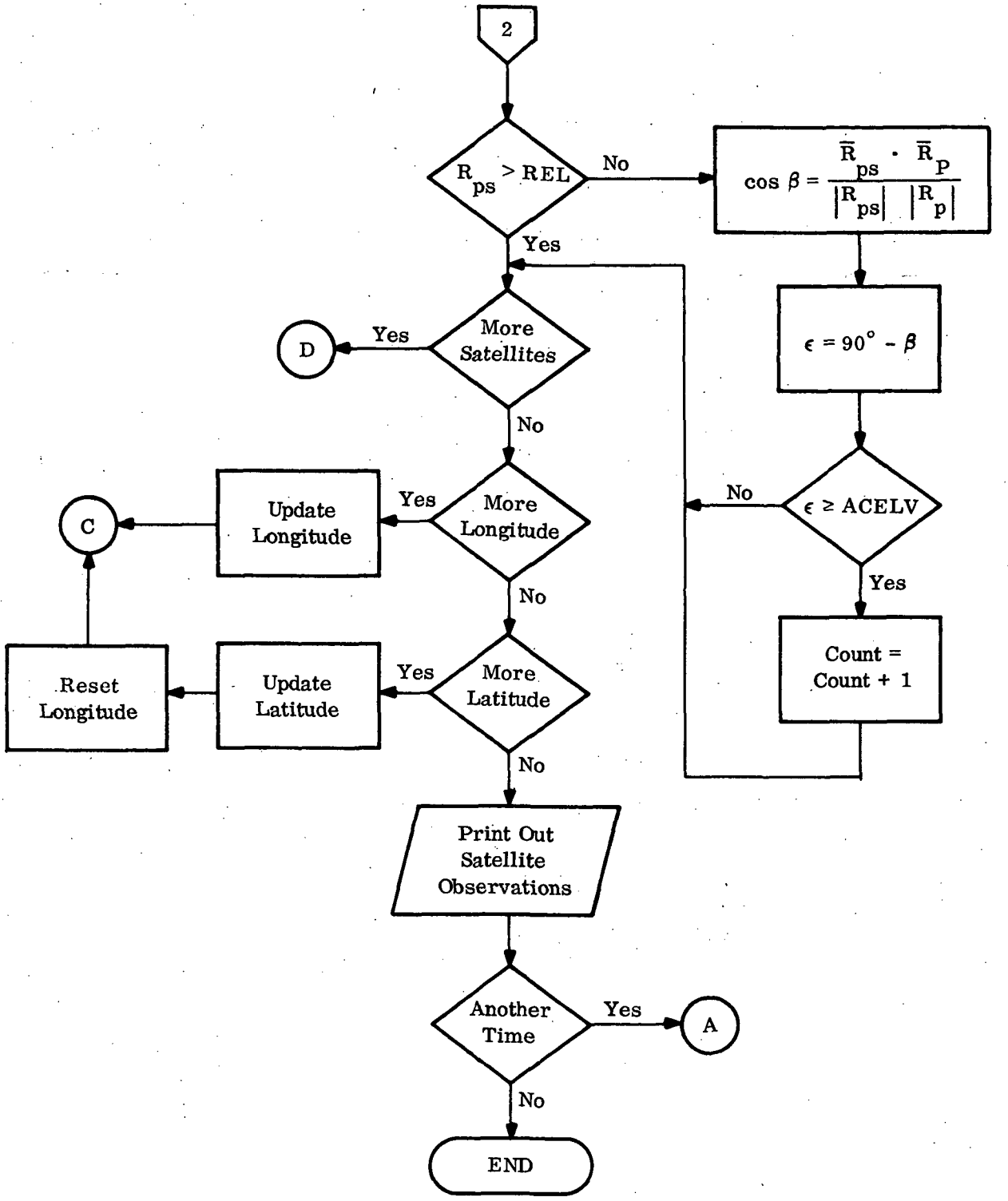
2
$R_{ps} > REL$
No
$\cos \beta = \frac{\bar{R}_{ps} \cdot \bar{R}_{p}}{|R_{ps}| \; |R_{p}|}$
Yes
More Satellites
Yes
D
No
$\epsilon = 90^{\circ} - \beta$
$\epsilon \geq ACELV$
No
Yes
Count = Count + 1
More Longitude
Yes
Update Longitude
C
No
More Latitude
Yes
Update Latitude
Reset Longitude
No
Print Out Satellite Observations
Another Time
Yes
A
No
END

SYMBOLS

R_e - Radius of earth

R_p - Distance from center of earth to observation point

ω_e - Earth's rotational rate

a - Semimajor axis

e - Eccentricity

T_p - Time of perigee

ξ_N - Longitude of ascending node

i - Inclination

ζ_p - Argument of perigee

T - Satellite period

n - Mean motion

p - Semilatus rectum

$\bar{n}$ - Mean value of mean motion

R_s - Distance from center of earth to satellite

R_{ps} - Distance from satellite to observation point

$\bar{m}$ - Mean value of mean anomaly

$\bar{\zeta}_u$ - Mean value of perturbed true anomaly

$\bar{\xi}_N$ - Mean value of longitude of ascending node

ϕ_s - Geodetic latitude of satellite

ξ - Inertial longitude

θ_s - Longitude of satellite

ϕ_p - Latitude of observation point

θ_p - Longitude of observation point

INPUT

Card 1

	ACELV	F10.5	Acceptance value for angle of elevation (degrees)
	STIM	F10.5	Start time for observations (minutes)
	ETIM	F10.5	End time for observations (minutes)
	DTIM	F10.5	Time increment (minutes)
	DLAT	I10	Delta latitude (degrees)
	DLONG	I10	Delta longitude (degrees)

Card 2

	NSTOT	15	Number of satellites
	NORB	15	Number of orbits
T	PER	F10.5	Period of satellites (minutes)
e	E	F10.5	Eccentricity
T_p	TP(1)	F10.5	Time of perigee for first satellite (minutes)
ξ_N	XIN(1)	F10.5	Longitude of ascending node for first satellite (degrees)
i	AIN	F10.5	Angle of inclination (degree)
ζ_p	ARGPER	F10.5	Argument of perigee for first satellite (degrees)

Appendix I

MARITIME USE OF SATELLITES

Appendix I

MARITIME USE OF SATELLITES

I.1 INTRODUCTION

During the past 25 years or more, electronic aids to navigation and collision avoidance have been used aboard ship. While certainly improving matters, each of the various systems has its problems. For example, Loran A has a range limitation of 600 to 900 miles by day and 1400 miles by night, insufficient for a truly world-wide system. Loran C has a longer range, but its lower reliability and higher cost make it unsuitable for commercial users.[1] Radar has proven so unsatisfactory with respect to collision-avoidance that the term "radar-assisted collisions" has come into use. This is not to say that the equipment causes collisions, but that ship's personnel either have difficulty interpreting the information provided by the radar or do not take the trouble to determine the proper action. The interpretation problem can arise from interference, such as rain and sea clutter, traffic density, which stresses the ability of even a competent operator, or simply lack of training. Recognition of the density problem has led to the development of a variety of automated systems capable of tracking multiple targets.[2,3,4] These systems certainly ease the burden of the individual ship's officers. However, it remains to be seen whether the systems prove accurate enough for all types of users and suitable for ever-increasing traffic densities. The latter in particular will highlight, if it hasn't already, the absence of a marine equivalent of the current air traffic control arrangements among nations. Satellites appear an attractive approach both to increased accuracy and cooperative traffic control.

I.2 USER COMMUNITY AND ITS REQUIREMENTS

Table I-1 summarizes the results of a study performed for the US Coast Guard in 1969.[5] This study provided estimates of current quantities, and forecasts for 1980, of the world's maritime vessels exceeding 100 gross tons. Not surprisingly, those vessels engaged in the transportation of raw materials and the search and acquiring of food had the fullest utilization. In all, there were in 1969 some 21,000 vessels at sea, of which nearly half were fishing vessels. The projections for 1980 were for an almost 50% increase in ships at sea, most of the increase accounted for by yet more fishing vessels. A geographic distribution appears in Table I-2.

While the overall traffic does indicate the magnitude of the navigation/collision-avoidance problem, the predominance of fishing vessels in itself has certain consequences. The traffic patterns of such vessels are much less predictable than for carriers of raw materials or manufactured products, as fishing boats are engaged in continuing search

Table I-1

FORECAST OF VESSEL POPULATION GROWTH

Type of Ship	1969		1980	
	Total	At-Sea	Total	At-Sea
Tankers	5,869	4,637	7,039	5,559
Ore and bulk carriers	2,378	1,474	5,370	3,519
General cargo and passenger	26,100	5,269	19,565	4,935
Other	3,980	270	2,984	254
Total exclusive of fishing vessels	38,327	11,650	34,958	14,267
Fishing vessels	11,949	9,323	19,156	14,946
Overall total (over 100 gt)	50,276	20,973	54,114	29,213

Table I-2

SUMMARY OF SHIP DISTRIBUTION TRENDS

Location	1969	1980
Atlantic	9,507	11,130
Pacific	7,431	10,790
Indian	2,465	5,776
Miscellaneous	1,570	1,517
Total (over 100 gt)	20,973	29,213

operations. Moreover, such vessels ever-increasingly operate in fleets, so that the collision-avoidance problem is aggravated for ships encountering them on the high seas and perhaps within the fleets themselves. Still further, fishing boats require an accuracy of less than 0.1 mile in all oceans and under virtually all weather conditions, and for reasons of business security would prefer a navigation system which does not require position reporting.[6]

Table I-3 presents accuracy and other user requirements for a variety of ship types.[7] Considering the usual estimates of satellite lifetimes, (5 to 7 years), the 1975-1985 column is of the most interest here. Note that the 0.1-mile or better accuracy is a requirement for several types of vessels, with 0.5-mile or better specified for all but recreational craft. The requirement for "instantaneous" determination of position mandates some form of automated system. Coverage capability of world-wide or near-world-wide extent underscores the need for a multination approach to traffic control, weather reporting, and search and rescue missions.

I.3 SATELLITE TECHNIQUES AND THEIR ADVANTAGES

A variety of experiments[8] have demonstrated that satellites can provide satisfactory marine surveillance and communications under a wide variety of conditions, some of which render HF and lower frequencies unusable. In fact, satellite communications are about as good as bridge-to-bridge communications in a harbor, which themselves are very useful. Obviously, the flexibility of such a system would be far greater than a line-of-sight system using such media as HF radio and cable. One of the questions to be answered (but not here) is that of orbit altitude. The Navy's TRANSIT system, which is the only fully operational satellite navigation system for marine use, has satellites in 600-mile polar orbits. One analysis[9] alleges that this type of system is less costly than one using synchronous orbits, and states that a synchronous system is superior only when service over a limited portion of the globe is required. However, the cost figures in that analysis are quite close, and one can argue that limited coverage per satellite or constellation is desirable as it minimizes tracking and handover problems. Another analysis[10] indicates a preference for mid-altitude satellites (6,500 to 14,000 miles). Still another study[11] refers to "preferred deployments" of geostationary orbits. How a marine satellite system eventually would be configured has yet to be resolved, but the TRANSIT system has already demonstrated an accuracy capability meeting the requirements set forth in Table I-3.[12]

A cost-benefit analysis for six possible satellite configurations was performed by the National Academy of Sciences.[13] These configurations were

1) Not appropriate for marine application
2) Two geostationary satellites using the VHF band and having limited capacity for marine service, primarily traffic control

Table I-3
MARTIME USER REQUIREMENTS

Type of Marine User	Accuracy 95% of Time (Accuracy when fix is available)						Order of Time to Determine Position						Coverage Capability of Systems			Cost Limitations (Per complete equipment including aux equipment but exclusive of installation costs)		
	1. 0 - 0.1 Mile 2. 0.1 - 0.5 Mile 3. 0.5 - 1.0 Mile 4. 1.0 - 2.0 Mile						1. Instantaneous 2. To 3 minutes 3. Over 3 minutes						1. World Wide 2. World Wide less Polar Regions 3. North Atlantic & North Pacific & U.S. Lakes and Rivers			1 Under $200 2 $200-$1500 3 $1500-$5K 4 $5K-$20K 5 Over $20K		
	Coastal and Confluence			High Seas			Coastal and Confluence			High Seas			All Waters			All Waters		
	Present	1975 - 1985	Post 1985	Present	1975 - 1985	Post 1985	Present	1975 - 1985	Post 1985	Present	1975 - 1985	Post 1985	Present	1975 - 1985	Post 1985	Present	1975 - 1985	Post 1985
Merchant Ship, Large	3	2	1	4	3	2	2	1	1	3	1	1	2	1	1	4	5	5
Merchant Ship, Small	3	2	1	4	3	2	2	1	1	3	1	1	2	1	1	4	5	5
Hydrofoil	2	1	1	4	2	1	1	1	1	1	1	1	3	2	2	4	5	5
Surface Effect Ship (GEM)	2	1	1	4	2	1	1	1	1	1	1	1	3	1	1	4	5	5
Fishing Craft, Large	2	1	1	2	2	2	2	1	1	2	1	1	2	1	1	4	4	4
Fishing Craft, Small	2	1	1	2	2	2	2	1	1	2	1	1	2	1	1	2	3	4
Recreation Craft	3	3	1	4	3	2	3	2	2	3	2	2	3	3	2	1	2	3
Scientific Survey Craft	2	1	1	2	1	1	1	1	1	1	1	1	1	1	1	5	5	5
Submersibles	2	1	1	2	1	1	1	1	1	1	1	1	1	1	1	5	5	5

3) Two geostationary satellites using both the VHF and L bands, and providing position fixing and communications for both air and marine traffic surveillance

4) A similar system using only L band

5) One geostationary satellite with communications in L band and position fixing at L or C band

6) A worldwide system (Systems 1-5 are transoceanic) using six geostationary satellites.

The costs of these systems are summarized in Table I-4. The R&D and the launch costs are assumptions, as is a satellite lifetime of 5 years and a launch malfunction factor of 1.2. The nature and amount of the benefits is summarized in Table I-5. It turns out that there is an unquestioned advantage (defined by the intersection of the lowest estimate of benefits with the highest estimates of cost) for Systems 3, 4, 5, and 6 if the systems are available to both US and foreigh users. The points of advantage are reached from 2 to 4 years following the date of availability of the satellite if aircraft as well as maritime applications are included. System 2 takes longer than ten years to reach the same point. Obviously, other configurations would have different cost-benefit tradeoffs, but the NAS study illustrates the kind of analysis that can be made to justify a continuing effort.

Table I-4

COSTS ASSOCIATED WITH SATELLITE SYSTEMS

Capital Equipment Costs ($ Million)	System					
	1	2	3	4	5	6
R&D	10-20	10-20	20-40	20-40	30-50	20-40
No. of Satellites	1	2	2	2	1	6
Cost of Flight Model Satellites	2-4	2-4	6-9	6-9	7-10	6-9
Cost of Launch (per satellite)	5	5	15	15	15	15
Total Cost of Satellite Portion of System (R&D plus Satellites plus Launch, including 1.2 Malfunction Factor)	18-31	27-42	70-98	70-98	56-80	171-213
Ground Complex Costs (including Marine Control for systems 3-6)	3-4	3-4	6-8	6-8	6-8	18-24
Total Capital Costs	21-35	30-46	76-106	76-106	62-88	189-237
Operation and Maintenance of Ground Complex (per year)	2-3	2-3	3-5	3-5	3-5	9-15
Replacement of Satellites (per year)	1.6-2	3.2-4	5-11.5	5-11.5	5.3-6	15-35
Total Annual Costs	3.6-5	5.2-7	8-16.5	8-16.5	8.3-11	24-50
User Equipment Costs ($ Thousand)						
Capital Costs (Equipment + Installation)						
Aircraft Users (each)	20-40	20-40	20-40	60-120	60-120	60-120
Ship Users (each)	*	7-15	25-50	25-50	25-50	25-50
Operation and Maintenance (per year)						
Aircraft Users (each)	2-4	2-4	2-4	6-12	6-12	6-12
Ship Users (each)	*	0.7-1.5	2.5-5	2.5-5	2.5-5	2.5-5

*Not appropriate

Table I-5

BENEFITS OF VARIOUS SATELLITE SYSTEMS

Benefit	Beneficiary	Reason for Benefit	Average Monetary Return per Year per Aircraft or Ship	
			Average	Net (10 year Amortization of Costs of User Equipment
Improvement in Air Traffic Control	Owners of Aircraft	Savings in fuel and increased utilization of aircraft by reduction in en route delays	Reduction in delay for 700 flights per year at $20-40 savings per flight in an early time frame, rising to $80-160 per flight by 1980, $14k-28k to $56-102k	$2-4k rising to $44-88k
Marine Traffic Control	Owners of Ships	Reduction in insurance premiums through increased safety	Lowering of negotiated rate of premium if experience warrants it by 0.5%-1.0% of cost of vessel, ($10M-20M average cost) $50k-200k	(A ship would receive benefits from both with a single installation of equipment) $51k-$202k
En route Navigation for Ships	Owners of Ships	Savings in fuel and increased utilization of ships by improved course keeping	1% of fuel cost (300k-500k); 1% gain in days available for revenue carrying purposes ($300k-$700k per year), $6k-$12k	
Aid to Commercial Fishing	Owners of Ships	Savings in manpower and fuel by enabling ship to return directly to proven fishing grounds	10% of manpower and fuel costs, ($50k-$250k per year) $5k-$25k	Zero-$15k

*Column 4 less user costs from Table 4

k = Thousand
M = Million

I.4 REFERENCES

1 G. D. Dunlap, Major Developments in Marine Navigation During the Last 25 Years; Navigation, Vol. 18, No. 1, Spring 1971, pp. 63-76.

2 A. E. Fiore et al, Historical Approach to Marine Collison Avoidance; Navigation, Vol. 18, No. 1, Spring 1971, pp. 116-133.

3 N. C. Dickerson, Automatic Omega Receiver: Computer-Augmented Approach to Low Cost Marine Navigation; Navigation, Vol. 18, No. 2, Summer 1971, pp. 147-154.

4 K. H. Chase and B. V. Tiblin, INCAS Integrated Navigation and Collision Avoidance System; Navigation, Vol. 18, No. 2, Summer 1971, pp. 205-214.

5 R. P. Thompson, Size and Ocean Distribution of the World Merchant Fleet: Present and Future; Navigation, Vol. 18, No. 2, Summer 1971, pp. 176-187.

6 National Academy of Sciences, Useful Applications of Earth-Oriented Satellites: Navigation and Traffic Control; 1969, Section 4.

7 A. E. Fiore and P. Rosenberg, Earth Satellite Systems for Marine and Transoceanic Air Navigation and Traffic Control; Navigation, Vol. 17, No. 3, Fall 1970, pp. 234-245.

8 A. E. Fiore et al, op. cit.

9 R. B. Kershner, Low Altitude Satellite System, 1969 EASCON Record, pp. 174-179.

10 R. L. Easton, Mid-Altitude Navigation Satellites, 1969 EASCON Record, pp. 180-183.

11 National Academy of Sciences, op. cit., Section 5.

12 T. A. Stansell, Using the Navy Navigation Satellite System; Navigation, Vol. 17, No. 2, Summer 1970, pp. 170-185.

13 National Academy of Sciences, op. cit., Section 8.

(Last page of document)

IBM Electronics Systems Center, Gaithersburg, Maryland 20760